5-2011

Carbon and Sulfur Cycling in Early Paleozoic Oceans

Cara Kim Thompson
cara.k.thompson@gmail.com

To the Graduate Council:

I am submitting herewith a dissertation written by Cara Kim Thompson entitled "Carbon and Sulfur Cycling in Early Paleozoic Oceans." I have examined the final electronic copy of this dissertation for form and content and recommend that it be accepted in partial fulfillment of the requirements for the degree of Doctor of Philosophy, with a major in Geology.

Linda C. Kah, Major Professor

We have read this dissertation and recommend its acceptance:

Chris Fedo, Kula Misra, Lee Cooper

Accepted for the Council:

Carolyn R. Hodges

Vice Provost and Dean of the Graduate School

(Original signatures are on file with official student records.)

To the Graduate Council:

I am submitting herewith a dissertation written by Cara Kim Thompson entitled “Carbon and Sulfur Cycling in Early Paleozoic Oceans”. I have examined the final electronic copy of this dissertation for form and content and recommend that it be accepted in partial fulfillment of the requirements for the degree of Doctor of Philosophy, with a major in Geology.

Linda C. Kah, Major Professor

We have read this dissertation
and recommend its acceptance:

Chris Fedo

Kula Misra

Lee Cooper

Accepted for the Council:

Carolyn R. Hodges
Vice Provost and Dean of the Graduate School

(Original signatures are on file with official student records)

CARBON AND SULFUR CYCLING IN EARLY PALEOZOIC OCEANS

A Dissertation
Presented for the
Doctor of Philosophy Degree
The University of Tennessee, Knoxville

Cara Kim Thompson
May 2011

Dedication

This dissertation is dedicated to my grandfather, Thomas W. Schoelen, who first sparked my interest in science, encouraged me not to sell myself short, and inspired me to reach my fullest potential. I am finally Dr. Doogie!

Acknowledgements

I would like to thank everyone who offered assistance to help me complete this Doctor of Philosophy degree in Geology. I would like to thank Linda Kah for all of her helpful insight and guidance as I worked through my dissertation research. I would also like to thank my committee members, Chris Fedo, Kula Misra, and Lee Cooper for their insight and support, and in particular Kula for agreeing to join my committee at a late date and for also serving on my Master of Science committee and Lee, who made a special trip to Knoxville for my defense.

Most importantly, I would like to thank my parents, Thomas and Trina Thompson, my brother, Kevin Thompson, my grandmother, Bonnie Schoelen, and my husband, Craig, for all of their love and support during these many long years in graduate school. Finally, I would like to thank Vincent for reminding me to relax and take a walk every once in a while.

Abstract

Here, I evaluate biospheric evolution during the Ordovician using high-resolution inorganic carbon and sulfur (carbonate-associated sulfate and pyrite) isotope profiles for Early Ordovician to early Late Ordovician strata from geographically distant sections in Western Newfoundland and the Argentine Precordillera. Additionally, I present new, high-resolution U-Pb ages for volcanic ash beds within strata of the Argentine Precordillera. Carbon isotope data record subdued variation that is typical of Early to Middle Ordovician strata worldwide. By contrast, sulfur isotopic compositions of carbonate-associated sulfate reveal a complex signal of short-term, rhythmic variation superimposed over a longer-term signal. This short-term, rhythmic variation occurs in all sections and appears to be unrelated to lithology or depositional environment, suggesting preservation of an oceanographic signal. I interpret this signal to reflect a combination of a marine sulfate reservoir that was likely much smaller than the modern, the persistence of a substantial deep-ocean hydrogen sulfide reservoir, and the episodic oxidation of a portion of the deep-ocean euxinic reservoir. Persistent euxinia likely resulted from decreased solubility of oxygen in warmer water and/or sluggish oceanic circulation during greenhouse conditions that reduced vertical ventilation. A dramatic change in the behavior of carbonate-associated sulfate and pyrite in the Middle Ordovician is interpreted to reflect a major oceanographic event that records the initial transition from Ordovician greenhouse to icehouse states. I suggest that the initiation of downwelling of increasingly cool, oxygen-rich surface water resulted in widespread oxidation of much of the deep ocean hydrogen sulfide reservoir and concomitant limitation of marine pyrite formation. It is unknown, however, why sea surface temperatures declined through the Early to Middle Ordovician. Explosive volcanism does not appear to be a primary climate driver, based on the timing of Argentinian K-bentonite formations relative to marine records of sea surface temperature, carbon and strontium isotopic composition. Rather, long-term positive feedback between organic carbon burial rates and productivity may have increased carbon dioxide drawdown, ultimately driving a gradual decrease in sea surface temperatures in the Early to Middle Ordovician.

Table of Contents

List of Figures

Page

Part 2

Part 3

List of Tables

Part 2

Part 3

Nomenclature

Abbreviations

SPICE	Steptoean Positive Carbon Isotope Excursion
MDICE	Middle Darriwilian Carbon Isotope Excursion
BSR	bacterial sulfate reduction
OC	organic carbon
DIC	dissolved inorganic carbon
pCO_2	partial pressure of carbon dioxide
CAS	carbonate-associated sulfate
PY	pyrite
δ	isotopic composition relative to a standard
VPDB	Vienna Pee Dee Belemnite
VCDT	Vienna Canyon Diablo Troilite
$\delta^{13}C_{carb}$	isotopic composition of carbonate carbon
$\delta^{18}O_{carb}$	isotopic composition of carbonate oxygen
$\delta^{34}S_{SO4}$	isotopic composition of sulfate sulfur
$\delta^{34}S_{CAS}$	isotopic composition of CAS
$\delta^{34}S_{PY}$	isotopic composition of pyrite sulfur
ΔS	isotopic difference between CAS and pyrite
FOV	field of view

Units

Ma	megaanum
Myr	million years
‰	parts per thousand
mM	millimolar

Part 1
Introduction

1. Overview

This dissertation is divided into three parts, two that present high-resolution Ordovician carbon and sulfur isotope chemostratigraphic curves and a third that incorporates high-resolution U-Pb geochronology data from K-bentonites. These data sets are used to understand the timing and drivers of oceanographic and climate change in the Ordovician. In particular, data in Parts 2 and 3 are used to constrain sulfate reservoir size and understand changes in the extent of deep ocean anoxia and data in Part 4 are used to evaluate potential climate forcing by explosive volcanism, which was prevalent in the Ordovician.

Biospheric oxygenation in the terminal Proterozoic (Hurtgen et al., 2009) and the advent of biomineralization in the earliest Cambrian likely paved the way for increased biodiversification in the Ordovician. Recent evidence, however, suggests deep-water anoxia persisted in the Late Cambrian (Gill et al., 2011). In Parts 2 and 3, carbon and sulfur isotope profiles from marine platform rocks from the Argentine Precordillera and Western Newfoundland are evaluated to show that anoxia likely persisted into at least the Middle Ordovician, when sea surface temperature cooling initiated downwelling of cool, oxygen-rich surface waters. In Part 4, high-resolution U-Pb zircon ages of K-bentonites that span a globally correlated, low magnitude C-isotope excursion are used to show that timing of Argentinian K-bentonite deposition is inconsistent with climate forcing via explosive volcanism.

2. The Ordovician carbon and sulfur isotope record

Paired carbon and sulfur isotope records offer valuable insight into the degree of water column oxygenation since the processes that govern marine carbon and sulfur isotopic composition are largely a function of redox conditions. Like carbon, biological processes preferentially fractionate isotopically light sulfur into the reduced phase (hydrogen sulfide, which is buried as pyrite), therefore, conditions that promote the removal of this reduced phase result in an isotopically heavy oxidized phase (marine sulfate). The carbon and sulfur cycles are linked because the primary mechanism for sulfate removal in marine settings, bacterial sulfate-

reduction, requires the respiration of organic matter. The coupling of these two isotope systems, therefore, helps constrain not only organic carbon production and burial rates, but also sulfate availability and pyrite burial, both of which are closely tied to ocean redox conditions.

Despite evidence for increased ocean-atmosphere oxygenation in the terminal Neoproterozoic (Fike et al., 2006; Ries et al., 2009), widespread, deep-ocean anoxia persisted (Canfield et al., 2008), and low-oxygen, low-sulfate conditions resulted in variable euxinia across the global ocean (Wille et al., 2008; Li et al., 2010). Evaluation of marine carbon and sulfur isotope records from Late Cambrian successions suggest that oceanic euxinia persisted through, and may have even increased within, the Cambrian (Hurtgen et al., 2009; Gill et al., 2011) despite marine oxidation represented by carbon burial during the Late Cambrian SPICE (Steptoean Positive Carbon Isotope Excursion) event (Saltzman et al., 1998; 2000; 2004). Part 2 presents the first long-term, high-resolution record of marine sulfur isotope variation for the Ordovician. These records reveal short-term variation superimposed over a longer-term signal. Short-term, rhythmic variation occurs in geographically disparate, lithologically distinct sections, suggesting preservation of an oceanographic signal. The rapidity of short-term isotopic variation requires the marine sulfate reservoir size to be much smaller (<10%) than that of the modern ocean, which agrees with previous estimates of low marine sulfate concentration in the Ordovician ocean (e.g., Horita et al., 2002; Brennan et al., 2004; Hough et al., 2006; Hurtgen et al., 2009; Gill et al., 2011). Single-reservoir box model calculations suggest the rhythmic nature of the short-term variability is best explained by episodic oxidation of at least a portion of a persistent deep-water hydrogen sulfide reservoir. Early-Middle Ordovician greenhouse conditions permitted the build-up of a deep-water hydrogen sulfide reservoir either through the decreased oxygen solubility of warmer water, sluggish ocean circulation, or both, and enhanced bacterial sulfate reduction in the water column.

Part 3 presents a continued examination of the Ordovician marine sulfur cycle in to the Middle-Late Ordovician. Long-term sulfur isotope signals vary little until the late Middle Ordovician, when a large, rapid decrease in sulfate sulfur occurs and is followed by a progressive increase in the isotopic composition of pyrite sulfur to values heavier than coeval sulfate. Such dramatic

change in the behavior of the marine sulfur cycle likely reflects decreased sea surface temperature (Trotter et al., 2008) and initiation of downwelling of cool, oxygen-rich surface waters which resulted in substantial oxidation of the deep-water hydrogen sulfide reservoir. Reoxidation of hydrogen sulfide, along with continued ocean ventilation and the combination of sulfide oxidation and restriction of bacterial sulfate reduction to the sediment aided in driving pyrite sulfur to superheavy values.

3. Relationship between K-bentonite deposition and climate

The Ordovician represents an interval of high sea level, large epicontinental seas, and elevated atmospheric carbon dioxide that resulted in super greenhouse climate in the Early-Middle Ordovician (Berner, 1984; Brenchley, 1994). Greenhouse conditions were interrupted by widespread glaciation in the Late Ordovician, which is associated with the end Ordovician mass extinction (Brenchley et al., 1994). A recent push to attribute Ordovician climate forcing to explosive volcanism (Young et al., 2009; Buggisch et al., 2010) has garnered interest in the relationship between K-bentonite deposition and high-resolution marine geochemical records. The Ordovician represents a time of expansive volcanism where two prominent suites of K-bentonites are recognized, Early to Middle Ordovician Famatina K-bentonites in Argentina and Late Ordovician K-bentonites primarily in North America. In Part 4, high-resolution ID-TIMS U-Pb zircon ages of K-bentonites from measured sections of the San Juan Formation (Talacasto and Cerro La Chilca) in the Argentine Precordillera are used to explore the relationship between explosive volcanism and global climate change. These K-bentonites span a low-magnitude, globally correlatable negative excursion in marine carbon isotopic composition. K-bentonites yield mean ages that range from 469.53 to 473.45±0.40 Ma. These ages agree well with C-isotope correlation of the Cerro La Chilca and Talacasto sections, but suggest an overall older age for the upper San Juan Formation than is sometimes reported (Buggisch et al., 2003). The discrepancy between U-Pb zircon ages and reported biostratigraphy points to the difficulty in placing biostratigraphic constraints on the regionally diachronous boundary between the San Juan Formation and overlying strata. The timing of K-bentonite deposition also does not coincide with major perturbations in marine records of sea surface temperature, strontium, carbon and

sulfur isotopic composition, which suggests explosive volcanism did not substantially alter the marine environment on a long-term scale.

4. Summary

This study provides the first high-resolution, long-term sulfur isotope records for the Ordovician. Marine carbon isotopic composition shows only subdued isotopic variability and it is consistent with global patterns observed during Paleozoic greenhouse times. Sulfur isotope records are highly variable and support and interpretation of a reduced sulfate reservoir size in the Ordovician, which is consistent with previous estimates of marine sulfate concentration. Short-term, rhythmic fluctuations in the marine sulfur isotope record are best explained by partial reoxidation of a deep-water hydrogen sulfide reservoir, and an abrupt decrease in marine sulfur isotopic composition in the Middle Ordovician are interpreted to reflect the onset of downwelling of cool, oxygenated waters and oxidation of this deep-water hydrogen sulfide reservoir. Proxy records for sea surface temperature and strontium isotope ratios suggest that the transition from Ordovician greenhouse to icehouse climate states initiated substantially earlier than the onset of Hirnantian glaciation. Additionally, new U-Pb zircon ages from Argentina K-bentonites constrain the age of a small, yet globally correlatable negative excursion in carbon isotope values. Comparison of the timing of these K-bentonites with records for marine carbon (Saltzman et al., 1998; 2000; Saltzman and Young, 2005; Young et al., 2005; 2008; this study), sulfur (this study), strontium (Shields et al., 2003) and sea surface temperature (Trotter et al., 2008) suggests explosive volcanism in the Early and Middle Ordovician likely did not significantly alter marine chemistry on a long-term scale and was likely not a driver for the observed long-term decrease in sea surface temperatures.

References cited

Berner, R.A., 1984. Sedimentary pyrite formation: An update. Geochimica et Cosmochimica Acta 48, 605-615.

Brenchley, P.J., Marshall, J.D., Carden, G.A.F., Robertson, D.B.R., Long, D.G.F., Meidla, T., Hints, L., Anderson, T.F., 1994. Bathymetric and isotopic evidence for a short-lived Late Ordovician glaciation in a greenhouse period. Geology 22, 295-298.

Brennan, S.T., Lowenstein, T.K., Horita, J., 2004. Seawater chemistry and the advent of biocalcification. Geology 32, 473-476.

Buggisch, W., Joachimski, M.M., Lehnert, O., Bergström, S.M., Repetski, J.E., Webers, G.F., 2010. Did intense volcanism trigger the first Late Ordovician icehouse? Geology 38, 327-330.

Gill, B. C., Lyons, T. W., Young, S. A., Kump, L. R., Knoll, A. H. & Saltzman, M. R. Geochemical evidence for widespread euxinia in the later Cambrian ocean. *Nature* (2011).

Horita, J., Zimmerman, H., Holland, H.D., 2002. Chemical evolution of seawater during the Phanerozoic: Implications from the record of marine evaporites. Geochimica et Cosmochimica Acta 66, 3733-3756.

Hough, M.L., Shields, G.A., Evins, L.Z., Strauss, H., Henderson, R.A., Mackenzie, S., 2006. A major sulphur isotope event at c. 510 Ma: a possible anoxia-extinction-volcanism connection during the Early-Middle Cambrian transition? Terra Nova 18, 257-263.

Hurtgen, M.T., Pruss, S.B., Knoll, A.H., 2009. Evaluating the relationship between the carbon and sulfur cycles in the later Cambrian ocean: An example from the Port au Port Group, western Newfoundland, Canada. Earth and Planetary Science Letters 281, 288-297.

Saltzman, M.R., Young, S.A., 2005. Long-lived glaciation in the Late Ordovician? Isotopic and sequence-stratigraphic evidence from western Laurentia. Geology 33, 109-112.

Saltzman, M.R., Runnegar, B., Lohmann, K.C., 1998. Carbon isotope stratigraphy of Upper Cambrian (Steptoean Stage) sequences of the eastern Great Basin: Record of a global oceanographic event. Geological Society of America, Bulletin 110, 285-297.

Saltzman, M.R., Brasier, M.D., Ripperdan, R.L., Ergaliev, G.K., Lohmann, KC, Robison, R.A., Chang, W.T., Peng, S., Runnegar, B., 2000. A global carbon isotope excursion during the Late Cambrian: Relation to trilobite extinctions, organic matter burial and sea level: Palaeogeography, Palaeoclimatology, Palaeoecology 162, 211-223.

Shields, G.A., Carden, G.A.F., Veizer, J., Meidla, T., Rong, J.Y., Rong, Y.L., 2003. Sr, C, and O isotope geochemistry of Ordovician brachiopods: a major isotopic event around the Middle–Late Ordovician transition. Geochimica Cosmochimica Acta 67, 2005-2025.

Sial, A.N., Peralta, S., Ferreira, V.P., Toselli, A.J., Acenolaza, F.G., Parada, M.A., Gaucher, C., Alonso, R.N., Pimentel, M.M., 2007. Upper Cambrian carbonate sequences of the Argentine Precordillera and the Steptoean C-Isotope positive excursion (SPICE). Gondwana Research 13, 437-452.

Trotter, J.A., Williams, I.S., Barnes, C.R., Lécuyer, C., Nicoll, R.S., 2008. Did cooling oceans trigger Ordovician biodiversification? Evidence from conodont thermometry. Science 321, 550-554.

Young, S.A., Saltzman, M.R., Bergström, S.M., 2005. Upper Ordovician (Mohawkian) carbon isotope ($\delta^{13}C$) stratigraphy in eastern and central North America: Regional expression of a perturbation of the global carbon cycle. Palaeogeography, Palaeoclimatology, Palaeoecology 222, 53-76.

Young, S.A., Saltzman, M.R., Bergström, S.M., Leslie, S.A., Chen, X., 2008. Paired δ^{13}Ccarb and δ^{13}Corg records of Upper Ordovician (Sandbian-Katian) carbonates in North America and China: implications for paleoceanographic change. Palaeogeography, Palaeoclimatology,

Palaeoecology 270, 166-178.

Young, S.A., Saltzman, M.R., Foland, K.A., Linder, J.S., Kump, L.R., 2009. A major drop in seawater $^{87}Sr/^{86}Sr$ during the Middle Ordovician (Darriwilian): links to volcanism and climate. Geology 37, 951-954.

Part 2

Sulfur isotope evidence for widespread euxinia and a fluctuating oxycline in Early to Middle Ordovician greenhouse oceans

This chapter is a reformatted version of a paper by the same title that was submitted for publication to Palaeogeography, Palaeoclimatology, Palaeoecology in 2011.

Thompson, C.K., Kah, L.C. (*in review*). Sulfur isotope evidence for widespread euxinia and a fluctuating oxycline in Early to Middle Ordovician greenhouse oceans. Palaeogeography, Palaeoclimatology, Palaeoecology.

Abstract

Despite marine geochemical records indicating widespread oxygenation of the biosphere in the terminal Neoproterozoic, Late Cambrian records point to the persistence of deep-water anoxia and potential for development of euxinic conditions. The Late Cambrian SPICE event, however, is a globally recognized chemostratigraphic marker that likely represents significant organic carbon burial and subsequent liberation of oxygen to the biosphere. Here, we present high-resolution inorganic carbon and sulfur isotope profiles from Early to Middle Ordovician carbonate rocks from the Argentine Precordillera and Western Newfoundland to constrain oceanic redox conditions in the post-SPICE world. Marine C-isotope profiles record relatively stable behavior (excursions <3‰) that is characteristic of greenhouse climates. Marine S-isotope profiles record short-term (<10^6 yr), rhythmic variation superimposed over a longer-term (~10^7 yr) signal. Substantial isotopic heterogeneity between average S-isotope values of different sections (15-25‰) suggests the Ordovician marine sulfate reservoir was not well mixed, indicating a low marine sulfate concentration (likely <2 mM or less than 10% modern). Short-term variation (7‰ excursions over 1 Myr) is consistent with a small sulfate reservoir size and is best explained by the rhythmic oxidation of a deep-water reactive HS^- reservoir. Greenhouse intervals are often associated with deep-water anoxia (either through decreased ocean ventilation or reduced O_2 solubility of warmer water), and the presence of a persistent, deep water HS^- reservoir that is fed through BSR is not unexpected. A broadly sympathetic relationship between carbon and sulfur isotope systems over long time scales (~10^7 yr) suggests that the extent of deep-ocean euxinia was moderated by changes in organic productivity, which fueled BSR and production of reduced sulfide species. By contrast, short-term (<10^6 yr) sulfur isotope variation

appears to be decoupled from the marine carbon isotope signal. We suggest that this apparent decoupling reflects a combination of elevated pCO_2 during greenhouse times—which acts to dampen C-isotope response—and relatively small-scale fluctuations in organic productivity that affected the position of the marine oxycline and the balance of HS^- production and reoxidation.

1. Introduction

Isotopic compositions recorded in sedimentary successions suggest that in the terminal Neoproterozoic, widespread, deep-ocean anoxia persisted (Canfield et al., 2008) and low-oxygen, low-sulfate conditions resulted in variable euxinia across the global ocean (Wille et al., 2008; Li et al., 2010) despite evidence for increased ocean-atmosphere oxygenation (Logan et al., 2995; Fike et al., 2006; Halverson and Hurtgen 2007; Ries et al., 2009), Furthermore, evaluation of marine C- and S-isotope records from Late Cambrian successions suggest that oceanic euxinia persisted through, and may have even increased within, the Cambrian (Hough et al., 2006; Hurtgen et al., 2009; Gill et al., 2011).

Recent work by Hurtgen et al. (2009) and Gill et al. (2011) has provided particularly interesting insights because these studies examined relationships between linked C- and S-isotope records preceding and during the time of the globally recognized SPICE event (Steptoean Positive Carbon Isotope Excursion; Saltzman et al, 1998; 2000; 2004). The SPICE event is a globally correlative, 4-6‰ increase in marine $\delta^{13}C$ and comprises one of the most well documented carbon isotope excursions in the Early Paleozoic. Paired C- and S-isotope analyses record both large and rapid variation in $\delta^{13}C$ and $\delta^{34}S$ during this interval and a generally sympathetic correlation between $\delta^{13}C$ and $\delta^{34}S$ trends (Hurtgen et al., 2009; Gill et al., 2011). In these models, expanded anoxia, potentially driven by relatively elevated organic productivity (Saltzman et al., 2004; Saltzman, 2005), promotes an increase in bacterial sulfate reduction (BSR) in the water column and a subsequent increase in pyrite burial (Hurtgen et al., 2009; Gill et al., 2011). In both these studies, an increase in pyrite burial relative to organic carbon burial (i.e. a decrease in ΔS) is also observed through this interval, which results in a decreased C/S ratios to values that are substantially lower than that observed in modern marine environments

(2.8 by weight%; Berner and Raiswell, 1983). A decreased C/S ratio, combined with a decrease in Mo enrichment during the SPICE event (Gill et al., 2011), is consistent with a transient increase in oceanic euxinia in the Late Cambrian.

Evidence for increased euxinia during the SPICE event is important because it highlights the question as to what extent high-magnitude positive C-isotope excursions, such as the SPICE event, may have had lasting effects on the composition of the marine biosphere. For instance, excess carbon burial associated with the SPICE event has been estimated at ~10^{19} g C (Saltzman et al., 1998). Carbon burial, however, can be linked plausibly to *either* an increase or a decrease in marine oxygenation. If the SPICE event was driven primarily by organic carbon burial resulting from increased productivity by oxygenic photoautotrophs in a well-ventilated water column, long-term effects might include an increase in organic carbon burial and biospheric oxygenation (Garrels and Perry, 1974; Kump and Garrels, 1986; Berner, 1987; Berner and Canfield, 1989; Canfield, 2005). By contrast, if productivity was associated with ocean stratification and effective decoupling of the ocean-atmosphere system (equivalent to well-documented OAEs in the Paleozoic; Meyer and Kump, 2008), long term effects might include an increase in the global extent of anoxia, an expansion of oceanic euxinia, and depletion of bioessential trace metals (Anbar and Knoll, 2002; Saltzman, 2005). Because both oceanic oxygenation and differential availability of food sources—driven by enhanced euxinia and the effects of nutrient-limitation on the biological pump (Butterfield, 2009)—have been linked to trends in biological diversification (Munnecke & Servais, 2007; Martin et al., 2008; Dahl et al., 2010), it is critical to understand what effect the SPICE event may have had on the evolution of post-SPICE environments, such as those that span the Great Ordovician Biodiversification Event (GOBE; Webby et al., 2004; Harper, 2006; Servais et al., 2009).

The C-isotope record, unfortunately, provides only limited insight into the oxygenation state of marine environments in the Early Paleozoic. The Paleozoic C-isotope record is characterized by extended intervals of relative isotopic stability (excursions <3‰) that alternate with shorter intervals of isotopic volatility (excursions to 6‰; Figure 2.1). These alternating signals have

Figure 2.1. Paleozoic marine C-isotope curve (modified from Saltzman, 2005). Intervals of carbon isotope stability (grey boxes) occur during "greenhouse" climates and are interpreted to reflect nitrogen limitation of primary productivity. Intervals of isotopic volatility (white boxes) occur during "icehouse climates, when increased oceanic ventilation is believed to have reduced the effects of nitrogen limitation. The Late Cambrian SPICE event (Steptoean Positive Isotope Carbon Excursion) is a globally recognized 4-6‰ C-isotope excursion (Saltzman et al., 1998; 2000) that directly precedes Early to Middle Ordovician greenhouse times.

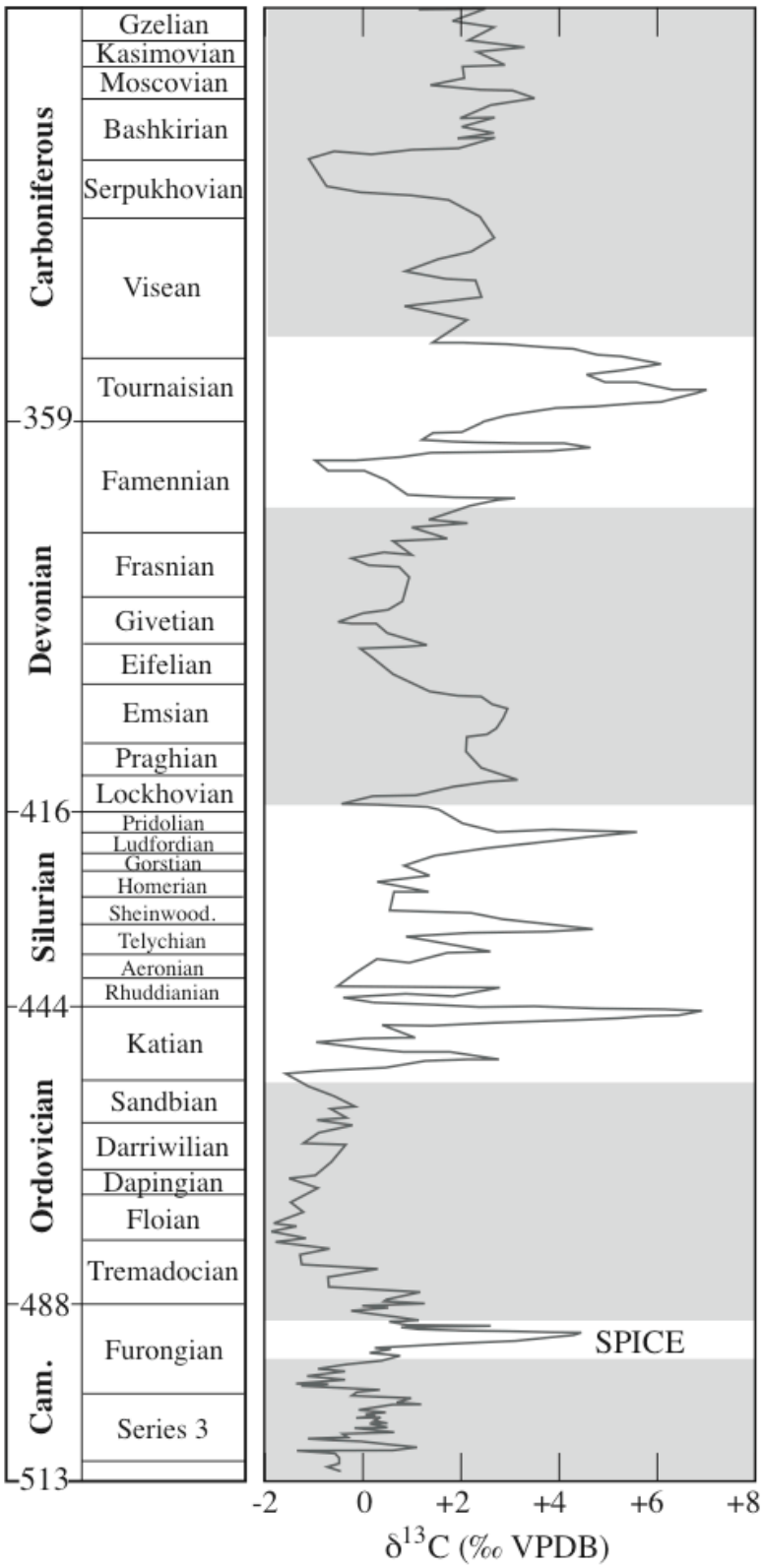
Carboniferous
Devonian
Silurian
Ordovician
Cam.
Gzelian
Kasimovian
Moscovian
Bashkirian
Serpukhovian
Visean
Tournaisian
Famennian
Frasnian
Givetian
Eifelian
Emsian
Praghian
Lockhovian
Pridolian
Ludfordian
Gorstian
Homerian
Sheinwood.
Telychian
Aeronian
Rhuddianian
Katian
Sandbian
Darriwilian
Dapingian
Floian
Tremadocian
Furongian
Series 3
359
416
444
488
513
SPICE
-2
0
+2
+4
+6
+8
δ13C (‰ VPDB)

been associated with changing states of global climate, oceanic circulation, and nutrient availability (Saltzman, 2005). In this model, enhanced circulation and oceanic ventilation during "icehouse" periods increases both nitrogen and phosphorus delivery to the surface oceans, resulting in enhanced photosynthetic productivity, higher organic carbon burial, and development of large, positive $\delta^{13}C$ excursions. By contrast, restrictive circulation in greenhouse oceans promotes development of a strong oxycline and nitrogen limitation through anoxic denitrification, ultimately producing a negative feedback between productivity and nitrogen availability and limiting the magnitude of C-isotope excursions (Saltzman, 2005).

In an alternative scenario, limited C-isotope variability that characterizes most of the Paleozoic can also plausibly be explained by a combination of high pCO_2 (Berner and Kothavala, 2001; Berner, 2006) and elevated marine dissolved inorganic carbon (DIC) (Bartley and Kah, 2004; Ridgwell and Zeebe, 2004). Because a large oceanic DIC reservoir is resistant to short-term changes in the magnitude and isotopic composition of carbon fluxes into and out from the oceanic system (Kump and Arthur, 1999), elevated pCO_2 conditions are consistent with minimal variability of the C-isotope record. In the Early Paleozoic, this effect might have been accentuated by the dramatic diversification of shelled marine invertebrates (i.e., the Great Ordovician Biodiversification Event), which would effectively couple marine carbonate and organic carbon burial across the continental shelves and further reduce the potential for isotopic variability (Bartley and Kah, 2004). Under these conditions, the primary source for C-isotope variability becomes the production of organic carbon by non-calcifying pelagic phytoplankton (Ridgwell, 2003; Bartley and Kah, 2004). In this scenario, increased C-isotope variability observed during "icehouse" states may represent a combination of lower pCO_2 and enhanced extinction of skeletonizing platform organisms, which would effectively decouple marine carbonate and organic carbon burial, resulting in increased organic carbon burial (Bartley and Kah, 2004).

Since the C-isotope record alone can provide only limited insight into oceanic oxygenation in the early Paleozoic, we focus on a combination of C- and S-isotope records. The biogeochemical cycles of carbon and sulfur are intimately linked, with their behavior largely dependent upon the

ambient state of biospheric oxygenation, therefore, combined C-S analysis can provide unique insight into oceanic oxygenation. Under relatively oxidizing conditions, inhibition of BSR can result in enhanced nutrient flux, higher rates of organic carbon burial, and a greater oxygen release, ultimately driving enhanced oxidative weathering and delivery of sulfate to the marine system (Kump and Garrels, 1986; Berner, 1987; Berner and Canfield, 1989; Canfield, 2005). Conversely, under conditions of anoxia, organic input will enhance BSR, resulting in either increased pyrite burial—provided there was sufficient availability of Fe—or expansion of oceanic euxinic conditions that may ultimately lead to a drawdown of oceanic sulfate concentration (Garrels and Perry, 1974; Veizer et al., 1980; Garrels and Lerman, 1981). Furthermore, generally low marine sulfate concentrations in the lower Paleozoic (Horita et al., 2002; Brennan et al., 2004; Hough et al., 2006; Hurtgen et al., 2009; Gill et al., 2011; Thompson et al., *in review*) should show a greater sensitivity of the marine S-isotope record to biogeochemical change, and thus provide a substantially more detailed and nuanced view of marine geochemical processes.

Here we present high-resolution, C- and S-isotope profiles of Latest Cambrian through Middle Ordovician strata from the Argentine Precordillera (La Silla and San Juan formations) and Western Newfoundland. Deposition of these units initiated shortly after the end of the globally recognized SPICE C-isotope event, and represents deposition through more than 20 Myr that are marked by relatively invariant C-isotope compositions. These strata thus provide an opportunity to use C-S relationships to test contrasting hypotheses regarding oceanic behavior in the aftermath of the SPICE event and ocean anoxia during global "greenhouse" conditions of the Ordovician.

2. Geologic setting and biostratigraphy

2.1. Ordovician paleogeography

Cambrian and Ordovician-aged marine carbonate and siliciclastic rocks crop out over large sections of the Argentine Precordillera (Baldis et al., 1984; Ramos et al., 1986) and Western

Newfoundland (Williams and Stevens, 1974; James et al., 1989). Both localities record intertidal to subtidal carbonate platform deposition in the Iapetus ocean, thereby avoiding potential issues of decoupling of geochemistry between epeiric and marine water masses (Holmden et al., 1998; Panchuk et al., 2006; Newton et al., 2011). Furthermore Ordovician biostratigraphic and paleomagnetic records place Western Newfoundland at equatorial latitudes (Ross and Ingham, 1970; Hall and Evans, 1988; Neuman and Harper, 1992; Cocks and McKerrow, 1993; Harper et al., 1996) and the Argentine Precordillera at moderately high southern latitudes (Figure 2.2; Herrera and Benedetto, 1991; Niocaill et al., 1997), suggesting that these sections, combined, provide a broad view of the Iapetus ocean. Finally, although there are relatively few absolute chronostratigraphic constraints for these successions, abundant biostratigraphic work has provided a necessary time-correlation of these geographically widespread successions (Herrera and Benedetto, 1991, Lehnert and Keller, 1994; Astini et al., 1995; Albanesi and Ortega, 2002).

2.2. Argentine Precordillera

Lower Paleozoic strata of the Argentine Precordillera comprise >2500 meters of siliciclastic, carbonate, evaporite-bearing sedimentary rocks, as well as associated mafic rocks, that record rifting of the Precordilleran microcontinent from the southeast margin of Laurentia in the Cambrian (Thomas and Astini, 1996; 1999), its subsequent drift across the Iapetus Ocean during the Early Ordovician, and eventual docking with Gondwana in the Middle to Late Ordovician (Ramos, 1988a; Benedetto et al., 1999). Initiation of Precordilleran docking with Gondwana is marked by the formation of the Famatina volcanic arc, which is the source of widespread bentonites in Middle Ordovician strata of the Argentine Precordillera (Huff et al., 1998). K-bentonites with ages of 469.5 ±3.2 Ma, 470.1 ±3.3 Ma (U-Pb_{zircon}; Fanning et al., 2004), and 464 ±2 Ma (U-Pb_{zircon}; Huff et al., 1997) suggest initiation of the pre-docking stage of the Precordillera in the Dapingian-early Darriwilian. Ultimately the Precordilleran terrane was uplifted by east-directed faulting of the Andean thrust belt in the Cenozoic (Thomas and Astini, 1999) and currently is exposed along the western margin of Argentina, striking north-south along the eastern margin of the Andean mountain range between 28°45′S and 33°15′S (Figure 2.3A; Ramos, 1988b; 2004). Strata are subdivided into eastern and western tectofacies, which record

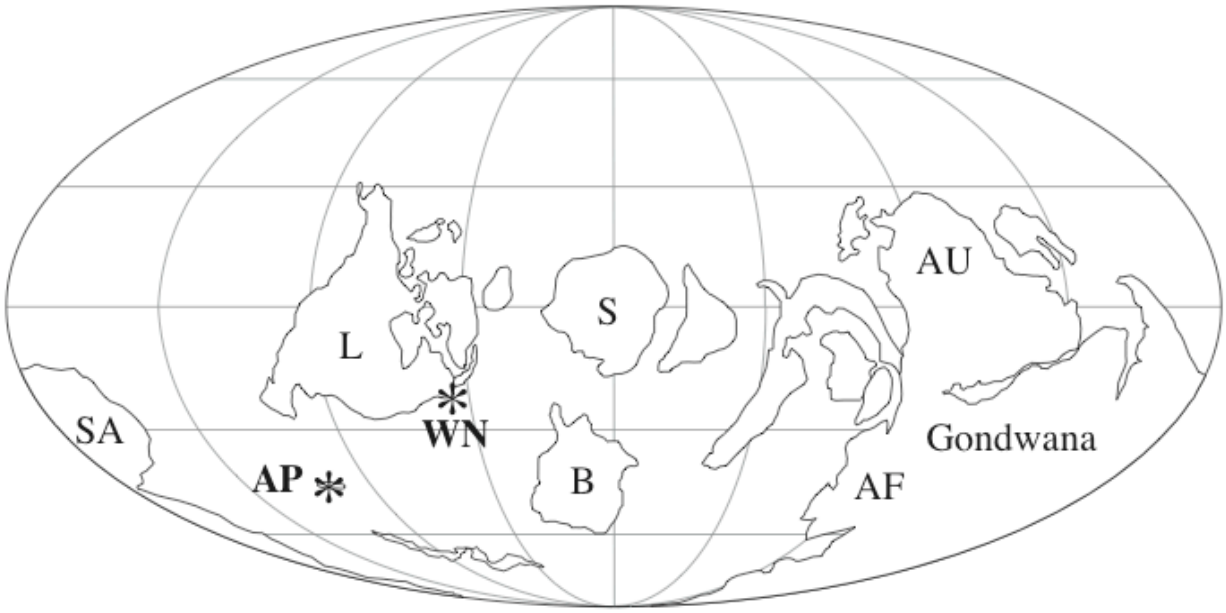

Figure 2.2. Paleogeographic reconstruction of the Early Ordovician (modified from Scotese and McKerrow, 1990). Whereas Western Newfoundland (WN) was positioned in subtropical latitudes throughout the Early and Middle Ordovician, during this time the Argentine Precordillera (AP) drifted from mid to high southerly latitudes, ultimately to collide with Gondwana in the Middle Ordovician. SA = South America, L = Laurentia, B = Baltica, S = Siberia, AF = Africa, AU = Australia, G = Gondwana.

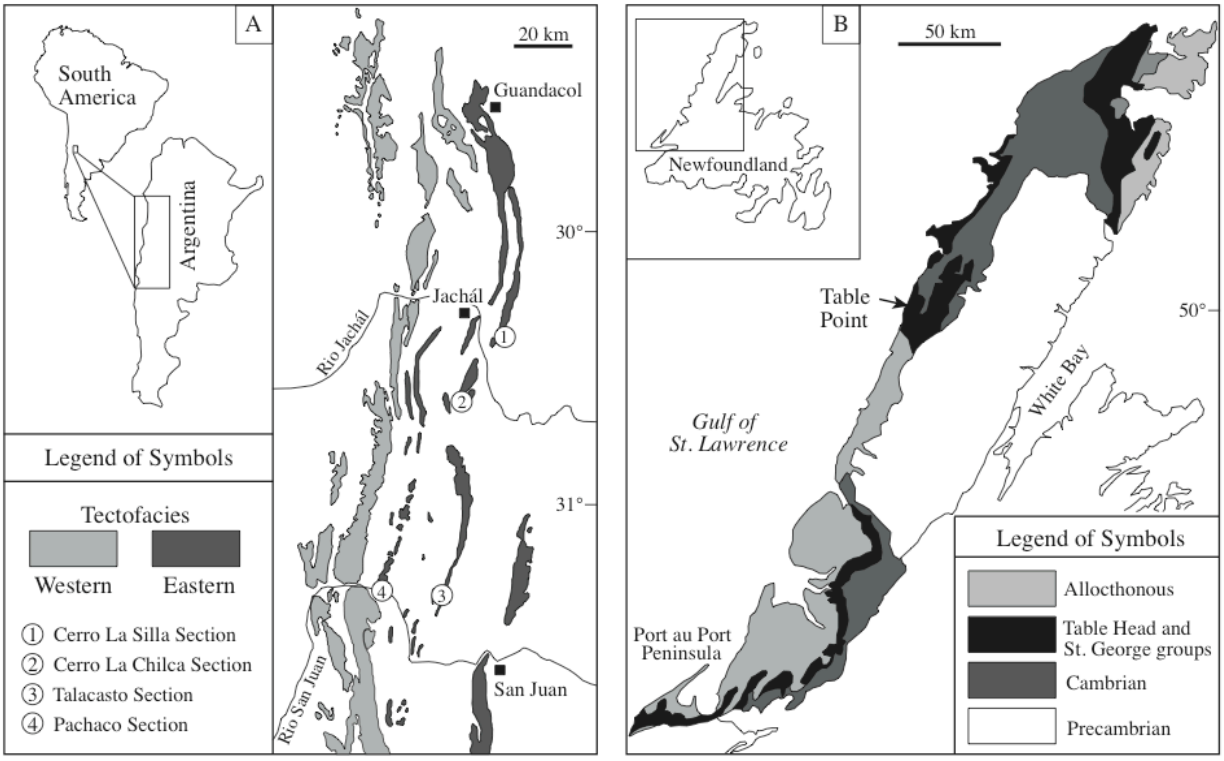

Figure 2.3. Geologic maps of the Argentinian and Newfoundland sections (modified from Williams, 1987 and Keller, 1994). A) Geographic locality of Argentinian sections. Both the La Silla and San Juan Formations were sampled at the type section, Cerro La Silla. The San Juan Formation was also sampled at Cerro La Chilca, Talacasto and Pachaco. B) Geographic locality of the Western Newfoundland sections. The Aguathuna Formation and Table Head Group were both sampled at Table Point.

carbonate, siliciclastic, and evaporite platform deposition on the Precordilleran platform and outer platform, respectively. Outer platform deposits, in particular, are comprised of basin deposits with slump features and conglomerates containing large olistoliths (Thomas and Astini, 2007).

2.2.1. La Silla Formation

The La Silla Formation consists of approximately 375 meters of shallow, subtidal limestone and dolostone that represent restricted carbonate platform deposition. The base of the La Silla Formation yields conodonts of the *C. proavus* zone, indicating a Late Furongian (Figure 2.4; Late Cambrian; Lehnert et al., 1997). The uppermost strata yield conodonts of the *P. Proteus* zone, indicating a Late Tremadocian age (Keller et al., 1994; Lehnert, 1995; Lehnert et al., 1997). The La Silla Formation was sampled at Cerro La Silla (30°21′10″S, 68°39′09″W), where the boundary with both the underlying La Flecha Formation and overlying San Juan Formation is exposed. The boundary between the La Flecha and La Silla formations is marked by a 20 cm thick dark grey silty dolostone and a shift from cyclic stromatolitic to thrombolitic, cherty dolostone of the La Flecha Formation to predominantly non-stromatolitic calcareous facies of the La Silla Formation (Keller, 1999). At the Cerro La Silla section, the La Silla Formation is composed of calcareous peloidal and intraclast grainstone, oolites, and fine-grained microbial laminates, with minor dolomite and chert. The boundary between the La Silla Formation and overlying San Juan Formation is conformable and marked by a major transgressive surface and the sudden appearance of facies that contain a diverse, open marine fauna (Keller et al., 1994; Keller, 1999).

2.2.2. San Juan Formation

The San Juan Formation consists of shallow subtidal deposits that record open ocean carbonate platform deposition. The base of the San Juan Formation yields conodonts of the *P. elongatus-deltifer* zone, indicating a Late Tremadocian-Early Floian age (Lindström, 1971, Löfgren, 1978; 1996). The uppermost strata yield conodonts of the *E. suecicus* zone (Lindström, 1971, Löfgren,

Figure 2.4. Biostratigraphic correlation of the Argentinian and Western Newfoundland sections compiled from Williams (1987), Stouge (1984), Lehnert and Keller (1997), Albanesi et al. (1999), and Albanesi and Ortega (2000). International stage names and time slices are from Bergström et al. (2008) and Walker and Geissman (2009). Age of the base of the section (here, the base of the La Silla Formation) is estimated based on a combination of biostratigraphic constraints, ages of stage boundaries, and an assumption of constant sedimentation rate for the individual sections.

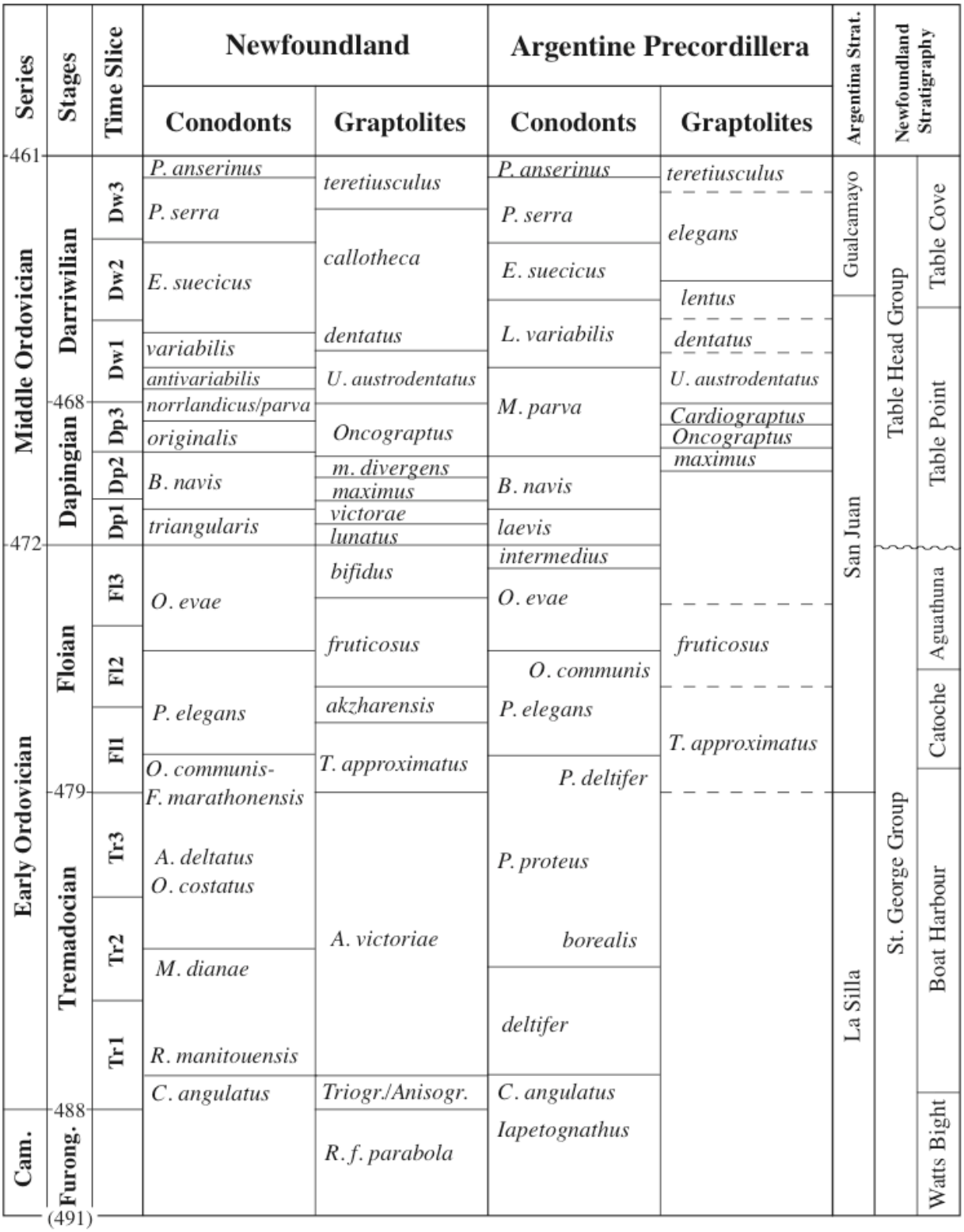
Series
Stages
Time Slice
Newfoundland
Conodonts
Graptolites
Argentine Precordillera
Conodonts
Graptolites
Argentina Strat.
Newfoundland Stratigraphy
461
Middle Ordovician
Darriwilian
Dapingian
468
472
Early Ordovician
Floian
Tremadocian
479
488
Cam.
Furong.
(491)
Dw3
Dw2
Dw1
Dp3
Dp2
Dp1
Fl3
Fl2
Fl1
Tr3
Tr2
Tr1
P. anserinus
P. serra
E. suecicus
variabilis
antivariabilis
norrlandicus/parva
originalis
B. navis
triangularis
O. evae
P. elegans
O. communis-
F. marathonensis
A. deltatus
O. costatus
M. dianae
R. manitouensis
C. angulatus
teretiusculus
callotheca
dentatus
U. austrodentatus
Oncograptus
m. divergens
maximus
victorae
lunatus
bifidus
fruticosus
akzharensis
T. approximatus
A. victoriae
Triogr./Anisogr.
R. f. parabola
P. anserinus
P. serra
E. suecicus
L. variabilis
M. parva
B. navis
laevis
intermedius
O. evae
O. communis
P. elegans
P. deltifer
P. proteus
borealis
deltifer
C. angulatus
Iapetognathus
teretiusculus
elegans
lentus
dentatus
U. austrodentatus
Cardiograptus
Oncograptus
maximus
fruticosus
T. approximatus
Gualcamayo
San Juan
La Silla
Table Head Group
St. George Group
Table Cove
Table Point
Aguathuna
Catoche
Boat Harbour
Watts Bight

1978; 1996) indicating a mid-Darriwilian age (Figure 2.4). The San Juan Formation is lithologically heterogeneous, consisting of fossiliferous mudstone and wackestone, nodular wackestone, oncolitic packstone, and reef boundstone. The top of the San Juan Formation is time-transgressive; it is conformably overlain by deep-water shale of the Gualcamayo Formation (Figure 2.5), and by mixed carbonate to shale deposition of the regional Las Chacritas and Las Aguaditas formations (not pictured), and is, in places, unconformably overlain by Silurian-aged strata. The San Juan Formation was sampled at its type section, Cerro La Silla. At Cerro La Silla, the uppermost San Juan Formation is absent, and was sampled at the nearby Cerro La Chilca section (Figure 2.3A). At Cerro La Chilca, uppermost San Juan strata consist of interbedded shale and limestone, yielding conodonts of the *E. suecicus* zone, and mark the conformable transition to the overlying Gualcamayo Formation. Incomplete sections of the San Juan Formation were also sampled at Talacasto and Pachaco (Figure 2.3A). In these sections substantial faulting and duplication prohibited measurement of their lower sections. The San Juan Formation at both Talacasto and Pachaco are unconformably overlain by Silurian-aged green shale. The Cerro La Chilca, Talacasto, and Pachaco sections also contain discrete K-bentonites in the upper portion of exposed San Juan strata. Several bentonites in the Talacasto have been dated using U-Pb zircon techniques and give ages that range from 470.1 ±3.3 Ma to 469.5 ±3.2 Ma (Fanning et al., 2004). Similarity in age to a porphyritic rhyolite from the Famatinian magmatic arc links these bentonites to the Famatina volcanism and initial docking of the Precordillera to Gondwana (Fanning et al., 2004).

2.3. Western Newfoundland

More than 2500 m of Early Paleozoic strata exposed in the Humber Zone of Western Newfoundland (Figure 2.3B) record the development and demise of a long-lived passive margin (Stenzel and James, 1987; James et al., 1989). Early Cambrian rifting resulted in predominantly siliciclastic deposition that shifted to predominantly carbonate deposition by the late Cambrian. Strata of the Aguathuna Formation and Table Head Group represent carbonate platform deposition during marine transgression (James et al., 1989; Knight and Cawood, 1991) and rapid

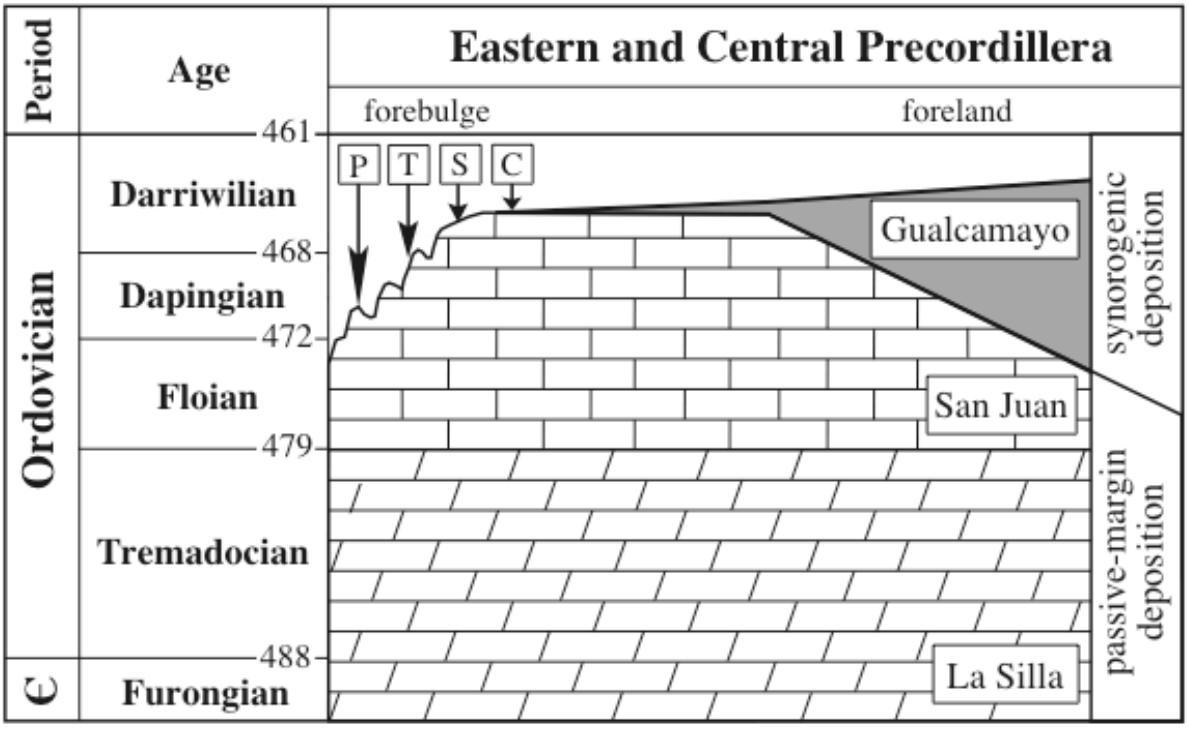

Figure 2.5. Time correlation of the Argentinian sections sampled for this study. The contact between the San Juan Formation and overlying Gualcamayo Formation is diachronous, as shown in the SW to NE directed section. Northward deepening reflects facies changes across the carbonate platform in response to higher rates of subsidence associated with tectonic convergence with Gondwana. P = Pachaco, T = Talacasto, S = Cerro La Silla, C = Cerro La Chilca.

drowning of the carbonate platform in the early stages of the Taconic orogeny (Stenzel et al., 1990).

2.3.1. Aguathuna Formation

The Aguathuna Formation represents the uppermost St. George Group and is generally reported to be approximately 70 meters thick. It is composed primarily of dolostone deposited in a shallow-water, restricted setting. The base of the Aguathuna Formation yields conodonts considered equivalent to the *P. fruticosus* zone (Williams et al., 1987) indicating a mid-Floian age (Figure 2.4). The upper Aguathuna Formation correlates with the *Orthidiella* brachiopod zone (Early Dapingian; Williams et al., 1987), suggesting the Floian-Dapingian boundary lies in the upper part of the Aguathuna Formation. For this study, the entire Aguathuna Formation (76 meters) was sampled at Table Point (50°22′22″ N, 57°31′44″ W; Figure 2.3B). Here, the Aguathuna Formation conformably overlies the Catoche Formation and is unconformably overlain by the Table Point Formation. At Table Point, the boundary between the Aguathuna Formation and overlying Table Head Group is marked by an abrupt change from coarsely-recrystalline, buff-colored dolomite to dark grey lime mudstone and wackestone.

2.3.2. Table Head Group

Table Head Group was also sampled at Table Point, where it comprises ~300 meters of bioturbated, fossiliferous wackestone and packstone. These deposits yield conodonts from the *H. tableheadensis* to *P. anserinus* zone that span the Dapingian to late Darriwilian (Figure 2.4; Stouge, 1982; Williams et al., 1987). At Table Point, the Table Head Group is divided into the Table Point, Table Cove, and Black Cove formations, which represent subtidal shelf deposition in increasingly deepening marine environments (Jacobi, 1981; Stouge, 1982; Knight and James, 1991). The Table Point Formation represents the lower 250 meters and consists of a homogeneous succession of subtidal, nodular limestone. The Table Point Formation is conformably overlain by the Table Cove Formation that consists, where sampled, of intercalated limestone and shale, with distinct intervals of slumping. Interbedded limestone and shale give

way upsection to predominantly black shale of the upper Table Cove and overlying Black Cove formations (Stenzel, 1990), which were not sampled for this study.

3. Methods

3.1. Petrographic screening

Prior to isotope and elemental analyses, samples were examined using standard petrographic and cathodoluminescence (CL) techniques (Hemming et al., 1989; Kaufman et al., 1991; Kah et al., 1999; Frank et al., 2003; Bartley et al, 2007) to evaluate secondary alteration that may affect the interpretation of geochemical profiles. Mirror-image slabs of samples were cut using a water-cooled rock saw and made into thin and thick sections for petrographic and CL analysis, respectively. Petrographic observations were used to characterize carbonate fabrics and to identify primary and secondary phases. Past studies have demonstrated that primary depositional phases, particularly micritic and fine-grained microsparitic fabrics, that show little evidence of secondary recrystallization, often preserve geochemical signatures that also show little evidence of overprinting by diagenetic fluids (Kaufman et al., 1991; Frank et al., 1997; Bartley et al., 2007). Similarly, coarsely recrystallized fabrics and secondary phases, such as spar-filled fractures and voids, commonly preserve a geochemical signal related to post-depositional fluid flow. Combined, such data permit careful evaluation of the range of geochemical signatures retrieved from samples and interpretation of the degree of diagenesis that samples have undergone.

Petrographic analyses show that, on the whole, both the Argentina and Newfoundland sections are comprised primarily of variably fossiliferous wackestone, packstone, and grainstone that contain abundant micritic and fine-grained microsparitic components (Figure 2.6). Petrographic fabrics of the Table Head Group are lithologically homogenous compared to the Argentina sections, which contain a variety of grainstone fabrics (La Silla and San Juan formations), and more poorly fossiliferous mudstone facies (La Silla Formation). A noted exception is the Aguathuna Formation, which contains patches of coarse-grained, euhedral, fabric-obliterative

Figure 2.6. Characteristic microfabrics of Ordovician strata, Argentina and Newfoundland. A) Peritidal facies of the La Silla Formation are dominated by peloidal and microbial intraclastic carbonate containing abundant fenestrae filled with equant calcite cements (FOV = 6.9 mm). B) Oolitic intraclastic grainstone of the La Silla Formation (FOV = 6.9 mm). C) Erosional surface in fossiliferous wackestone of the San Juan Formation, overlain by intraclastic grainstone (FOV = 6.9 mm). D) Micritic carbonate of the San Juan Formation showing abundant calcified microbial filaments (girvanella; FOV = 1.37 mm). E) Coarsely crystalline, fabric destructive dolomite of the Aguathuna Formation showing fractures modified by secondary dissolution (FOV = 2.74 mm). F) Finely-crystalline microspar within sparsely fossiliferous wackestone of the Table Head Group, showing minor shelter porosity and superb preservation of fossil microstructures (FOV = 6.9 mm).

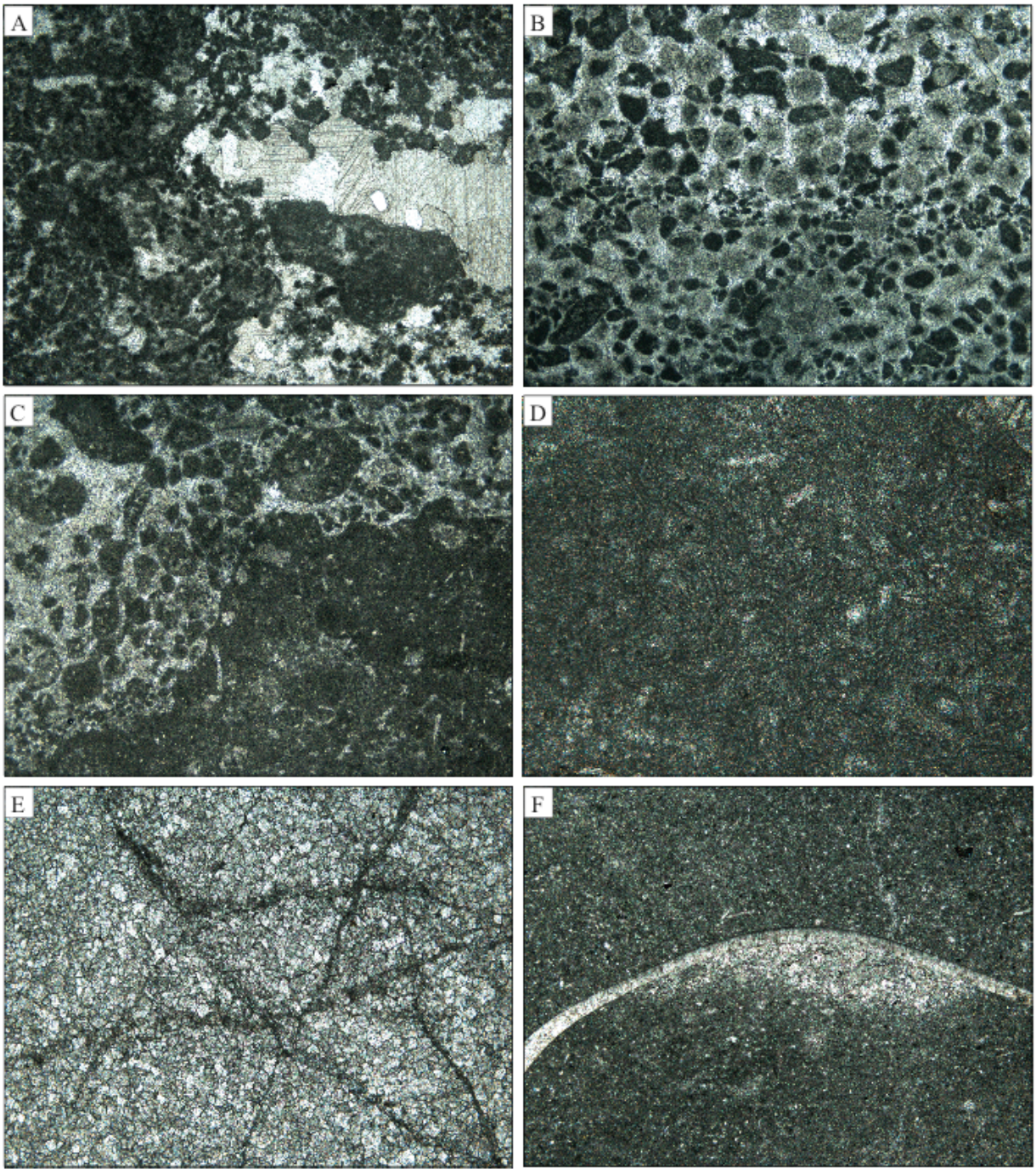
A
B
C
D
E
F

dolomite that indicates substantial potential for diagenetic overprinting of geochemical signals. Additionally, the La Silla Formation contains a number of primary depositional phases consisting of coarse, sparry cement (e.g., fenestrae with microbial laminates) that indicate early diagenetic interaction with meteoric fluids. Such fabrics are consistent with deposition in a shallow marine environment that is susceptible to periodic subaerial exposure, but also marks substantial potential for geochemical alteration.

In addition to standard petrographic analysis, cathodoluminescence petrography was used to diagnose the potential for alteration within primary and secondary phases. Luminescence in carbonate minerals is activated by the presence of Mn^{2+} in the carbonate lattice and suppressed by the presence of Fe^{2+} (Hemming et al., 1989). Because both Mn^{2+} and Fe^{2+} are incorporated in carbonates either during deposition from or dissolution and re-precipitation within diagenetic fluids, evidence for incorporation via CL analysis provides a quick measure of the degree of alteration (Brand and Veizer, 1980; Veizer, 1983; Banner, 1995). Caution must be taken, however, since previous studies have shown that CL need not accurately reflect the true extent of geochemical alteration (Rush and Chafetz, 1990; Marshall, 1992; Savard et al., 1995), and might also reflect primary incorporation of Mn or Fe from unusual marine fluids. All samples were examined under vacuum (50-80 mtorr) using a Luminoscope cathodoluminescence system at the University of Tennessee.

On the whole, CL analyses revealed dully luminescent, fine-grained limestones with local brightly luminescent, spar-filled fractures and voids. A noted difference between the Newfoundland and Argentina sections is the relative luminescence of fossil fragments. In the Argentina sections, fossil fragments tend to be more variable in both their microfabric preservation and their luminescence, whereas in the Newfoundland sections, fossil components tend to have better fabric preservation but more brightly luminescent than the matrix, suggesting the potential for either a greater degree of post-depositional recrystallization or primarily enhanced Mn incorporation. Additionally, the La Silla Formation is notably more dully luminescent than the other sections.

After petrographic evaluation, selected regions of polished thick sections were micro-sampled using 0.5 mm dental drill bits attached to a micro-drill press. Petrographically uniform phases were drilled to retrieve 2-5 mg of powder to be used as splits for the C- and O-isotope and elemental analyses. When possible, a range of fabrics was sampled in order to compare the geochemical properties of both primary and secondary phases.

3.2. Major and trace element analyses

Micro-drilled carbonate phases were analyzed for major (Ca, Mg) and trace (Sr, Mn, Fe) element concentration. Approximately 1 mg of microdrilled powder was dissolved in 10 mL of trace metal grade 2% HNO_3, agitated, then left overnight to assure complete dissolution. To remove any insoluble material that might clog intake tubing during analysis, each sample was centrifuged for 10 minutes at 3000 rpm and the top ~9 mL decanted into a clean centrifuge tube. Centrifuging was repeated as often as necessary to ensure removal of visible insoluble material. Elemental analyses for the San Juan Formation and Table Head Group were conducted at the University of West Georgia using a Perkin-Elmer inductively coupled plasma-optical emission spectrometer (ICP-OES) fitted with a Meinhardt concentric nebulizer calibrated to a series of gravimetric standards. Elemental analyses of the La Silla Formation were completed at the University of Tennessee, Knoxville using a Perkin-Elmer Optima 2100 DV ICP-OES with a Scott spray chamber. All analyses were calibrated using a series of gravimetric standards that were run before and after every six unknowns. Analyses were determined to be reproducible to within ±10% by analysis of standards and duplicate samples.

3.3. Total organic carbon concentration

Total organic carbon concentration was determined using a UIC, Inc carbon dioxide coulometer with a combustion apparatus at the University of Tennessee. Five grams of whole-rock powder were acidified overnight using 10% HCl to dissolve carbonate components. Samples were then rinsed with at least 1 L of Milli-Q water until filtrate reached a pH > 6 to ensure removal of chlorine. Insoluble residues were dried for 24-48 hours at 30°C, then hand-ground to a fine

powder. 150-200 mg was then loaded into pre-cleaned and dried porcelain boats. Each sample was combusted between 900 and 1000ºC for 11 minutes to ensure complete combustion. CO_2 resulting from combustion was then measured via coulometric titration. Analytical error was <0.1%, based upon duplicate sample and calcite standard analyses.

3.4. Carbon and oxygen isotope analyses

Approximately 1.0 to 1.5 mg of powder from microdrilled carbonate phases were loaded into silver caps, reacted with anhydrous phosphoric acid at a reaction temperature of 120°C, and cryogenically distilled using a Carbo-Flo automated sampler attached to a dual-inlet Finnigan MAT Delta Plus gas source isotope ratio mass spectrometer at the University of Tennessee. Data are reported in delta notation as per mil (‰) deviations from Vienna Pee Dee Belemnite (VPDB). Analyses were determined to be reproducible to within ±0.1‰ from analysis of duplicate and internal lab standards. Two internal standards were used for isotope calibration, Chihuahua calcite (CHCC; $\delta^{13}C$ = +1.35‰, $\delta^{18}O$ = –6.16‰ at 25°C) was used for analyses of the Table Head Group and San Juan Formation, and Australian National University "M1" (ANU-M1: $\delta^{13}C$ = -10.66‰, $\delta^{18}O$ = -9.23‰ at 25°C) was used for analyses on La Silla and Aguathuna formation samples.

3.5. Sulfur extraction and isotope analyses

$\delta^{34}S_{SO4}$ profiles were constructed using carbonate-associated sulfate (CAS). CAS substitutes into the carbonate lattice during initial carbonate precipitation and is regarded as a reliable proxy for marine sulfate $\delta^{34}S$ (Burdett et al., 1989; Strauss, 1999). For instance, in the modern ocean, the isotopic composition of CAS ($\delta^{34}S_{CAS}$) of brachiopod shells (+21.2±0.8‰) is analytically indistinguishable from mean ocean $\delta^{34}S_{SO4}$ (+20.9±0.5‰; Kampschulte et al., 2001). In ancient sediments, CAS has been demonstrated to be isotopically similar to coeval evaporite deposits (Burdett et al., 1989; Strauss, 1997; Kah et al., 2001). Additionally, $\delta^{34}S_{SO4}$ has been shown to be resistant to diagenetic alteration and retain a record of primary $\delta^{34}S_{SO4}$ despite large decreases in sulfate concentration during diagenetic recrystallization (Lyons et al., 2004; Gill et al., 2008).

CAS was extracted using acid dissolution and barite precipitation methods modified from Burdett et al. (1989), Kah et al. (2001), and Hurtgen et al. (2002). Approximately 200 grams of bulk rock was first etched with 10% HCl to remove surface weathering products, then crushed and powdered. Approximately 100 grams of powdered sample was soaked overnight in 250 mL of 5.65-6% laboratory grade sodium hypochlorite (NaOCl), rinsed four times with Milli-Q water (typically 1.0-1.5 L), and filtered. An initial NaOCl leach is necessary to remove soluble iron sulfide and organically bound sulfur that might oxidize to sulfate during acidification (Burdett et al., 1989) and was completed although the potential for organically-bound sulfur is low in ancient samples. Geologically ancient samples typically have low concentration (here <0.6 wt%) of preserved organic carbon concentration is low, and the organic material is dominantly kerogen, which suggests that most labile organic components containing organically bound sulfur have long since degraded.

Approximately 50-100 g of dried and weighed sample were dissolved slowly with up to 600 mL of 3N hydrochloric acid. Dissolution was monitored to maintain a pH >3 to prevent the exchange of oxygen between sulfate and water and to minimize pyrite oxidation (Chiba and Sakai, 1985). Samples were then filtered to remove insoluble and undissolved residue. The filtrate was then brought to a pH of 9 using sodium hydroxide (NaOH) pellets to precipitate any dissolved iron oxides, and filtered. Approximately 140 mL of saturated barium chloride solution (250 g/L) was added to the filtrate to recover CAS as barium sulfate. The reaction was allowed to continue overnight at room temperature to ensure complete precipitation. Barium sulfate precipitate was then filtered using 0.45 μm Millipore filters, dried at 30°C, and weighed. Sulfate concentration was estimated from weight measurements of barium sulfate precipitate from extraction.

For S-isotope analyses, 1.5-2.0 μg of $BaSO_4$ was weighed into tin cups along with excess V_2O_5 (~10x weight to ensure complete combustion). Samples were analyzed for $\delta^{34}S$ using a Finnigan MAT 252 gas source mass spectrometer fitted with an elemental analyzer at Indiana University. S-isotope composition is expressed as per mil (‰) deviation from Vienna Canyon Diablo Troilite (VCDT). Analytical precision was determined to be ±1‰ by analysis of four lab standards, ERE Ag_2S (-4.7‰), EMR Cp (+0.9‰), NBS 127 (+20.3‰), and PQB (+39.8‰).

4. Results and interpretation

Geochemical results are presented in Tables 2.1 - 2.6 and presented in Figures 2.7, 2.8, and 2.9.

4.1. Geochemical signals of alteration

It is important to constrain the degree to which carbonate rocks have been altered to establish whether geochemical trends are likely to be representative of syndepositional oceanic values (Given and Lohmann, 1985; Zempolich et al., 1988; Carpenter et al., 1991; Frank and Lohmann, 1996; Kah, 2000). Primary depositional fluids, whether at the seafloor or of meteoric origin can result in the production of sedimentary grains and the precipitation of primary cement phases. Primary depositional components, such as skeletal grains, micrite, and marine cements, have the potential to retain signatures of these depositional fluids. However, all secondary fluids—from the seafloor, to early diagenetic influx of meteoric fluids, to deep-burial fluids, to fluids involved in modern weathering— also have the potential to result in dissolution and recrystallization of carbonate phases. Of these, only stabilization of carbonate phases by syndepositional marine fluids may result in recrystallization at high water:rock ratios that may still preserve marine geochemical signals. In all other cases, preservation of marine signals will reflect the relative composition of water and rock and the degree of water:rock interaction (Banner and Hanson, 1990).

Relative to marine carbonate rocks, meteoric fluids typically have low Sr concentration and more depleted $\delta^{18}O$ and $\delta^{13}C$ isotope compositions. Similarly, anoxic fluids may contain substantially higher concentrations of redox-sensitive divalent ions, such as Mn and Fe, as well (Brand and Veizer, 1980; Banner and Hanson, 1990). Numerous studies have shown that, because of the low carbon content of most diagenetic fluids, $\delta^{18}O$, Sr, Mn and Fe are much more sensitive indicators of post depositional alteration, especially at low water to rock ratios. Alteration of $\delta^{13}C$, however, can occur during diagenesis if fluids contain large amounts of dissolved inorganic carbon from the remineralization of organic carbon (Brand and Veizer, 1980; Banner and Hanson, 1990; Derry, 2010). To help constrain the degree of alteration and the potential for

Figure 2.7. Isotopic and elemental data from Ordovician marine carbonates. A) A cross plot of C- and O-isotope values show no covariance and little indication of alteration of C-isotope values by postdepostional alteration. B) A cross plot of S- and O-isotope shows distinct separation of S-isotopic composition for different units, suggesting postdepositional alteration has not overprinted S-isotope compositions. C) Across the range of preserved O-isotope compositions, Sr typically falls between 150 and 500 ppm, which is consistent with well-preserved marine limestone. Sr concentrations < 50 ppm in the Aguathuna Formation likely represent substantial interaction with late stage, low Sr fluids, which is consistent with petrographic indicators for alteration. D) Similarly, Mn/Sr fall largely below 1.5, which is often considered an acceptable values for little altered carbonate rocks. Elevated Mn/Sr occurs predominantly in the Aguathuna Formation, which shows strong petrographic indication of secondary recrystallization. Several samples with anomalously high Mn concentration occur in the Cerro La Chilca section. These fall near the boundary between the San Juan and overlying Gualcamayo Formation suggesting the potential for fluid interaction confined to this lithologic transition. C = Cerro La Chilca, T = Talacasto, S = Cerro La Silla.

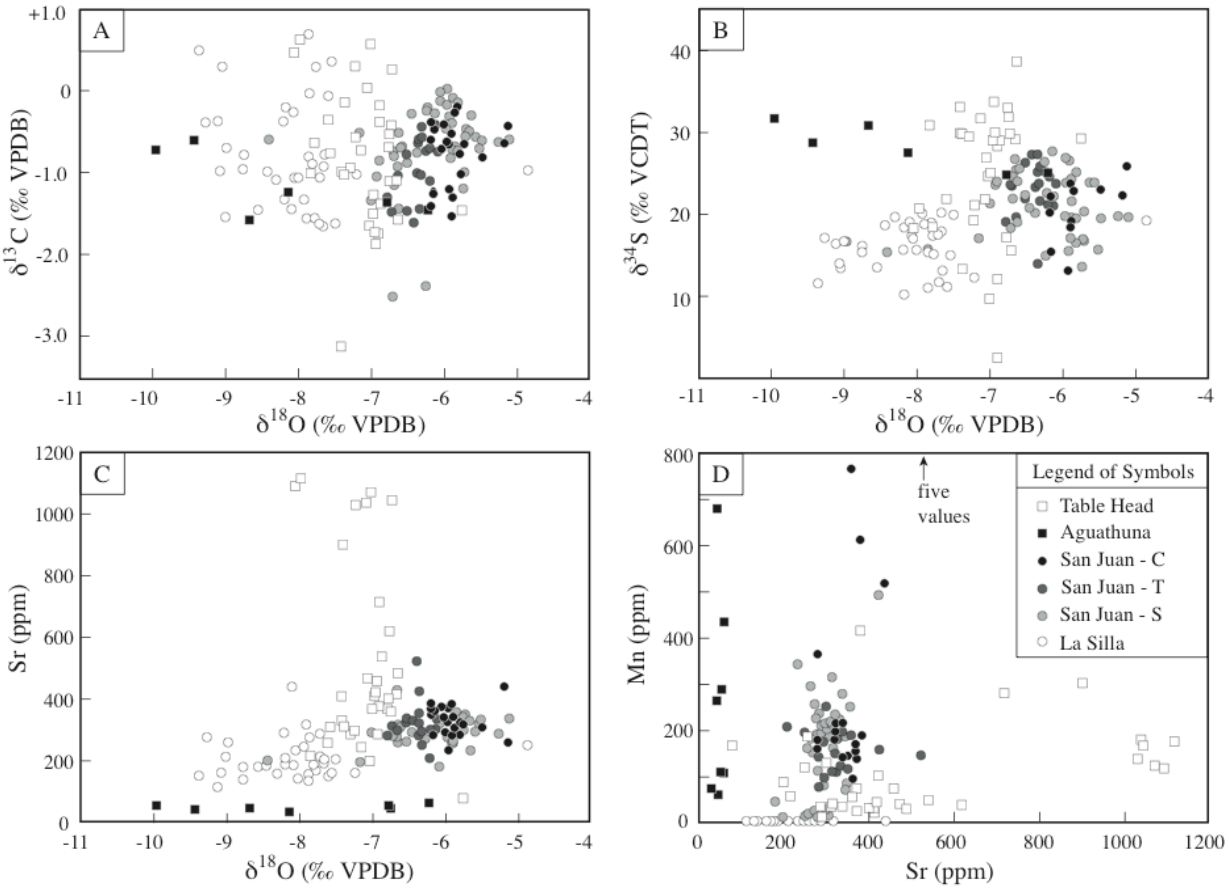
A
B
C
D
δ13C (‰ VPDB)
δ34S (‰ VCDT)
δ18O (‰ VPDB)
Sr (ppm)
Mn (ppm)
five values
Legend of Symbols
Table Head
Aguathuna
San Juan - C
San Juan - T
San Juan - S
La Silla

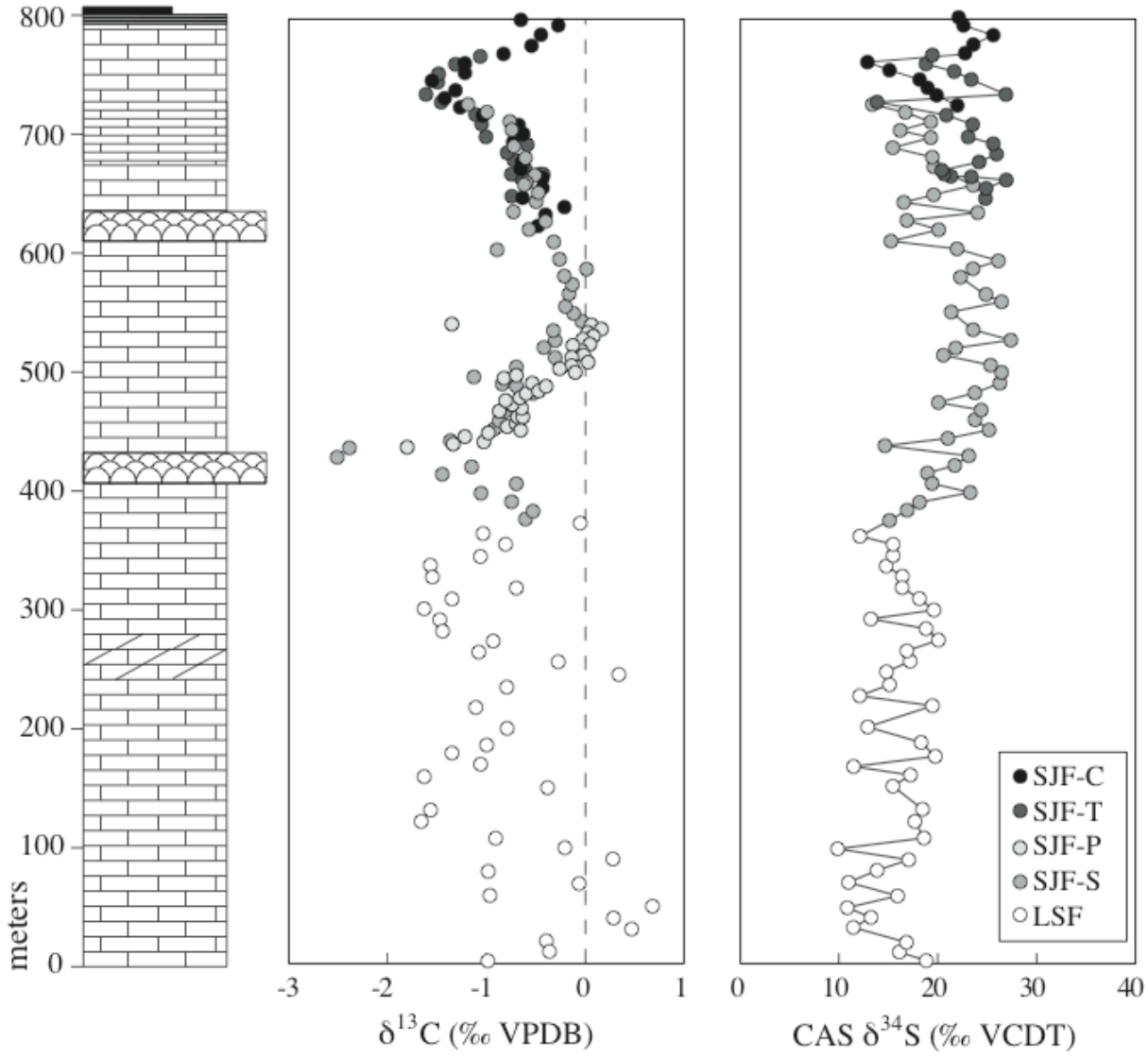

Figure 2.8. Carbon and sulfur isotope records from the Argentine Precordillera. Chemostratigraphic profiles show coherent carbon isotope trends through the San Juan Formation, although the underlying La Silla Formation records more stratigraphic variability. Sulfur isotopes show relatively stable long-term stratigraphic trends overprinted by a clear, short-term isotopic signal. Measured sections were correlated using a combination of biostratigraphic and carbon isotope data. SJF = San Juan Formation, LSF = La Silla Formation, C = Cerro La Silla, T = Talacasto, P = Pachaco, S = Cerro La Silla.

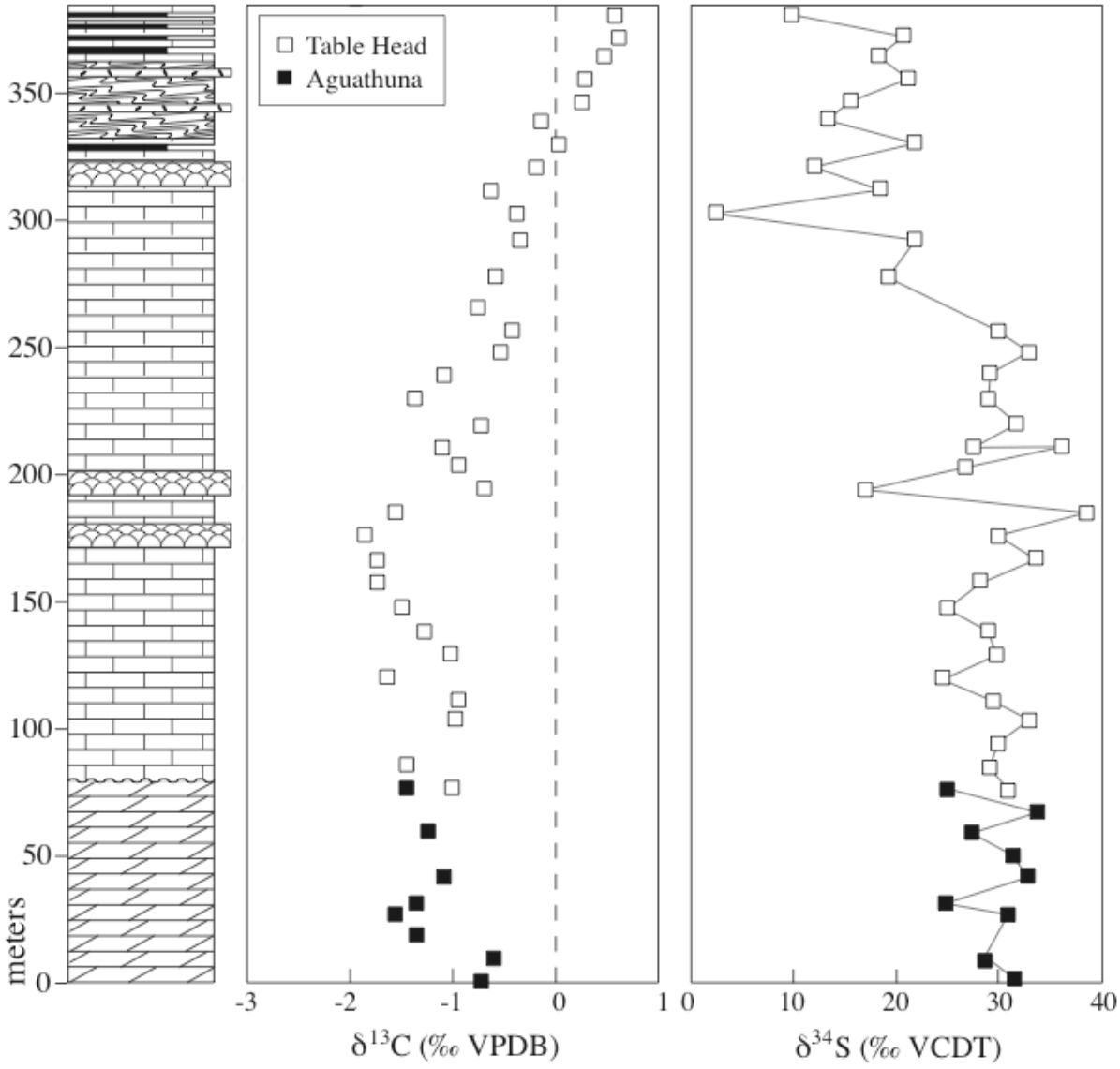

Figure 2.9. Carbon and sulfur isotope records from Western Newfoundland. Strata from Newfoundland show patterns similar to those recorded in the Argentinian sections. Carbon isotopes show relatively stable isotopic compositions and sulfur isotopes are characterized by clear, short-term isotopic variation. Despite petrographic evidence of fabric-obliterative dolomite and low Sr values in the Aguathuna Formation, carbon and sulfur values are not drastically different than the well-preserved Table Head Group, Western Newfoundland.

preservation of C- and S-isotope trends, we compared petrographic characteristics (optical and cathodoluminescence) to geochemical (Mn, Sr, $\delta^{13}C$ and $\delta^{18}O$ and $\delta^{34}S$) characteristics.

4.1.1. $\delta^{18}O$ and trace element data

The majority of $\delta^{18}O$ values of primary depositional phases fall between -9 and -5‰ (Figure 2.6A). $\delta^{18}O$ values from the La Silla and Aguathuna Formations broadly overlap and represent the most depleted isotopic values (-10 to -7‰), whereas the San Juan Formation preserved the least depleted isotopic values (-7 to -5‰). O-isotope values from the Table Head Group are intermediate and fall within a relatively narrow range (-8 to -6.5‰). Most of these values fall within the range of data from other well-preserved, non-evaporative carbonate units in the Paleozoic (-9 to -5‰) (Wadleigh and Veizer, 1992; Qing and Veizer, 1994; Veizer et al., 1999). Since O-isotopes are easily exchanged during diagenesis, $\delta^{18}O$ values more positive than -9‰ in depositional phases that show little petrographic evidence of recrystallization are generally interpreted to represent minimal water-rock interaction (Banner and Hanson, 1990; Wadleigh and Veizer, 1992; Qing and Veizer, 1994). Extensive dolomitization and the occurrence of the isotopically lightest $\delta^{18}O$ values in the Aguathuna Formation, however, suggests a higher degree of water-rock interaction. Similarly, $\delta^{18}O$ depleted values in the La Silla Formation likely reflect observed contributions from and interaction with meteoric fluids.

More positive isotopic values in the San Juan Formation suggest this section may represent a lesser degree of post-depositional alteration or higher degree of evaporation of primary marine fluids, although the presence of open ocean facies does not support this interpretation. Another possibility is that generally more positive values in the San Juan Formation preserve secular change in the isotopic composition of marine $\delta^{18}O$, such as that inferred from previous studies of Ordovician brachiopods, which show $\delta^{18}O$ values generally increasing through the Ordovician (Wadleigh and Veizer, 1992; Qing and Veizer, 1994; Veizer et al., 1999). O-isotope values in those studies are derived from brachiopod shells that meet stringent criteria for quality of preservation (well-preserved microfabrics, high Sr and Na and low Mn and Fe concentrations; Banner and Hanson, 1990). Additional evidence for diagenetic alteration of $\delta^{18}O$ variation are

refuted since variation is observed in geologically disparate basins and because these samples also preserve other, globally correlative isotopic trends ($^{87}Sr/^{86}Sr$, $\delta^{13}C$). Mechanisms driving $\delta^{18}O$ variation, however, are still under debate. Sea surface temperature, extent of glacial ice and high-temperature interaction with ocean crust have all been considered as potential mechanisms of $\delta^{18}O$ variation (Wadleigh and Veizer, 1992; Qing and Veizer, 1994; Veizer et al., 1999). Based on petrographic and CL analyses, we consider $\delta^{18}O$ values between -5.5‰ and -7.5‰ are consistent with marine rocks that have undergone minimal post-depositional alteration.

Mn and Sr concentrations also provide insight into the degree of post-depositional fluid interaction since they are exchanged readily in the presence of secondary fluids (Banner and Hanson, 1990). Sr concentrations fall primarily between 200-1200 ppm (Figure 2.6, C and D), which are typical for marine calcites that have undergone limited exchange with post-depositional fluids (Banner and Hanson, 1990). The highest Sr concentrations occur in the Table Head Group and San Juan Formation, which support O-isotope and petrographic evidence for limited exchange with post-depositional fluids. Notably, Sr concentrations within the Aguathuna Formation fall well below 200 ppm, consistent with petrographic evidence for post-depositional fluid interaction. Sr concentration also fall below 200 ppm in the La Silla Formation, potentially reflects some interaction with meteoric fluids. The low Sr concentration in the La Silla Formation is also consistent with isotopically light O-isotope values that were observed petrographically, and provide evidence for early interaction with meteoric fluids, although the observed $\delta^{18}O$ values still primarily fall within the range of accepted values for well-preserved carbonate rocks.

Mn concentrations of all formations fall predominantly below 400 ppm, with all but five values falling below 800 ppm (four from the Cerro La Chilca section of the San Juan Formation, one and one from the Pachaco section) (Figure 2.6D). An Mn concentration below 400 ppm is consistent, as well, with an interpretation of relatively limited water-rock interaction (Banner and Hanson, 1990). The one value that is >800 ppm in the Pachaco section occurs at the top of the section, where it is associated with a major subaerial exposure surface that marks a significant depositional hiatus between the Middle Ordovician San Juan Formation and overlying Silurian

strata (Astini et al., 1995). This sample also yields anomalously low $\delta^{18}O$ values, supporting an interpretation that elevated Mn concentration is a result of alteration along this boundary. Similarly, all Mn values that are >400 ppm in the Cerro La Chilca section occur in the upper 55 meters of the section indicating the potential for stratigraphic control. In this case, however, there is no indication of subaerial exposure. Rather, elevated Mn concentrations coincide with marine transgression and potential interaction with reduced, Mn-rich fluids. These observations suggest potential transgression of high Mn, low O_2 waters, which can facilitate the deposition of Mn in marine sediments (Grill, 1978; Davison, 1982) and may explain elevated Mn concentration in the upper San Juan Formation at the Cerro La Chilca section. Extraordinarily low Mn in the La Silla Formation (Mn concentrations <50 ppm) along with the presence of meteoric cements suggests precipitation from oxic, low Mn fluids. Early diagenetic interaction with oxic, meteoric fluids may also account for some of the scatter in $\delta^{13}C$ in the La Silla Formation (Figures 2.7A and 2.8), because such fluids would also be expected to oxidize depositional organic matter and provide variable $\delta^{13}C$ for incorporation into early diagenetic phases. By contrast, the large range of Mn concentrations in the Aguathuna Formation, along with low Sr and petrographic evidence for replacive dolotimization, suggest this interval has experienced substantially greater post-depositional alteration. Despite evidence for at least some interaction with post-depositional fluids, in no case is there clear evidence that interaction with post-depositional fluids proceeded to such a degree as to strongly affect the C-isotope values of the samples.

4.1.2. $\delta^{34}S_{CAS}$ signal

Although we concluded that carbonate rocks sampled in this study have undergone only limited water-rock interaction and therefore are likely to preserve reliable records of marine $\delta^{13}C$, we also need to consider whether $\delta^{34}S_{CAS}$ is likely to preserve a reliable record of marine $\delta^{34}S$. A cross plot of $\delta^{34}S_{CAS}$ and $\delta^{18}O$ shows no clear trends in any of the studied sections (Figure 2.7B). In particular, the Table Head Group, which represents an interval where $\delta^{34}S_{CAS}$ shows dramatic stratigraphic variability, reveals a large range in $\delta^{34}S_{CAS}$ over a only about a 1.5‰ range in $\delta^{18}O$, suggesting that variation in $\delta^{34}S_{CAS}$ is not related to post-depositional alteration of the host carbonate. Similarly, although the La Silla and San Juan formations show a broader range in

$\delta^{18}O$, there is no clear correlation with $\delta^{34}S_{CAS}$ that might suggest covariance resulting from post-depositional alteration. Additionally, diagenetic fluids have substantial oxygen, whereas only scant amounts of sulfate are expected in early Paleozoic fluids since oxygen levels were likely low. Because of this relative imbalance between O_2 and SO_4 concentration in diagenetic fluids, $\delta^{18}O$ should alter much more quickly that $\delta^{34}S_{CAS}$ (Banner and Hanson, 1990). These interpretations are consistent with other studies (Burdett et al., 1989; Kampschulte et al., 2001; Lyons et al., 2004; Gill et al., 2007), which suggest that CAS faithfully records marine $\delta^{34}S$ in samples of minor to moderate diagenetic recrystallization.

5.2 Interpretation of C- and S-isotope profiles

5.2.1. Global stability of the Middle Ordovician C-isotope record

$\delta^{13}C$ values from all sections overlap in range (between -1.5 and +0.5‰) and show no clear covariance with $\delta^{18}O$ or other common indicators of diagenetic alteration. A further test of the preservation of marine $\delta^{13}C$ is provided by comparison with coeval C-isotope records. C-isotope records from the Argentine Precordillera (Figure 2.8) and Western Newfoundland (Figure 2.9) reveal a clear and coherent signal with correlative excursions. C-isotope values average -1‰ in the latest Cambrian through the Early Ordovician (Tremadocian), drop briefly to values near -2.5‰ in the early Floian, before returning to near zero values by the late Floian (Figure 2.10). Isotopic compositions drop again to near -1.5‰ in the Dapingian, and then increase through the Darriwilian to values near 0.5‰. C-isotope data in this study are consistent with data from published curves for Early and Middle Ordovician marine carbonate rocks worldwide (Wadleigh and Veizer, 1992; Qing and Veizer, 1994; Ainsaar et al., 1999; Buggisch et al., 2003; Saltzman, 2005; Saltzman and Young, 2005; Bergström et al., 2008; Kah et al., *in prep*). The one exception to this coherence is at the very top of the Pachaco section, where a single sample near -1.5‰ is substantially more depleted than the underlying C-isotope values in the Pachaco section and values recorded in the coeval Cerro La Silla section. The occurrence of high Mn, low $\delta^{18}O$ and $\delta^{13}C$ in this sample likely represents meteoric alteration of $\delta^{13}C$ values as would be expected in

Figure 2.10. Composite carbon and sulfur isotope records from the Early to Middle Ordovician. Section were correlated using a combination of previously published biostratigraphic data and matched with carbon isotope data from this study. Heterogeneity in recorded sulfur isotope data, here apparent in the uppermost Floian and Dapingian, is interpreted to reflect true heterogeneity in a low sulfate marine system. Despite regional heterogeneity, all sections are marked by a short-term ($< 10^6$ yr) oscillation in the isotopic composition of marine sulfate. International stage names and time slices are from Bergström et al. (2008) and Walker and Geissman (2009). The age of the base of the section (here at the base of the La Silla Formation) is estimated based on a combination of biostratigraphic constraints, ages of stage boundaries, and an assumption of constant sedimentation rate for the individual sections.

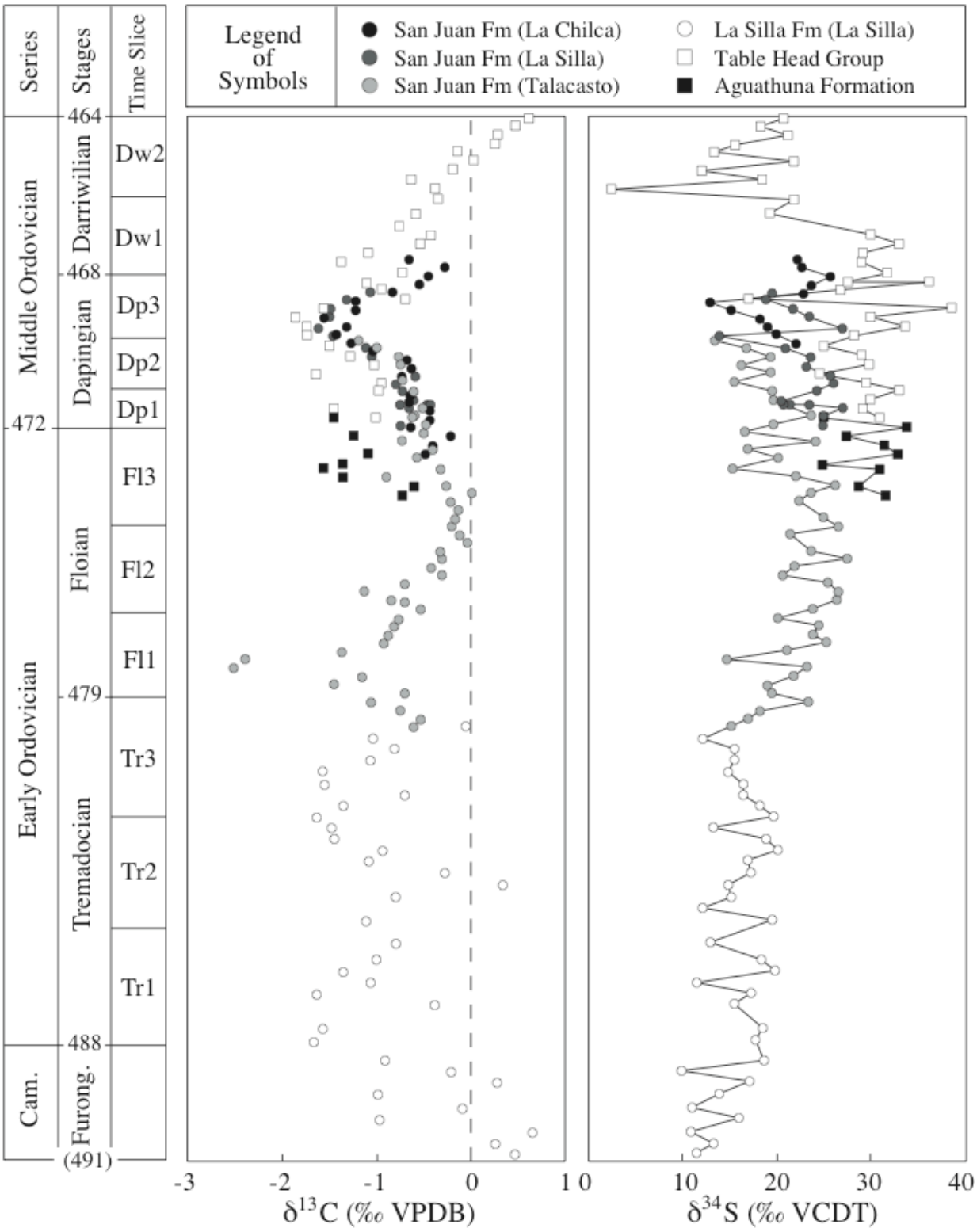
Series
Stages
Time Slice
Middle Ordovician
Early Ordovician
Cam.
Darriwilian
Dapingian
Floian
Tremadocian
Furong.
464
468
472
479
488
(491)
Dw2
Dw1
Dp3
Dp2
Dp1
Fl3
Fl2
Fl1
Tr3
Tr2
Tr1
Legend of Symbols
San Juan Fm (La Chilca)
San Juan Fm (La Silla)
San Juan Fm (Talacasto)
La Silla Fm (La Silla)
Table Head Group
Aguathuna Formation
-3
-2
-1
0
1
0
10
20
30
40
δ13C (‰ VPDB)
δ34S (‰ VCDT)

subaerial exposure and interaction with meteoric fluids, which produce ^{12}C-enriched limestone (e.g., Allan and Matthews, 1982).

C-isotope profiles from the La Silla, San Juan and Table Head formations (Figures 2.8, 2.9, and 2.10) record limited isotopic variation (< 3‰), in striking contrast to either the Late Cambrian (Steptoean) SPICE excursion (Ripperdan et al., 1992; Braiser, 1993; Glumac and Walker, 1998; Saltzman et al., 1998) or Late Ordovician excursions (GICE, HICE; Kump et al., 1999; Saltzman and Young, 2005; Young et al., 2005) (cf., Figure 2.1). Limited variation in marine $\delta^{13}C$ values during global greenhouse intervals has been attributed to nitrogen-limitation of organic productivity (Saltzman, 2005) or the combination of high DIC values (Berner, 1998; Bartley and Kah, 2004) and the coupling of organic and inorganic $\delta^{13}C$ in widespread epeiric seas (Ridgwell, 2003; Bartley and Kah, 2004). Our data is consistent with relatively stable marine $\delta^{13}C$ values, although confirming the specific mechanisms maintaining this stability is outside the scope of this study.

5.2.2. Sectional heterogeneity in $\delta^{34}S$

Comparison of $\delta^{34}S$ values shows clear heterogeneity both between the Argentina and Newfoundland sections and locally within the Argentine Precordillera (Figures 2.8, 2.9, and 2.10). In coeval (Dapingian) intervals of the San Juan Formation, the isotopic composition of CAS in the Talacasto section is typically enriched in ^{34}S, with $\delta^{34}S$ values 4.5‰ more positive than the Cerro La Silla section (Figure 2.10). Similarly, $\delta^{34}S$ values from the Table Head Group are 10‰ heavier than the Cerro La Silla section of the San Juan Formation and 6.6‰ heavier than the Talacasto section. Furthermore, comparison of $\delta^{34}S$ of the Tremadocian Gasconade Formation (Gill et al., 2007) to $\delta^{34}S$ profiles presented here shows that La Silla Formation $\delta^{34}S$ values are 10‰ more negative relative to the Gasconade Formation. Combined, these data suggest the potential for substantial regional heterogeneity in marine sulfur isotope composition.

Heterogeneity in isotopic composition between the different stratigraphic sections could plausibly arise from non-conservative isotopic behavior under conditions of low marine sulfate

concentration or potentially from vertical variation in $\delta^{34}S$ that results from chemical stratification of the water column. Variation in $\delta^{34}S_{SO4}$ with depth in the water column has been documented in the modern day Black Sea (Vinogradov et al., 1962; Sweeney and Kaplan, 1980; Calvert et al., 1996; Lyons, 1997). In the Black Sea, the isotopic composition of deep-water sulfate is 1.5-2‰ more positive than surface water sulfate, due to high rates of bacterial sulfate reduction in deeper anoxic waters (Sweeney and Kaplan, 1980). The ^{34}S-depleted values CAS of the San Juan Formation relative to deeper water deposits of the Table Head Group potentially result from proximity of these deeper water deposits to anoxic fluids and water-column BSR. $\delta^{34}S$ values from the Table Head Group, however, are more depleted in the deeper water Table Cove Formation, suggesting $\delta^{34}S$ stratification is not the primary cause of spatial heterogeneity, and that heterogeneity more likely derives from the simple non-conservative behavior of $\delta^{34}S$ in a low-sulfate ocean. Numerous studies of fluid inclusions in marine evaporites (Lowenstein et al., 2001; Horita et al., 2002; Lowenstein et al., 2003; Brennan et al., 2004) suggest Early Paleozoic marine sulfate concentration may have been only 2-12 mM (or <50% of modern marine sulfate concentrations; 28mM, Bottrell and Newton, 2006), and isotopic heterogeneity appears to be a hallmark of these low-sulfate oceans (Gill et al., 2011).

5.2.3. Instability of the Middle Ordovician S-isotope record

Despite spatial heterogeneity, all sections show a strikingly similar stratigraphic pattern in marine $\delta^{34}S$. In sharp contrast to the marine C-isotope record, marine S-isotopes record repeated short-term oscillation superimposed over more subtle, longer-term trends. The duration of $\delta^{34}S$ these two scales of isotopic variation is estimated using a combination of biostratigraphic constraints and an assumption of constant sedimentation rate for each of the individual sections. From the latest Cambrian (here estimated to be the upper 3 Ma of the Furongian) through the Early Ordovician (Tremadocian), average S-isotope composition shows little long-term variation (Figure 2.10). In the Cerro La Silla section of the San Juan Formation, $\delta^{34}S$ values increase from approximately +16‰ to +22‰ through the Floian, then decrease to approximately +18‰ through the Dapingian (Figure 2.10). The Cerro La Chilca section of the San Juan formation shows the same trend, although these values are offset by about +2‰ (Figure 2.10). The Table

Head Group shows similarly elevated $\delta^{34}S$ in Dapingian and early Darriwilian, but then records a dramatic shift from +30‰ to near +15‰ in the mid-Darriwilian (Thompson et al., *in review*). Combined, these observations suggest broad, long-term stability of marine sulfur isotope composition, with potential variation of 6-15‰ over time spans of 0.5 Myr.

Despite long periods of time that show no apparent change in the average sulfate isotope composition of the marine system, regular, short-term oscillation of $\delta^{34}S_{CAS}$ appears to be characteristic of the Lower to Middle Ordovician, and shows striking similarity in duration and magnitude (average 7‰ excursion over 0.9 Myr) through all of the measured sections. Because oscillation in $\delta^{34}S_{CAS}$ occurs in all sections, is commonly defined by multiple data points, and does not appear to be directly related to either depositional environment or changes in lithology within the different sections, we suggest that observed short-term change in the isotopic composition of marine systems represents a true oceanographic signal with a driving mechanism that occurs on at least a basin-wide scale.

6. Discussion

6.1. Marine depositional environments of the Ordovician

The Early to Middle Ordovician represents a global greenhouse interval (Frakes et al., 1992) when high sea level (Hallam, 1992; Miller et al., 2005; Haq and Schutter, 2008) and extensive epeiric seas promoted widespread carbonate platform deposition (Algeo and Seslavinsky, 1995; Pratt and Holmden, 2008). Elevated pCO_2 associated with greenhouse, or potentially supergreenhouse, conditions (Berner, 1994; Brenchley, 1994) resulted in elevated sea surface temperatures (Trotter et al., 2008; Finnegan et al., 2011) and potentially sluggish ocean circulation (Brenchley et al., 1995; Saltzman, 2005). Deep-water anoxia is often attributed to organic matter production in global greenhouse climate conditions, either through sluggish ocean circulation or the decreased O_2 solubility of warm water, or both (Sarmiento et al., 1988; Meyer and Kump, 2008). Decreased deep-ocean ventilation, in turn, may result in the effective

decoupling of surface and deep-ocean waters as has been suggested for Late Paleozoic ocean anoxic events (Meyer and Kump, 2008).

Under these conditions hydrogen sulfide (HS^-) can build up in the water column via bacterial sulfate reduction, wherein photosynthetically produced organic matter provides a carbon source for bacterial sulfate reduction (BSR), which in turn reduces oceanic sulfate to produce hydrogen sulfide (Garrels and Lerman, 1981; Berner et al., 1985). Under well-oxygenated marine conditions, BSR is restricted to the sediment-column and >90% of HS^- produced by BSR is immediately reoxidized to sulfate or intermediate sulfur species (Jørgensen et al., 1990), with remaining HS^- available to react with Fe^{2+} to form pyrite (Berner et al., 1985). Under anoxic marine conditions, reoxidation of bacterially reduced HS^- is likely to be substantially less, and euxinic conditions arise when Fe^{2+} availability is insufficient to strip the water column of bacterially produced HS^- (Rozanov et al., 1974).

6.2. Biogeochemical cycling of carbon and sulfur

Isotopic composition of marine dissolved inorganic carbon (DIC) and sulfate are a function of the magnitude and isotopic composition of carbon and sulfur fluxes into and out from the marine system. The primary sources of marine DIC are the input of crustal carbon from metamorphic, volcanic outgassing and the weathering of marine carbonates, air-water gas exchange and associated organic matter (Kump and Arthur, 1999). Marine DIC is removed via photosynthetic organic carbon production and subsequent burial, and through marine carbonate deposition. Similarly, sources of marine sulfate include oxidative weathering of crustal sulfides (Berner, 1987), dissolution of evaporite minerals (Holser et al., 1988), and oxidation of volcanogenic sulfur species (Bischoff and Dickson, 1975; Seyfried and Bischoff, 1979; Alt, 1995). Sinks include burial of S-bearing phases such as bacterially mediated sedimentary sulfides (Berner and Raiswell, 1983; Berner, 1984; Kump; 1989), precipitation of sulfur-bearing evaporite minerals in the shallow oceans (Holser, 1966) and at mid-ocean ridge hydrothermal circulation systems (Edmond et al., 1979), and sulfate substitution into the marine carbonate lattice (Takano et al., 1985; Kitano et al., 1985). Evaporite precipitation and dissolution (Ault and Kulp, 1959; Thode

et al., 1961; Holser and Kaplan, 1966; Raab and Spiro, 1991), volcanogenic sulfur fluxes (Petsch, 1999), and trace sulfate account for only a small amount of the total fluxes of marine sulfate. Furthermore, they do not impart substantial isotopic fractionation and are thus not typically considered as drivers of variation of marine sulfate isotopic composition. Instead, riverine delivery of oxidatively weathered sulfide is considered the primary input of marine sulfate, whereas the burial of bacterially-mediated sulfide is considered the primary export (Garrels and Lerman, 1984; Berner and Petsch, 1998; Berner, 2001).

The isotopic composition of carbon input into the oceans is variable, with metamorphic and volcanic outgassing typically -5%, weathering of marine carbonates near 0‰, and weathering of organic carbon near -22‰ (Kump and Arthur, 1999), but ultimately approximates the crustal value of -5‰ (Garrels and Lerman, 1984). Marine DIC is then removed from the oceanic system via the autotrophic production of organic matter, which typically imparts a fractionation of 28-30‰. Similarly, modern riverine sulfate, derived from the oxidative weathering of crustal components (e.g., sulfide and evaporite minerals), ranges from 0-10‰ (Holser et al., 1988), and bacterially reduced sulfide can impart fractionations of 2 to 46‰ (Harrison and Thode, 1957; Habicht and Canfield; 1997; Canfield, 2001). Under conditions where BSR is not limited by sulfate availability, fractionations are commonly observed to be 35-45‰, with restricted fractionation observed with greater sulfate limitation. Additionally, S-isotope fractionation of up to 70‰ can result from disproportionation in the oxidative parts of the bacterial sulfur cycle (Canfield and Thamdrup, 1994; Habicht and Canfield, 1996; 1997; 2001).

Variation in the isotopic composition of both carbon and sulfur can be modeled as a function of the isotopic composition and magnitude of these fluxes (e.g., Kump and Arthur, 1999). Change in the isotopic composition of the marine dissolved inorganic carbon reservoir (δ_{DIC}) is defined as a time-dependent relationship (Kump and Arthur, 1999):

$$\partial\delta_{DIC}/\partial t = [F_W(\delta_W - \delta_{DIC}) - (F_{ORG} \bullet \Delta C)] \bullet 1/M_{DIC} \qquad [1]$$

where F_W and F_{ORG}, and δ_W and $\delta_{ORG,}$ represent the magnitude and isotopic composition of weathering input to the ocean and removal of carbon as organic carbon, respectively; ΔC represents the fractionation between oxidized and reduced carbon reservoirs; and M_{DIC} represent the magnitude of dissolved inorganic carbon in the marine reservoir.

Similarly, change in the isotopic composition of the oceanic sulfate reservoir (d_{SO4}) can also be defined as a time-dependent relationship (e.g. Kah et al., 2004):

$$\partial\delta_{SO4}/\partial t = [F_W(\delta_W - \delta_{SO4}) - (F_{PY} \bullet \Delta S)] \bullet 1/M_{SO4} \qquad [2]$$

wherein δ_{SO4}, δ_W and δ_{PY} are the isotopic composition of marine sulfate, weathered sulfate input to the ocean and buried pyrite, respectively; F_W and F_{PY} represent the magnitude of weathering and pyrite burial fluxes; ΔS represents the fractionation between organic and inorganic sulfur reservoirs; and M_{SO4} represent the magnitude of sulfate in the marine reservoir. The relationships expressed in Eq. [1] and [2] highlight reservoir size effects, with small reservoir size facilitating more rapid changes in $\delta^{13}C_{DIC}$ and $\delta^{34}S_{SO4}$. The maximum rate of marine C-isotope variability ($\partial\delta_{DIC}/\partial t_{MAX}$) can then be estimated by allowing the weathering input to approach zero ($F_W \rightarrow 0$) and the remaining carbon to be removed via organic carbon burial ($F_{ORG} = F_W$), giving:

$$\partial\delta_{DIC}/\partial t_{MAX} = F_W \bullet \Delta C/M_{DIC} \qquad [3]$$

Likewise, $\partial\delta_{SO4}/\partial t_{MAX}$ can be estimated for the marine sulfate reservoir as weathering input approaches zero ($F_W \rightarrow 0$) and the remaining sulfate reservoir is removed via pyrite burial ($F_{PY} = F_W$), giving:

$$\partial\delta_{SO4}/\partial t_{MAX} = F_W \bullet \Delta S/M_{SO4} \qquad [4]$$

At steady state, carbonate and sulfate input fluxes are equivalent to output fluxes ($F_W = F_{DIC} + F_{ORG}$ and $F_W = F_{SO4} + F_{PY}$, respectively) and $\partial d_{SO4}/\partial t = 0$ (Kump and Arthur, 1999; Rothman, 2003). From Eq. [1], this gives:

$$F_{ORG} = [F_W \bullet (\delta_W - \delta_{DIC})] / \Delta C \quad [5]$$

for the marine carbon cycle and from Eq. [2], this gives:

$$F_{PY} = [F_W \bullet (\delta_W - \delta_{SO4})] / \Delta S \quad [6]$$

for the marine sulfur cycle. Dividing Eq. [5] and [6] by F_W gives:

$$f_{ORG} = (\delta_W - \delta_{DIC}) / \Delta C \quad [7]$$

$$f_{PY} = (\delta_W - \delta_{SO4}) / \Delta S \quad [8]$$

where f_{ORG} is the relative fraction of carbon that is removed from the system as organic carbon ($f_{ORG} = F_{ORG}/(F_{ORG} + F_{DIC})$) and f_{PY} is the relative fraction of sulfur that is removed from the system as pyrite ($f_{PY} = F_{PY}/(F_{PY} + F_{SO4})$). The relationships in Eq. [7] and [8] are valid for times scales longer than the residence time of marine DIC (τ_{DIC}) and marine sulfate (τ_{SO4}). In the modern ocean sulfate residence time is very long (approximately 20 Myr, Böttcher et al., 2007), but in the early Paleozoic, the residence time was potentially much shorter since the sulfate reservoir size was likely much smaller than in the modern ocean (Horita et al., 2002; Hurtgen et al., 2009; Gill et al., 2011; Thompson et al., *in review*) and residence time is a function of sulfate reservoir size ($\tau_{SO4} = M_o/F_W$). Therefore, the steady state relationship [Eq. 4] is potentially applicable to short-term (<10^6 Myr) $\delta^{34}S_{SO4}$ variation.

6.3. Long-term C- and S-isotope trends

Over longer time scales (10^7 yr), carbon and sulfur isotope data show sympathetic variation with a 1‰ increase in $\delta^{13}C$ values from the early to mid-Floian that corresponds to a 15‰ increase in average $\delta^{34}S$ (Figure 2.10). Similar sympathetic behavior in $\delta^{13}C$ and $\delta^{34}S$ values has been recognized in the Lower Paleozoic, particularly during the Late Cambrian SPICE event (Hurtgen et al., 2009; Gill et al., 2011). This covariant behavior has been interpreted as increased organic

carbon input to an anoxic and sulfidic deep-ocean (Hurtgen et al., 2009; Gill et al., 2011). Under these conditions, enhanced delivery of organic carbon results in increased bacterial sulfate reduction and expansion of ocean euxinia. Ordovician sulfur isotope records show an excursion of similar magnitude to that recorded at the time of the SPICE event (15‰) occurring over an interval approximately 2x longer than the SPICE event (~2 Myr SPICE; Saltzman et al., 2004; versus approximately 4 Myr from early to mid-Floian). If we assume, as in Gill et al. (2011), that the increase in $\delta^{34}S$ is driven by enhanced delivery of organic carbon under low oxygen, potentially sulfidic conditions, the longer duration of the observed sulfur isotope shift may reflect a longer duration of enhanced organic carbon input. Alternatively, it may also reflect a slower response time to enhanced organic carbon input because of a larger marine sulfate reservoir.

Gill et al. (2011) suggests that marine sulfate concentration at the time of the SPICE event would have to have been <1.5 mM in order to produce a S-isotope excursion that would recover within the 2 Myr time-frame afforded by the SPICE isotopic records. Hurtgen et al. (2009) suggests even lower (<1 mM) marine concentrations for this same time. Recent evaluation of a sharp 15‰ shift in the marine sulfur isotope record in the upper Table Head Group, Thompson et al. (*in review*) calculated marine sulfate concentration to be approximately 2 mM in the Early to Middle Ordovician. These models would therefore suggest that marine sulfate reservoir size potentially doubled in the aftermath of the SPICE event as a result of organic carbon burial and release of oxidative potential.

In either case, if marine sulfur isotope change was ultimately driven by enhanced delivery of organic carbon, then the 15‰ shift in $\delta^{34}S$ would have required a net organic carbon flux of $4x10^{18}$ mol (Gill et al., 2011). In the Middle Ordovician, however, the enhanced organic carbon flux necessary to drive a 15‰ sympathetic shift in $\delta^{34}S$ is not reflected in the apparent $\delta^{13}C$ composition of marine DIC (as recorded in carbonates), which only increases 1‰. This dramatically muted response of DIC may result from a larger DIC reservoir during greenhouse times. Another potential factor would be increased coupling between marine organic and inorganic carbon (Ridgwell, 2003; Bartley and Kah, 2004) resulting from a globally sustained increase in skeletal biomass during this time (i.e. GOBE; Harper, 2006; Servais et al., 2009). If

the muted carbon isotope response resulted entirely from increased DIC related to greenhouse climate, a time-dependent mass balance requires the DIC reservoir to be 10x larger than that assumed by Gill et al (2011). Although extreme pCO_2 of up to 10x present atmospheric level may have been present during Ordovician greenhouse times (Berner, 1998; Berner, 2006), there are little data to support such a dramatic change in pCO_2 (and thus DIC) from the Late Cambrian to the Middle Ordovician. Even at lower levels of pCO_2, however, a muted carbon isotope response may occur if organic and inorganic carbon production are strongly coupled via metazoan skeletonization (i.e., limited production of organic carbon by pelagic, non-calcifying organisms (Ridgwell, 2003; Bartley and Kah, 2004). Such a scenario might be expected under potentially nutrient-limiting conditions during greenhouse times (Saltzman, 2005). Under these conditions, small changes in organic carbon flux may result in changes in $\delta^{34}S$ that are largely uncompensated by changes in $\delta^{13}C$. This apparent decoupling is readily observed in Ordovician data from Argentina and Western Newfoundland in terms of the dramatic, short-term ($<10^6$ yr) oscillation in $\delta^{34}S$ that is recorded in all studied sections (Figure 2.10).

6.4. Potential origins of short-term S-isotope variation

The most dramatic feature of the Ordovician marine sulfur isotope record is a short-term oscillation with an amplitude of 7‰ and wavelength of approximately 1 Myr. This oscillation is observed in each of the measured section and is surprising in its uniformity through Lower and Middle Ordovician strata sampled at these two very disparate sections. This short-term sulfur isotope variability, which records rates of isotopic change of approximately 14‰ per Myr (or 7‰ per 0.5 Myr) suggests a fundamentally different response of the marine system than traditional models. Marine S-isotope variation is usually considered to be primarily driven by pyrite burial (Garrels and Lerman, 1984; Kump, 1989; Petsch and Berner, 1998; Petsch, 1999; Berner, 2001). Here, we evaluate the potential for alternate drivers such as a change in the fractionation between oxidized and reduced sulfur reservoirs, the magnitude of pyrite burial, and the magnitude and isotopic composition of the weathering flux as keys to understanding the short-term S-isotope variation.

6.4.1. ΔS control

The degree of fractionation between oxidized and reduced marine sulfur reservoirs (ΔS) can vary as a function of sulfate availability (Habicht et al., 2002), sulfur disproportionation (Jørgensen, 1990; Canfield and Teske, 1996), and the burial efficiency of pyrite (Hurtgen et al., 2005). The kinetic isotope effect associated with bacterial sulfate reduction imparted a 2-46‰ fractionation between sulfide and residual sulfate (Canfield, 1997; 2001; Detmers et al., 2001). Fractionation greater than 46‰ is commonly attributed to bacterial disproportionation, wherein intermediate sulfur species, thiosulfate ($S_2O_3^{2-}$) and elemental sulfur (S^0), are recycled, producing sulfide that is depleted by 7-20‰ relative to the residual intermediate sulfur species (Jørgensen et al., 1990; Canfield and Thamdrup, 1994; Habicht et al., 1998; Cypionka et al., 1998; Böttcher et al., 2001). Late Cambrian to Ordovician records of δ_{SO4} and $\delta^{34}S_{PY}$ suggest ΔS values <46‰ (Hurtgen et al., 2009; Gill et al., 2011, Thompson et al., *in review*). Because bacterial communities responsible for sulfur disproportionation have been active in the marine realm since the latter half of the Proterozoic (Canfield and Teske, 1996; Johnston et al., 2005), these reduced fractionations are generally interpreted to reflect BSR under sulfate-limiting conditions. To evaluate whether changes in ΔS required to produce observed short-term variation in marine sulfate S-isotope composition are plausible, steady state (Eq. [8]) constraints on the magnitude and f_{PY} required are first considered, then time dependent relationships (Eq. [2] and [4]) are used to determine the magnitude of ΔS and changes in ΔS required to achieve the observed rate of S-isotope change and its potential oscillation. All models use values provided in Table 2.7.

Steady state estimates of ΔS indicate either a high fraction of pyrite burial (f_{PY}) or large changes in ΔS are required to achieve average observed magnitude of S-isotope excursions (7‰) (Figure 2.11A). At modern f_{PY} (0.2-0.4; Holland, 1973; Berner and Raiswell, 1983; Garrels and Lerman, 1984; Canfield, 2005), ΔS must change by 25‰ to produce a 7‰ shift in δ_{SO4}. Even at unreasonably high pyrite burial fractions (f_{PY} = 0.9), ΔS would need to change by nearly 8‰ in to produce a 7‰ shift in δ_{SO4}. Time dependent modeling of the magnitude of ΔS required to produce observed rates of S-isotope change (14‰/Myr) also indicate low marine sulfate reservoir size is required to produce short-term marine S-isotope variation. Maximum possible

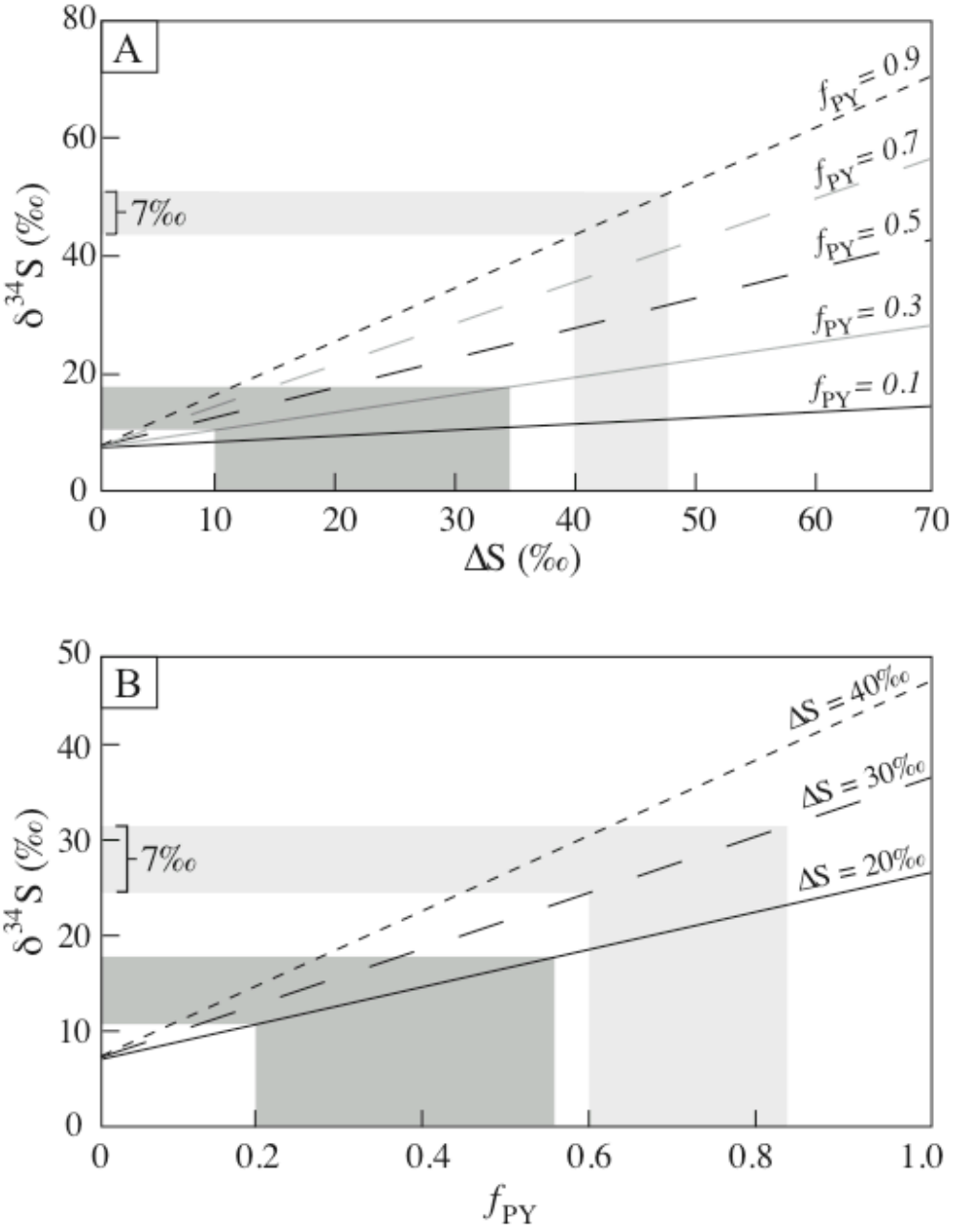

Figure 2.11. Steady state model estimates for production of small amplitude isotopic excursions. A) Approximately 20% increase in relative pyrite burial is required to produce an average 7‰ increase in δ_{SO4} at ΔS = 30‰. At lower values of ΔS, as is commonly observed in low sulfate systems, even greater increase in relative pyrite burial is required. B) δ_{SO4} over a range of f_{PY}. These plots highlight the sensitivity of δ_{SO4} to high ΔS and high f_{PY} values.

rates of change ($\partial\delta_{SO4}/\partial t_{MAX}$) were estimated using Eq. [4] for a range of ΔS values. Since sulfate reservoir size is unknown, we used M_o values that correspond to a range of sulfate concentrations from 0.5 to 28 mM. Estimates of $\partial\delta_{SO4}/\partial t_{MAX}$ indicate that a rate of change of 14‰/Myr requires either large ΔS or small reservoir size, or both. At modern sulfate reservoir size (28 mM), observed rate of S-isotope variation can only be achieved at values of ΔS >50‰ (Table 2.8). At values of ΔS closer to those commonly observed in the Cambrian and Ordovician (0 to 30‰), M_{SO4} <2 mM is required to achieve observed rate of S-isotope variation. Estimates of $\partial\delta_{SO4}/\partial t$ at varying ΔS values using the time dependent relationship in Eq. [2] further indicate the necessity of a small sulfate reservoir (<2 mM) and large changes in ΔS (>25‰) to achieve observed oscillation of S-isotope composition (Table 2.9).

It is clear that both steady state and time dependent estimates suggest low marine sulfate concentration and large fluctuations in ΔS (approximately 25‰). Low marine sulfate concentration is consistent with high-resolution Late Cambrian and Ordovician records of δ_{SO4} (Hurtgen et al., 2009; Gill et al., 2011; Thompson et al., *in review*) and marine evaporite data (Horita et al., 2002; Petrychenko et al., 2005) that suggest marine sulfate concentrations of <2 mM. Although parallel records of Cambrian and Ordovician δ_{SO4} and δ_{PY} record ΔS fluctuations of great enough magnitude (>25‰) to result in observed isotopic variation (Hurtgen et al., 2009; Gill et al., 2011; Thompson et al., *in review*), observed changes in ΔS all occur over substantially longer time frames (2-4 Myr), suggesting this mechanism is unlikely as a driver for short-term oscillation in the isotopic composition of marine sulfate.

6.4.2. Pyrite burial control

In most traditional models of marine sulfur cycling, pyrite burial is considered to be the primary control on changes in the isotopic composition of marine sulfate (Garrels and Lerman, 1984; Kump, 1989; Petsch and Berner, 1998; Petsch, 1999; Berner, 2001) and is, in itself, a function of water column oxygenation, the availability of organic carbon for bacterial sulfate reduction, and the availability of Fe^{2+} for pyrite burial (Westrich, 1983; Westrich and Berner 1984; Berner et al., 1985). In modern, well-oxygenated marine waters, bacterial sulfate reduction is typically

restricted to within the sediment column and, since highly reactive organic matter is also degraded by oxygen in the water column, bacterial sulfate reduction is further limited by the concentration and quality of organic carbon within sediments (Berner and Raiswell, 1983; Westrich, 1983; Westrich and Berner, 1984; Boudreau and Westrich, 1984). Under well-oxygenated conditions, organic matter availability is controlled primarily by factors extrinsic to the marine system, e.g., increased sedimentation rate, which enhances deposition of highly reactive organic matter and leads to higher rates of bacterial sulfate reduction, or increased terrigenous weathering and delivery of nutrients to the marine system, which enhances organic productivity within the water column and its subsequent deposition. By contrast, under anoxic to euxinic oceanic conditions—resulting from lower biospheric oxygen (Canfield et al., 2007), decreased oxygen solubility (Meyer and Kump, 2008), or ocean stagnation (Saltzman, 2005)—even slight changes in the extent of marine redox can result in an intrinsic increase in nutrient delivery to the surface oceans, which can enhance organic productivity within the water column.

Permanent removal of marine sulfur by pyrite burial additionally relies on the availability of reactive iron, which facilitates the removal of biogenically-mediated hydrogen sulfide as pyrite (Berner, 1984; 1985; Lyons and Berner, 1992; Hurtgen et al., 2005). The availability of reactive iron to the marine system is controlled by a combination of hydrothermal influx and the delivery of iron via riverine and atmospheric sources (Fung et al., 2000). The dynamics of this system, however, are also affected by the rate at which reduced sulfur is rexoidized prior to its transformation to pyrite. In well-oxygenated environments, as much as 95% of HS^- is reoxidized to sulfate and intermediate sulfide species before it can react with iron to form pyrite (Jørgensen, 1982; Canfield and Teske, 1996). Under anoxic to euxinic oceanic conditions, however, the degree of HS^- reoxidation was likely reduced, leading to a greater efficiency of pyrite burial (Hurtgen et al., 2005).

A greater efficiency of pyrite burial might have the potential to drive observed short-term variation in the isotopic composition of marine sulfate. Steady state estimates of f_{PY} using Eq. [8] indicate that at $\Delta S = 30‰$, f_{PY} must fluctuate by approximately 20% to achieve the observed average 7‰ shift in $\delta^{34}S$ (Figure 2.11B). At smaller values of ΔS (e.g., 20‰ or less, which is

commonly observed in low-sulfate systems), f_{PY} increases dramatically to >40%. Although such a large increase in f_{PY} may not be unreasonable over long time scales, such change becomes substantially more difficult when examined using a time-dependent model.

Time dependent estimates of S-isotope variation reinforce requirements that both a small reservoir size and large fluctuations in F_{PY} are needed to achieve the observed rate of δ_{SO4} variation (Table 2.10). Estimates suggest that observed $\partial\delta S_{SO4}/\partial t$ cannot be achieved with a sulfate reservoir size >2 mM except at very high pyrite burial rates ($>>F_W$), which would result in a rapid drawdown of marine sulfate concentrations. Even at sulfate concentrations much lower than the estimated 2 mM, the bi-directional change in δ_{SO4} observed in this study would require changes in F_{PY} from near zero to $0.8x10^{18}$ mol/Myr (Table 2.10). Large fluctuations in pyrite burial are best explained by the presence of a persistent HS^- reservoir in an ocean that is stratified with respect to dissolved oxygen. In this scenario, HS^- produced by BSR in anoxic bottom waters is removed from the overlying sulfate reservoir and is effectively sequestered as a distinct sulfur reservoir (Meyer and Kump, 2008). In an iron-limited system, variability in the isotopic composition of the marine sulfate reservoir would reflect expansion or contraction of a deep-ocean euxinic reservoir resulting from changes in organic carbon availability. Ultimately, such a scenario in which rates of BSR are decoupled from rates of pyrite burial (i.e., where modeled values of F_{PY} effectively reflect F_{BSR} rather than pyrite burial) could result in substantial changes in the isotopic composition of marine sulfate even in the absence of evidence (such as changes in ΔS) for enhanced efficiency of pyrite burial. Furthermore, although it is difficult to separate extrinsic from intrinsic controls on C_{ORG} availability, we suggest that the rapid ($<10^6$ yr) time-frame of observed sulfur isotope change is consistent with changes in C_{ORG} availability resulting from intrinsic changes in marine redox structure and nutrient availability.

6.4.3. Weathering flux control

In a final model examination, we examine the potential for changes in the magnitude and isotopic composition of sulfate weathering to result in short-term oscillation of marine sulfur isotope composition. Flux of sulfate to the marine system includes the oxidative weathering of

crustal sulfide minerals, dissolution of marine evaporite minerals, and the input of magmatic sulfur, with the isotopic composition of this flux being a function of the relative contribution of these sulfur sources (Garrels and Lerman, 1984; Carpenter and Lohmann, 1997; Berner and Petsch, 1998; Berner, 2001). Typically, volcanogenic sulfur input is inferred to be low relative to crustal weathering, and is typically ignored (Kump, 1989; Petsch and Berner, 1998; Petsch, 1999; Berner, 2001; see Carpenter and Lohmann, 1997 who argue for the addition of a significant mantle flux). Additionally, because there is little fractionation associated with the precipitation of sulfate-bearing evaporites from seawater (Holser et al., 1988; Raab and Spiro, 1991), their dissolution plays only a minor role in determining the isotopic composition of a crustal weathering flux, which is, instead, dominated by the oxidative weathering of crustal pyrite.

Because crustal weathering, and thus the flux and isotopic composition of weathering input to the marine sulfur system, is primarily controlled by long term ($>10^7$ yr) processes (Berner, 1994; Canfield et al., 2000), weathering input typically affects marine $\delta^{34}S$ only on long time scales (Garrels and Lerman, 1984; Veizer et al., 1999; Kampschulte et al., 2001). To constrain the magnitude of weathering flux change required for $\partial\delta_{SO4}/\partial t = 14‰/Myr$, we used Eq. [2] to calculate $\partial\delta_{SO4}/\partial t$ for a range of M_{SO4} and F_W (Table 2.11). These estimates again emphasize that observed $\partial\delta_{SO4}/\partial t$ requires low marine sulfate concentration (<2 mM) and large fluctuations in F_W. Modern sulfate reservoir size (equivalent to a concentration of 28 mM) cannot achieve observed rates even at F_W that is 10x estimates for Phanerozoic weathering rates. Even at a marine sulfate concentration of 0.5 mM a near doubling of F_W is required to shift from δ_{SO4} variation in the negative direction to the positive direction (F_W from $2.5x10^{18}$ mol/Myr to $5x10^{18}$ mol/Myr). The combination of large fluxes and rapid change in the magnitude of these fluxes suggests that F_W is not a primary control on marine S-isotope variation.

Additionally, time-dependent estimates (Eq. [2]) of the sensitivity of marine sulfate isotopic composition to changes in the isotopic composition of the weathering flux (δ_W) suggest great difficulty in achieving observed rates of S-isotope change at modern concentrations of marine sulfate (Table 2.12). Even at very low marine sulfate concentrations (0.5 mM), observed

oscillation of marine δ_{SO4} would require shifts in δ_W from approximately -13‰ to > 3 (Table 2.12). Estimates of Early Paleozoic the isotopic composition of sulfate weathering flux range from +3 to +12‰ (Hurtgen et al., 2009; Gill et al., 2011). Although early Paleozoic δ_W values are admittedly difficult to constrain, values much below 0‰ are unlikely from a continental source since these values represent a mixture of sulfate and sulfide weathering (Holser et al., 1988). Under conditions of a persistent euxinia, however, a deep water HS^- reservoir could provide a potentially large reservoir of highly reactive, isotopically light sulfur. Model estimates provided here suggest that partial reoxidation of this source (i.e., where modeled values of F_W and δ_W effectively reflect a combination of a traditional crustal weathering flux plus a flux of oxidized hydrogen sulfide, $F_W + F_{OX}$) could result in substantial changes in the isotopic composition of marine sulfate.

6.5. Short-term sulfur isotope oscillation driven fluctuating oxycline

Time-dependent analyses indicate that it is unlikely that observed, systematic oscillations in marine $\delta^{34}S$ result from changes in the isotopic fractionation between oxidized and reduced sulfur phases. We suggest that difficulties in generating large, yet short-term, changes in the either pyrite burial (F_{PY}) or weathering (F_W) flux can be reconciled by treating the Ordovician sulfur cycle as a dual-reservoir system, with marine sulfate and HS^- treated as distinct, reactive reservoirs (Thompson et al., *in review*; cf. Rothman et al., 2003). Numerous studies suggest early Paleozoic oceans were susceptible to deep-ocean anoxia and fluctuating euxinia (Wille et al., 2008; Hurtgen et al., 2009; Gill et al., 2011). Here we consider that short-term, rapid oscillation in the marine CAS record may be best explained by the intrinsic expansion and contraction of a reactive deep-ocean HS^- reservoir responding to small-scale changes in marine redox.

If we first consider a single-reservoir model (Figure 2.12A), the composition of the marine sulfate reservoir depends only on the magnitude and isotopic composition of input fluxes (from weathering) and output fluxes (from deposition of marine evaporates, including deposition of carbonate-associated sulfate, and pyrite). Because marine evaporite deposition has little fractionation from original marine compositions (Holser et al., 1988; Raab and Spiro, 1991),

pyrite burial is the quantitatively critical flux. The inherent assumption in this single-reservoir model—suitable for a well-ventilated water column—is that all bacterially reduced HS^- that is not extracted by reaction with available iron is immediately reoxidized, through a range of intermediate sulfur phases, to sulfate.

By contrast, a dual-reservoir model acknowledges the potential existence of a reactive, deep-ocean HS^- reservoir in addition to the marine sulfate reservoir. Deep-ocean euxinia is treated as a distinct reservoir with its own input and output fluxes that can affect both the behavior of the individual reservoirs as well as the degree of linkage between them (Thompson et al., *in review*; cf., Rothman et al., 2003). In a dual-reservoir model (Figure 2.12B) the isotopic composition of marine sulfate is affected directly by the magnitude and isotopic composition of traditional input and output fluxes (from weathering and deposition of marine evaporates, including deposition of carbonate-associated sulfate, respectively) that act over long time-scales, as well as a suite of transitory input and output fluxes (from BSR and a combination of chemical and biological sulfide oxidation; Kaplan and Rittenberg, 1964; Fry et al, 1988). In this scenario, the composition of marine sulfate will be influenced directly by the magnitude and isotopic composition of pyrite burial only when the transitory fluxes between the two reservoirs, bacterial sulfate reduction (F_{BSR}) and sulfide oxidation (F_{OX}), are in equilibrium (Figure 2.12B). When transitory fluxes are not in equilibrium, it is critical to consider the time-scales of these fluxes with respect to the size of the individual reactive reservoirs (cf. Rothman et al., 2003). For instance, if BSR or HS^- oxidation occurs over time scales that are shorter than the residence time of the marine HS^- reservoir (τ_{HS}), but longer than the residence time of the marine sulfate (τ_{SO4}) these processes will preferentially affect the composition of the marine sulfate reservoir but not that of the marine HS^- reservoir. The implications of this two-reservoir model indicate that rapid oscillation in the isotopic composition of marine sulfate may reflect transitory changes in the balance of BSR and HS- oxidation in a low-sulfate, euxinic marine system (Figure 2.13). In this scenario, reduced oceanic ventilation (via sluggish circulation or reduced oxygen solubility) promotes deep-water anoxia and buildup of an HS^- reservoir. During intervals of increased marine anoxia (Figure 2.13A), HS^- produced via BSR is effectively removed from the overlying marine sulfate reservoir. The high position of the marine oxycline prevents substantial

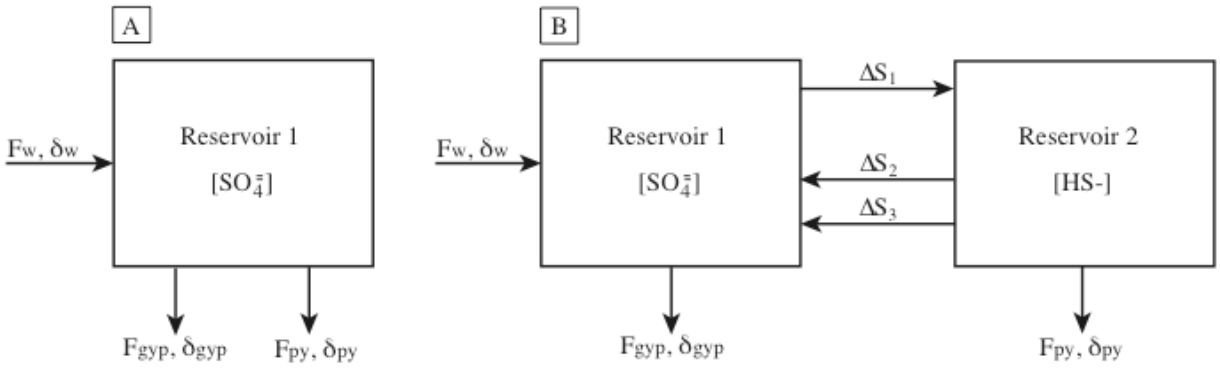

Figure 2.12. Conceptual diagrams of single and dual reservoir marine sulfur models. A) In a single reservoir model (cf., Kurtz et al., 2003) the isotopic composition of marine sulfate is controlled primarily by the magnitude and isotopic composition of input fluxes (from weathering) and output fluxes (from deposition of marine evaporites, including deposition of carbonate-associated sulfate and pyrite). Because marine evaporite deposition imparts little fractionation from the original marine composition, pyrite burial is the quantitatively critical flux. B) In a dual reservoir sulfur model (cf., Rothman et al., 2003) both marine sulfate and marine hydrogen sulfide serve as reactive reservoirs. The isotopic composition of the marine sulfate reservoir can be affected not only by endmember input fluxes and output fluxes, but also by the magnitude and isotopic composition of processes that occur between the two reservoirs, such as bacterial sulfate reduction and biotic/abiotic sulfide oxidation.

reoxidation of HS^-, which results in isotopically heavy marine sulfate. During times of decreased marine anoxia (Figure 2.13B), partial reoxidation of HS^- in the water column and sediment releases a flux of isotopically light marine sulfate to the marine sulfate reservoir, resulting in a negative shift in the isotopic composition of marine sulfate.

We envision the primary driver behind fluctuating marine redox to be organic productivity. In this model, expansion of euxinic deep-waters occurs when productivity leads to enhanced oxygen consumption and increased rates of BSR within the water column. Modeled C/S ratios of 0.8-1.8 and diminished evidence for restricted ΔS support the hypothesis of syngenetic pyrite formation within a euxinic water column (Thompson et al., *in review*), although, in this case, the isotopic composition of marine pyrite is buffered by HS^- rather than by pyrite burial. We expect that such conditions are self-limiting and have internal feedback. For example, a strong oxycline will foster anoxic denitrification, ultimately resulting in a negative feedback between nitrogen availability and organic productivity. As nitrate limitation forces a reduction in productivity, oxygen consumption will decline, resulting in a lowering of the marine oxycline. Even these potentially small changes in nutrient availability and organic productivity, may result in cyclic changes in oceanic redox that is reflected in an oscillation in the isotopic composition of marine sulfate. Regardless of the driving mechanism, it is clear that the transitory nature of observed isotopic changes requires consideration of a dual-reservoir model for marine sulfur cycling. In this scenario, the total flux of bacterially reduced sulfur, less the reduced sulfur removed from the system as pyrite, represents the extent of euxinia and the amount of reactive sulfur available for reoxidation. The stability of the observed short-term oscillation of $\delta^{34}S$ indicates that, over the long time-frame of this study (>20 Myr), extrinisic factors such as increased crustal weathering and its affect on organic productivity on expansion and contraction of marine euxinia was largely decoupled from changes driven by intrinsic changes in nutrient flux.

7. Conclusions

Marine S-isotope records from the Early to Middle Ordovician Argentine Precordillera and Western Newfoundland show robust short-term variation superimposed over a longer-term

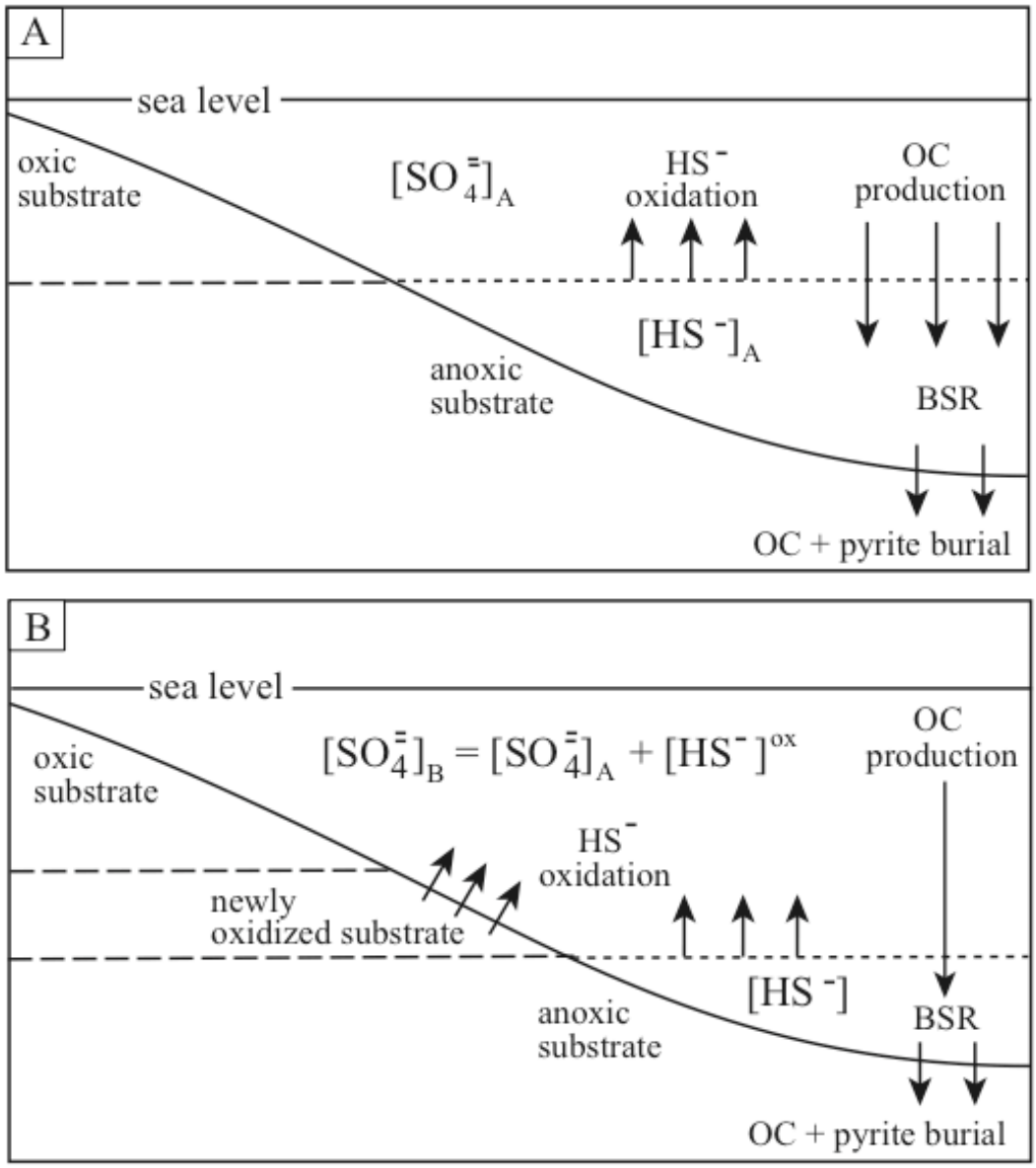

Figure 2.13. Conceptual model of a fluctuating oxycline in the poorly ventilated Ordovician greenhouse ocean. A) During intervals of widespread anoxia (high marine oxycline) low rates of hydrogen sulfide reoxidation results in effective removal of sulfur from the marine sulfate reservoir and buildup of a large hydrogen sulfide reservoir. B) Contraction of deep ocean euxinia and partial oxidation of the reactive hydrogen sulfide reservoir results in an increased flux of isotopically light sulfate to the marine sulfate reservoir and a concomitant decrease in the isotopic composition of the marine sulfate reservoir.

signal. Long-term S-isotope variation is sympathetic to marine C-isotope variation, indicating organic carbon burial was a driver of C- and S-isotope variation. Comparison to long-term C- and S-isotope variation to trends observed during the Late Cambrian SPICE event shows $\delta^{34}S$ variation that is similar in magnitude, but which occurs over a time interval twice as long as during the Late Cambrian. We suggest this longer duration of average variation in marine sulfur isotope composition reflects an approximate doubling of the marine sulfate reservoir after SPICE (equivalent to a concentration change from approximately 1 to 2 mM). Marine $\delta^{13}C$ variation is notably muted in the Ordovician relative to SPICE (1‰ excursion versus 5‰ during SPICE). The muted response of marine $\delta^{13}C$ in the Ordovician likely reflects a combination of increased pCO_2 in a supergreenhouse climate and organic and inorganic carbon production that was strongly coupled via metazoan skeletonization (Ridgwell, 2003; Bartley and Kah, 2004).

Traditional single-reservoir modeling of the sulfur cycle is not sufficient to account, however, for a persistent short-term oscillation in the isotopic composition of marine sulfur. Short-term variation in marine sulfate isotopic composition is indicative of expansion and contraction of deep-ocean euxinia, and is best explained by an intrinsically controlled fluctuation in the marine oxycline that results in an alternation between enhanced BSR and enhanced reoxidation of marine HS^- in a poorly ventilated Ordovician greenhouse ocean.

The potential for a large, reactive HS^- reservoir demands consideration of the sulfur cycle as a dual-reservoir model (cf. Rothman et al., 2003), and suggests that Precambrian and Early Paleozoic records of S-isotope variation should be re-evaluated in terms of a dual reservoir model, especially during intervals when the water column was potentially euxinic. The results from this and other recent studies (Thompson et al., *in review*) indicate the persistence of deep-ocean euxinia well into the Ordovician despite the potential for large-scale organic carbon burial during the Late Cambrian SPICE event. We suggest that the extent of oxygen liberated to the biosphere during the SPICE event, although sufficient to double the size of the marine sulfate reservoir, was insufficient fully ventilate the deep ocean environment, particularly during greenhouse climates.

Acknowledgements

Funding for this project was provided by the National Geographic Society (NGS 7866-05 to Kah), National Science Foundation (NSF-EAR 0745768 to Kah), the American Chemical Society (ACS-PRF 48166 to Kah), along with student grants from Sigma Xi, the Geological Society of America, and SEPM (to Thompson). We give special thanks to Ricardo Astini and Fernando Gomez (University of Cordoba) and Geoff Gilleaudeau (University of Tennessee) for help in conducting field work in Argentina; and Lisa Pratt and Anna Synkiewicz (Indiana University) and Zheng-hua Li and Michael Peretich (University of Tennessee) for help with isotopic and elemental analyses.

References cited

Ainsaar, L., Meidlha, T., Martma, T., 1999. Evidence for a widespread carbon isotopic event associated with late Middle Ordovician sedimentological and faunal changes in Estonia. Geological Magazine 136, 49-62.

Albanesi G.L, Ortega, G., 2002. Advances on conodont-graptolite biostratigraphy of the Ordovician system of Argentina. Serie Correlacion Geologica 16, 143-165.

Algeo, T.J., Seslavinsky, K.B., 1995. The Paleozoic world; continental flooding, hypsometry, and sea level. American Journal of Science 295, 878-822.

Allan, J.R., Matthews, R.K., 1982. Isotope signatures associated with early meteoric diagenesis. Sedimentology 29, 797-817.

Alt, J.C., 1995. Sulfur isotopic profile through the oceanic crust: Sulfur mobility and seawater-crustal sulfur exchange during hydrothermal alteration. Geology 23, 7, 585-588.

Anbar, A.D., Knoll, A.H., 2002. Proterozoic ocean chemistry and evolution: a bioinorganic bridge? Science 297, 1137-1142.

Arthur, M.A., 1983. Secular variations in amounts and environments of organic carbon burial during the Phanerozoic. Geology Newsletters 12, 235-348.

Astini, R.A., Benedetto, J.L., Vaccari, N.E., 1995. The early Paleozoic evolution of the Argentine Precordillera as a Laurentian rifted, drifted, and collided terrane: A geodynamic model. Geological Society of America Bulletin 107, 3, 253-273.

Ault, W.U., Kulp, J.L., 1959. Isotopic geochemistry of sulfur. Geochimica et Cosmochimica Acta 16, 201-235.

Baldis, B.A.J., Beresi, M.S., Bordonaro, O.L., Vaca, A., 1984. The Argentine Precordillera as a key to Andean structure. Episodes 7, 14-19.

Banner, J.L., Hanson, G.N., 1990. Calculation of simultaneous isotopic and trace element variations during water-rock interaction with applications to carbonate diagenesis. Geochimica et Cosmochimica Acta 54, 3123-3137.

Banner, J.L., 1995. Application of the trace element and isotope geochemistry of strontium to studies of carbonate diagenesis. Sedimentology 42, 805-824.

Bartley, J.K., Kah, L.C., 2004. Marine carbon reservoir, C_{org}-C_{carb} coupling, and the evolution of the Proterozoic carbon cycle. Geology 32, 129-132.

Bartley, J.K., Kah, L.C., Williams, J.L., Stagner, A.F., 2007. Carbon isotope chemostratigraphy of the Middle Riphean type section (Avzyan Formation, Southern Urals, Russia): Signal recovery in a fold-and-thrust belt. Chemical Geology 237, 211-232.

Benedetto, J.L., Sánchez, T.M., Carrera, M.G., Brussa, E.D., Salas, M.J., 1999. Paleontological constraints on successive paleogeographic positions of Precordillera terrane during the early Paleozoic. Geological Society of America, Special Paper 336, 21-42.

Bergström, S.M., Chen, X., Gutierrez-Marco, J.C., Dronov, A., 2008. The new chronostratigraphic classification of the Ordovician System and its relations to major regional series and stages and to $\delta^{13}C$ chemostratigraphy. Lethaia 42, 97-107.

Berner R.A., Canfield D.E., 1989. A new model of atmospheric oxygen over Phanerozoic time. American Journal of Science 289, 333-361.

Berner, R.A., De Leeuw, J.W., Spiro, B., Murchison, D.G., Eglington, G., 1985. Sulfate reduction, organic matter decomposition and pyrite formation. Philosophical Transactions of the Royal Society, London 315, 25-38.

Berner, R.A., Kothavala, Z., 2001. GEOCARB III: a revised model of atmospheric CO_2 over Phanerozoic time. American Journal of Science 301, 182-204.

Berner R.A., Petsch S.T., 1998. The sulfur cycle and atmospheric oxygen. Science 282, 1426-1427.

Berner, R.A., Raiswell, R., 1983. Burial of organic carbon and pyrite sulfur in sediments over Phanerozoic time: a new theory. Geochimica et Cosmochimica Acta 47, 855-862.

Berner, R.A., 1984. Sedimentary pyrite Formation: an update. Geochimica et Cosmochimica Acta 48, 605-615.

Berner, R.A., 1987. Models for carbon and sulfur cycles and atmospheric oxygen: applications to Paleozoic geologic history. American Journal of Science 287, 177-190.

Berner, R.A., 1994. GEOCARB II: a revised model of atmospheric CO_2 over Phanerozoic time. American Journal of Science 294, 56-91.

Berner, R.A., 2001. Modeling atmospheric O_2 over Phanerozoic time. Geochimica et Cosmochimica Acta 65, 685-694.

Berner, R.A., 2006. GEOCARBSULF: a combined model for Phanerozoic atmospheric O_2 and CO_2. Geochimica et Cosmochimica Acta 70, 5653-5664.

Bischoff, J.L., Dickson, F.W., 1975. Seawater-basalt interaction at 200 degrees C and 500 bars; implications for origin of sea-floor heavy-metal deposits and regulation of seawater chemistry. Earth and Planetary Science Letters 25, 385-397.

Boudreau, B.P., Westrich, J.T., 1984. The dependence of bacterial sulfate reduction on sulfate concentration in marine sediments. Geochimica et Cosmochimica Acta 48, 2503-2516.

Brand, U., Veizer, J., 1980. Chemical diagenesis of a multicomponent carbonate system—1: Trace elements. Journal of Sedimentary Petrology 50, 1219-1236.

Brennan, S.T., Lowenstein, T.K., Horita, J., 2004. Seawater chemistry and the advent of biocalcification. Geology 32, 473-476.

Buggisch, W., Keller, M., Lehnert, O., 2003. Carbon isotope record of the Late Cambrian to Early Ordovician carbonates of the Argentine Precordillera. Palaeogeography, Palaeoclimatology, Palaeoecology 195, 357-373.

Burdett, J.W., Arthur, M.A., Richardson, M., 1989. A Neogene seawater sulfur isotope age curve from calcareous pelagic microfossils. Earth and Planetary Science Letters 94, 189-198.

Butterfield, N.J., 2009. Oxygen, animals and oceanic ventilation: an alternative view. Geobiology 7, 1-7.

Canfield D.E., Teske A., 1996. Late Proterozoic rise in atmospheric oxygen concentration inferred from phylogenetic and sulfur- isotope studies. Science 382, 127-132.

Canfield, D.E., Thamdrup, B., 1994. The production of ^{34}S-depleted sulphide during bacterial disproportionation of elemental sulphur. Science, 266, 1973-1975.

Canfield, D.E., Poulton, S.W., Knoll, A.H., Narbonne, G.M., Ross, G., Goldberg, T., Strauss, H., 2008. Ferruginous conditions dominated later Neoproterozoic deep-water chemistry. Science 321, 949-952.

Canfield, D.E., 2001. Biogeochemistry of sulphur isotopes. In: Valley, J.W., Cole, D.R. (Eds.), Stable Isotope Geochemistry, 607-633.

Canfield D.E., 2005. The early history of atmospheric oxygen: homage to Robert M. Garrels. Annual Review of Earth and Planetary Science 33, 1-36.

Carpenter, S.J., Lohmann, K.C., 1997. Carbon isotope ratios of Phanerozoic marine cements: Re-evaluating the global carbon and sulfur systems. Geochimica et Cosmochimica Acta 61, 4831-4846.

Carpenter S.J., Lohmann K.C., Holden P., Walter L.M., Huston, T., Halliday A.N., 1991. $\delta^{18}O$ values, $^{87}Sr/^{86}Sr$ and Sr/Mg ratios of Late Devonian abiotic marine calcite: Implications for composition of ancient seawater. Geochimica et Cosmochimica Acta 55, 1991-2010.

Chambers, L.A., Trudinger, P.A., 1979. Microbiological fractionation of stable sulfur isotopes. Geomicrobiology Journal 1, 249-293.

Chiba, H., Sakai, H., 1985. Oxygen isotope exchange rate between dissolved sulfate and water at hydrothermal temperatures. Geochimica et Cosmochimica Acta 49, 993-1000.

Cocks, L.R.M., McKerrow, W.S., 1993. A reassessment of the Early Ordovician "Celtic" brachiopod province. Journal of the Geological Society, London 150, 1039-1042.

Dahl, T.W., Hammarlund, E.U., Anbar, A.D., Bond, D.P.G., Gill, B.C., Gordon, G.W., Knoll, A.H., Nielsen, A.T., Schovsbo, N.H., Canfield, D.E., 2010. Devonian rise in atmospheric oxygen correlated to the radiations of terrestrial plants and large predatory fish. Proceedings of the National Academy of Sciences 107, 17911-17915.

Edmond, J.M., Measures, C., McDuff, R. E., Chan, L.H., Collier, R.W., Grant B., Gordon, L.I., Corliss, J.B., 1979. Ridge crest hydrothermal activity and the balance of the major and minor elements in the ocean: The Galapagos data. Earth and Planetary Sciences Letters 46, 1-18.

Fanning, C.M., Pankhurst, R.J., Rapela, C.W., Baldo, E.G., Casquet, C., Galindo, C., 2004. K-bentonites in the Argentine Precordillera contemporaneous with rhyolite volcanism in the Famatinian Arc. Journal of the Geological Society, London 161, 747-756.

Fike, D.A., Grotzinger, J.P., Pratt, L.M., Summons, R.E., 2006. Oxidation of the Ediacaran ocean. Nature 444, 744-747.

Frakes, L.A., Francis, J.E., Syktus, J.I., 1992. Climate modes of the Phanerozoic. Cambridge

University Press, Cambridge 274 p.

Frank, T.D., Lohmann, K.C., 1996. Diagenesis of fibrous magnesian calcite marine cement: Implications for the interpretation of $\delta^{18}O$ and $\delta^{13}C$ values of ancient equivalents. Geochimica et Cosmochimica Acta 60, 2427-2436.

Frank, T.D., Lyons, T.W., Lohmann, K.C., 1997. Isotopic evidence for the paleoenvironmental evolution of the Mesoproterozoic Helena Formation, Belt Supergroup, Montana, USA. Geochimica et Cosmochimica Acta 61, 5023-5041.

Frank, T.D., Kah, L.C., Lyons, T.W., 2003. Changes in organic matter production and accumulation as a mechanism for isotopic evolution in the Mesoproterozoic ocean. Geological magazine 140, 397-420.

Fry, B., Ruf, W., Gest, H., Hayes, J.M., 1988. Sulfur isotope effects associated with oxidation of sulfide by O_2 in aqueous solution. Isotope Geoscience 73, 205-210.

Garrels, R.M., Lerman, A., 1981. Phanerozoic cycles of sedimentary carbon and sulfur. Proceedings of the National Academy of Sciences 78, 4652-4656.

Garrels R.M., Lerman A., 1984. Coupling of the sedimentary sulfur and carbon cycles—an improved model. American Journal of Science 284, 989-1007.

Garrels, R.M., Perry, E.A., Jr., 1974. Cycling of carbon, sulfur, and oxygen through geologic time. In: Goldberg, E.D. (Ed.), The Sea; Volume 5, Marine Chemistry—the Sedimentary Cycle. John Wiley and Sons, New York, 303-336.

Gill, B. C., Lyons, T.W., Saltzman, M.R., 2007, Parallel, high-resolution carbon and sulfur isotope records of the evolving Paleozoic marine sulfur reservoir. Palaeogeography, Palaeoclimatology, Palaeoecology 256, 156-173.

Gill, B.C., Lyons, T.W., Frank, T.D., 2008. Behavior of carbonate-associated sulfate during meteoric diagenesis and implications for the sulfur isotope paleoproxy. Geochimica et Cosmochimica Acta 72, 4699-471.

Gill, B.C., Lyons, T.W., Young, S.A., Kump, L.R., Knoll, A.H., Saltzman, M.R., 2011. Geochemical evidence for widespread euxinia in the Late Cambrian ocean. Nature (2011).

Given, R.K., Lohmann, K.C., 1985. Derivation of the original isotopic composition of Permian marine cements. Journal of Sedimentary Petrology 55, 430-439.

Habicht, K.S., Canfield, D.E., 1996. Sulphur isotope fractionation in modern microbial mats and the evolution of the sulphur cycle. Nature 382, 342-343.

Habicht, K.S., Canfield, D.E., 1997. Sulfur isotope fractionation during bacterial sulfate reduction in organic-rich sediments. Geochimica et Cosmochimica Acta 61, 5351-5361.

Habicht, K., Canfield, D., 2001. Isotope fractionation by sulfate reducing natural populations and the isotopic composition of sulfide in marine sediments. Geology 29, 555-558.

Habicht, K.S., Gade, M., Thamdrup, B., Berg, P., Canfield, D.E., 2002. Calibration of sulfate levels in the Archean ocean. Science 298, 2372-2374.

Habicht, K.S., Salling, L., Thamdrup, B., Canfield, D.E., 2005. Effect of low sulfate concentrations on lactate oxidation and isotope fractionation during sulfate reduction by Archaroglobus fulgidus strain Z. Applied and Environmental Microbiology 71, 3770-3777.

Hall, S.A., Evans, I., 1988. Paleomagnetic study of the Ordovician Table Head Group, Port au Port Peninsula, Newfoundland. Canadian Journal of Earth Sciences 25, 1407-1419.

Hallam, A., 1992. Phanerozoic sea-level changes. In: Bottjer, D.J., Bambach, R.K., (Eds.), The perspectives in paleobiology and Earth history series. Columbia University Press, New York, 1-266.

Halverson, G.P., Hurtgen, M.T., 2007. Ediacaran growth of the marine sulfate reservoir. Earth and Planetary Science Letters 263, 32-44.

Haq, B.U., Schutter, S.R., 2008. A chronology of Paleozoic sea-level changes. Science 322, 64-68.

Harper, D.A.T., MacNiocaill, C., Williams, S.H., 1996. The palaeogeography of early Ordovician Iapetus terranes: an integration of faunal and palaeomagnetic constraints. Palaeogeography, Palaeoclimatology, Palaeoecology 121, 297-312.

Harper, D.A.T., 2006. The Ordovician biodiversification: Setting and agenda for marine life. Palaeogeography, Palaeoclimatology, Palaeoecology 232, 148-166.

Harrison, A.G., Thode, H.G., 1957. The kinetic isotope effect in the chemical reduction of sulphate. Transactions of the Faraday Society 53, 1648-1651.

Hemming, N.G., Meyers, W.J., Grams, J.C., 1989. Cathodoluminescence in diagenetic calcites: the roles of Fe and Mn as deduced from electron probe and spectrophotometric measurements. Journal of Sedimentary Petrology 59, 404-411.

Herrera, Z.A., Benedetto, J.L., 1991. Early Ordovician brachiopod faunas of the Precordillera Basin, Western Argentina: Biostratigraphy and paleobiogeographical affinities. In: MacKinnon, D.L., Lee, D.E., Campbell, J.D. (Eds.), Brachiopods through time. Balkema, Rotterdam, 283-301.

Holmden, C., Creaser, R.A., Muehlenbachs, K., Leslie, S.A., Bergström, S.M., 1998. Isotopic evidence for geochemical decoupling between ancient epeiric seas and bordering oceans: Implications for secular curves. Geology 26, 567-570.

Holser, W.T., Kaplan, I.R., 1966. Isotope geochemistry of sedimentary sulfates. Chemical Geology 1, 93-135.

Holser, W.T., Schidlowski, M., Mackenzie, F.T., Maynard, J.B., 1988. Geochemical cycles of carbon and sulfur. In: Gregor, C.B., Garrels, R.M., Mackenzie, F.T., Maynard, J.B. (Eds.), Chemical Cycles in the Evolution of the Earth. Wiley, New York, pp. 105-173.

Horita, J., Zimmermann, H., Holland, H.D., 2002. Chemical evolution of seawater during the Phanerozoic: Implications from the record of marine evaporites. Geochimica et Cosmochimica Acta 66, 3733-3756.

Hough, M.L., Shields, G.A., Evins, L.Z., Strauss, H., Henderson, R.A., Mackenzie, S., 2006. A major sulphur isotope event at c. 510 Ma: a possible anoxia-extinction-volcanism connection during the Early-Middle Cambrian transition? Terra Nova 18, 257-263.

Huff, W.D., Davis, D., Bergström, S.M., Krekeler, M.P.S., Kolata, D.R., Cingolani, C., 1997. A biostratigraphically well-constrained K-bentonite U-Pb zircon age of the lowermost Darriwilian State (Middle Ordovician) from the Argentine Precordillera. Episodes 20, 29-33.

Huff, W.D., Bergström, S.M., Kolata, D.R., Cingolani, C.A., Astini, R.A., 1998. Ordovician K-bentonites in the Argentine Precordillera: relations to Gondwana margin evolution. In: Pankhurst, R.J., Rapela, C.W. (Eds.), The Proto-Andean Margin of Gondwana. Geological Society, London, Special Publication 142, 107-126.

Hurtgen, M., Arthur, M., Suits, N., Kaufman, A., 2002. The sulfur isotopic composition of Neoproterozoic seawater sulfate: implications for snowball Earth? Earth and Planetary Science Letters 203, 413-429.

Hurtgen, M.T., Arthur, M.A., Halverson, G.P., 2005. Neoproterozoic sulfur isotopes, the evolution of microbial sulfur species, and the burial efficiency of sulfide as sedimentary sulfide. Geology 33, 41-44.

Hurtgen, M.T., Pruss, S.B., Knoll, A.H., 2009. Evaluating the relationship between the carbon and sulfur cycles in the later Cambrian ocean: An example from the Port au Port Group, western Newfoundland, Canada. Earth and Planetary Science Letters 281, 288-297.

Jacobi, R.D., 1981. Peripheral bulge—a causal mechanism for the Lower/Middle Ordovician unconformity along the western margin of the Northern Appalachians. Earth and Planetary Science Letters 56, 245-251.

James, N.P, Barnes, C.R., Stevens, R.K., Knight, I., 1989. A lower Paleozoic continental margin carbonate platform, northern Canadian Appalachians. In: Crevello, T., Sarg, R., Read, J.F., Wilson, J.L. (Eds.), Controls on carbonate platforms and basin development. Society of Economic Paleontologists and Mineralogists, Special Publications 44, 123-146.

Johnston, D.T., Wing, B.A., Farquhar, J., Kaufman, A.J., Strauss, H., Lyons, T.W., Kah, L.C., and Canfield, D.E., 2005. Active microbial sulfur disproportionation in the Mesoproterozoic. Science 310, 1466-1479.

Jørgensen, B.B., 1982. Mineralization of organic matter in the sea bed—the role of sulphate reduction. Nature 296, 643- 645.

Jørgensen, B.B., Bang, M., Blackburn, T.H., 1990. Anaerobic mineralization in marine sediments from the Baltic Sea–North Sea transition: Marine Ecology Progress Series 59, 39-54.

Kah, L.C., Sherman, A.B., Narbonne, G.M., Kaufman, A.J., Knoll, A.H., 1999. $\delta^{13}C$ stratigraphy of the Proterozoic Bylot Supergroup, northern Baffin Island: Implications for regional lithostratigraphic correlations. Canadian Journal of Earth Sciences 36, 313-332.

Kah, L.C., Lyons, T.W., Chesley, J.T., 2001. Geochemistry of a 1.2 Ga carbonate-evaporite succession, northern Baffin and Bylot Islands: implications for Mesoproterozoic marine evolution. Precambrian Research 111, 203-234.

Kah, L.C., Lyons, T.W., Frank, T.D., 2004. Low marine sulphate and protracted oxygenation of the Proterozoic biosphere. Nature 431, 834-838.

Kah, L.C., Zhan, R., and Thompson, C.K. Ocean oxygenation did not drive the Great Ordovician Biodiversification Event. (*in preparation*).

Kah, L.C., 2000. Depositional $\delta^{18}O$ signatures in Proterozoic dolostones: constraints on seawater chemistry and early diagenesis. SEPM Special Publication 67, 345-360.

Kampschulte, A., Bruckschen, P., Strauss, H., 2001. The sulphur isotopic composition of trace sulphates in Carboniferous brachiopods: implications for coeval seawater correlation with other geochemical cycles and isotope stratigraphy. Chemical Geology 175, 149-173.

Kampschulte, A., Strauss, H., 2004. The sulfur isotopic evolution on Phanerozoic seawater based on the analysis of structurally substituted sulfate in carbonates. Chemical Geology 204, 255-286.

Kaplan, I.R., Rittenberg, S.C., 1964. Microbiological fractionation of sulphur isotopes. Journal of General Microbiology 34, 195-212.

Kaufman, A.J., Hayes, J.M., Knoll, A.H., Germs, G.J.B., 1991. Isotopic compositions of carbonates and organic carbon from upper Proterozoic successions in Namibia: stratigraphic variation and the effects of diagenesis and metamorphism. Precambrian Research 49, 301-327.

Keller, M., Canas, F., Lehnert, O., Vaccari, N.E., 1994. The upper Cambrian and Lower Ordovician of the Precordillera (Western Argentina): Some stratigraphic reconsiderations. Newsletters Stratigraphy 31, 115-132.

Keller, M., Eberlein, S., Lehnert, O., 1993. Sedimentology of Middle Ordovician carbonates in the Argentine Precordillera: evidence of regional relative sea-level changes. Geologische Rundschau 82, 362-377.

Keller, M., 1999. Argentine Precordillera: Sedimentary and plate tectonic history of a Laurentian crustal fragment in South America. Geological Society of America, Special Paper 341, 131 pp.

Kitano, Y., Okumura, M., Idogake, M., 1985. Incorporation of sodium, chloride and sulfate with calcium carbonate. Geochemistry Journal 9, 75-84.

Knight, I., Cawood, P.A., 1991. Paleozoic geology of western Newfoundland: an exploration of a deformed Cambro-Ordovician passive margin and foreland basin, and Carboniferous successor basin. St. John's, Newfoundland, Centre for Earth Resources Research, 1-403.

Knight, I., James, N. P., Lane, T. E., 1991. The Ordovician St. George unconformity, northern Appalachians: the relationship of plate convergence at the St. Lawrence Promontory to the Sauk /Tippecanoe sequence boundary. Geological Society of America, Bulletin 103, 1200-1225.

Kump, L.R., Arthur, M.A., 1999. Interpreting carbon isotope excursions: Carbonates and organic matter. Chemical Geology 161, 181-198.

Kump L.R., Garrels R.M., 1986. Modeling atmospheric O_2 in the global sedimentary redox cycle. American Journal of Science 286, 336-360.

Kump, L.R., Arthur, M.A., Patzkowsky, M.E., Gibbs, M.T., Pinkus, D.S., Sheehan, P.M., 1999. A weathering hypothesis for glaciation at high atmospheric pCO_2 during the Late Ordovician. Palaeogeography, Palaeoclimatology, Palaeoecology 152, 173-187.

Kump, L.R., 1989. Alternative modeling approaches to the geochemical cycles of carbon, sulfur, and strontium isotopes. American Journal of Science 289, 390-410.

Lehnert, O., Keller, M., 1994. The conodont record of the Argentine Precordillera: Problems and possibilities. Zentralblatt für Geologie und Paläontologie 1, 231-244.

Lehnert, O., 1995. The Tremadoc/Arenig Transition in the Argentine Precordillera. Proceedings of the International Symposium on the Ordovician System 6, 145-148.

Lehnert, O, Miller, J.F., Repetski, J.E.,1997. Paleogeographic significance of *Clavohamulus hintzei* Miller (Conodonta) and other Ibexian conodonts in an early Paleozoic carbonate platform facies of the Argentine Precordillera. GSA Bulletin 109, 429-443.

Li, C., Love, G.D., Lyons, T.W., Fike, D.A., Sessions, A.L., Chu, X., 2010. A stratified redox model for the Ediacaran ocean. Science 328, 80-83.

Lindström, M. 1971. Lower Ordovician conodonts of Europe. Geological Society of America, Memoir 127, 21-61.

Löfgren, A., 1978. Arenigian and Llanvirnian conodonts from Jämtland, northern Sweden. Fossils and Strata 13, 1-129.

Löfgren, A., 1996. Lower Ordovician conodonts, reworking, and biostratigraphy of the Orreholmen Quarry, Västergötland, south-central Sweden. GFF 118, 169-183.

Logan, G.A., Hayes, J.M., Hieshima, G.B., Summons, R.E., 1995. Terminal Proterozoic reorganization of biogeochemical cycles. Nature 376, 53-56.

Lowenstein, T.K., Timofeeff, M.N., Brennan, S.T., Hardie, L.A., Demicco, R.V., 2001. Oscillations in Phanerozoic seawater chemistry: evidence from fluid inclusions. Science 294, 1086-1088.

Lowenstein, T.K., Hardie, L.A., Timofeeff, M.N., Demicco, R.M., 2003. Secular variation in seawater chemistry and the origin of calcium chloride basinal brines. Geology 31, 857-860.

Lyons, T.W., 2004. Sites of anomalous organic remineralization in the carbonate sediments of South Florida, USA: The sulfur cycle and carbonate-associated sulfate. Geological Society of America Special Paper 379, 161-176.

Marshall, J.D., 1992. Climatic and oceanographic isotopic signals from the carbonate rock record and their preservation. Geological Magazine 129, 143-160.

Martin, R.E., Quigg, A., Podkovyrov, V., 2008. Marine biodiversification in response to evolving phytoplankton stoichiometry. Palaeogeography, Palaeoclimatology, Palaeoecology 258, 277-291.

Meyer, K.M., Kump, L.R., 2008. Ocean Euxinia in Earth History: Causes and Consequences. Annual Review of Earth and Planetary Science 36, 251-288.

Miller, K.G., Kominz, M.A., Browning, J.V., Wright, J.D., Mountain, G.S., Katz, M.E., Sugarman, P.J., Cramer, B.S., Christie-Blick, N., Pekar, S.F., 2005. The Phanerozoic record of global sea-level change. Science 310, 1293-1298.

Munnecke, A., Servais, T., 2007. What caused the Ordovician biodiversification? Palaeogeography, Palaeoclimatology, Palaeoecology 245, 1-4.

Neuman, R.B., Harper, D.A., 1992. Paleogeographic significance of Arenig-Llanvirn Toquima-Table Head and Celtic brachiopod assemblages. Proceeding of the International Symposium on the Ordovician System 6, 241-254.

Niocaill, C.M., van der Pluijm, B.A., Van der Voo, R., 1997. Ordovician paleogeography and the evolution of the Iapetus ocean. Geology 25, 159-162.

Panchuk, K.M., Holmden, C.E., Leslie, S.A., 2006. Local controls on carbon cycling in the Ordovician midcontinent region of North America, with implications for carbon isotope secular curves. Journal of Sedimentary Research 76, 200-211.

Petsch S.T., Berner R.A., 1998. Coupling the long-term geochemical cycles of carbon, phosphorus, sulfur, and iron: the effect on atmospheric O_2 and the isotopic records of carbon and sulfur. American Journal of Science 298, 246-262.

Petsch, S.T., 1999. Comment on "Carbon isotope ratios of Phanerozoic marine cements: Re-evaluating global carbon and sulfur systems". Geochimica et Cosmochimica Acta 63, 307-310.

Pratt, B.R. Holmden, C., (Eds.), 2008. Dynamics of Epeiric Seas. Geological Association of Canada Special Paper 48, 1-406.

Qing, H., Veizer, J., 1994. Oxygen and carbon isotopic composition of Ordovician brachiopods: Implications for coeval seawater. Geochimica et Cosmochimica Acta 58, 20, 4429-4442.

Raab, M., Spiro, B., 1991. Sulfur isotopic variations during seawater evaporation with fractional crystallization. Chemical Geology. Isotope Geoscience Section 86, 323-333.

Ramos, V.A., Jordan, T.E., Allmendinger, R.W., Mpodozis, C., Kay, S.M., Cortés, J.M., Palma, M., 1986. Paleozoic terranes of the central Argentine-Chilean Andes. Tectonics 5, 855-880.

Ramos, V.A., 1988a. Tectonics of the Late Proterozoic – Early Paleozoic: a collisional history of southern South America. Episodes 11, 168-174.

Ramos, V.A., 1988b. The Tectonics of the Central Andes: 30"-33"s latitude. Geological Society of America, Special Paper 218, 31-54.

Ridgwell, A., Zeebe, R.E., 2004. The role of the global carbonate cycle in the regulation and evolution of the Earth system. Earth and Planetary Science Letters 234, 299-315.

Ridgwell, A., 2003. A Mid-Mesozoic revolution in the regulation of ocean chemistry. Marine Geology 217. 339-357.

Ries, J.B., Fike, D.A., Pratt, L.M., Lyons, T.W., Grotzinger, J.P., 2009. Superheavy pyrite in the terminal Proterozoic Nama Group, southern Namibia: a consequence of low seawater sulfate at the dawn of animal life. Geology 37, 743-746.

Ross, R.J., Jr., Ingham, J.K., 1970. Distribution of the Toquima-Table Head (Middle Ordovician Whiterock) faunal realm in the Northern Hemisphere. Geological Society of America Bulletin 81, 393-408.

Rothman, D.H., Hayes, J.M., Summons, R.E., 2003. Dynamics of the Neoproterozoic carbon cycle. Proceedings of the National Academy of Sciences 100, 8124-8129.

Rush, P.F., Chafetz, H.S., 1990. Fabric retentive, non-luminescent brachiopods as indicators of original $\delta^{13}C$ and $\delta^{18}O$ compositions: a test. Journal of Sedimentary Petrology 60, 968-981.

Saltzman, M.R., Young, S.A., 2005. Long-lived glaciation in the Late Ordovician? Isotopic and sequence-stratigraphic evidence from western Laurentia. Geology 33, 109-112.

Saltzman, M.R., Runnegar, B., Lohmann, K.C., 1998. Carbon isotope stratigraphy of Upper Cambrian (Steptoean Stage) sequences of the eastern Great Basin: Record of a global oceanographic event. Geological Society of America, Bulletin 110, 285-297.

Saltzman, M.R., Brasier, M.D., Ripperdan, R.L., Ergaliev, G.K., Lohmann, KC, Robison, R.A., Chang, W.T., Peng, S., Runnegar, B., 2000. A global carbon isotope excursion during the Late Cambrian: Relation to trilobite extinctions, organic matter burial and sea level: Palaeogeography, Palaeoclimatology, Palaeoecology 162, 211-223.

Saltzman, M.R., Groessens, E., Zhuravlev, A.V., 2004. Carbon cycle models based on extreme changes in d13C: an example from the lower Mississippian. Palaeogeography, Palaeoclimatology, Palaeoecology 213, 359-377.

Saltzman, M.R., 2005. Phosphorus, nitrogen, and the redox evolution of the Paleozoic oceans. Geology 33, 7, 573-576.

Sarmiento, J.L., Herbert, T., Toggweiler, J.R., 1988. Causes of anoxia in the world ocean. Global Biogeochemical Cycles 2, 115-128.

Savard, M.M., Veizer, J., Hinton, R., 1995. Cathodoluminescence at low Fe and Mn concentrations; a SIMS study of zones in natural calcites. Journal of Sedimentary Research 65, 208-213.

Servais, T., Harper, D.A.T., Li, J., Munnecke, A., Owen, A.W., Sheehan, P.M., 2009. Understanding the Great Ordovician biodiversification Event (GOBE): Influences of paleogeography, paleoclimate, or paleoecology? GSA Today 19, 4-10.

Seyfried, W.E, Bischoff, J.L., 1979. Low temperature basalt alteration by seawater: an experimental study at 70°C and 150°C. Geochimica et Cosmochimica Acta 43, 1937-1947.

Stenzel, S.R., James, N.P., 1987. Death and destruction of an early Paleozoic carbonate platform, western Newfoundland [abstract]. Society of Economic Paleontologists and Mineralogists, Annual Midyear Meeting. Abstract 4, 80.

Stenzel, S.R., Knight, I, James, N.P., 1990. Carbonate platform to foreland basin: revised stratigraphy of the Table Head Group (Middle Ordovician), western Newfoundland. Canadian Journal of Earth Sciences 26, 14-26.

Stouge, S., 1982. Preliminary conodont biostratigraphy and correlation of Lower to Middle Ordovician carbonates of the St. George Group, Great Northern Peninsula, Newfoundland. Newfoundland Department of Mines and Energy Report 82-83, 1-59.

Strauss, H., 1997. The isotopic composition of sedimentary sulfur through time. Palaeogeography, Palaeoclimatology, Palaeocology 132, 97-118.

Strauss, H., 1999. Geologic evolution from isotope proxy signals—Sulphur. Chemical Geology 161, 89-101.

Sweeney, R.E., Kaplan, I.R., 1980. Stable isotope composition of dissolved sulfate and hydrogen sulfide in the Black Sea. Marine Chemistry 9, 145-152.

Takano, B., 1985. Geochemical implications of sulfate in sedimentary carbonates. Chemical Geology 49, 393-403.

Thode, H.G., Monster, J., Dunford, H.B., 1961. Sulphur isotope geochemistry. Geochimica et Cosmochimica Acta 25, 159-174.

Thomas, W.A. Astini, R.A., 1996. The Argentine Precordillera: A Traveler from the Ouachita Embayment of North America from Laurentia. Science 273, 752-757.

Thomas, W.A., Astini, R.A., 1999. Simple-shear conjugate rift margins of the Argentine Precordillera and the Ouachita embayment of Laurentia. Geological Society of America, Bulletin 111, 1069-1079.

Thomas, W.A. Astini, R.A., 2007. Vestiges of an Ordovician west-vergent thin-skinned Ocloyic thrust belt in the Argentine Precordillera, southern Central Andes. Journal of Structural Geology 29, 1369-1385.

Thompson, C.K., Kah, L.C., Kaufman, A.J., 2011. Did ventilation of euxinic oceans herald the end of Ordovician greenhouse climate? Nature Geoscience (*in review*).

Veizer, J., Holser, W.T., Wilgus, C.K., 1980. Correlation of $^{13}C/^{12}C$ and $^{34}S/^{32}S$ secular variations. Geochimica et Cosmochimica Acta 44, 579-587.

Veizer J., Ala D. Azmy K., Bruckschen P., Buhl D., Bruhn F., Carden G. A. F., Diener A., Ebneth S., Godderis Y., Jasper T., Korte C., Pawellek F., Podlaha O. G., Strauss H., 1999. $^{87}Sr/^{86}Sr$, $\delta^{13}C$ and $\delta^{18}O$ evolution of Phanerozoic seawater. Chemical Geology 161, 59-88.

Veizer, J., 1983. Chemical diagenesis of carbonates: theory and application of trace element technique. Society of Economic Paleontologists and Mineralogists, Short Course Notes 10, 1-100.

Vinogradov, A.P, Grinenko, V.A., 1962. Isotopic composition of sulfur compounds in the Black Sea. Geochemistry 10, 973-997.

Wadleigh, M.A., Veizer, J., 1992. $^{18}O/^{16}O$ and $^{13}C/^{12}C$ in lower Paleozoic brachiopods: implications for the isotopic composition of sea water. Geochimica et Cosmochimica Acta 56, 431-443.

Webby, B.D., Paris, F., Droser, M.L., Percival, I.G., 2004. The Great Ordovician Biodiversification Event. Columbia University Press, New York, 1-484.

Westrich, J.T., Berner, R.A., 1984. The role of sedimentary organic matter in bacterial sulfate reduction: the G model tested. Limnology and Oceanography 29, 236-249.

Westrich, J.T., 1983. The consequences and controls of bacterial sulfate reduction in marine sediments. Ph.D. thesis, Yale University.

Wille, M., Nägler, T.F., Lehmann, B., Schröder, S., Kramers, J.D., 2008. Hydrogen sulphide release to surface waters at the Precambrian/Cambrian boundary. Nature 453, 767-769.

Williams, H., Stevens, R.K., 1974. The ancient continental margin of eastern North America. In: Burk, C.A., Drake, C.L. (Eds.), The geology of continental margins. Springer-Verlag, New York, NY, 781-796.

Williams, H., Boyce, W.D., James, N.P., 1987. Graptolites from the Lower-Middle Ordovician St. George and Table Head groups, western Newfoundland, and their correlation with trilobite, brachiopod, and conodont zones. Canadian Journal of Earth Sciences 24, 3, 456-470.

Young, S.A., Saltzman, M.R., Bergström, S.M., 2005. Upper Ordovician (Mohawkian) carbon isotope ($\delta^{13}C$) stratigraphy in eastern and central North America: Regional expression of a perturbation of the global carbon cycle. Palaeogeography, Palaeoclimatology, Palaeoecology 222, 53-76.

Zempolich, W.G., Wilkinson, B.H., Lohmann, K.C., 1988. Diagenesis of late Proterozoic carbonates; the Beck Springs Dolomite of eastern California. Journal of Sedimentary Petrology 58, 656-672.

Appendix

Table 2.1. Range of isotopic compositions and elemental concentrations recorded in the La Silla Formation, Argentina. *Stratigraphic height is cumulative based on measured section and carbon isotope correlation of individual sections.

Sample	Strat. Height*	Age	$\delta^{13}C$	$\delta^{18}O$	$\delta^{34}S$	Mg/Ca	Mn	Fe	Sr
	(m)	(Myr)	(‰ VPDB)		(‰ VCDT)			(ppm)	
LS-1	1	491.0	-1.0	-4.8	19.1	0.48	10	406	248
LS-9	9	490.7	-0.4	-9.1	16.3	0.00	0	11	111
LS-18	18	490.4	-0.4	-9.3	17.0	0.01	0	216	273
LS-30	29.5	490.0	0.5	-9.4	11.6	0.00	0	103	150
LS-39	38.5	489.8	0.3	-9.0	13.4	0.01	0	168	156
LS-48	47.5	489.5	0.7	-7.8	11.0	0.00	0	149	152
LS-58	57.7	489.1	-1.0	-8.7	16.1	0.01	0	91	136
LS-67	66.7	488.9	-0.1	-7.6	11.2	0.01	0	4	148
LS-78	78	488.5	-1.0	-9.1	13.9	0.00	0	118	158
LS-87	87	488.2	0.3	-7.8	17.3	0.01	0	127	164
LS-96	96	487.9	-0.2	-8.2	10.1	0.00	0	148	187
LS-105	105	487.6	-0.9	-7.8	18.8	0.01	0	74	186
LS-120	120	487.1	-1.7	-7.7	17.9	0.00	0	100	190
LS-131	130.5	486.8	-1.6	-7.9	18.7	0.01	0	378	315
LS-149	149.3	486.2	-0.4	-8.2	15.6	0.00	0	40	290
LS-159	158.3	485.9	-1.6	-7.7	17.4	0.00	0	0	209
LS-167	167.3	485.6	-1.1	-7.7	11.7	0.00	0	122	287
LS-176	176.3	485.3	-1.3	-7.9	19.9	0.00	0	90	246
LS-185	185.3	485.0	-1.0	-8.4	18.5	0.00	0	112	182
LS-199	199	484.6	-0.8	-7.6	13.1	0.00	0	10	204
LS-217	217	484.0	-1.1	-8.3	19.5	0.00	0	18	158
LS-227	226.8	483.7			12.2	0.00	0	30	166
LS-236	235.8	483.4	-0.8	-8.7	15.3	0.00	0	31	177
LS-246	245.6	483.1	0.3	-7.5	14.9	-0.01	0	228	159
LS-255	255.4	482.8	-0.3	-8.1	17.3	0.00	0	0	183
LS-264	264.4	482.5	-1.1	-8.0	17.0	0.01	0	158	232
LS-273	273.4	482.2	-0.9	-7.6	20.1	0.00	0	132	201
LS-282	282.4	481.9	-1.4	-8.1	19.0	0.00	0	40	440
LS-291	291.4	481.6	-1.5	-8.5	13.4	0.00	0	0	177
LS-300	300.4	481.3	-1.6	-7.5	19.8	0.01	0	179	203
LS-309	309	481.0	-1.3	-8.2	18.3	0.01	0	50	209
LS-318	317.6	480.8	-0.7	-9.0	16.6	0.01	0	86	258
LS-327	326.6	480.5	-1.6	-9.0	16.6	0.00	0	21	210
LS-337	336.6	480.2	-1.6	-7.8	15.0	0.01	0	198	168
LS-346	345.5	479.9	-1.1	-8.0	15.7	0.00	0	130	139
LS-355	354.5	479.6	-0.8	-7.8	15.6	0.01	0	98	132
LS-364	363.5	479.3	-1.0	-7.2	12.3	0.00	0	128	158
LS-373	372.5	479.0	0.0	-7.8	15.3	0.00	0	107	273

Table 2.2. Range of isotopic compositions and elemental concentrations recorded in the Cerro La Silla section of the San Juan Formation. *Stratigraphic height is cumulative based on measured section and carbon isotope correlation of individual sections.

Sample	Strat. Height*	Age	$\delta^{13}C$	$\delta^{18}O$	$\delta^{34}S$	Mg/Ca	Mn	Fe	Sr
	(m)	(Myr)	(‰ VPDB)		(‰ VCDT)			(ppm)	
SJ-0	375.2	479.0	-0.6	-8.4	15.3	0.00	8	8	200
SJ-8	382.7	478.8	-0.5	-7.2	17.1	0.00	9	42	196
SJ-15	390.2	478.6	-0.7	-6.7	18.3	0.00	12	81	277
SJ-23	397.7	478.4	-1.1	-6.9	23.5	0.01	12	76	279
SJ-31	405.8	478.1	-0.7	-5.9	19.6	0.01	14	71	251
SJ-39	413.7	477.9	-1.5	-6.6	19.0	0.01	17	123	257
SJ-46	421.2	477.7	-1.2	-6.7	21.7	0.01	13	91	303
SJ-55	429.7	477.5	-2.5	-6.7	23.3	0.01	24	203	299
SJ-62	437.2	477.2	-2.4	-6.2	14.9	0.01	21	92	271
SJ-70	444.7	477.0	-1.4	-7.0	21.2	0.01	76	718	291
SJ-77	452.2	476.8	-0.9	-6.6	25.3	0.00	107	1119	277
SJ-85	459.7	476.6	-0.9	-6.9	23.8	0.00	232	1652	281
SJ-92	467.2	476.4	-0.8	-6.7	24.5	0.01	214	1637	309
SJ-100	474.7	476.2	-0.8	-6.4	20.2	0.00	121	1455	303
SJ-107	482.2	476.0	-0.5	-6.6	23.9	0.00	184	1251	315
SJ-115	489.7	475.8	-0.7	-6.6		0.01	210	2144	312
SJ-116	491.2	475.7	-0.8	-5.9	26.5	0.01	158	1252	255
SJ-124	498.7	475.5	-1.1	-6.6	26.6	0.00	491	1025	425
SJ-131	506.2	475.3	-0.7	-6.6	25.5	0.01	182	1556	307
SJ-139	513.7	475.1	-0.3	-6.4	20.7	0.01	206	1332	291
SJ-146	521.2	474.9	-0.4	-6.1	22.0	0.01	194	1523	308
SJ-154	528.7	474.7	-0.3	-6.1	27.6	0.01	201	1207	300
SJ-162	536.2	474.4	-0.3	-5.6	23.8	0.00	340	977	233
SJ-169	543.7	474.2	0.0	-6.1		0.01	312	1477	313
SJ-176	551.2	474.0	-0.1	-5.9	21.5	0.00	294	862	262
SJ-184	558.7	473.8	-0.2	-6.0	26.7	0.01	232	943	321
SJ-191	566.2	473.6	-0.2	-5.8	25.0	0.00	186	855	280
SJ-199	573.7	473.4	-0.1	-6.1		0.00	43	229	179
SJ-206	581.2	473.2	-0.2	-6.2	22.5	0.01	167	572	285
SJ-214	588.7	473.0	0.0	-6.0	23.7	0.01	223	1201	274
SJ-221	596.2	472.7	-0.3	-6.2	26.3	0.01	148	1114	269
SJ-229	603.7	472.5	-0.9	-6.5	22.2	0.01	178	1281	261
SJ-236	611.2	472.3	-0.3	-5.9	15.5	0.00	106	217	324
SJ-246	621.4	472.0	-0.6	-5.7	20.2	0.01	81	290	347
SJ-253	628.9	471.8	-0.4	-5.9	17.1	0.01	70	274	345
SJ-261	636.4	471.6	-0.7	-5.9	24.2	0.00	255	1301	270
SJ-269	643.9	471.4	-0.5	-5.7	16.8	0.01	110	321	332
SJ-277	651.7	471.2	-0.5	-6.0	19.7	0.01	158	780	314
SJ-284	659.2	471.0	-0.6	-5.6	23.7	0.00	211	556	295
SJ-292	666.7	470.7	-0.5	-5.6		0.02	218	691	327
SJ-299	674.2	470.5	-0.6	-5.2	19.7	0.01	190	655	287
SJ-307	681.7	470.3	-0.6	-5.1	19.6	0.01	180	532	334
SJ-316	690.7	470.1	-0.7	-5.5	15.6	0.01	159	456	317

SJ-323	698.2	469.8	-0.6	-5.5	19.4	0.01	217	404	332
SJ-331	705.7	469.6	-0.7	-5.8	16.4	0.01	276	657	337
SJ-338	713.2	469.4	-0.8	-5.8	19.4	0.01	248	512	354
SJ-346	720.7	469.2	-1.0	-5.7	16.8	0.01	184	427	341
SJ-353	728.2	469.0	-1.2	-5.7	13.5	0.01	127	290	297

Table 2.3. Range of isotopic compositions and elemental concentrations recorded in the Talacasto section of the San Juan Formation, Argentina. *Stratigraphic height is cumulative based on measured section and carbon isotope correlation of individual sections.

Sample	Strat. Height*	Age	$\delta^{13}C$	$\delta^{18}O$	$\delta^{34}S$	Mg/Ca	Mn	Fe	Sr
	(m)	(Myr)	(‰ VPDB)		(‰ VCDT)			(ppm)	
SJT-0	647.9	471.2	-0.7		25.1	0.01	184	798	359
SJT-7	655.1	471.0	-0.6	-6.3	25.0	0.01	141	563	283
SJT-16	663.9	470.7	-0.7	-6.3	27.1				
SJT-19T	667.2	470.7	-0.7	-6.1	23.6	0.01	193	767	337
SJT-19B1	666.9	470.7	-0.4	-6.1	20.9	0.01	249	475	298
SJT-19B2	666.9	470.7	-0.5	-6.3	21.5	0.01	170	491	292
SJT-22	670.2	470.6	-0.6	-6.3	20.6	0.01	155	347	424
SJT-31	679	470.3	-0.7	-6.2	24.4	0.01	131	294	298
SJT-38	686.1	470.1	-0.8	-6.5	26.2	0.01	175	454	325
SJT-45	693.2	469.9	-0.6	-6.3	25.8	0.00	191	392	248
SJT-54	701.5	469.7	-1.0	-6.4	23.2	0.01	143	222	522
SJT-63	710.4	469.4	-1.0	-6.3	23.7	0.01	114	333	350
SJT-71	718.5	469.2	-1.1	-6.2	21.1	0.00	204	1991	206
SJT-82	729.4	468.9	-1.5	-6.3	13.9	0.01	147	427	321
SJT-89	736.6	468.7	-1.6	-6.4	27.1	0.01	107	181	326
SJT-99	747.1	468.4	-1.5	-6.7	23.5	0.00	107	244	311
SJT-106	754.4	468.2	-1.5	-6.5	21.9	0.01	117	227	334
SJT-115	762.7	467.9	-1.3	-6.8	19.0	0.00	73	286	282
SJT-121	769.2	467.8	-1.1	-6.6	19.6	0.01	94	125	295

Table 2.4. Range of isotopic compositions and elemental concentrations recorded in the Cerro La Chilca section of the San Juan Formation, Argentina. *Stratigraphic height is cumulative based on measured section and carbon isotope correlation of individual sections.

Sample	Strat. Height*	Age	$\delta^{13}C$	$\delta^{18}O$	$\delta^{34}S$	Mg/Ca	Mn	Fe	Sr
	(m)	(Myr)	(‰ VPDB)		(‰ VCDT)			(ppm)	
SJC-0	624.7	472.7	-0.5	-6.1		0.01	91	399	362
SJC-8	632.2	471.7	-0.4	-6.2		0.01	185	342	383
SJC-17	641.2	471.5	-0.2	-5.8		0.00	171	457	287
SJC-24	648.7	471.3	-0.6	-6.0		0.00	211	533	322
SJC-32	656.2	471.0	-0.4	-6.0		0.01	170	267	291
SJC-39	663.7	470.8	-0.4	-6.0		0.00	212	344	338
SJC-48	672.7	470.6	-0.6	-5.9		0.01	166	340	368
SJC-56	680.2	470.4	-0.7	-5.7		0.01	176	342	320
SJC-63	687.7	470.1	-0.8	-5.8		0.00	197	335	322
SJC-71	695.2	469.9	-0.7	-6.0		0.00	136	220	372
SJC-78	702.4	469.7	-0.6	-6.2		0.01	151	272	368
SJC-86	710.6	469.5	-0.7	-5.9		0.00	158	189	280
SJC-94	718.2	469.3	-1.0	-5.8		0.00	145	152	283
SJC-101	725.7	469.1	-1.3	-6.1	22.1	0.00	176	264	280
SJC-109	733.2	468.9	-1.4	-6.2	20.1	0.01	142	244	349
SJC-116	740.7	468.6	-1.3	-5.9	19.1	0.00	139	236	338
SJC-124	748.2	468.4	-1.6	-5.9	18.3	0.00	362	1177	280
SJC-131	755.7	468.2	-1.2	-6.1	15.3	0.01	764	2449	359
SJC-139	763.2	468.0	-1.2	-5.9	13.0	0.00	1535	3528	232
SJC-147	771.2	467.8	-0.8	-5.5	23.0	0.00	2102	3800	306
SJC-154	778.9	467.6	-0.5	-5.9	23.7	0.00	610	871	381
SJC-162	787	467.3	-0.4	-5.1	25.7	0.02	1592	4126	257
SJC-171	795.3	467.1	-0.3	-5.8	22.8	0.01	2006	3660	308
SJC-178	802.4	466.9	-0.6	-5.2	22.2	0.02	517	1174	437

Table 2.5. Range of isotopic compositions and elemental concentrations recorded in the Pachaco section of the San Juan Formation, Argentina. *Stratigraphic height is cumulative based on measured section and carbon isotope correlation of individual sections.

Sample	Strat. Height*	Age	$\delta^{13}C$	$\delta^{18}O$	Mg/Ca	Mn	Fe	Sr
	(m)	(Myr)	(‰ VPDB)				(ppm)	
SJP-0	437.5		-1.8	-7.0	0.00	80	611	219
SJP-8	440.6		-1.3	-7.0	0.00	136	400	225
SJP-13	442.6		-1.0	-6.8	0.02	60	902	232
SJP-21	445.9		-1.2	-7.0	0.01	127	727	225
SJP-28	448.9		-1.0	-6.9	0.00	182	1149	208
SJP-36	452.0		-0.6	-7.2	0.00	195	1783	264
SJP-44	455.3		-0.8	-7.3	0.00	205	2346	273
SJP-51	458.4		-0.7	-6.9	0.00	192	1753	247
SJP-58	461.3		-0.7	-6.9	0.01	179	1965	241
SJP-66	464.4		-0.7	-6.9	0.00	296	1820	232
SJP-66(*)	464.4		-0.6	-7.2	0.01	185	2653	242
SJP-73	467.5		-0.9	-7.0	0.01	220	2171	224
SJP-81	470.5		-0.6	-7.1	0.01	334	2712	265
SJP-89	473.7		-0.7	-7.1	0.00	263	2111	212
SJP-96	476.7		-0.8	-6.7	0.01	278	2006	253
SJP-103	479.8		-0.7	-7.2	0.00	241	2095	248
SJP-111	482.9		-0.6	-7.0	0.00	226	1909	250
SJP-119	485.9		-0.5	-6.8	0.00	416	1999	256
SJP-126	489.0		-0.4	-6.9	0.00	261	1414	209
SJP-133	492.0		-0.5	-7.0	0.00	374	1692	192
SJP-141	495.1		-0.8	-6.6	0.00	373	1750	248
SJP-149	498.2		-0.7	-6.7	0.01	442	1799	237
SJP-156	501.2		-0.1	-6.6	0.00	213	1136	209
SJP-164	504.3		-0.3	-6.4	0.00	258	1422	250
SJP-171	507.4		-0.1	-6.2	0.00	180	1184	246
SJP-179	510.4		0.0	-6.5	0.00	158	1466	323
SJP-186	513.5		-0.1	-7.0	0.00	212	1425	237
SJP-194	516.6		0.0	-6.7	0.00	180	1251	236
SJP-201	519.6		0.0	-7.0	0.01	267	1141	244
SJP-209	522.7		-0.1	-7.1	0.00	363	1727	238
SJP-216	525.8		0.1	-7.0	0.01	359	1524	221
SJP-224	528.8		0.0	-7.0	0.00	474	1299	218
SJP-231	531.9		0.1	-7.3	0.01	313	833	194
SJP-239	534.9		0.0	-7.7	0.02	252	1291	177
SJP-246	538.0		0.2	-9.6	0.00	210	967	173
SJP-254	541.1		0.1	-10.8	0.01	372	1012	172
SJP-257	542.5		-1.3	-14.3	0.00	2044	2698	243

Table 2.6. Range of isotopic compositions and elemental concentrations recorded in the Western Newfoundland sections. *Stratigraphic height is cumulative based on measured section and carbon isotope correlation of individual sections. † AG = Aguathuna Formation and TH = Table Head Group

Sample†	Strat. Height*	Age	$\delta^{13}C$	$\delta^{18}O$	$\delta^{34}S$	TOC	Mg/Ca	Mn	Fe	Sr
	(m)	(Myr)	(‰ VPDB)		(‰ VCDT)	(wt%)			(ppm)	
AG-0B	0	473.8	-0.7	-10.0	31.6					
AG-9	9.4	473.6	-0.6	-9.4	28.7					
AG-18	18.4	473.3	-1.4	-11.0						
AG-26	26.4	473.1	-1.6	-8.7	30.9					
AG-31	30.9	473.0	-1.4	-6.8	24.8					
AG-41	41.4	472.7	-1.1	-6.7	32.9					
AG-50	50.4	472.5			31.3					
AG-59	59.4	472.2	-1.2	-8.1	27.4					
AG-67	67.4	472.0			33.7					
AG-76	76.4	471.8	-1.5	-6.2	25.0					
TH-1	76.4	471.8	-1.0	-7.8	30.9	0.01	0.1	56	1088	214
TH-9	85.4	471.6	-1.5	-5.7	29.2	0.06	0.5	167	5084	78
TH-18	94.4	471.3	-3.1	-7.4	29.9	0.08	0.0	32	672	332
TH-27	103.4	471.1	-1.0	-7.4	33.0	0.10	0.0	23	108	410
TH-35	110.9	470.9	-0.9	-7.3	29.4	0.05	0.0	11	299	286
TH-43	119.9	470.6	-1.6	-7.0	24.6	0.04	0.1	86	1109	198
TH-52	128.9	470.4	-1.0	-7.4	29.8	0.06	0.0	33	397	309
TH-61	137.9	470.2	-1.3	-7.0	28.9	0.05	0.0	28	653	411
TH-70	146.9	469.9	-1.5	-7.0	25.0	0.04	0.0	22	639	369
TH-81	157.4	469.7	-1.7	-6.9	28.2	0.06	0.0	32	797	284
TH-90	166.4	469.4	-1.7	-6.9	33.6	0.06	0.0	98	394	422
TH-99	175.4	469.2	-1.9	-6.9	30.0	0.05	0.0	72	381	458
TH-108	184.8	468.9	-1.6	-6.6	38.6	0.05	0.0	27	597	486
TH-117	193.8	468.7	-0.7	-6.8	17.1	0.07	0.0	71	1625	368
TH-126	202.8	468.5	-0.9	-7.1	26.8	0.06	0.0	39	1022	469
TH-133	210	468.3	-1.1	-6.7	31.8		0.0	35	545	619
TH-142	219	468.0	-0.7	-7.1	31.6	0.06	0.0	118	425	246
TH-153	229.5	467.8	-1.4	-6.9	29.0	0.06	0.0	48	722	538
TH-162A	238.5	467.5	-1.1	-6.7	29.2	0.05	0.0	41	431	417
TH-171	247.5	467.3	-0.5	-6.8	32.9	0.05	0.0	30	391	400
TH-180	256.5	467.1	-0.4	-6.7	29.9	0.05	0.0	52	578	361
TH-189	265.4	466.8	-0.8	-7.6			0.1	40	279	311
TH-201	277.4	466.5	-0.6	-7.2	19.2	0.06	0.0	127	275	297
TH-215	292.1	466.1	-0.4	-7.6	21.8	0.06	0.0	184	503	255
TH-226	302.6	465.8	-0.4	-6.9	2.6	0.09	0.0	413	1368	377
TH-235	311.6	465.6	-0.6	-7.8	18.5					
TH-244	320.6	465.4	-0.2	-6.9	12.2	0.11	0.0	279	2578	715
TH-253	329.6	465.1	0.0	-7.1	21.8	0.10	0.0	178	2217	1040
TH-262	338.6	464.9	-0.1	-7.4	13.3	0.19	0.0	301	3132	901
TH-270	346.1	464.7	0.3	-6.7	15.6	0.23	0.0	164	2232	1045

TH-278	355.1	464.5	0.3	-7.2	21.1	0.19	0.0	134	2148	1031
TH-287	364.1	464.2	0.5	-8.1	18.2	0.14	0.0	116	1528	1094
TH-295	371.6	464.0	0.6	-8.0	20.7	0.08	0.0	173	1787	1118
TH-304	380.6	463.8	0.6	-7.0	9.7	0.12	0.0	121	1889	1073

Table 2.7. Values used for carbon and sulfur isotopic modeling. Values for fluxes and isotopic compositions were estimated from typical values used for Phanerozoic studies (Kump and Arthur, 1999; Kurtz et al., 2003; Gill et al., 2011). Values for ΔS used are less than traditional values (Kah et al., 2004), but reflect the values recorded by data in an earlier study for the early Darriwilian (Thompson et al., *in review*); δ_{carb} and δ_{SO4} were estimated from data recorded in the current study (see Figs. 8, 9, and 10).

Carbon	**Sulfur**
$F_w = 3x10^{19}$ mol/My	$F_w = 1.5x10^{18}$ mol/My
$F_{ORG} = 1x10^{19}$ mol/My	$F_{PY} = 0.5x10^{18}$ mol/My
δ_w = -4‰	δ_w = +7‰
ΔC = -28‰	ΔS = -30‰
δ_{carb} = -1‰	δ_{SO4} = +15‰

Table 2.8. Estimates of maximum rate of change in sulfur isotope composition ($\partial\delta_{SO4}/\partial t$) with ΔS. Sulfate concentration is expressed in millimoles (mM) and weathering flux is expressed in ‰/Myr.

$[SO_4]$	ΔS = 0‰	ΔS = 10‰	ΔS = 20‰	ΔS = 30‰	ΔS = 40‰	ΔS = 50‰
0.5	0	21	41	62	82	102
1	0	10	21	31	41	51
2	0	5	10	15	21	26
14	0	1	2	2	3	4
28	0	0	1	1	2	2

Table 2.9. Estimates of rate of change in sulfur isotope composition ($\partial\delta_{SO4}/\partial t$) with ΔS. Sulfate concentration is expressed in millimoles (mM) and weathering flux is expressed in ‰/Myr.

$[SO_4]$	ΔS = 0‰	ΔS = 10‰	ΔS = 20‰	ΔS = 30‰	ΔS = 40‰	ΔS = 50‰
0.5	-17	-3	11	25	38	52
1	-8	-1	5	12	19	26
2	-4	-1	3	6	10	13
14	-1	0	0	1	1	2
28	0	0	0	0	1	1

Table 2.10. Estimates of rate of change in sulfur isotope composition ($\partial\delta_{SO4}/\partial t$) with F_{PY}. Sulfate concentration is expressed in millimoles (mM) and weathering flux is expressed in ‰/Myr.

$[SO_4]$	$F_{PY} = 0$	$F_{PY} = 0.5 \times 10^{18}$	$F_{PY} = 1 \times 10^{18}$	$F_{PY} = 1.5 \times 10^{18}$	$F_{PY} = 2 \times 10^{18}$
0.5	-16	4	25	45	66
2	-4	1	6	11	16
14	-1	0	1	2	2
28	0	0	0	1	1

Table 2.11. Estimates of rate of change in sulfur isotope composition ($\partial\delta_{SO4}/\partial t$) with F_W. Sulfate concentration is expressed in millimoles (mM) and weathering flux is expressed in ‰/Myr.

$[SO_4]$	$F_W = 0$	$F_W = 1x10^{18}$	$F_W = 1.5x10^{18}$	$F_W = 2x10^{18}$	$F_W = 3x10^{18}$	$F_W = 4x10^{18}$	$F_W = 5x10^{18}$
0.5	41	30	25	19	8	-3	-14
1	20	15	12	10	4	-1	-7
2	10	8	6	5	2	-1	-3
14	1	1	1	1	0	0	0
28	1	1	0	0	0	0	0

Table 2.12. Estimates of rate of change in sulfur isotope composition ($\partial\delta_{SO4}/\partial t$) with δ_W. Sulfate concentration is expressed in millimoles (mM) and weathering flux is expressed in ‰/Myr.

$[SO_4]$	$\delta_W = -15‰$	$\delta_W = -10‰$	$\delta_W = -5‰$	$\delta_W = 0‰$	$\delta_W = +5‰$	$\delta_W = +10‰$	$\delta_W = +15‰$
0.5	-20	-10	0	10	20	31	41
1	-10	-5	0	5	10	15	20
2	-5	-3	0	3	5	8	10
14	-1	0	0	0	1	1	1
28	0	0	0	0	0	1	1

Part 3

Sulfur isotopes mark end of Ordovician greenhouse climate in Darriwilian

This chapter is a reformatted version of a paper by the same title submitted for publication to Nature Geoscience in 2011 by Cara K. Thompson, Linda C. Kah and Alan Jay Kaufman. Journal format requires a short paper and an additional document of supplementary online material.

Thompson, C.K., Kah, L.C., Kaufman, A.J., in review, Sulphur isotopes mark end of Ordovician greenhouse climate in Darriwilian. Nature Geoscience.

Abstract

Climatic cooling in the terminal Ordovician Period (Finnegan et al., *in press*) resulted in widespread Gondwanan glaciation (Brenchley et al., 1994) and a catastrophic loss of marine biodiversity (Sheehan, 2001). Icehouse climates, however, may have been initiated earlier in the Ordovician, as marked by C-isotope volatility in the Sandbian associated with oceanic ventilation (Saltzman, 2005; Saltzman and Young, 2005) or by a >25 Myr low in tropical sea surface temperatures (SSTs) in the Darriwilian (Trotter et al., 2008) which would be expected to drive oceanic ventilation. To test this hypothesis, we constructed high-resolution geochemical profiles across Middle-to-Late Ordovician (472-457 Ma) marine successions from Argentina and Newfoundland. Our results reveal profound changes in the S-isotope composition of carbonate associated sulphate (CAS) and co-existing pyrite. S-isotope data are consistent with an abrupt flux of oxygen into the oceans as surface temperatures cooled, resulting in widespread ventilation of euxinic bottom waters and subsequent growth of the marine sulfate reservoir. Synchronous changes in the isotopic composition of both C and pyrite S suggest that oceanic ventilation resulted in both enhanced organic productivity and increased efficiency of pyrite burial, ultimately driving the isotopic composition of pyrite heavier than that of marine sulphate. Coincidence of superheavy pyrite with marine Sr-isotope change supports a critical increase in iron delivery to the oceans, most likely from hydrothermal sources associated with seafloor spreading. This unique dataset demonstrates that deep-water euxinia and the complex C-S relationships that result from these conditions persisted through at least the Middle Ordovician.

1. Introduction

The terminal Ordovician is marked by a dramatic shift in global climate resulting in widespread glaciation and the catastrophic extinction of >100 marine invertebrate families (Finnegan et al., in press; Brenchley et al., 1994; Sheehan, 2001). Recent evidence, however, suggests that the transition to icehouse conditions may have occurred as early as the Katian (Saltzman and Young, 2005; Pope and Steffen, 2003; Young et al., 2010) in association with oceanic ventilation, enhanced productivity, and atmospheric CO_2 drawdown (Saltzman, 2005). Oxygen-isotope measurements of conodont phosphate (Trotter et al., 2008), however, indicate conditions for oceanic ventilation may have been initiated 10 Myr earlier, in the Darriwilian. In order to better understand oceanic ventilation and the timing of the greenhouse to icehouse transition, we focus on marine geochemical records from the Middle-to-Late Ordovician of western Newfoundland and the Argentina Precordillera (Figure 3.1). Biostratigraphically correlated sections include critical intervals defined by variation in SST (Trotter et al., 2008) and a prominent decrease in marine $^{87}Sr/^{86}Sr$ (Shields et al., 2003; Young et al., 2009). Sections comprise dominantly open marine, subtidal environments in tropical to high paleolatitudes, respectively, and geochemical comparison of correlative intervals supports the global nature of observed isotopic trends (see supplementary information for discussion of sections and preservation of geochemical records).

Our understanding of Middle-to-Late Ordovician marine geochemical change is rooted within studies of Proterozoic and earlier Paleozoic seawater proxies. High resolution S-isotope data from Proterozoic (Kah et al., 2004; Hurtgen et al., 2006; Fike et al., 2006; Ries et al., 2009) and Cambrian (Hurtgen et al., 2009; Gill et al., 2011) successions show rapid fluctuation in $\delta^{34}S$ compositions of CAS (herein designated δ_{SO4}) that indicate low concentrations and non-conservative behavior of marine sulphate. Time-dependent models (Hurtgen et al., 2009; Gill et al., 2011), fluid inclusions (Horita et al., 2002; Brennan et al., 2004), and a combination of C/S ratios and Mo concentration (Gill et al., 2011) from late Cambrian strata further indicate sulphate concentrations <2-12 mM and suggest the persistence of regional euxinic conditions that first arose in the Proterozoic (Canfield, 1998).

2. Results and interpretation

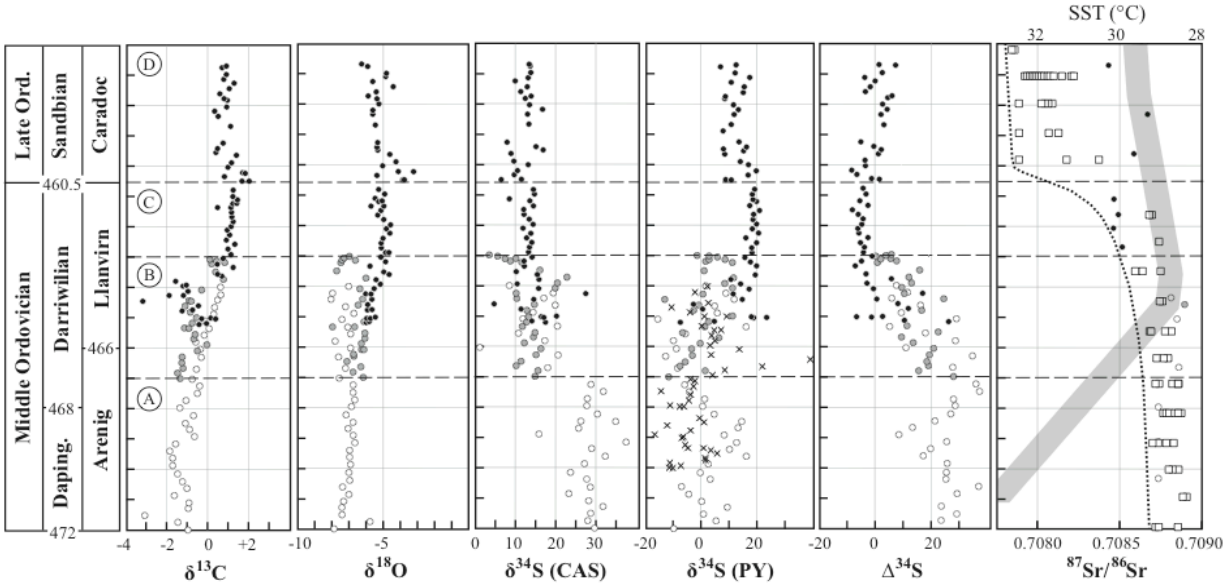

Figure 3.1. Chemostratigraphic data for Middle to Late Ordovician marine rocks of Western Newfoundland and the Argentine Precordillera. In all plots isotopic analyses are represented as follows: open circles = Table Head Group; hatch marks = Gualcamayo Formation; grey circles = Las Chacritas Formation; black circles = Las Aguaditas Formation. Open squares are $^{87}Sr/^{86}Sr$ data from Shields et al. (2003) and references therein and the sea surface temperature curve is from Trotter et al. (2008). Dotted lines separate (A) baseline values representative of pre-early Darriwilian marine systems, (B) Darriwilian transitional oceanic compositions representing dynamic disequilibrium between $[SO_4^{=}]$ and $[HS^-]$ reservoirs, (C) Late Darriwilian interval of superheavy pyrite representing maximum extent of disequilibrium between $[SO_4^{=}]$ and $[HS^-]$ reservoirs, and (D) inferred end of the period of dynamic disequilibrium. Stable isotope values are recorded in parts per thousand (‰) relative to VPDB (for carbon and oxygen) and VCDT (for sulfur) with an analytical error of ±0.2 or better.

Results (Figure 3.1) suggest that euxinic conditions likely persisted through at least the Middle Ordovician. Preserved isotopic fractionation between sulphate and sulphide (ΔS) is distinctly less than that commonly attributed to fractionation effects associated with bacterial sulfate reduction (BSR) and S-disproportionation in the oxidative part of the sulphur cycle (Canfield and Teske, 1996). Non-photosynthetic sulfide-oxidizing bacteria responsible for S-disproportionation were well established by the Neoproterozoic (Johnston et al., 2005), so a diminished ΔS likely reflects a combination of low sulfate concentration and syngenetic pyrite formation within a euxinic water column (Hurtgen et al., 2005). Euxinic conditions are also supported by low C/S ratios (=0.82; Berner, 1984) and rapid fluctuations in δ_{SO4}, which are interpreted to reflect transient perturbations associated with a fluctuating marine oxycline.

An abrupt 15‰ shift in δ_{SO4} in the Darriwilian (c. 467 Myr), however, marks a profound perturbation from steady-state conditions. We suggest that disequilibrium conditions arose from a combination of decreased pyrite burial and oxidation of a deep-water HS^- reservoir as cooling SSTs initiated deep ocean ventilation. In the aftermath of this event, the isotopic composition of both marine C and pyrite S increase, with a 20‰ shift in F_{PY} culminating in an interval of superheavy pyrite and unusual inverse fractionation between sulfate and sulfide reservoirs ($\Delta S = \delta_{SO4} - \delta_{PY}$) that persisted for >3 Myr, into the Late Ordovician. Across this same interval, Sr-isotopes reveal a remarkable stepwise decline in $^{87}Sr/^{86}Sr$ (0.7087 to 0.7079), with notably lower values in the late Darriwilian than previously reported (Shields et al., 2003; Young et al., 2009). Observed records of C, S, and Sr can plausibly be linked through enhanced nutrient delivery to the oceans, wherein oceanic ventilation reduced nitrogen-limitation and stimulated organic productivity, and iron delivery associated with enhanced hydrothermal input increased the efficacy of pyrite burial. Alternatively, it has been suggested that Sr-isotope change could be related to input of Sr from rapidly weathered juvenile volcanic rocks (Young et al., 2009), although widespread Ordovician ash falls both pre-date and post-date observed Sr- and S-isotope anomalies.

Using time-series isotopic data to test hypotheses regarding persistent euxinia and oceanic ventilation requires consideration of a model for S-cycling in which the Earth's oceans are

represented by two distinct pools of reactive sulphur (Figure 3.2; cf. Rothman et al., 2003). In a single-reservoir model, the size (M_{SO4}) and composition (δ_{SO4}) of the marine sulphate reservoir is controlled through time by the balance of input flux via weathering (F_W, δ_W) and output fluxes of S as gypsum or CAS (F_{SO4}, = δ_{SO4}) and pyrite (F_{PY}, δ_{PY}). Assuming the steady-state condition that $Fw = F_{SO4} + F_{PY}$ and that the pyrite fraction of the output flux can be expressed as $f_{PY} = F_{PY} / [F_{PY} + F_{SO4}]$, this relationship can be expressed as:

$$\partial\delta_{SO4}/\partial t = 1/M_{SO4} * [F_W (\delta_W - \delta_{SO4}) - (F_{PY} \cdot \Delta S)] \qquad [1]$$

Significant kinetic isotope effects associated with BSR make F_{PY} the primary driver of changes in the isotopic composition of the marine sulphate reservoir. By contrast, consideration of a dual-reservoir model requires that the isotopic composition of the marine sulphate reservoir be influenced directly by F_{PY} only when the fluxes between the two reservoirs (F_{BSR} and bacterial or abiotic sulphide oxidation, F_{OX}) are in equilibrium as, for instance, under very low oxygen conditions of the Proterozoic. Under conditions of enhanced marine oxygenation, increased F_{OX} may mask the effect of F_{PY}. Similarly, increased anoxia may lead to enhanced water column BSR and an increase in the size of the marine sulphide reservoir—assuming that the supply of soluble Fe^{2+} is insufficient for quantitative removal of HS^- as pyrite. Availability of Fe^{2+} will, as well, affect the degree to which BSR fractionation (ΔS_1) is recorded in the isotopic composition of F_{PY} (Hurtgen et al., 2005). We conclude that the relationships afforded by a dual-reservoir model are essential for a more complete understanding of the Early Paleozoic sulphur cycle.

At 467 Ma, S-isotope data record an abrupt shift in marine δ_{SO4} from 30‰ to 15‰ (Figure 3.1). In terms of a single-reservoir steady-state model, maximum rates of isotopic change are reached when S input to the oceans approaches zero (F_W=0) and the standing marine sulphate reservoir is removed in its reduced form (F_{PY}) giving, from equation [1]:

$$\partial\delta_{SO4}/\partial t = (F_W * \Delta S) * 1/M_{SO4} \qquad [2]$$

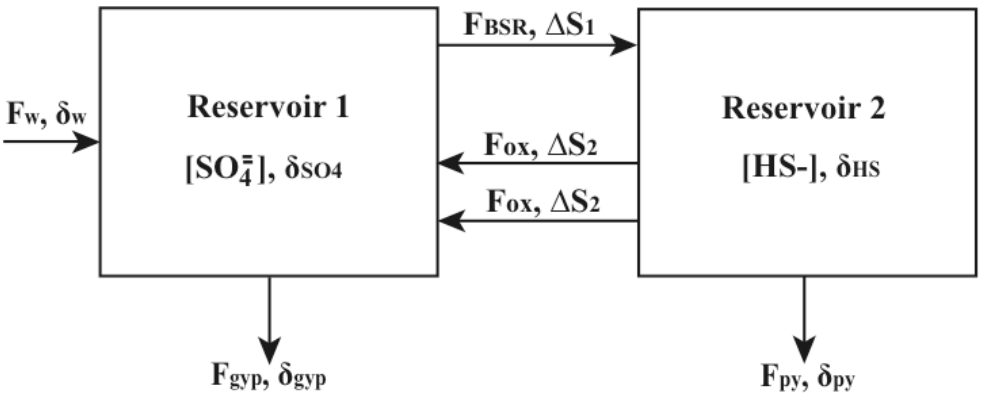

Figure 3.2. Dual reservoir model of sulfur cycling in early Earth oceans. Marine sulfur is divided into two chemically distinct reservoirs: sulfate [$SO_4^{=}$] and reduced sulfur [HS^-], which includes all transient reduced sulfur species. Fluxes and their isotopic compositions include input from crustal weathering (F_W, δ_W), output via deposition of sedimentary sulfates (F_{GYP}, δ_{GYP}) or pyrite (F_{PY}, δ_{PY}), and bacterial sulfur reduction with or without expression of sulfur disproportionation (F_{BSR}, ΔS_1). In terms of model application, although biotic and abiotic sulfide oxidation (ΔS_2) are associated with substantially different fractionations (Fry et al., 1988; Kaplan and Rittenburg, 1964), difficulty in distinguishing oxidation pathways will results in condensation of these terms into a single flux. In a dual reservoir system (cf. Rothman et al., 2003), model behavior is indistinguishable from a single reservoir model (Canfield, 2001) when $F_{BSR} = F_{OX}$. When $F_{BSR} \neq F_{OX}$, F_{PY} is decoupled from F_{BSR} and represents $F_{PY} = F_{BSR} - F_{OX}$ indicating a dynamically maintained disequilibrium between the two reservoirs. In this dynamic system, the rate of processes acting as fluxes between the two reservoirs is critical to understanding the relative behavior of the reservoirs (Rothman et al., 2003), where rates shorter than the residence time of the larger reservoir, but shorter than the residence time of the smaller reservoir will affect the size and isotopic composition of the smaller reservoir, but will have no effect on the larger reservoir. Additionally, behavior of this dual reservoir sulfur model will also be affected by availability of organic carbon and reactive iron. Organic carbon may act as a limiting factor in either bacterial sulfate reduction or biological sulfide oxidation and availability of reactive iron can limit pyrite burial relative to bacterial sulfate reduction rates.

In terms of a dual-reservoir model, this relationship assumes that F_W includes potential input from F_{OX}, and that F_{PY} includes sulphate removed as either pyrite or HS^- (F_{BSR}). Thus, the rapid (<0.5 Myr) isotopic shift recorded in early Darriwilian CAS suggests a maximum marine reservoir size of approximately 1.5 to $1.7x10^{18}$ mol (1-2 mM), and potentially less if isotopic compositions record only a fraction of maximum isotopic change (Kah et al., 2004). This abrupt change in marine δ_{SO4} occurs coincident with marine equatorial SSTs reaching their lowest point in >25 Myr (Trotter et al., 2008). From this perspective, it seems plausible that lower equatorial SSTs reflect global cooling in the Darriwilian, intensified thermohaline circulation, and delivery of cool, oxygenated waters to the deep ocean (Figure 3.3).

This conceptual model is tested through calculation fluxes of F_{PY} from single- and dual-reservoir models in order to better estimate the extent of HS^- oxidation. A critical difference between single- and dual-reservoir models is that, in a single-reservoir model, F_{PY} is presumed to reflect all byproducts of BSR that are not immediately reoxidized to sulfate and intermediate sulphide species (up to 95% HS^- in modern oceans; Jørgensen et al., 1990). In a dual-reservoir model, F_{BSR} (and F_{OX}) are decoupled from F_{PY} in such a way that F_{BSR} reflects all byproducts of BSR that are not immediately reoxidized to sulphate (e.g. the flux of HS^- available for oxidation, F_{OX}), and F_{PY} reflects only sulphide species that are transformed into syngenetic or diagenetic pyrite. Thus, an estimation of the oxidized flux can be determined by modeling the single-reservoir, steady-state F_{PY} before (F_{PY1} which, in our dual-reservoir model, equals $F_{PY} + F_{BSR}$) and after (F_{PY2} which, in our model equals $F_{PY} + F_{BSR} - F_{OX}$) the observed change in δ_{SO4}. Our results indicate that approximately $1.5x10^{18}$ mol (1 mM) of HS^- was oxidized during this event.

Both modeled C/S ratios (=1.8) and observed short-term variation in δ_{SO4} suggest that euxinic conditions likely persisted in the aftermath of this oxidation event, although the oxidation of approximately $1.5x10^{18}$ mol of HS^- had substantial effects on the evolution of Ordovician marine biogeochemical cycles: first, the oxidation event increased the marine sulphate reservoir by 50-100%; second, a substantial decrease in euxinia is proposed to have resulted in a reduction of N-limitation via anoxic denitrification (Saltzman, 2005) and an increase in organic carbon production; and third, rapid oxidation of a reactive HS^- reservoir resulted in a dynamic

Figure 3.3. Conceptual model of sulfur cycling in the early Paleozoic. Individual panels correspond to time steps (A), (B), and (C) in Figure 3.1. Reservoir labels [$SO_4^{=}$] and [HS^-] correspond to dual, reactive reservoirs in Figure 3.1. (A) Pre-early Darriwilian marine systems express evidence for low oceanic sulfate concentration and the presence of sulfidic deep oceans (Ries et al., 2009; Hurtgen et al., 2009; this study). Under such conditions, nitrogen limitation arises because the area of oxic substrate available for nitrogen fixation is reduced relative to anoxic substrate, which promotes denitrification (Saltzman, 2005). Transient variability in δ_{SO4} likely represents a low level of disequilibrium between [$SO_4^{=}$] and [HS^-]. Over longer time scales, F_{BSR} and F_{OX} are in dynamic disequilibrium. Under such conditions, calculation of F_{PY} from a single reservoir model of sulfur cycling will give a value that includes both pyrite burial and bacterial sulfate reduction. (B) Long-term cooling of oceans (Trotter et al., 2008) results in enhanced flux of cool, oxygen-rich surface waters to the deep ocean and substantial oxidation of hydrogen sulfide, initiating a period of dynamic disequilibrium between the [$SO_4^{=}$] and [HS^-] reservoirs. Effects of oxidation are recorded immediately in δ_{SO4} with only a delayed response in δ_{PY}, suggesting that [HS^-] was initially much larger than [$SO_4^{=}$]. Diminished anoxia is suggested to have reduced denitrification and increased nitrogen availability (Saltzman, 2005) promoting enhanced organic productivity. Decreased ΔS is interpreted to reflect a combination of increased F_{PY} relative to F_{BSR} under more oxygenated conditions and change in the isotopic composition of [HS^-] resulting from a kinetic isotope effects associated with a combination of biotic and abiotic sulfide oxidation (Fry et al., 1988; Kaplan and Rittenberg, 1964). (C) A continuation of $F_{PY} > F_{BSR}$, potentially enhanced by progressive cooling, in addition to more vigorous oceanographic oxidation of [HS^-] and depletion of euxinic conditions (shown here), results in superheavy pyrite (i.e. $\Delta S < 0$) formation. Isotope effects associated with dynamic disequilibrium can occur over time scales longer that the residence time of the larger reservoir (Rothman et al., 2003). We interpret the end of consistently superheavy pyrite values to mark the nominal end of dynamic disequilibrium conditions.

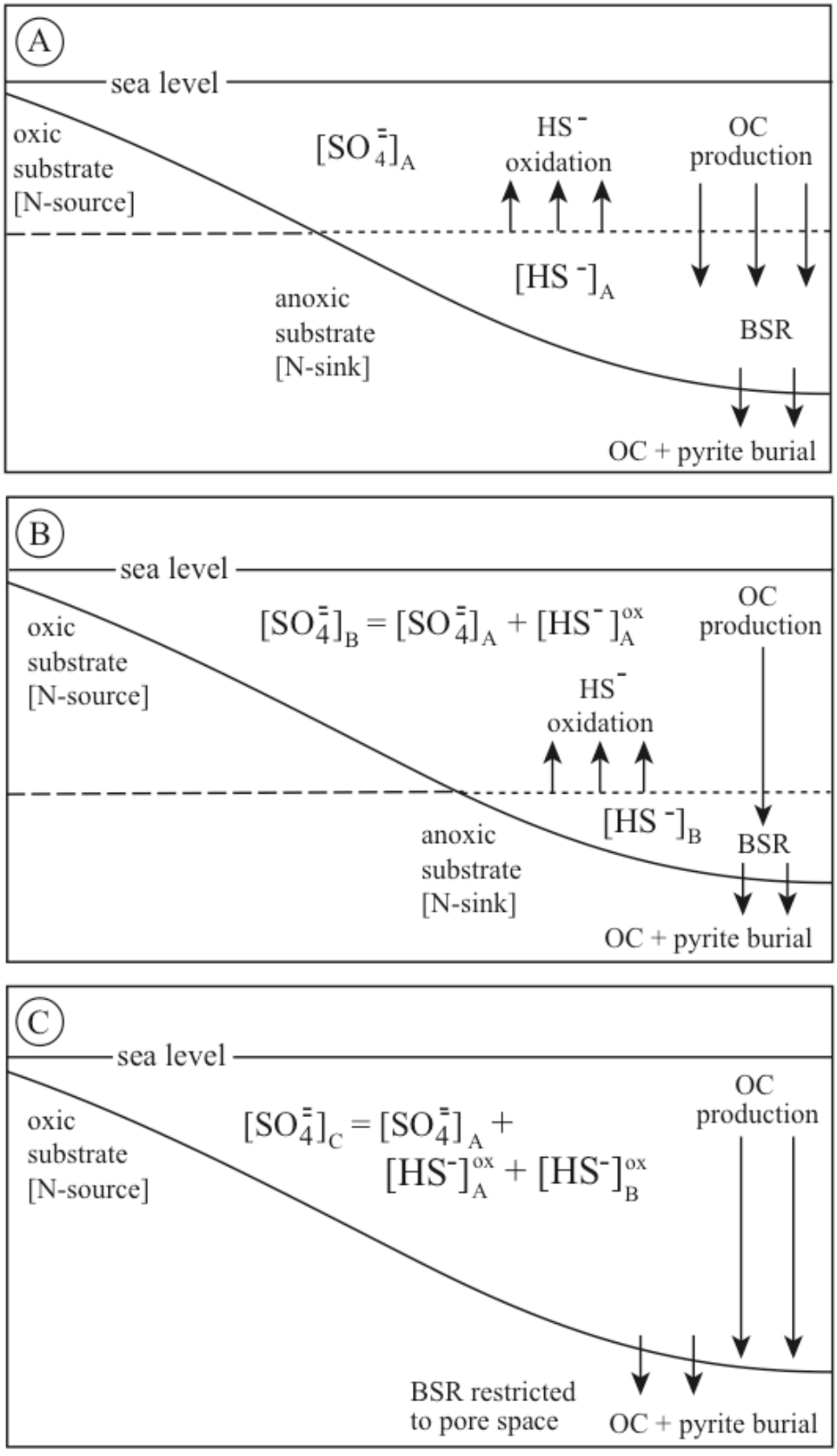
A
sea level
oxic
substrate
[N-source]
$[SO_4^{=}]_A$
HS^-
oxidation
OC
production
$[HS^-]_A$
anoxic
substrate
[N-sink]
BSR
OC + pyrite burial
B
sea level
oxic
substrate
[N-source]
$[SO_4^{=}]_B = [SO_4^{=}]_A + [HS^-]_A^{ox}$
OC
production
HS^-
oxidation
$[HS^-]_B$
anoxic
substrate
[N-sink]
BSR
OC + pyrite burial
C
sea level
oxic
substrate
[N-source]
$[SO_4^{=}]_C = [SO_4^{=}]_A +$
$[HS^-]_A^{ox} + [HS^-]_B^{ox}$
OC
production
BSR restricted
to pore space
OC + pyrite burial

disequilibrium that potentially persisted for time scales much longer than the residence time of marine sulfate (cf. Rothman et al., 2003). Although we do not observe an increase in CAS abundance in our samples across the ventilation interval, increased organic carbon burial is predicted from the >2‰ positive shift in $\delta^{13}C$ after 467 Ma, which persists for at least 11 Myr.

Evidence for dynamic disequilibrium between oxidized and reduced water masses is observed in the behavior of δ_{PY} in the aftermath of HS^- oxidation (Figure 3.1). In the four Myr after the HS^- oxidation event, δ_{PY} increases from 0‰ to 20‰, with a concomitant decrease in ΔS to approximately -5‰, which persists for an additional three Myr. Values of $\Delta S<0$ are contrary to traditional understanding of pyrite formation where pyrite is derived from coeval marine sulphate (Canfield, 2001). This data represents the first report of "superheavy" pyrite from Paleozoic strata. Earlier studies attribute $\Delta S<0$ in the Proterozoic to either Rayleigh distillation within a sulphate-poor water body decoupled from overlying sulphate-rich waters (Tie-bing et al., 2006; Shen et al., 2008), or to fractionation effects associated with intense aerobic reoxidation of sedimentary sulfide (Ries et al., 2009). Experimental data suggests that residual sulphide is enriched by 4-5‰ for abiotic oxidation (Fry et al., 1988) and up to 18‰ for biotic oxidation (Kaplan and Rittenberg, 1964). We suggest that superheavy pyrite reflects both an increase in F_{PY} relative to F_{BSR} and a change in the isotopic composition of the HS^- reservoir resulting from HS^- oxidation during progressive oceanic ventilation. Furthermore, a global rise in sea level—reflected by a rapid decrease in $^{87}Sr/^{86}Sr$ beginning at 463 Myr (Figure 3.1)—may have enhanced production of cool, oxygenated waters and their delivery to the deep ocean, accelerating oxidation of the remaining HS^- reservoir and resulting in the disappearance of short-term δ_{SO4} variability and predominance of superheavy pyrite (Figure 3.3).

3. Conclusions

Data presented here lend new insight into the complex linkages between Ordovician ocean chemistry and climate, and provide a temporal framework for understanding the biological responses to deep ocean ventilation. Elevated SSTs during greenhouse climates of the early Middle Ordovician resulted in sluggish oceanic circulation, enhanced ocean anoxia and

maintenance of a substantial HS^- reservoir. Ventilation of the deep oceans, driven by a progressive reduction in SST, began in the early Darriwilian—10 Myr before the traditional onset of icehouse climates—and is marked by the widespread oxidation of a deep-ocean HS^- reservoir and establishment of a dynamic disequilibrium between $SO_4^=$ and HS^- reservoirs. Together, results from this study suggest a dynamic and rapidly evolving Ordovician system sensitive to environmental perturbations, wherein long-term cooling initiated in the Darriwilian ultimately progressed into full-scale glaciation and mass extinction some 25 Myr later.

4. Supplementary online material

4.1. Geologic setting

Cambrian-Ordovician marine carbonate and siliciclastic rocks outcrop in large sections in both the Argentine Precordillera (Baldis et al., 1984; Ramos, 1986) and Western Newfoundland (Williams and Stevens, 1974; James et al., 1989). Although both localities preserve carbonate platform deposition in the Iapetus ocean, Ordovician biostratigraphic and paleomagnetic records place Western Newfoundland at near equatorial latitudes (Ross and Ingham, 1970; Hall and Evans, 1988; Neuman and Harper, 1992; Cocks and McKerrow, 1993; Harper et al, 1996) while the Argentine Precordillera was positioned at higher latitudes in the southern hemisphere (Figure 3.4; Herrera and Benedetto, 1991; Niocaill et al., 1997). Although relatively few absolute chronostratigraphic dates exist for these successions, abundant biostratigraphic work has provided the basis for the time-correlation of these geographically widespread successions (Herrera and Benedetto, 1991; Lehnert and Keller, 1994; Astini et al., 1995; Albanesi and Ortega, 2002).

4.1.1. Precordilleran sections, Argentina

Lower Paleozoic strata of the Argentine Precordillera comprise >2500 meters of siliciclastic, carbonate, evaporite-bearing and mafic rocks that record rifting of the Precordilleran microcontinent from the southeast margin of Laurentia in the Cambrian (Thomas and Astini,

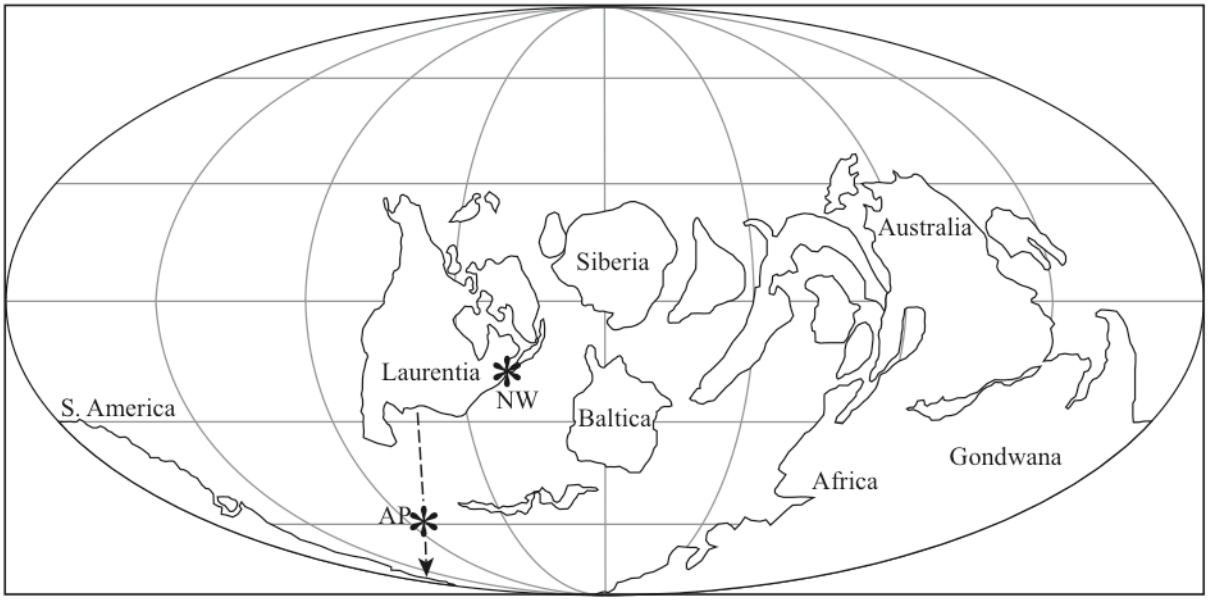

Figure 3.4. Paleogeographic reconstruction of the Middle-Late Ordovician (late Darriwilian to early Sandbian) landmasses (adapted from Scotese and McKerrow, 1990). The approximate locations of sections sampled for this study are marked by asterisks. The Argentine Precordillera drifted southward towards Gondwana during the Ordovician. Western Newfoundland sections were located closer to equatorial latitudes.

1996; 1999), its subsequent drift across the Iapetus ocean during the Early Ordovician, and eventual docking with Gondwana in the Middle to Late Ordovician (Ramos, 1988; Benedetto et al., 1999). Precordilleran docking with Gondwana is marked by the formation of the Famatinian volcanic arc, which is the source of widespread bentonites in Middle Ordovician San Juan strata of the Argentine Precordillera (Huff et al., 1998). Several discrete K-bentonites have been dated using zircon U-Pb zircon geochronology techniques and give a Dapingian-early Darriwilian age (469.5 ±3.2 Mya, 470.1 ±3.3 Mya; Fanning et al., 2004; 464 ±2 Mya; Huff et al., 1997) for the pre-docking stage of the Precordillera.

The Precordilleran terrane was uplifted by east-directed faulting of the Andean thrust belt and currently is exposed along the western margin of Argentina, striking north-south along the eastern margin of the Andean mountain range between 28°45′S and 33°15′S (Figure 3.5; Ramos, 1988; 2004). Strata are subdivided into eastern and western tectofacies, which record carbonate, siliciclastic, and evaporite platform deposition on the Precordilleran platform and outer platform, respectively. Outer platform deposits, in particular, include slump features and mafic to ultramafic sills, and lava flows (Thomas and Astini, 2003). Sections sampled for this study, including the Gualcamayo, Las Chacritas and Las Aguaditas formations, represent Late Dapingian to early Sandbian-aged strata of the eastern tectofacies (Figure 3.5 and 3.6).

4.1.1.1. Gualcamayo Formation

Carbonaceous and graptolitic black shale deposits of the Gualcamayo Formation overlie San Juan Formation limestone and are overlain by thick carbonate breccias of the Trapiche Formation (Astini et al., 1995). The Gualcamayo Formation is interpreted to reflect regional drowning of the San Juan carbonate platform during a combination of global transgression and regional subsidence related to the collision of the Precordilleran terrane with Gondwana (Astini, 1995; Cañas, 1995). The contact between the Gualcamayo and San Juan Formation is regionally diachronous (Astini, 1995; Albanesi et al., 1999), and reflects differential subsidence during the docking of the Precordilleran microcontinent (Astini, 1995).

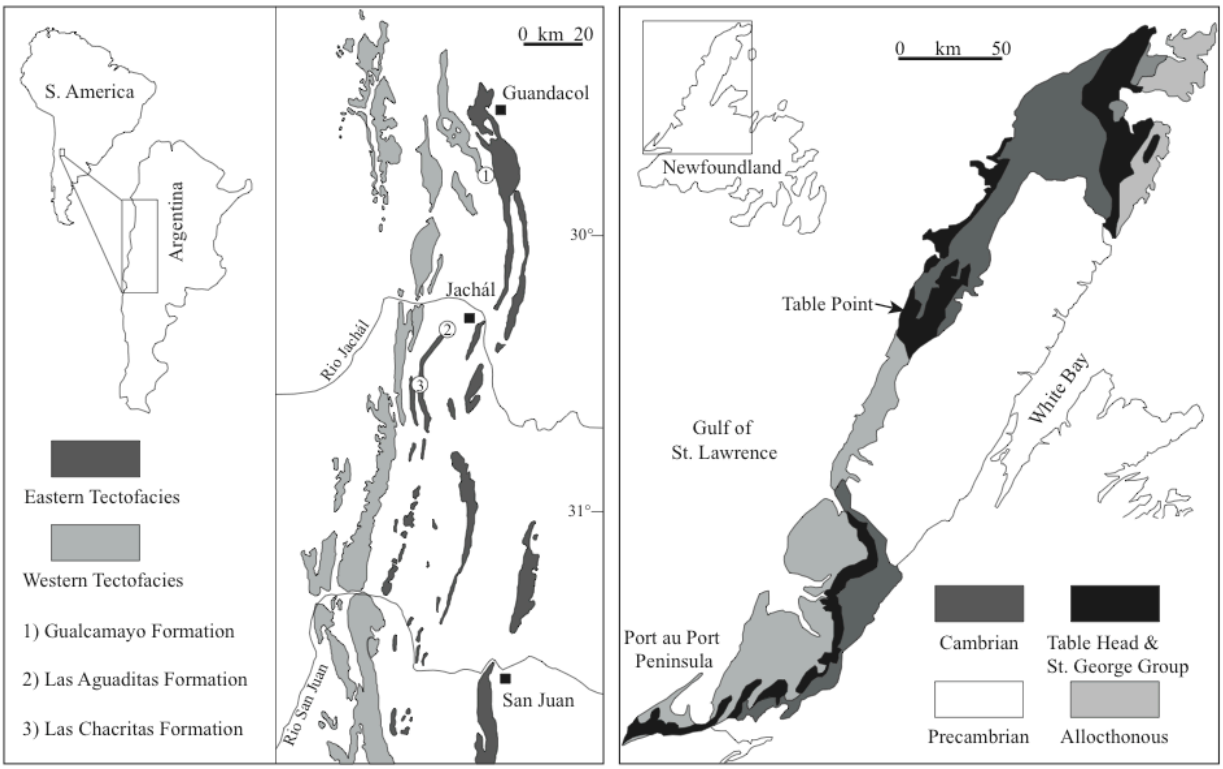

Figure 3.5. Geologic map of the Argentine Precordillera in western Argentina and the Humber Zone of the Appalachian-Caledonian fold belt in Western Newfoundland. Figures were adapted from Williams et al. (1987) and Astini et al. (1995). Strata were sampled at the Las Aguaditas, Las Chacritas, and Gualcamayo formations (numbered) in the Argentine Precordillera and at Table Point (arrow) in Western Newfoundland.

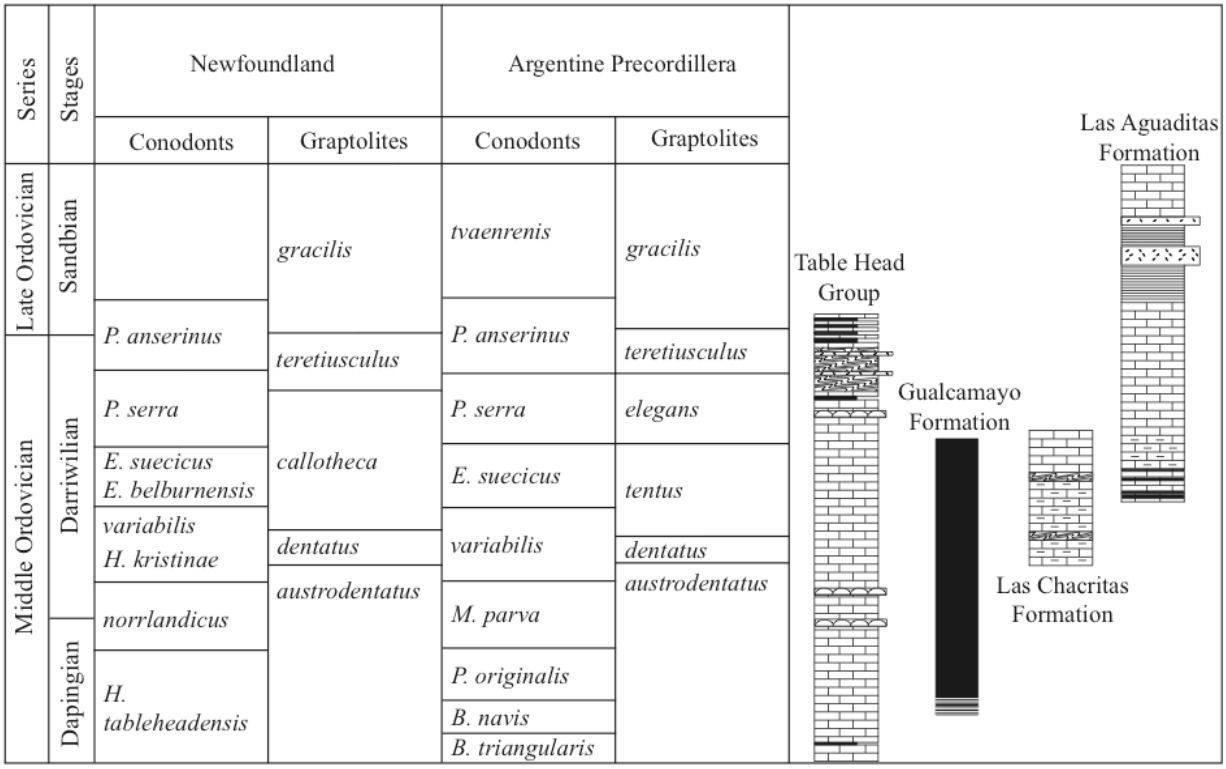

Figure 3.6. Biostratigraphic correlation of studied sections. Western Newfoundland conodont and graptolite biostratigraphic data are from Williams et al. (1987) and Argentinian conodont and graptolite biostratigraphic data are from Albanesi and Ortega (2002).

The Gualcamayo Formation was sampled at the type section, Las Corriditas Creek (29°35′41″S; 68°3′14″W), where conodont-graptolite data indicate an age spanning the Dapingian-Darriwilian (Albanesi et al., 1999). At this locality, the basal 40 meters consist of alternating platy limestone and black shale and are considered as a distinct, lower member of the Gualcamayo Formation (Figure 3.5 and 3.6; Astini, 1995; Albanesi et al., 1999). The upper 200 meters of the Gualcamayo Formation consists primarily of graptolitic black shale, which is interpreted to represent deep ramp deposition.

4.1.1.2. Las Chacritas Formation

The Las Chacritas Formation consists of 55 meters of thin to medium bedded, marly limestone and fossiliferous black shale that represents deposition in outer carbonate ramp environments (Peralta et al., 1999). The lower member (38 meters) yields conodonts of the *L. variabilis* zone indicating an early Darriwilian age (Heredia et al., 2005). Occurrence of the conodont *H. kristinae* in the very top of the Las Chacritas Formation correlates this part of the section with the internationally recognized *E. suecicus* zone and indicates a mid-Darriwilian age (Heredia et al., 2005). The Las Chacritas Formation was sampled at Las Chacritas Creek (30°33′41″ S, 68°51′49″ W), where it conformably overlies the San Juan Formation and is unconformably overlain by the Las Aguaditas Formation (Heredia et al., 2005). While the basal 38 meters are interpreted to represent outer platform deposition (Peralta et al., 1999; Heredia et al., 2005), the upper member (17 meters) is comprised of fossiliferous wackestones and mudstones that are interpreted to represent deposition in a shallow subtidal environment.

4.1.1.3. Las Aguaditas Formation

The Las Aguaditas Formation consists of ~300 meters of black shale with intercalated, mudstone and carbonate breccia, that are interpreted to represent deposition in upper slope environments (Keller et al. 1993). The Las Aguaditas Formation overlies pertidal to subtidal limestone of the San Juan Formation and is overlain by the La Chilca Formation, which records uplift and erosion

resulting from collision of the Precordilleran terrane with Gondwana (Astini, 1995; Astini et al., 1995).

The Las Aguaditas Formation was sampled at Las Aguaditas Creek (30°20′15″ S, 68°49′49″ W), where *P. tentaculatus* and *N. gracilis* graptolite zones indicate a Darriwilian to Sandbian age (Brussa, 1996). In the region sampled for this study, the Las Aguaditas Formation consists of interbedded lime mudstone and shale with abundant small-scale slump features.

4.1.2. Table Head Group, Western Newfoundland

The Table Head Group is exposed in the Humber Zone of western Newfoundland (Figure 3.5). The Table Head Group represents passive margin platform carbonate deposition during marine transgression (James et al., 1989; Knight and Cawood, 1991) and rapid drowning of the carbonate platform in the early stages of the Taconic orogeny (Stenzel et al., 1990).

Table Head Group was sampled at the type section, Table Point, in Western Newfoundland (50°22′22″ N, 57°31′44″ W), where it comprises ~300 meters of bioturbated, lime-mudstone and wackestone. These deposits yield conodonts from the *H. tableheadensis* to *P. anserinus* zone that span the Dapingian to late Darriwilian (Stouge, 1982; Williams et al., 1987). The Table Head Group conformably overlies the Aguathuna Formation, where the contact is marked by an abrupt change from coarsely-recrystalline, buff-colored dolomite to dark grey lime mudstone and wackestone. At Table Point, the Table Head Group is divided into the Table Point, Table Cove, and Black Cove formations (Stouge, 1982). The Table Point Formation represents the lower 250 meters and consists of a homogeneous succession of subtidal, bioturbated carbonate. The conformably overlying Table Cove Formation is comprised, at its base, of intercalated ribbon limestone and shale, with distinct intervals of slumping that give way to predominantly shale in the upper portion. Strata of the Table Point and Table Cove formations represent subtidal shelf deposition in an increasingly deepening environment (Stouge, 1982; Jacobi, 1981; King et al., 1991).

4.2. Geochemical methods

4.2.1. Initial petrographic screening

Samples were evaluated using standard petrographic and cathodoluminescence (CL) techniques (Hemming et al., 1989; Kaufman et al., 1991; Kah et al., 1999; Frank et al., 2003) prior to isotope and elemental analyses to evaluate secondary alteration that is a concern when constructing geochemical profiles. Mirror-image slabs of samples were cut using a water-cooled rock saw and made into thin and thick sections for petrographic and CL analysis, respectively. Petrographic analyses were used to characterize carbonate fabrics and to identify primary and secondary phases. Past studies have demonstrated that primary depositional phases, particularly micritic and fine-grained microsparitic fabrics that show little physical evidence of secondary recrystallization, often preserve geochemical signatures that also show little evidence of overprinting by diagenetic fluids (Kaufman et al., 1991; Frank et al., 2003; Bartley et al., 2007). Similarly, coarsely crystalline fabrics and secondary phases, such as spar-filled fractures and voids, commonly preserve a geochemical signal related to post-depositional fluid flow. Combined, such data permit careful evaluation of the range of geochemical signatures retrieved from samples and interpretation of the degree of diagenesis that samples have undergone.

In addition to standard petrographic analysis, cathodoluminescence petrography was used to distinguish the potential for alteration of within primary and secondary phases. Luminescence in carbonate minerals is activated by the presence of Mn^{2+} in the carbonate lattice and suppressed by the presence of Fe^{2+} (Hemming et al., 1989). Because both Mn^{2+} and Fe^{2+} are incorporated in carbonates either during deposition from or dissolution and re-precipitation within diagenetic fluids, evidence for incorporation via CL analysis provides a quick measure of the degree of alteration (Brand and Veizer, 1980; Veizer, 1983; Banner, 1995). Caution must be taken, however, since previous studies have shown that CL does not always accurately reflect alteration (Rush and Chafetz, 1990; Marshall, 1992; Savard et al., 1995), and might also reflect primary incorporation from unusual marine fluids. All samples were examined under vacuum (50-80 mtorr) using a cathodolumnescence microscope at the University of Tennessee.

After petrographic evaluation, selected regions of polished thick sections were micro-sampled using 0.5 mm dental drill bits attached to a micro-drill press. Petrographically uniform phases were drilled to retrieve 2-5 mg of powder to be used as splits for the C- and O-isotope and elemental analyses. When possible, a range of fabrics was sampled in order to compare the geochemical properties of both primary and secondary phases.

4.2.2. Carbon and oxygen isotope analyses

Microdrilled powders were stored in a desiccator prior to C- and O-isotope analyses. Each sample (1.5-2 mg) was loaded into silver capsules and reacted individually with anhydrous phosphoric acid at 90°C (Table Head Group) and 120°C (Las Chacritas and Las Aguaditas formations) and analyzed using a Carbo-Flo dual inlet Finnigan Delta Plus gas source isotope ratio mass spectrometer fitted with a auto sampler at the University of Tennessee, Knoxville. Data are reported in delta notation as per mil (‰) deviations from Vienna Pee Dee Belemnite (VPDB). Analyses were determined to be reproducible to within ±0.1‰ from analysis of duplicate samples and internal lab standards. Two internal standards were used for isotope calibration, Chihuahua calcite (CHCC; $\delta^{13}C$ = +1.35‰, $\delta^{18}O$ = –6.16‰ at 25°C) was used for the Table Head Group analyses, and Australian National University "M1" (ANU-M1: $\delta^{13}C$ = -10.66‰, $\delta^{18}O$ = -9.23‰ at 25°C) was used for the Las Chacritas and Las Aguaditas formations.

4.2.3. Major and trace element analyses

Micro-drilled carbonate phases were also analyzed for major (Ca, Mg) and trace (Sr, Mn, Fe) element concentrations. Approximately 1 mg of microdrilled powder was quantitatively dissolved in 10 mL of trace metal grade 2% HNO_3. After acidification each sample was centrifuged for 10 minutes at 3000 rpm and the top ~9 mL decanted into a clean centrifuge tube. Elemental analyses for the San Juan Formation and Table Head Group were conducted at the University of West Georgia using a Perkin-Elmer inductively coupled plasma optical emission spectrometer (ICP-OES) fitted with a Meinhardt concentric nebulizer calibrated to a series of gravimetric standards. Elemental analyses of the Las Chacritas, and Las Aguaditas formations

were completed at the University of Tennessee using a Perkin-Elmer Optima 2100 DV ICP-OES with a Scott spray chamber calibrated with a series gravimetric standards. Standards were run before and after every six unknowns. Analyses were determined to be reproducible to within ±10% by analysis of duplicate samples and standards.

4.2.4. Carbonate-associated sulfate extraction

$\delta^{34}S_{SO4}$ profiles were constructed using carbonate-associated sulfate (CAS). CAS substitutes into the carbonate lattice during initial deposition and is suggested to have potential as a proxy for the sulfur isotopic composition of marine sulfate $\delta^{34}S$ (Burdett et al., 199; Strauss, 1999). In the modern ocean, the isotopic composition of CAS ($\delta^{34}S_{CAS}$) of brachiopod shells (+21.2±0.8‰) has been shown to record mean ocean $\delta^{34}S_{SO4}$ (+20.9±0.5‰; Kampschulte et al., 2001). In ancient sediments, CAS has been demonstrated to be isotopically similar to coeval evaporite deposits (Burdett et al., 1989; Strauss, 1999; Kah et al., 2001). Additionally, $\delta^{34}S_{SO4}$ has been shown to be resistant to diagenetic alteration and retain a record of primary $\delta^{34}S_{SO4}$ despite large drops in sulfate concentration during diagenetic recrystallization (Lyons et al., 2004; Gill et al., 2008).

CAS was extracted using acid dissolution and barite precipitation methods modified from (Burdett et al., 1989; Kah et al., 2001; Hurtgen et al., 2002). Approximately 200 grams of bulk rock was first etched with 10% HCl to remove surface weathering products, then crushed and powdered. Approximately 100 grams of powdered sample was soaked overnight in 250 mL of 5.65-6% laboratory grade sodium hypochlorite (NaOCl), rinsed four times with Milli-Q water (typically 1.0-1.5 L), and filtered. Initial NaOCl leach was performed to remove soluble iron sulfide and organically bound sulfur that might oxidize to sulfate during acidification (Burdett et al., 1989). The potential for organically-bound sulfur was low since organic carbon concentration is low (<0.6 wt%) in all samples, and since organic material is dominantly kerogen, indicating that most labile organic components have long since degraded.

Dried and weighed samples were then dissolved slowly with 3M hydrochloric acid and monitored in order to maintain a pH > 3 to prevent the exchange of oxygen between sulfate and water and to minimize pyrite oxidation (Chiba and Sakai, 2002). Samples were then filtered to remove insoluble residue. The filtrate from HCl dissolutions was then brought to a pH of 9 using sodium hydroxide (NaOH) pellets to precipitate any dissolved iron oxides, and filtered. Approximately 140 mL of saturated barium chloride solution (250 g/L) was added to the filtrate to recover CAS as barium sulfate. The reaction was allowed to continue overnight to ensure complete precipitation. Barium sulfate precipitate was then filtered using 0.45 μm Millipore filters, dried at 30°C, and weighed. Sulfate concentration of samples was estimated from weight measurements of barium sulfate precipitates after extraction.

4.2.5. Pyrite extraction

Pyrite sulfur was extracted from bulk rock powders by sequential acid extraction (Canfield et al., 1986) at Indiana University. Elemental and organically-bound sulfur were extracted from approximately 5 grams of sample in a heated Soxhlet setup for 12-18 hours using 250 mL of dichloromethane. Copper pellets were submerged in the dichloromethane trap during digestion to collect elemental sulfur (S^0). Elemental sulfur was later removed from copper pellets by acid digestion under a nitrogen atmosphere and collected using silver nitrate traps. S^0 was proved to be negligible by weight. The remaining sample powders were dried under a fume hood and weighed before the next extraction step.

Acid-soluble sulfur (sulfate and monosulfide) was extracted by dissolution of powders in 6M hydrochloric acid under a nitrogen atmosphere. The resulting hydrogen sulfide gas was bubbled through a silver nitrate trap, precipitating Ag_2S. The precipitate was then filtered, dried and weighed in preparation for isotope analyses.

Pyrite sulfur was extracted from the remaining sample by dissolution in a 1:1 12N hydrochloric acid and chromium chloride solution under a nitrogen atmosphere for pyrite extraction. Like the acid soluble sulfur extraction step, the resulting hydrogen sulfide gas was bubbled through silver

nitrate traps where it precipitated as Ag_2S. Samples were filtered and dried overnight prior to weighing for isotopic analysis.

4.2.6. Sulfur isotope analyses

For S-isotope analyses, Ag_2S was weighed into tin cups along with excess V_2O_5 (~10x Ag_2S weight to ensure complete combustion). Samples were analyzed for $\delta^{34}S$ using a Finnigan MAT 252 gas source mass spectrometer fitted with an elemental analyzer at Indiana University. S-isotope composition is expressed as per mil (‰) deviation from Vienna Canyon Diablo Troilite (VCDT). Analytical precision was determined to be ±0.1‰ by analysis of four lab standards, ERE Ag_2S (-4.7‰), EMR Cp (+0.9‰), NBS 127 (+20.3‰), and PQB (+39.8‰).

4.2.7. $^{87}Sr/^{86}Sr$ analyses

Strontium was separated from ~5 mg of carbonate powder by stepwise leaching and dissolution steps. Each powder was weighed into a microcentrifuge tube and ~1 mL of 0.2M ammonium acetate monitored to have pH~8.2 was added and allowed to leach unbound Sr from the samples for one hour. The samples were then centrifuged and the leachate discarded. This step was repeated three times, and the samples were then washed with Milli-Q ultrapure water and centrifuged three times. Remaining powder was dissolved in ultra-pure 0.5M acetic acid overnight, taken to dryness under a heat lamp, and the precipitate then dissolved with 200 µl of 3M HNO_3. Strontium was isolated from the acidified fraction using Sr spec resin and a variety of acid and neutral solutions. The dried Sr fraction was dissolved in 2 µl of 3M HNO_3 and then loaded with ~0.8 µl of TaO onto a Rhenium filament and then allowed to dry under a heat lamp. Samples were loaded into a carousel for analysis on the VG Sector 54 thermal ionization mass spectrometer in the University of Maryland Geochemistry Laboratories, and each analyzed at between 1450-1650°C, which produced a stable 1V beam on mass $^{88}Sr^{+}$ that was measured with other isotopes for over 100 ratios. Repeated analysis of NBS 987 over the course of the investigation resulted in a value of 0.710250 ± 0.000008.

4.3. Preservation of geochemical signals

It is important to constrain the degree to which carbonate rocks have been altered to establish if geochemical trends are representative of primary or little-altered oceanic values (Given and Lohmann, 1985; Zempolich et al., 1988; Carpenter et al., 1991; Frank and Lohmann et al., 1996; Kah, 2000). Early diagenesis often results in the production of additional, secondary cements, whereas meteoric diagenesis can result in dissolution and recrystallization. Primary depositional components, such as skeletal grains, micrite, and marine cements have the potential to retain signatures of depositional fluids. However, all secondary fluids—meteoric fluids to deep-burial fluids to fluids involved in modern weathering—have the potential to result in recrystallization of carbonate phases and alteration of the geochemical signals.

Relative to marine carbonate rocks, meteoric fluids typically have low Sr concentration and more depleted $\delta^{18}O$ and $\delta^{13}C$ isotope compositions; if these fluids are anoxic, they may also contain substantially higher concentrations of divalent Mn and Fe (Brand and Veizer, 1980; Banner and Hanson, 1990). Numerous studies have shown that, because of the low carbon content of most diagenetic fluids, $\delta^{18}O$, Sr, Mn and Fe are much more sensitive indicators of post depositional alteration, especially at low water to rock ratios; alteration of $\delta^{13}C$, however, can occur during burial diagenesis if fluids contain large amounts of organic carbon (Kaufman et al., 1991; Brand and Veizer, 1980; Frank and Lohmann, 1996; Banner and Hanson, 1990). To help constrain the degree of alteration and the potential for preservation of geochemical trends, we compared petrographic characteristics (optical and cathodoluminescence) to geochemical (Mn, Sr, $\delta^{13}C$ and $\delta^{18}O$ and $\delta^{34}S$) characteristics.

Petrographic analyses show that carbonate samples from the Table Head Group, Las Chacritas and Las Aguaditas formations are primarily composed of micrite and microspar, with only a small degree of recrystallization. On the whole, the Table Head Group is more fine-grained than the Las Chacritas and Las Aguaditas formations, although all sections show a similar degree of recrystallization to coarser grain sizes. Fossil fragments (brachiopod, crinoid, bivalve shells, and sponge spicules) compose the majority of larger grains within the samples. Although most fossil

fragments show at least some evidence of recrystallization, many retain evidence of their primary microstructure (brachiopods and crinoid ossicles, in particular), which suggests relatively low degrees of post-depositional. Evidence for post-secondary fluid flow and burial diagenesis (spar-filled fractures, late-stage void fills, and stylolites) was present in all sections, although relatively rare in most.

Cathodoluminescence petrography (CL) was used to screen samples for diagenetic overprinting not necessarily apparent in thin sections. CL helps distinguish primary and secondary phases by revealing distribution of diagenetic indicators (Mn and Fe) in samples (Hemming et al., 1989). CL analyses of polished thick sections revealed micrite and fine-grained marine cements to be largely homogeneous, non- to dully luminescent, indicating overall low Mn concentration, which is consistent with the interpretation of these phases as having undergone only limited recrystallization. In most samples coarse-grained, spar-filled regions that were identified in thin section showed bright orange luminescence, suggesting deposition from post-depositional fluids. Additionally, many fossil fragments showed bright luminescence, supporting petrographic evidence of recrystallization. It is important to note, however, that although individual phases showed bright luminescence, these phases appear distinct from surrounding phases, indicating that diagenetic fluids did not affect the chemistry of depositional components uniformly, which further supports that dully-luminescent, fine-grained phases experienced only minimal resetting of geochemical signatures.

Although the abundance of later stage cement and spar varied stratigraphically throughout all the studied sections, there was no clear difference between the degree of alteration of one section versus another. When possible, both primary and secondary phases were sampled for C-, O-isotope, and elemental analyses to establish geochemical characteristics of endmember phases as an additional assessment of the preservation of geochemical trends. Isotopic and elemental data are provided in Tables 3.1 - 3.4.

The bulk of $\delta^{18}O$ values of primary phases fall between -4 and -8‰ (Figure 3.7). $\delta^{18}O$ values from the Table Head Group and Las Chacritas Formation broadly overlap (-6 to -8‰) and are,

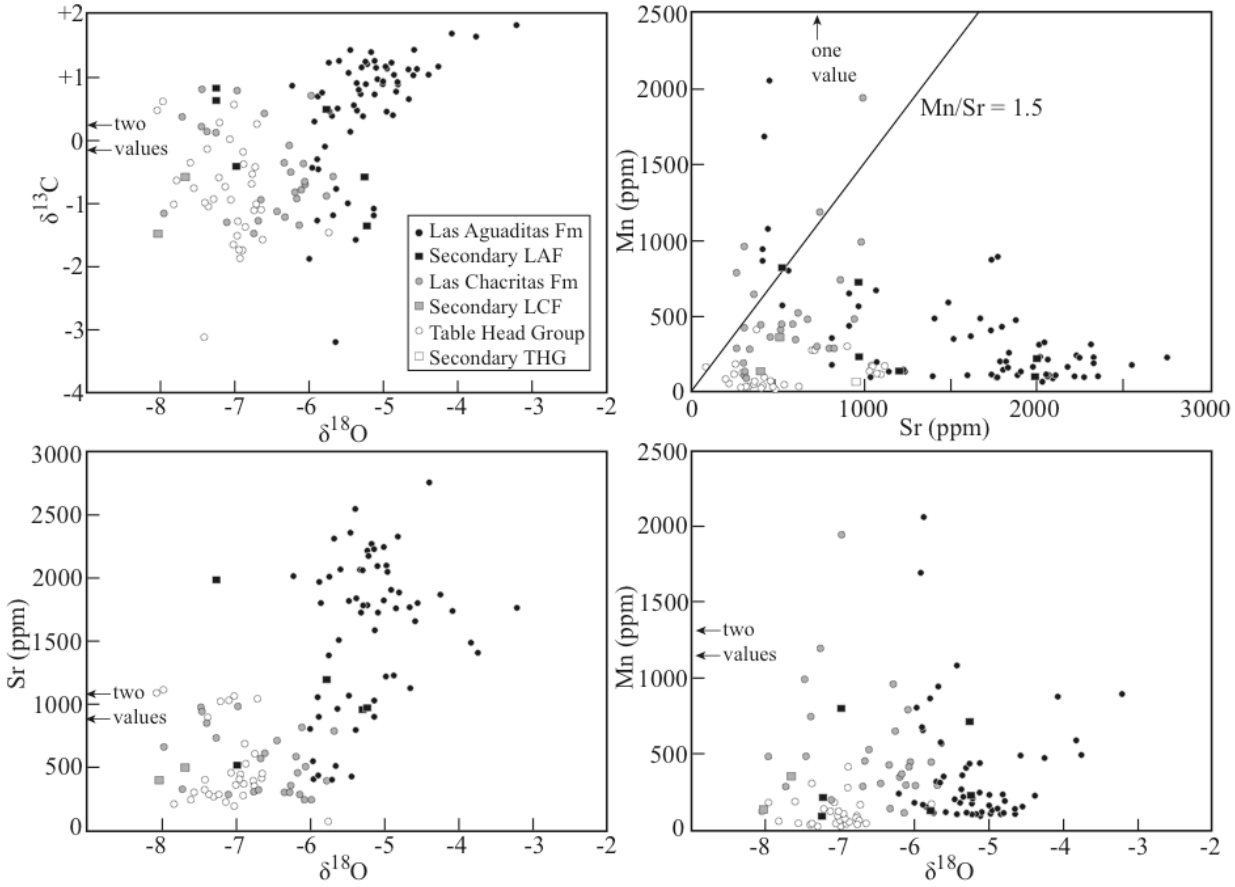

Figure 3.7. Elemental, carbon and oxygen isotope data from studied sections. Oxygen isotope values from the Table Head Group (-8.1 to -5.7‰, average -7.1‰ ±0.4) and Las Chacritas Formation (-8.0 to -5.7‰, average -6.6‰ ±0.6) broadly overlap and are, on the whole, isotopically depleted relative to the Las Aguaditas Formation (-6.2 to -3.2‰, average -5.2‰ ±0.6). Marine $\delta^{13}C$ values range from -1.9 to +2.0‰, where values average -1.3‰ ±0.6 from the Dapingian to the lower Darriwilian and increase to an average of +1.0‰ ±0.4 during the Darriwilian and into the Sandbian. Oxygen isotope values fall within the range of Ordovician values (Wadleigh and Veizer, 1992; Qing and Veizer, 1994; Veizer, 1999) and show no trend with carbon or sulfur isotopes. Mn/Sr values are consistent with well-preserved samples (<1.5) for the majority of samples and fall below the accepted value for little altered carbonate rocks (4.0).

on the whole, isotopically depleted by ~2‰ relative to the Las Aguaditas Formation (-4 to -6‰). All of these values fall within the range of data from other well-preserved, non-evaporative carbonate units (Wadleigh and Veizer, 1992; Qing and Veizer, 1994; Veizer, 1999). Since O-isotopes are easily exchanged during diagenesis, $\delta^{18}O$ values more positive than -8‰ in primary phases is generally interpreted to represent good preservation; more positive isotopic values in the Las Aguaditas Formation suggest this section may represent a slightly lesser degree of post-depositional alteration. $\delta^{18}O$ values of identified secondary phases are generally depleted relative to micrite $\delta^{18}O$ by <4‰ in the Table Head Group, <2‰ in the Las Chacritas Formation and <1‰ in the Las Aguaditas Formation. Another possibility is that generally heavier values in the younger Las Aguaditas Formation preserve secular change in the isotopic composition of marine $\delta^{18}O$, such as that inferred from previous studies of Ordovician brachiopods that show $\delta^{18}O$ values generally increasing through the Ordovician (Wadleigh and Veizer, 1992; Qing and Veizer, 1994; Veizer, 1999). Critically, the corresponding values of $\delta^{13}C$ of secondary phases, however, were identical to micrite $\delta^{13}C$ in the Table Head Group and depleted by 0.6‰ in the Las Chacritas Formation and 0.2‰ in the Las Aguaditas Formation, suggesting diagenetic overprinting did not alter $\delta^{13}C$ values.

Mn and Sr concentrations also provide insight into the degree of alteration experienced by these samples, since they are altered quickly in the presence of secondary fluids (Banner and Hanson, 1990). Sr values fall primarily between 200-2000 ppm (Figure 3.7), which are typical for marine calcites that have undergone limited exchange with post-depositional fluids (Banner and Hanson, 1990). Highest Sr concentrations occur in the Las Aguaditas Formation, which might support O-isotope evidence for more limited exchange by post-depositional fluids. Similarly, Mn concentrations fall largely below 500 ppm, with all but 5 values (3 in Las Aguaditas and 2 in Las Chacritas) falling below 1000 ppm (Figure 3.6). Mn concentration below 500 ppm suggests relatively limited water/rock interaction (Banner and Hanson, 1990). Unlike Sr, there is no difference in Mn concentration among the three units. In nearly all samples, Mn/Sr falls below 1.5, which is a common standard for samples that have undergone only limited postdepositional alteration[70]. For both Mn and Sr, there is no clear evidence that alteration proceeded to such a degree as to affect C-isotope values of the samples.

The bulk of marine $\delta^{13}C$ values lie between -1.5 and +1.5‰ (Figure 3.6). A further test of the preservation of marine $\delta^{13}C$ values is comparison with coeval C-isotope records. C-isotope records presented here provide a broadly coherent signal with only rare deviations (e.g. Argentine sections show slightly more negative values that the Newfoundland section from 465-464 Ma; Figure 3.2) that plausibly represent true oceanic heterogeneity (Saltzman, 2000; Saltzman et al., 2004). C-isotope data in this study, however, are strikingly consistent with data from published curves for Middle Ordovician marine carbonate rocks (Wadleigh and Veizer, 1992; Qing and Veizer, 1994; Ainsaar et al., 1999; Buggisch et al., 2003; Saltzman, 2005; Saltzman and Young, 2005). Within this global context, we see that even the most positive values, recorded as a positive shift in $\delta^{13}C$ in the Las Aguaditas Formation, is coeval to a small, globally-correlatable shift in $\delta^{13}C$ (Middle Darriwilian carbon isotope excursion or MDICE; Ainsaar et al., 2010).

Although we would suggest that carbonate rocks sampled in this study preserve reliable records of marine $\delta^{13}C$, we consider whether $\delta^{34}S_{CAS}$ is likely to preserve a reliable record of marine $\delta^{34}S$. A cross plot of $\delta^{34}S_{CAS}$ and $\delta^{18}O$ shows no clear correlation in any of the studied sections (Figure 3.8). In particular, the Table Head Group, which represents an interval where $\delta^{34}S_{CAS}$ shows dramatic stratigraphic variability, reveals a large spread in $\delta^{34}S_{CAS}$ over a only about a 1.5‰ range in $\delta^{18}O$, suggesting that variation in $\delta^{34}S_{CAS}$ is not related to post-depositional alteration. Similarly, although the Las Chacritas and Las Aguaditas show a broader range in $\delta^{18}O$, there is no clear correlation with $\delta^{34}S_{CAS}$ that might suggest covariance resulting from postdepositional alteration. This same pattern is apparent when examining different indicators of diagenesis: the greatest variability in $\delta^{34}S_{CAS}$ corresponds to samples that all show very low Mn concentrations. Furthermore, if we consider the potential for alteration by the addition of oxidized sulfide either during sub-recent weathering or during the CAS extraction (Marenco et al., 2008; Mazumder et al., 2008), we find no correlation between $\delta^{34}S_{CAS}$ and the concentration of either CAS or pyrite (Figure 3.8). Together, these observations suggest that measured $\delta^{34}S_{CAS}$ compositions were not affected by pyrite oxidation. These interpretations are consistent with other studies (Burdett et al., 1989; Kampschulte et al., 2001; Lyons et al., 2004; Gill et al., 2008),

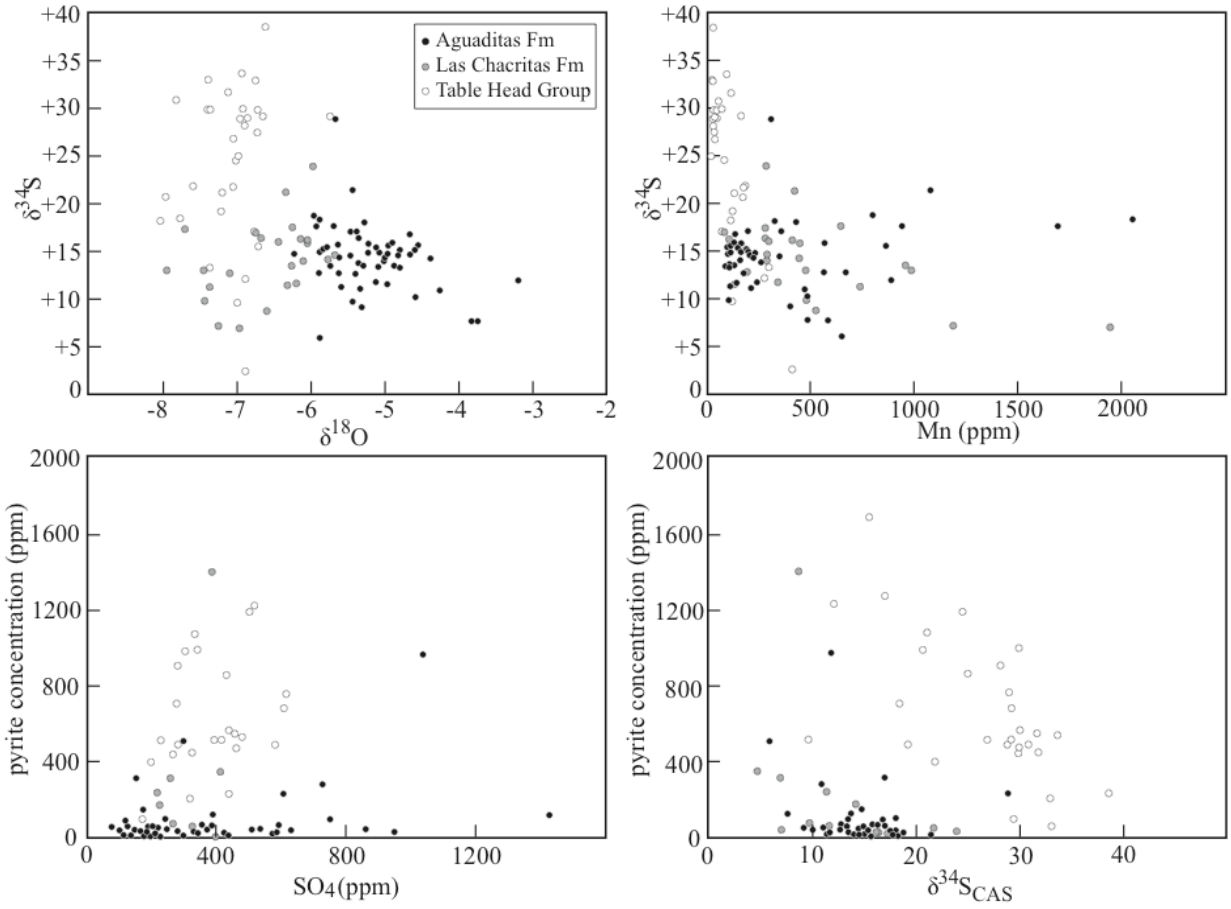

Figure 3.8. Elemental and sulfur isotope data from the studied sections. Sulfur isotope values range from +2.6 to +38.6‰ in the Table Head Group, from +4.8 to +24.0‰ (average (+24.9 ±8.1‰), in the Las Chacritas Formation, and from +6.0 to 28.9‰ (average +4.6 ±3.4‰) in the Las Aguaditas Formation. Sulfur isotope values from all sections overlap and fall within the range reported for the Ordovician, although the Table Head Group shows the largest range. Sulfur isotope values are not correlated with $\delta^{18}O$ or Mn concentration. Likewise, pyrite concentration is not correlated with SO_4 concentration or $\delta^{34}S$ as would be expected if sulfide oxidation contributed to sulfate during the extraction process.

which suggest that CAS faithfully records marine $\delta^{34}S$ in samples of minor to moderate diagenetic recrystallization.

Because Sr is particularly susceptible to alteration, it is necessary to evaluate $^{87}Sr/^{86}Sr$ values for diagenetic overprinting as well. Samples with aforementioned indicators of well-preserved carbonates (elevated Sr concentration, moderate $\delta^{18}O$ values, low Mn concentration, little petrographic indication of recrystallization) were selected for $^{87}Sr/^{86}Sr$ analyses. Cross plots of $^{87}Sr/^{86}Sr$ with $\delta^{18}O$ show no clear correlation within each section, although the most radiogenic Sr value in the Las Aguaditas Formation corresponds to the most depleted $\delta^{18}O$ value. Additionally, cross plots with Sr concentration also shows no systematic correlation within each formation although lowest Sr values in the Las Chacritas and Las Aguaditas formations correspond to the most radiogenic $^{87}Sr/^{86}Sr$ values. Correlation of the most radiogenic $^{87}Sr/^{86}Sr$ values with the lowest $\delta^{18}O$ and Sr concentration indicates these are potentially overprinted. Dapingian to lower Darriwilian $^{87}Sr/^{86}Sr$ values are very close to those of non-luminescent brachiopods, however, upper Darriwilian values are substantially lower than sparse, previously reported values (Shields et al., 2003). Sandbian-aged samples proved to be the most anomalous—despite elevated Sr concentrations, $^{87}Sr/^{86}Sr$ from these samples is substantially more radiogenic than coeval brachiopod data. We attribute these elevated values to the argillaceous nature of these limestone samples, wherein Rb in clays likely contributed to the increase in ^{87}Sr in these samples.

4.4. Single and dual reservoir modeling of marine sulfur

Traditional modeling of the sulfate cycle utilizes a single oceanic sulfate reservoir whose composition (δ_{SO4}) and size (M_{SO4}) is influenced by the combination of the magnitude and isotopic composition of input and output fluxes (Kah et al., 2004). In this model, input of sulfate results from crustal weathering (F_W, δ_W), and output occur as both deposition of sulfate as either gypsum or carbonate associated sulfate (F_{SO4}, δ_{SO4}), and the bacterial reduction of sulfate and its subsequent deposition as sedimentary pyrite (F_{py}, δ_{PY}). Change in the size of the oceanic sulfate reservoir is defined as a time-dependent relationship (Kah et al., 2004):

$$\partial\delta_{SO4}/\partial t = 1/M_{SO4} * [F_W (\delta_W - \delta_{SO4}) - (F_{PY} \cdot \Delta S)] \quad [1]$$

where ΔS represents the difference in isotopic fractionation between oxidized and reduced sulfur species. Assuming the steady state condition that $F_w = F_{SO4} + F_{PY}$ and that the pyrite fraction of the output flux can be expressed as $f_{PY} = F_{PY} / [F_{PY} + F_{SO4}]$, this relationship becomes:

$$\delta_{SO4} = \delta_W - (f_{PY} \cdot \Delta S)] \quad [2]$$

Using a combination of direct measurement of isotopic values and standard values listed in Table 3.5, we first applied steady state conditions to calculate f_{PY} and F_{PY} for the Dapingian and early Darriwilian (A in Figure 3.2). Although we consider that rapid variation in the CAS record is best explained by the presence and partial oxidation of a reactive deep-ocean HS^- reservoir, long-term stability of this CAS isotopic pattern (Thompson and Kah, 2008) indicates that the deep-ocean HS^- reservoir was, over the long-term, isolated from the oceanic sulfate reservoir and thus behaved as a sedimentary pyrite reservoir. These conditions permit us to use a single-reservoir model to calculate F_{PY} because, in a single reservoir model, we consider $F_{BSR} = F_{PY}$. Our calculations give us, for the early Darriwilian, $f_{PY} = 0.77$ and $F_{PY} = 1.7x10^{18}$ mol.

At 467 Ma, CAS data record an abrupt change in marine d_{SO4} composition from ~30‰ to ~15‰ over <0.5 Myr. In terms of a single-reservoir steady-state model, maximum rates of isotopic change are reached when S input to the oceans approaches zero ($F_W = 0$) and the standing marine sulfate reservoir is removed in its reduced form (F_{PY}) giving, from equation [1]:

$$\partial\delta_{SO4}/\partial t = (F_W * \Delta S) * 1/M_{SO4} \quad [3]$$

Thus, this isotopic shift suggests a maximum marine reservoir size of approximately 1.5 to $1.7x10^{18}$ Mol, or 1-2 mM, and potentially less, if isotopic compositions are presumed to record only a fraction of maximum isotopic change (Kah et al., 2004).

Instead, we suggest that the extraordinary rapidity of this change in marine sulfate composition can only be accounted for by rapid oxidation of a reactive, deep-ocean HS^- reservoir, which demands consideration of a dual-reservoir model for sulfur cycling. A dual-reservoir model acknowledges the persistence and reactivity of a deep-ocean HS- reservoir and permits its decoupling from the marine sulfate reservoir (Rothman et al., 2003). Whereas, in a single-reservoir model F_{PY} plays the largest role in determining the composition of the marine sulfate reservoir, in a dual-reservoir model, isotopic composition of marine sulfate will be influenced directly by F_{PY} only when the fluxes between the two reservoirs—bacterial sulfate reduction and sulfide oxidation—are in equilibrium. Furthermore, in a dual-reservoir model, $F_{BSR} \neq F_{PY}$, as is assumed in a single-reservoir model. Instead, the total flux of bacterially reduced sulfur, less the reduced sulfur removed from the system as pyrite, provides a measure of the amount of reactive reduced sulfur available for reoxidation (e.g., $F_{BSR} - F_{PY} = F_{OX}$).

Using this relationship, we can estimate the size of the deep-ocean HS^- reservoir that was oxidized to result in a 15% shift in the isotopic composition of CAS in the early Darriwilian. Across the abrupt shift in δ_{SO4}, there are no immediate observed changes in the isotopic composition of marine carbon or pyrite. We thereby infer that it is unlikely that large variation in organic carbon delivery occurred over this interval, suggesting that it is also unlikely that F_{BSR} changed dramatically over this interval. Considering the linkages in a dual-reservoir model, we must consider that our originally calculated F_{PY} (now termed F_{PY1}) actually reflects a combination of pyrite burial and sequestration of reactive HS^- in the deep-ocean reservoir (F_{BSR}). Similarly, a calculated value for F_{PY} after the oxidation event (now termed F_{PY2}) will represent pyrite burial and sequestration of reactive HS^- less the amount of reactive HS^- that was oxidized during the event. Thus, calculated values of F_{PY} before (F_{PY1}; from $f_{PY} = 0.77$) and after (F_{PY2}; from $f_{PY} = 0.27$) the inferred oxidation event will provide a measure of the amount of the HS^- reservoir that was oxidized ($F_{PY1} - F_{PY2} = F_{OX}$). F_{OX} is here calculated to be 1.5×10^{18} mol or 1 mM, which means that this early Darriwilian oceanographic event would have resulted in a 50-100% increase in the size of the marine sulfate reservoir.

Because active exchange of F_{BSR} and F_{OX} within a dual-reservoir modeling results in disequilibrium behavior that can extend for intervals much longer than the residence time of the two reservoirs (Rothman et al., 2003), direct modeling of the system is not easily accomplished. Furthermore, many variables (e.g. F_{BSR}, F_{PY}) cannot be uniquely determined from a sedimentary dataset. Here, we show that consideration of a dual-reservoir model can be used to infer a combination of parameters that are calculated using a more simplistic single-reservoir model.

Acknowledgements

We would like to thank the National Science Foundation and American Chemical Society who provided funding to Linda Kah for geochemical analyses, National Geographic Society who provided funding for fieldwork to Linda Kah, along with Sigma Xi, the Geological Society of America, and SEPM who provided student grants to Cara Thompson for fieldwork and geochemical analyses. Sample collection was aided by Mary Varnell, Geoff Gilleaudeau, Fernando Gomez, and Ricardo Astini. Isotopic analyses were aided by Lisa Pratt, Seth Young, Craig Moore, and Zheng-hua Li.

References cited

Ainsaar, L., Meidla, T., Martma, T., 1999. Evidence for a widespread carbon isotopic event associated with late Middle Ordovician sedimentological and faunal changes in Estonia. Geol. Magazine 136, 49-62.

Ainsaar, L., Kaljo, D., Martma, T., Meidla, T., Männik, P., Nõlvak, J., Tinn, O., 2010. Middle and Upper Ordovician carbon isotope chemostratigraphy in Baltoscandia: a correlation standard and clues to environmental history. Palaeogeography, Palaeoclimatology, Palaeoecology 294, 189-201.

Albanesi, G.L., Ortega, G., Barnes, C.R., Hunicken, M.A., 1999. Conodont-graptolite biostratigraphy of the Gualcamayo Formation (Middle Ordovician) in the Gualcamayo-

Guandacol rivers area, Argentina Precordillera. Acta Universitatis Carolinae, Geologica 43, 45-48.

Albanesi, G.L., Ortega, G., 2002. Advances on conodont-graptolite biostratigraphy of the Ordovician system of Argentina. Serie Correlación Geológica 16, 143-165.

Astini, R.A., 1995. Geologic meaning of Arenig-Llanvirn diachronous black shales (Gualcamayo Alloformation) in the Argentine Precordillera, tectonic or eustatic? SEPM Fieldtrip Guidebook 77, 217-220.

Astini, R.A., Benedetto, J.L., Vaccari, N.E., 1995. The early Paleozoic evolution of the Argentine Precordillera as a Laurentian rifted, drifted, and collided terrane: A geodynamic model. Geological Society of America Bulletin 107, 253-273.

Baldis, B.A., Beresi, M.S. Bordonaro, O., Vaca, A., 1984. The Argentine Precordillera as a key to the Andean structure. Episodes 17, 14-19.

Banner, J.L., Hanson, G.N., 1990. Calculation of simultaneous isotopic and trace element variations during water-rock interaction with applications to carbonate diagenesis. Geochimica et Cosmochimica Acta 54, 3123-3137.

Banner, J.L., 1995. Application of the trace element and isotope geochemistry of strontium to studies of carbonate diagenesis. Sedimentology 42, 805-824.

Bartley, J.K., Kah, L.C., McWilliams, J.L., Stagner, A.F., 2007. Carbon isotope chemostratigraphy of the Middle Riphean type section (Avzyan Formation, Southern Urals, Russia): Signal recovery in a fold-and-thrust belt. Chemical Geology 237, 211-232.

Benedetto, J.L., Sánchez, T.M., Carrera, M.G., Brussa, E.D., Salas, M.J., 1999. Paleontological constraints on successive paleogeographic positions of Precordillera terrane during the early Paleozoic. Geological Society of America Special Paper 336, 21-42.

Berner, R.A., 1984. Sedimentary pyrite formation: an update. Geochimica et Cosmochimica Acta 48, 605-615.

Brand, U., Veizer, J., 1980. Chemical diagenesis of a multicomponent carbonate system – 1: trace elements. Journal of Sedimentary Petrology 50, 1219-1236.

Brenchley, P.J., Marshall, J.D., Carden, G.A.F., Robertson, D.B.R., Long, D.G.F., Meidla, T., Hints, L., Anderson, T.F., 1994. Bathymetric and isotopic evidence for a short-lived Late Ordovician glaciation in a greenhouse period. Geology 22, 295-298.

Brennan, S.T., Lowenstein, T.K., Horita, J., 2004. Seawater chemistry and the advent of biocalcification. Geology 32, 473-476.

Brussa, E., 1996. Las graptofaunas Ordovicicas de la Formacion Las Aguaditas, Precordillera de San Juan, Argentina. Parte I: Faminilas thanmnograptidae, dichograptidae, abrograptidae y glossograptidae. Amedhiniana 33, 421-434.

Buggisch, W., Keller, M., Lehnert, O., 2003. Carbon isotope record of Late Cambrian to Early Ordovician carbonates of the Argentine Precordillera. Palaeogeography, Palaeoclimatology, Palaeoecology 195, 357-373.

Burdett, J.W., Arthur, M.A., Richardson, M.A., 1989. Neogene seawater sulfur isotope age curve from calcareous pelagic microfossils. Earth Planetary Science Letters 94, 189-198.

Cañas, F.L., 1995. Early Ordovician carbonate platform facies of the Argentine Precordillera: Restricted shelf to open platform evolution. SEPM Fieldtrip Guidebook 77, 221-224.

Canfield, D.E., 1998. A new model for Proterozoic ocean chemistry. Nature 396, 450-453.

Canfield, D.E., 2001. Biogeochemistry of sulphur isotopes. Reviews of Mineralogy and Geochemistry 43, 607-636.

Canfield, D.E., Raiswell, R., Westrich, J.T., Reaves, C.M., Berner, R.A., 1986. The use of chromium reduction in the analysis of reduced inorganic sulfur in sediments and shales. Chemical Geology 54, 149-155.

Canfield, D.E., Teske, A., 1996. Late Proterozoic rise in atmospheric oxygen concentration inferred from phylogenetic and sulphur-isotope studies. Nature 382, 127-132.

Carpenter, S.J., Lohmann, K.C., Holden, P., Walter, L.M., Huston, T.J., Halliday, A.N., 1991. $\delta^{18}O$ values, $^{87}Sr/^{86}Sr$ and Sr/Mg ratios of Late Devonian marine calcite: implications for the composition of ancient seawater. Geochimica et Cosmochimica Acta 55, 1991-2010.

Chiba, H., Sakai, H., 1985. Oxygen isotope exchange rate between dissolved sulfate and water at hydrothermal temperatures. Geochimica et Cosmochimica Acta 49, 993-1000.

Cocks, L.R.M., McKerrow, W.S., 1993. A reassessment of the Early Ordovician 'Celtic' brachiopod province. Journal of the Geological Society of London 150, 1039-1042.

Derry, L.A., Kaufman, A.J., Jacobsen, S.B., 1992. Sedimentary cycling and environmental change in the Late Proterozoic: Evidence from stable and radiogenic isotopes. Geochimica et Cosmochimica Acta 56, 1317-1329.

Fanning, C.M., Pankhurst, R.J., Rapela, C.W., Baldo, E.G., Casquet, C., Galindo, C., 2004. K-bentonites in the Argentine Precordillera contemporaneous with rhyolite volcanism in the Famatinian Arc. Journal of the Geological Society of London 161, 747-756.

Fike, D.A., Grotzinger, J.P., Pratt, L.M., Summons, R.E., 2006. Oxidation of the Ediacaran Ocean. Nature 444, 744-747.

Finnegan, S., Bergmann, K., Eiler, J.M., Jones, D.S., Fike, D.A., Eisenman, I., Hughes, N.C., Tripati, A.K., Fischer, W.W., 2011. The magnitude and duration of Late Ordovician-Early Silurian Glaciation. Science 331, 903-906.

Frank, T.D., Lohmann, K.C., 1996. Diagenesis of fibrous magnesian calcite marine cement: implications for the interpretation of $\delta^{18}O$ and $\delta^{13}C$ values from ancient equivalents. Geochimica et Cosmochimica Acta 60, 2427-2436.

Frank, T.D., Lyons, T.W., Lohmann, K.C., 1997. Isotopic evidence for the paleoenvironmental evolution of the Mesoproterozoic Helena Formation, Belt Supergroup, Montana. Geochimica et Cosmochimica Acta 61, 5023-5041.

Frank, T.D., Kah, L.C., Lyons, T.W., 2003 Changes in organic matter production and accumulation as a mechanism for isotopic evolution in the Mesoproterozoic ocean. Geological Magazine 140, 397-420.

Fry, B., Ruf, W., Gest, H., Hayes, J.M., 1988. Sulphur isotope effects associated with oxidation of sulphide by O_2 in aqueous solution. Isotope Geoscience 73, 205-210.

Gill, B.C., Lyons, T.W., Frank, T.D., 2008. Behavior of carbonate-associated sulfate during meteoric diagenesis and implications for the sulfur isotope paleoproxy. Geochimica et Cosmochimica Acta 72, 4699-4711.

Gill, B.C., Lyons, T.W., Young, S.A., Kump, L.R., Knoll, A.H., Saltzman, M.R., 2011. Geochemical evidence for widespread euxinia in the later Cambrian ocean. Nature 469, 80-83.

Given, R.K., Lohmann, K.C., 1985. Derivation of the original isotopic composition of Permian marine cements. Journal of Sedimentary Petrology 55, 430-439.

Hall, S.A., Evans, I., 1988. Paleomagnetic study of the Ordovician Table Head Group, Port au Port Peninsula, Newfoundland. Canadian Journal of Earth Science 25, 1407-1419.

Harper, D.A.T., MacNiocaill, C., Williams, S.H., 1996. The palaeogeography of Early Ordovician Iapetus terranes: an integration of faunal and palaeomagnetic constraint. Palaeogeography, Palaeoclimatology, Palaeoecology 121, 297-312.

Hemming, N.G., Meyers, W.J., Grams, J.C., 1989. Cathodoluminescence in diagenetic calcites: the roles of Fe and Mn as deduced from electron probe and spectrophotometric measurements. Journal of Sedimentary Petrology 59, 404-411.

Heredia, S., Beresi, M., Peralta, S., 2005. Darriwilian condodont biostratigraphy of the Las Chacritas Formation, Central Precordillera (San Juan Province, Argentina). Geologica Acta. **3**, 385-394.

Herrera, Z.A., Benedetto, J.L., 1991. Early Ordovician brachiopod faunas from the Precordillera basin, Western Argentina: biostratigraphy and paleobiogeographical affinities. In: McKinnon, D.I., Lee, D.E., Campbell, J.D. (Eds) Brachiopods Through Time, 283-301.

Horita, J., Zimmermann, H. & Holland, H. D., 2002. Chemical evolution of seawater during Phanerozoic: Implications from the record of marine evaporites. Geochimica et Cosmochimica Acta 66, 3733-3756.

Huff, W.D., Davis, D., Bergström, S.M., Krekeler, M.P.S., Kolata, D.R., Cingolani, C., 1997. A biostratigraphically well-constrained K-bentonite U-Pb zircon age of the lowermost Darriwilian stage (Middle Ordovician) from the Argentine Precordillera. Episodes. 20, 29-33.

Huff, W.D., Bergström, S.M., Kolata, D.R., Cingolani, C., Astini, R.A., 1998. Ordovician K-bentonites in the Argentine Precordillera: relations to Gondwana margin evolution. Geological Society of London, Special Publication 142, 107-126.

Hurtgen, M.T., Arthur, M.A., Suits, N.S., Kaufman, A.J., 2002. The sulfur isotopic composition of Neoproterozoic seawater sulfate: implications for a snowball Earth? Earth and Planetary Science Letters 203, 413-429.

Hurtgen, M.T., Arthur, M.A., Halverson, G.P., 2005. Neoproterozoic sulfur isotopes, the evolution of microbial sulfur species, and the burial efficiency of sulfide as sedimentary pyrite. Geology 33, 41-44.

Hurtgen, M.T., Halverson, G.P., Arthur, M.A., Hoffman, P.F., 2006. Sulfur cycling in the aftermath of a 635-Ma snowball glaciation: Evidence for a synglacial sulfidic deep ocean. Earth and Planetary Science Letters 245, 551-570.

Hurtgen, M.T., Pruss, S.B., Knoll, A.H., 2009. Evaluating the relationship between carbon and sulfur cycles in the later Cambrian ocean: an example from the Port au Prot Group, western Newfoundland, Canada. Earth and Planetary Science Letters 281, 288-297.

Jacobi, R.D., 1981. Peripheral bulge – a causal mechanism for the Lower/Middle Ordovician unconformity along the western margin of the northern Appalachians. Earth and Planetary Science Letters 56, 245-251.

James, N.P., Barnes, C.R., Stevens, R.K., Knight, I., 1989. A lower Paleozoic continental margin carbonate platform, northern Canadian Appalachians. SEPM Special Publication 44, 123-146.

Johnston, D.T., Wing, B.A., Farquhar, J., Kaufman, A.J., Strauss, H., Lyons, T.W., Kah, L.C., Canfield, D.E., 2005. Active microbial sulfur disproportionation in the Mesoproterozoic. Science 310, 1477-1479.

Jørgensen, B.B., Bang, M., Blackburn, T. H., 1990. Anaerobic mineralization in marine sediments from the Baltic Sea-North Sea transition. Marine Ecology Progress Series 59, 39-54.

Kah, L.C., 2000. Preservation of depositional $\delta^{18}O$ signatures in Proterozoic dolostones: geochemical constraints on seawater chemistry and early diagenesis. SEPM Special Publication 65, 345-360.

Kah, L.C., Sherman, A.G., Narbonne, G.M., Knoll, A.H., Kaufman, A. J., 1999. $\delta^{13}C$ stratigraphy of the Proterozoic Bylot Supergroup, Baffin Island, Canada: implications for regional lithostratigraphic correlations. Canadian Journal of Earth Science 36, 313-332.

Kah, L.C., Lyons, T.W., Chesley, J.T., 2001. Geochemistry of a 1.2 Ga carbonate-evaporite succession, northern Baffin and Bylot Islands: implications for Mesoproterozoic marine evolution. Precambrian Research 111, 203-234.

Kah, L.C., Lyons, T.W., Frank, T.D., 2004. Low marine sulfate and protracted oxygenation of the Proterozoic biosphere. Nature 431, 834-838.

Kampschulte, A., Bruckschen, P., Strauss, H., 2001. The sulfur isotopic composition of trace sulfates in Carboniferous brachiopods: implications for coeval seawater, correlation with other geochemical cycles and isotope stratigraphy. Chemical Geology 175, 149-173.

Kaplan, I.R., Rittenberg, S.C., 1964. Microbiological fractionation of sulphur isotopes. Journal of General Microbiology 34, 195-212.

Kaufman, A.J., Hayes, J.M., Knoll, A.H., Germs, G.J.B., 1991. Isotopic compositions of carbonates and organic carbon from upper Proterozoic successions in Namibia: stratigraphic variation and the effects of diagenesis and metamorphism. Precambrian Research 49, 301-327.

Keller, M., Eberlein, S., Lehnert, O., 1993. Sedimentology of Middle Ordovician carbonates in the Argentine Precordillera: Evidence of regional relative sea-level changes. Geologische Rundschau 82, 362-377.

Knight, I., Cawood, P.A., 1991. Paleozoic geology of western Newfoundland: an exploration of a deformed Cambro-Ordovician passive margin and foreland basin, and Carboniferous successor basin: St. John's, Newfoundland. Centre Earth Resources Research 1-403.

Knight, I., James, N.P., Lanes, T.E., 1991. The Ordovician St. George unconformity, northern Appalachians: the relationship of plate convergence at the St. Lawrence Promontory to the Sauk/Tippecanoe sequence boundary. Geological Society of America Bulletin 103, 1200-1225.

Kump, L.R., Arthur, M.A., 1999. Interpreting carbon isotope excursions: Carbonates and organic matter. Chemical Geology 161, 181-198.

Kurtz, A.C., Kump, L.R., Arthur, M.A., Zachos, J.C., Paytan, A., 2003. Early Cenozoic decoupling of the global carbon and sulfur cycles. Paleoceanography 18, 1090.

Lehnert, O., Keller, M., 1994. The conodont record of the Argentine Precordillera: Problems and possibilities. Zentralblatt für Geologie und Paleontologie 1-2, 231-244.

Lyons, T.W., Walter, L.M., Gellatly, A.M., Martini, A.M., Blake, R.E., 2004. Sites of anomalous organic remineralization in the carbonate sediments of South Florida, USA: the sulfur cycle and carbonate-associated sulfate. Geological Society of America Special Paper 379, 161-176.

Marenco, P.J., Corsetti, F.A., Hammond, D.E., Kaufman, A.J., Bottjer, D.J., 2008. Oxidation of pyrite during extraction of carbonate associated sulfate. Chemical Geology 247, 124-132.

Marshall, J.D., 1992. Climatic and oceanographic signals from the carbonate rock record and their preservation. Geological Magazine 129, 143-160.

Mazumder, A., Goldberg, T., Strauss, H., 2008. Abiotic oxidation of pyrite Fe (III) in acidic media and its implications for sulfur isotope measurements of lattice-bound sulfate in sediments. Chemical Geology 253, 30-37.

Neuman, R.B., Harper, D.A.T., 1992. Paleogeographic significance of Arenig-Llanvirn Toquima-Table Head and Celtic brachiopod assemblages. In: Webby, B.D., Laurie, J.R. (Eds) Global Perspectives in Ordovician Geology, 241-254.

Niocaill, C.M., van der Pluijm, B.A., Van der Voo, R., 1997. Ordovician paleogeography and the evolution of the Iapetus Ocean. Geology 25, 159-162.

Peralta, S.H., Heredia, S., Beresi, M.S., 1999. Upper Arenig-Lower Llanvirn sequence of the Las Chacritas River, Central Precordillera, San Juan Province, Argentina. Acta Universitatis Carolinae, Geologica 43, 123-126.

Pope, M.C., Steffen, J.B., 2003. Widespread, prolonged late Middle to Late Ordovician upwelling in North America: A proxy record of glaciation? Geology 31, 63-66.

Qing, H., Veizer, J., 1994. Oxygen and carbon isotopic composition of Ordovician brachiopods: Implications for coeval seawater. Geochimica et Cosmochimica Acta 58, 4429-4442.

Ramos, V.A., 1986. Paleozoic terranes of the central Argentine-Chilean Andes. Tectonics 5, 855-880.

Ramos, V.A., 1988. Late Proterozoic-Early Paleozoic of South America: a collisional history. Episodes 11, 168-174.

Ramos, V.A., 1988. The tectonics of the central Andes, 30° to 33° S. Geological Society of America Special Paper 218, 31-54.

Ramos, V.A., 2004. Cuyania, an exotic block to Gondwana: review of a historical success and the present problems. Gondwana Research 7, 1009-1026.

Ries, J.B., Fike, D.A., Pratt, L.M., Lyons, T.W., Grotzinger, J.P., 2009. Superheavy pyrite ($\delta^{34}S_{pyr} > \delta^{34}S_{CAS}$) in the terminal Proterozoic Nama Group, southern Namibia: A consequence of low seawater sulphate at the dawn of animal life. Geology 37, 743-746.

Ross, R.J., Jr., Ingham, J.K., 1970. Distribution of the Toquima – Table Head (Middle Ordovician Whiterock) faunal realm in the Northern Hemisphere. Geological Society of America Bulletin 81, 393-408.

Rothman, D.H., Hayes, J.M., Summons, R.E., 2003. Dynamics of the Neoproterozoic carbon cycle. Proceedings of the National Academy of Sciences 100, 8124-8129.

Rush, P.F., Chafetz, H.S., 1990. Fabric retentive, non-luminescent brachiopods as indicators of original $\delta^{13}C$ and $\delta^{18}O$ compositions: a test. Journal of Sedimentary Petrology 60, 968-981.

Saltzman, M.R., 2000. A global carbon isotope excursion (SPICE) during the Late Cambrian: relation to trilobite extinctions, organic-matter burial and sea level. Palaeogeography, Palaeoclimatology, Palaeoecology 162, 211-223.

Saltzman, M. R., 2005. Phosphorus, nitrogen, and the redox evolution of the Paleozoic oceans. Geology 33, 573-576.

Saltzman, M.R., Cowan, C.A., Runkel, A.C., Runnegar, B., Stewart, M.C., Palmer, A.R., 2004. The Late Cambrian SPICE ($\delta^{13}C$) event and the Sauk II-Sauk III regression: New evidence from Laurentian basins in Utah, Iowa, and Newfoundland. Journal of Sedimentary Research 74, 366-377.

Saltzman, M.R., Young, S.A., 2005. Long-lived glaciation in the Late Ordovician? Isotopic and sequence-stratigraphic evidence from western Laurentia. Geology 33, 109-112.

Savard, M.M., Veizer, J., Hinton, R., 1995. Cathodoluminescence at low Fe and Mn concentrations: a SIMS study of zones in natural calcite. Journal of Sedimentary Research A65, 208-213.

Scotese, C.R., McKerrow, W.S., 1990. Revised world maps and introduction. Geological Society of London Memoirs 12, 1-21.

Sheehan, P.M., 2001. The Late Ordovician mass extinction. Annual Reviews of Earth Planetary Science 29, 331-364.

Shen, B., Xiao, S., Kaufman, A.J., Bao, H., Zhou, C., Wang, H., 2008. Stratification and mixing of a post-glacial Neoproterozoic ocean: Evidence from carbon and sulphur isotopes in a cap dolostone from northwest China. Earth and Planetary Science Letters 265, 209-228.

Shields, G.A., Carden, G.A.F., Veizer, J., Meidla, T., Rong, Y., Li, R., 2003. Sr, C, and O isotope geochemistry of Ordovician brachiopods: A major isotopic event around the Middle-Late Ordovician transition. Geochimica et Cosmochimica Acta 67, 2005-2025.

Stenzel, S.R., Knight, I., James, N.P., 1990. Carbonate platform to foreland basin: revised stratigraphy of the Table Head Group (Middle Ordovician), western Newfoundland. *Canadian Journal of Earth Science* **27**, 14-26.

Stouge, S.S., 1982. Preliminary conodont biostratigraphy and correlation of Lower and Middle Ordovician carbonates of the St. George Group, Great Northern Peninsula, Newfoundland. Newfoundland Department of Mines and Energy, Mineral Development Division 82-83, 1-59.

Strauss, H., 1997. The isotopic composition of sedimentary sulfur through time. Palaeogeography, Palaeoclimatology, Palaeoecology 132, 97-118.

Strauss, H., 1999. Geological evolution from isotope proxy signals – sulfur. Chemical Geology 161, 89-101.

Thomas, W.A., Astini, R.A., 1996. The Argentine Precordillera: A traveler from the Ouachita embayment of North American Laurentia. Science 273, 752-757.

Thomas, W.A., Astini, R.A., 1999. Simple-shear conjugate rift margins of the Argentine Precordillera and the Ouachita embayment of Laurentia. Geological Society of America Bulletin 111, 1069-1079.

Thomas, W.A., Astini, R.A., 2003. Ordovician accretion of the Argentine Precordillera terrane to Gondwana: a review. Journal of South American Earth Science 16, 67-79.

Thompson, C.K., Kah, L.C., 2008. Redox cycling in the greenhouse ocean: exploring rapid sulfur isotope variation in the Middle Ordovician. Geological Society of America Abstracts 40, 321.

Tie-bing, L., Maynard, J.B., Alten, J., 2006. Superheavy S isotopes from glacier-associated sediments of the Neoproterozoic of south China: Oceanic anoxia or sulphate limitation? Geological Society of America Memoir 198, 205-222.

Trotter, J.A., Williams, I.A., Barnes, C.R., Lécuyer, C., Nicoll, R.S., 2008. Did cooling oceans trigger Ordovician biodiversification? Evidence from conodont thermometry. Science 321, 550-554.

Veizer, J., 1983. Trace elements and isotopes in sedimentary carbonates. Reviews of Mineralogy 11, 265-300.

Veizer, J., Ala, D., Azmy, K., Bruckschen, P., Buhl, D., Bruhn, F., Carden, G.A.F., Diener, A., Ebneth, S., Godderis, Y., Jasper, T., Korte, C., Pawellek, F., Podlaha, O.F., Strauss, H., 1999. $^{87}Sr/^{86}Sr$, $\delta^{13}C$ and $\delta^{18}O$ evolution of Phanerozoic seawater. Chemical Geology 161, 59-88.

Wadleigh M.A., Veizer, J., 1992. $^{18}O/^{16}O$ and $^{13}C/^{12}C$ in lower Paleozoic articulate brachiopods: Implications for the isotopic composition of seawater. Geochimica et Cosmochimica Acta 56, 431-443.

Williams, H., Stevens, R.K., 1974. The ancient continental margin of North America. In: Burke, C.A., Drake, C.L. (Eds) The Geology of Continental Margins 781-796.

Williams, S.H., Boyce, W.D., James, N.P., 1987. Graptolites from the Lower-Middle Ordovician St. George and Table Head groups, western Newfoundland, and their correlation with trilobite, brachiopod, and conodont zones. Canadian Journal of Earth Science 24, 456-470.

Young, S.A., Saltzman, M.R., Foland, K.A., Linder, J. S., Kump, L.R., 2009. A major drop in seawater $^{87}Sr/^{86}Sr$ during the Meddle Ordovician (Darriwilian): Links to volcanism and climate? Geology 37, 951-954.

Young, S.A., Saltzman, M.R., Ausich, W.I., Desrochers, A., Kaljo, D., 2010. Did changes in atmospheric CO_2 coincide with latest Ordovician glacial-interglacial cycles? Palaeogeography, Palaeoclimatology, Palaeoecology 296, 376-388.

Zempolich, W.G., Wilkinson, B.H., Lohmann, K.C., 1988. Diagenesis of Late Proterozoic carbonates: the Beck Springs Dolomite of Eastern California. Journal of Sedimentary Petrology 58, 656-672.

Appendix

Table 3.1. Isotopic compositions and elemental concentrations recorded in the Table Head Group, Western Newfoundland.

Sample	Age* (Myr)	$\delta^{13}C$ (‰ VPDB)	$\delta^{34}S_{CAS}$	$\delta^{34}S_{PY}$ (‰ VCDT)	$\Delta^{34}S$	Mn	Fe (ppm)	Sr	$^{87}Sr/^{86}Sr$
TH-1	472.0	-1.01	30.9	-9.8	40.7	56	1088	214	
TH-9	471.8	-1.46	29.2	5.6	23.6	167	5084	78	
TH-18	471.5	-3.12	29.9	1.1	28.8	32	672	332	
TH-27	471.3	-0.98	33.0	9.5	23.6	23	108	410	
TH-35	471.1	-0.94	29.4	0.5	28.9	11	299	286	
TH-43	470.9	-1.64	24.6	-4.5	29.1	86	1109	198	
TH-52	470.6	-1.03	29.8	-6.9	36.8	33	397	309	
TH-61	470.4	-1.28	28.9	3.6	25.3	28	654	411	0.708747
TH-70	470.1	-1.5	25.0	-0.2	25.2	22	639	369	
TH-81	469.9	-1.74	28.2	2.7	25.5	32	797	284	
TH-90	469.6	-1.73	33.6	16.5	17.1	98	394	422	
TH-99	469.4	-1.87	30.0	10.3	19.6	72	381	458	
TH-108	469.1	-1.57	38.6	13.1	25.5	34	608	486	0.7087485
TH-117	468.9	-0.69	17.1	8.5	8.6	71	1625	368	
TH-126	468.7	-0.94	26.8	13.5	13.4	39	1023	469	
TH-133	468.5	-1.11	36.1	14.8	21.4	35	545	619	
TH-142	468.2	-0.73	31.6	4.7	26.9	118	425	246	
TH-153	468.0	-1.37	29.0	0.7	28.3	48	722	538	0.7087389
TH-162A	467.7	-1.09	29.2	1.4	27.7	41	431	417	
TH-171	467.5	-0.53	32.9	-4.1	37.0	30	391	400	
TH-180	467.3	-0.42	29.9	-5.8	35.6	52	578	361	
TH-189	467.0	-0.76	–	–	–	40	279	311	
TH-201	466.7	-0.58	19.2	-8.3	27.5	127	275	297	0.708868
TH-215	466.3	-0.35	21.8	-12.7	34.5	184	503	255	
TH-226	466.1	-0.38	2.6	-8.5	11.1	413	1368	377	
TH-235	465.8	-0.63	18.5	-9.8	28.2	–	–	–	
TH-244	465.6	-0.18	12.2	-5.5	17.7	279	2206	715	
TH-253	465.3	0.03	21.8	16.4	5.4	178	2217	1040	
TH-262	465.1	-0.14	13.3	-15.5	28.8	301	3132	901	0.7088601
TH-270	464.9	0.25	15.6	6.3	9.3	164	2232	1045	
TH-278	464.7	0.29	21.1	5.0	16.1	134	2148	1031	
TH-287	464.4	0.47	18.2	12.1	6.1	116	1528	1094	0.708823
TH-295	464.2	0.62	20.7	8.9	11.8	173	1787	1118	
TH-304	464.0	0.58	9.7	2.0	7.7	121	1889	1073	

Table 3.2. Isotopic compositions and elemental concentrations recorded in the Gualcamayo Formation, Argentina.

Sample	Age* (Myr)	$\delta^{34}S_{PY}$ (‰ VCDT)
GF-0	470.0	-10.2
GF-1	470.0	-11.3
GF-3	469.9	-7.2
GF-6	469.9	-11.1
GF-10	469.7	1.7
GF-14	469.7	1.6
GF-19	469.5	5.8
GF-24	469.4	3.7
GF-28	469.3	-4.7
GF-32	469.2	-5.7
GF-36	469.1	–
GF-42	469.0	-6.6
GF-43	469.0	-6.4
GF-46	468.9	-16.5
GF-52	468.8	-3.7
GF-59	468.6	-12.1
GF-64	468.5	0.9
GF-69	468.3	-0.4
GF-85	468.0	-7.5
GF-87	467.9	-11.3
GF-93	467.8	-4.4
GF-100	467.6	-3.9
GF-107	467.4	-14.4
GF-113	467.3	-2.6
GF-119	467.1	-2.0
GF-122	467.1	-3.8
GF-128	466.9	4.1
GF-134	466.8	8.3
GF-141	466.6	22.1
GF-149	466.4	39.3
GF-155	466.3	3.5
GF-163	466.1	14.0
GF-169	465.9	3.5
GF-175	465.8	5.0
GF-183	465.6	4.0
GF-189	465.5	4.8
GF-195	465.3	0.6
GF-201	465.2	4.1
GF-208	465.0	1.4
GF-214	464.9	-4.1
GF-221	464.7	-10.5
GF-227	464.5	2.7
GF-233	464.4	–

GF-241	464.2	-2.0
GF-250	464.0	2.3

Table 3.3. Range of isotopic compositions and elemental concentrations recorded in the Las Chacritas Formation, Argentina.

Sample	Age* (Myr)	$\delta^{13}C$ (‰ VPDB)	$\delta^{34}S_{CAS}$	$\delta^{34}S_{PY}$ (‰ VCDT)	$\Delta^{34}S$	Mn	Fe (ppm)	Sr	$^{87}Sr/^{86}Sr$
LCF-0	467.0	-1.35	16.3	-11.4	27.7	110	261	299.3	
LCF-5	466.8	-1.47	17.0	1.6	15.4	90	472	317.0	
LCF-8	466.7	-1.22	11.5	-7.5	19.0	138	747	311.7	
LCF-13	466.5	-1.29	12.8	-5.6	18.3	192	704	301.6	
LCF-18	466.3	-1.27	16.4	-2.9	19.3	283	1405	334.9	
LCF-23A	466.1	-0.49	17.6	-3.2	20.7	649	2595	360.5	
LCF-23B	466.1	-0.36	–	–	–	788	2177	259.7	
LCF-28	465.9	-0.08	13.5	0.0	13.5	958	3881	303.7	
LCF-32	465.7	-0.70	15.8	6.4	9.4	447	2189	518.6	0.7092304†
LCF-37	465.5	-0.65	16.2	-6.4	22.6	412	3195	515.7	
LCF-41A	465.4	-1.15	13.0	1.7	11.3	478	7933	670.7	
LCF-41B	465.4	-0.94	–	–	–	451	2396	584.6	
LCF-47	465.2	-0.77	14.0	3.1	10.9	289	1589	827.8	
LCF-50	465.0	-0.57	14.7	11.7	3.0	291	3030	796.0	
LCF-55	464.8	-0.87	14.2	-2.4	16.6	446	1507	399.8	
LCF-59	464.6	-1.13	16.0	-0.7	16.7	301	1461	725.3	0.7089012
LCF-64-1	464.4	-0.81	11.7	-12.8	24.5	344	3232	599.8	
LCF-64-2	464.4	-0.92	–	–	–	363	1232	457.7	
LCF-69	464.3	–	11.5	0.9	10.6	–	–	–	
LCF-73	464.1	-0.36	21.3	11.7	9.6	425	1557	303.2	
LCF-77	463.9	–	21.7	8.6	13.1	–	–	–	
LCF-81	463.7	0.71	24.0	11.7	12.3	287	1814	259.2	
LCF-88	463.5	0.37	17.4	1.4	16.0	285	1293	336.9	
LCF-94	463.2	0.23	13.0	11.5	1.5	988	10189	982.8	
LCF-96	463.2	0.80	9.9	2.0	7.9	481	5124	941.4	
LCF-97	463.1	0.44	8.8	2.9	5.9	526	5211	617.0	
LCF-98	463.1	0.14	11.3	8.8	2.5	739	4976	861.2	
LCF-99	463.1	0.12	7.2	6.2	0.9	1191	13228	741.3	
LCF-100	463.0	0.79	7.0	3.0	4.0	1944	6950	992.5	
LCF-101	463.0	–	4.8	-1.2	6.0	–	–	–	

*The age of the Las Chacritas Formation was approximated using biostratigraphy of [30].
† Altered value, not plotted in Figure 3.2.

Table 3.4. Range of isotopic compositions and elemental concentrations in the Las Aguaditas Formation, Argentina.

Sample	Age* (Myr)	$\delta^{13}C$ (VPDB)	$\delta^{34}S_{CAS}$	$\delta^{34}S_{PY}$ (VCDT)	$\Delta^{34}S$	Mn	Fe (ppm)	Sr	$^{87}Sr/^{86}Sr$
AF-0	465.2	-0.42	18.8	-7.3	26.1	802	2809	559	
AF-1	465.2	-0.09	15.5	5.0	10.5	865	2664	409	
AF-6	465.1	-0.29	18.3	19.2	-0.8	2056	4146	451	
AF-7A	465.0	0.31	17.7	23.9	-6.2	1689	1862	422	
AF-7B	465.0	0.38	–	–	–	944	4395	409	
AF-7.1	465.0	0.14	21.4	18.4	3.0	1081	2893	440	
AF-17A	464.8	-1.26	12.7	0.8	11.9	671	17687	1067	0.7093401†
AF-17B	464.8	-0.75	–	–	–	568	8987	968	
AF-23	464.6	-0.46	6.0	-2.4	8.4	653	7243	913	
AF-30	464.4	-3.19	15.8	14.8	0.9	572	2884	526	
AF-37A	464.3	-1.87	28.9	11.9	16.9	177	2497	811	
AF-37B	464.3	-1.17	–	–	–	313	15348	2312	
AF-43	464.1	-0.99	17.1	17.5	-0.4	199	1431	1071	
AF-49A	463.9	-1.18	11.8	14.4	-2.6	436	2100	910	
AF-49B	463.9	-1.07	–	–	–	242	8091	2231	
AF-56	463.8	-1.57	17.1	11.1	6.0	360	1676	809	
AF-62	463.6	0.65	16.8	19.8	-3.0	137	3172	1139	
AF-65	463.5	0.46	11.6	–	–	147	2452	1229	
AF-73	463.4	1.23	13.6	20.1	-6.6	108	2650	1397	
AF-79	463.2	0.41	13.6	18.1	-4.5	134	3450	1236	
AF-85	463.0	0.73	15.3	16.1	-0.8	111	2537	1596	
AF-91X	462.9	1.13	14.7	18.6	-3.9	100	2166	1773	
AF-91Y	462.9	1.04	–	–	–	99	1887	1763	
AF-97	462.7	0.96	14.9	18.6	-3.7	116	2268	1736	
AF-103	462.6	1.27	15.5	20.1	-4.6	96	1108	1039	
AF-109	462.4	0.90	14.0	16.3	-2.3	162	1831	1832	
AF-115	462.3	1.03	15.2	20.8	-5.7	–	–	–	
AF-121	462.1	0.93	13.3	18.8	-5.5	111	1995	1886	0.7084642
AF-127	462.0	1.13	15.6	20.1	-4.5	147	4360	1801	
AF-133	461.8	1.18	14.8	18.9	-4.1	108	2157	2107	
AF-139	461.7	1.15	13.5	19.2	-5.6	105	1686	2061	
AF-145	461.5	1.16	13.5	21.1	-7.6	90	2508	2094	
AF-151	461.4	1.14	15.6	17.9	-2.2	116	2734	2054	
AF-151	461.4	0.46	–	–	–	316	5965	2013	
AF-157A	461.2	1.24	14.9	20.1	-5.2	104	2544	2220	

AF-157B	461.2	1.40	–	–	–	100	1768	2272	
AF-160	461.1	1.44	9.8	19.1	–	104	2121	2353	0.70847
AF-166	461.0	1.23	15.9	18.9	-3.0	135	2793	1908	
AF-172	460.8	1.22	15.8	19.7	-3.8	168	3954	2177	
AF-185A	460.5	1.65	7.8	8.9	-1.1	489	22688	1408	
AF-185B	460.5	2.01	–	–	–	589	31468	1489	
AF-191	460.4	0.81	11.1	17.3	-6.2	216	6316	2062	
AF-196	460.2	1.69	12.0	20.0	-8.1	873	39408	1738	
AF-196B	460.2	1.82	–	–	–	891	39330	1771	
AF-203	460.0	0.94	14.4	17.3	-2.9	228	6000	2247	
AF-208	459.9	1.17	11.0	14.4	-3.4	474	17124	1880	
AF-218	459.7	1.44	10.2	8.8	1.4	487	23274	1673	0.7085949
AF-223	459.5	0.39	18.1	15.4	2.6	432	9369	1798	
AF-228	459.4	0.47	16.4	16.3	0.0	–	–	–	
AF-234	459.3	0.74	9.2	13.8	-4.6	404	13489	1735	
AF-256	458.7	1.07	14.5	11.1	3.4	205	7311	1824	
AF-270	458.3	0.51	14.4	12.1	2.4	350	12959	1519	0.7086782
AF-276	458.2	0.33	18.1	13.6	4.6	326	19806	2041	
AF-283	458.0	0.90	14.9	12.0	2.9	203	6870	1786	
AF-290	457.8	0.91	13.8	8.9	4.9	261	10555	1837	
AF-293	457.8	0.76	15.3	9.0	6.3	151	3942	1808	
AF-299	457.6	0.57	12.7	15.6	-2.9	178	11295	2550	
AF-305	457.4	1.05	14.3	15.7	-1.4	225	7551	2756	
AF-312	457.3	1.25	11.3	11.1	0.1	113	2235	2075	
AF-318	457.1	0.78	14.6	17.8	-3.2	227	12772	2329	
AF-323	457.0	0.88	15.2	12.5	2.7	191	7633	2331	
AF-332	456.8	0.71	15.0	7.4	7.5	165	2451	1977	0.7084373
AF-334	456.7	0.87	14.8	13.0	1.8	235	2592	2020	

*The age of the Las Aguaditas Formation was approximated using the biostratigraphy of [31].
† Altered value, not plotted in Figure 3.2.

Table 3.5. Values for flux, mass and isotopic fractionation used for this study. Values for fluxes and isotopic compositions were estimated from typical values used for Phanerozoic studies (Kump and Arthur, 1999, Kurtz et al., 2003; Gill et al., 2011). Values for ΔS used are less than traditional values (Kah et al., 2004), but reflect the values recorded by data in this study for the early Darriwilian; δ_{carb} and δ_{SO4} were estimated from data recorded for intervals A and B of the current study (see Figure 3.2).

Carbon	Sulfur
$F_W = 3x10^{19}$ mol/My	$F_W = 1.5x10^{18}$ mol/My
$F_{CARB} = 2x10^{19}$ mol/My	$F_{GYP} = 0.5x10^{18}$ mol/My
δ_W = -4‰	δ_W = +7‰
ΔC = -28‰	ΔS = -30‰
δ_{CARB} (A) = -1‰	δ_{SO4} (A) = +30‰
δ_{CARB} (B) = +1.5‰	δ_{SO4} (B) = +15‰

Part 4

Bentonite geochronology, marine geochemistry, and the Great Ordovician Biodiversification Event (GOBE)

This chapter is a reformatted version of a paper by the same title submitted for publication to Palaeogeography, Palaeoclimatology, Palaeoecology in 2011 by Cara K. Thompson, Linda C. Kah, Ricardo Astini, Robert Buchwaldt, and Samuel Bowring.

Thompson, C.K., Kah, L.C., Astini, R., Buchwalt, R., Bowring, S. in review, Bentonite Geochronology, Marine Geochemistry, and the Great Ordovician Biodiversification Event (GOBE), Palaeogeography, Palaeoclimatology, Palaeoecology.

Abstract

Attribution of Ordovician climate forcing to explosive volcanism and its potential global importance in Ordovician biodiversification and extinction suggests the necessity of evaluating the relationships between K-bentonite deposition and increasingly high-resolution records of marine biogeochemical change. Globally, Ordovician strata preserve an extensive record of explosive volcanism—including the widely recognized Early to Middle Ordovician Famatina K-bentonite suite in Argentina and the Late Ordovician Millbrig-Diecke-Kinneulle suite of North America and Europe. Here, we present high-resolution ID-TIMS U-Pb zircon ages of K-bentonites from measured sections of the San Juan Formation (Talacasto and Cerro La Chilca section) of the Argentine Precordillera. These bentonites span a low-magnitude (2‰), globally-recorded negative excursion in marine carbon isotopic composition that provides an independent mechanism for global time-correlation.

K-bentonites from the Argentine Precordillera provide stratigraphically consistent (i.e., younging upward) ages that range from 473.45±0.70 Ma to 469.53±0.62 Ma. Evaluation of the timing of K-bentonite deposition in the Argentina Precordillera relative to marine biostratigraphic and biogeochemical records provides insight into relationships between explosive volcanism and regional to global environmental change. From a regional standpoint, these ages provide direct evidence for a Dapingian to earliest Darriwilian age of the upper San Juan Formation at these localities. These ages are consistent with recent carbon isotope correlation suggesting that the San Juan Formation in the region of its type section is coeval with only the base of the often-

correlated Table Head Group of Western Newfoundland and highlights the difficulties in using regional biostratigraphic data—particularly within erosionally truncated or otherwise diachronous units—to define the time-frame of carbon isotope chemostratigraphy. New geochronological data indicates that the pronounced negative carbon isotope excursion of the San Juan and Table Head formations is correlative to a globally recognized pre-MDICE negative excursion, and indicates that this aspect of the marine carbon isotope record can be used as a discrete chronologic marker. Argentinian bentonites, however, cannot be discretely correlated with observed, environmentally significant changes in the Middle Ordovician marine geochemical records of carbon, sulfur, strontium, or sea surface temperature, and suggests that the extent of volcanism represented by the Famatina bentonite suite was insufficient to affect global surface environments. These results suggest, in light of recent high-resolution records of marine chemistry during the Ordovician, that the relationship between explosive volcanism and environmental change—even during the Late Ordovician Millbrig-Diecke-Kinnekulle events—may not be straightforward.

1. Introduction

The Ordovician is characterized by a series of profound changes in Earth surface environments. Perhaps most dramatic of these changes was the expansion of marine life during the Great Ordovician Biodiversification Event (GOBE) (Harper, 2006). Over a 25 Myr period beginning in the early Ordovician, a cascade of diversification resulted in increased biodiversity at species, genus, and family levels (Droser and Sheehan, 1997; Webby et al., 2004; Harper, 2006). The peak of the GOBE broadly correlates with a maximum continental dispersion (Scotese and McKerrow, 1990; Crame and Owen, 2002; Webby et al., 2004), elevated pCO_2 (Berner and Kothavala, 2001; Herrmann et al., 2003), and global greenhouse climates. These conditions resulted in the largest area of tropical marine shelves in the Phanerozoic (Walker et al., 2002; Servais et al., 2009) and the potential for substantial diversification as a result of ecological interaction within an expanded ecosystem space (Droser and Finnegan, 2003; Harper et al., 2006; Achab and Paris, 2007; Servais et al., 2009; Servais et al., 2010). Yet there currently remains no single explanation for the GOBE (*see* Servais et al., 2009, 2010 *for review*), and a variety of

potential causes—including global cooling (Trotter et al., 2008; Zhang et al., 2010), changes in nutrient flux (Cardenas and Harries, 2010) and resulting expansion of phytoplankton (Servais et al., 2008; Hints et al., 2010), or even extraterrestrially-driven ecosystem disturbance (Schmitz et al., 2007)—remain under active investigation.

Second only to the GOBE is the end-Ordovician extinction, during which nearly 85% of this newly gained species-level diversity was lost (Jablonski, 1991; Sheehan, 2001). Although it is generally accepted that abrupt and widespread glaciation in the Hirnantian served as the primary mechanism for extinction (Brenchley et al., 1994; Sheehan 2001), the timing, extent, and mechanism of global cooling remains controversial. Although evidence for dramatic changes in sea level and sea surface temperature are typically restricted to a very short (approximately 1 Myr) interval in the Hirnantian (Brenchley et al., 1994; Finnegan et al., 2011), evidence for glacioeustatically driven sea level change (Pope and Read, 1998; Calner et al., 2010), expansion of cool-water depositional lithologies (Pope and Steffan, 2003; Cherns and Wheeley, 2007), carbon burial and CO_2 drawdown (Kump et al., 1995; Saltzman and Young, 2005; Young et al., 2005, 2008, 2010; Ainsaar et al., 2010), changes in oceanic circulation (Herrmann et al., 2004; Saltzman 2005; Thompson et al., 2010), and glacial deposition of strata in Africa (Theron, 1994; Hamoumi, 1999) suggest that onset of climate change may have been already underway at the height of the GOBE.

Recently, substantial attention has been given to the hypothesis of Barnes (2004), that large-scale volcanism and low-latitude emplacement of a continental basaltic province in the Ordovician may have played a role in both the GOBE and the climatic upheaval of the Hirnantian (Keller and Lehnert, 2010; Kidder and Worsley, 2010; Lefebvre et al., 2010). Unfortunately, with the exception of a sharp drop in marine $^{87}Sr/^{86}Sr$ in the Darriwilian (Qing et al., 1998; Shields et al., 2003) there is little direct evidence for the existence of such a basaltic province. Abundant evidence, however, for widespread bentonite deposits (Bergström et al., 1995; Kolata et al., 1996) associated with explosive volcanism in continental margin arc settings suggest that volcanism —as well as potential weathering of arc-related basaltic provinces—may have indeed

played a role in moderating environmental change in the Ordovician (Young et al., 2009; Buggisch et al., 2010).

Ordovician-aged bentonites have been reported in North America, South America, Europe, and Asia (Huff, 2008; Huff et al., 2010), with the Lower to Middle Ordovician Famatinian suite of Argentina (Huff et al., 1997; Fanning et al., 2004; Astini et al., 2007), and the predominantly Upper Ordovician Diecke-Millbrig-Kinekulle bentonite suite of North America and Sweden (Huff et al., 1992; Kolata et al., 1996, Bergström et al., 1995; 2004) being the most prominently discussed. Here, we examine age range of a portion of the Famatinian K-bentonite suite with respect globally recognized patterns of change in the marine records of carbon, sulfur, and strontium, in order to better understand the potential role of explosive volcanism in Ordovician biodiversification and climate change.

2. Geologic background

2.1. Argentine Precordillera

The Argentine Precordillera represents a microcontinent that rifted from the southeast margin of Laurentia in the Cambrian, drifted southward across Iapetus in the Early Ordovician, and eventually docked with Gondwana in the Late Ordovician (Figure 4.1) (Thomas and Astini, 1996; 1999; 2003). Biostratigraphic data for the Precordillera show a progression from fauna with predominantly Laurentian affinity in the Cambrian, through a period of increased endemicity and influence of Celtic-Baltic fauna in the Early Middle Ordovician, to fauna split between endemic and Gondwanan affinities by the Late Middle Ordovician (Benedetto, 1998; 2004; Benedetto et al., 1999; Albanesi and Ortega, 2002; Ramos, 1988). Biostratigraphic data are interpreted to reflect the tectonic position of the Precordilleran microcontinent as it drifted southward from Laurentia to Gondwana (Benedetto, 2004).

Sedimentary strata of the Precordillera are primarily comprised of mixed carbonate, siliciclastic, and evaporite deposits that represent a range of supratidal to deep subtidal environments (Astini

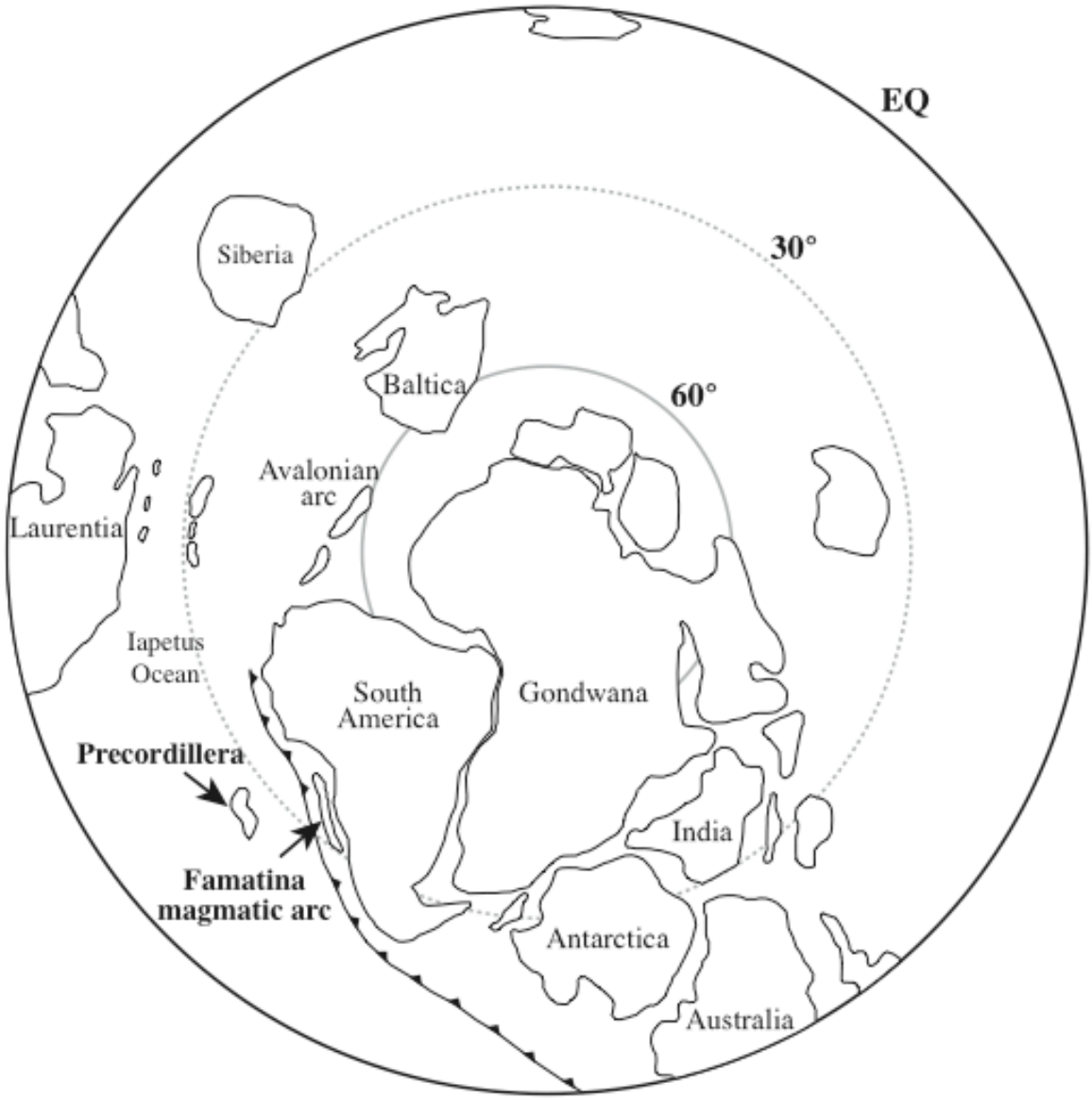

Figure 4.1. Paleogeographic reconstruction of the Middle Ordovician (c. 470 Ma; modified from Astini et al., 2007). The Argentine Precordillera drifted from mid-southerly latitudes, ultimately colliding with western Gondwana in the Middle-Late Ordovician. The Famatina magmatic arc has been identified as the source of voluminous ashfall deposits in the upper San Juan and lower Gualcamayo formations (Fanning et al., 2004).

et al., 1995). At the base of the Precordilleran succession, evaporite-bearing shale of the Lower Cambrian Cerro Totora Formation marks the initial rifting of the Precordilleran terrane rifted from southern Laurentia (Thomas and Astini, 2003), with passive-margin deposition initiating with the Lower to Middle Cambrian La Laja Formation (Gomez et al., 2007). Passive margin deposition continued from the Middle Cambrian through the Early Ordovician and is represented by the dominantly shallow-marine carbonate platform deposition of the Zonda, La Flecha, and La Silla formations (Cañas, 1999). Conformably overlying these deposits, deeper-water carbonate strata of the Lower to Middle Ordovician San Juan Formation (Astini et al., 1995), and north-south diachronous development of overlying deep-water shale, mixed carbonate-shale, and carbonate of the Gualcamayo, Las Chacritas, and Aguaditas formations in the Middle to Late Ordovician, reflect variation in subsidence rates with the approach of the Precordilleran microcontinent to Gondwana (Thomas and Astini, 1996; 2003). Finally, docking of the Precordillera with Gondwana is marked by Late Middle to Upper Ordovician clastic wedge deposits of the Trapiche Group and its equivalents, which are interpreted as recording development of a peripheral forebulge and steepening of slopes to the west, in response to tectonic loading during accretion (Thomas and Astini , 1996; 2003).

By the Latest Cambrian-Early Ordovician, an active margin had developed along the western Gondwanan margin (Astini, 2003; Astini and Dávila, 2004), and a series of Early Ordovician-aged K-bentonites in the Famatina terrane show compositional evolution from volcanic arc to more continental affinities (Astini et al., 2007). An absence of preserved bentonites in the Precordilleran terrane at this time suggests its spatial separation from the Gondwanan margin, with its approach to Gondwana marked by the widespread appearance of K-bentonite deposition in the Middle Ordovician (Huff et al., 1998; Astini et al., 2007).

Ultimately the Precordilleran terrane was uplifted by east-directed faulting of the Andean thrust belt in the Cenozoic (Thomas and Astini, 1999), and currently is exposed along the western margin of Argentina, striking north-south along the eastern margin of the Andean mountain range between 28°45′S and 33°15′S (Figure 4.2) (Ramos, 1988; 2004). To the west of the carbonate platform occur deep-water turbidites and ocean-floor mafic and ultramafic rocks

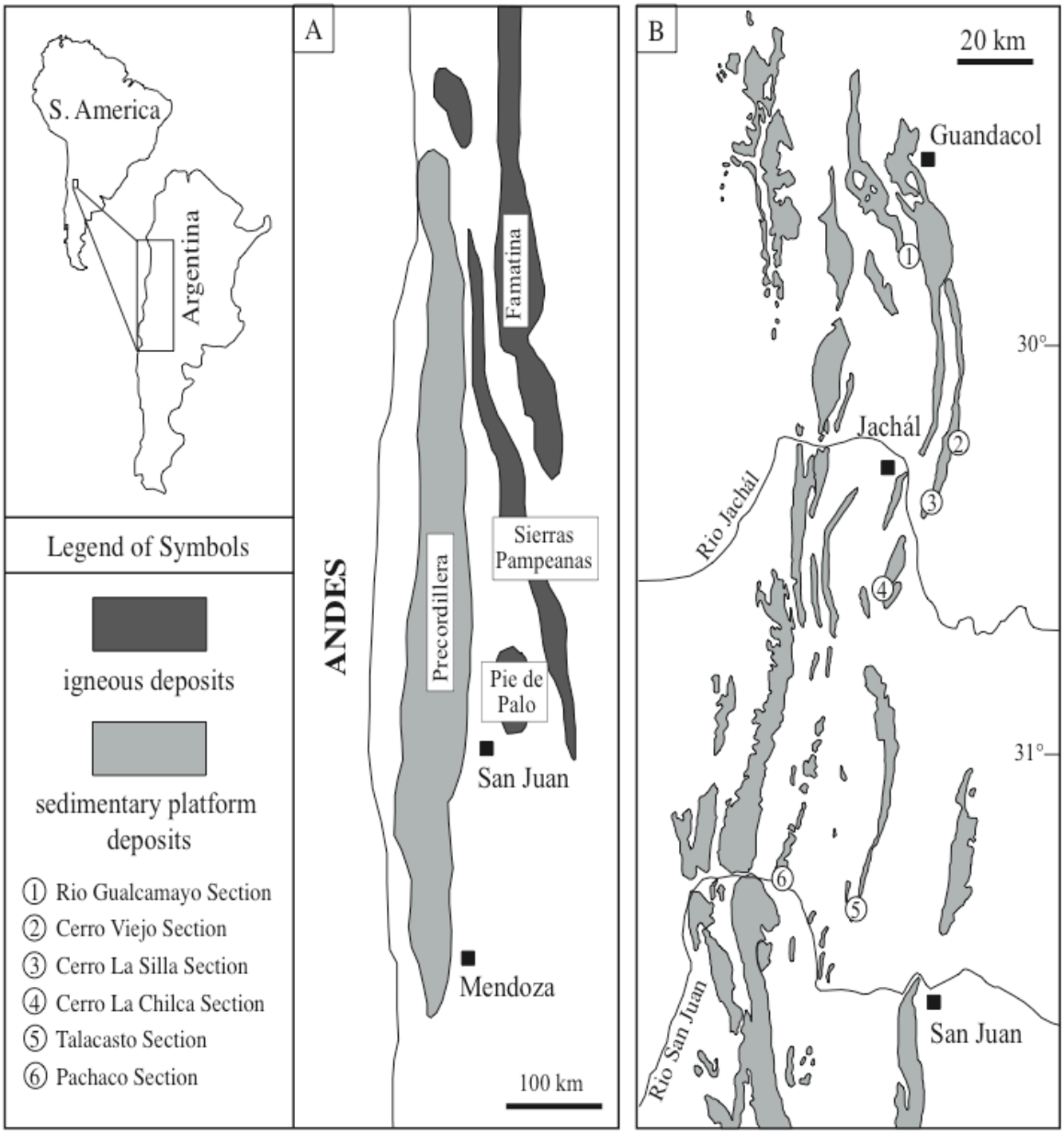

Figure 4.2. Geologic map of western Argentina (modified from Keller, 1994; Thomas and Astini, 2003). A) Geographic locality of the Precordilleran sedimentary terrane relative to the Sierra Pampeanas and Famatina magmatic arcs. B) Outcrop map of Precordilleran strata, noting sections of the San Juan and Gualcamayo formations. K-bentonites have been observed at all marked sections with the exception of the type section of the San Juan Formation at Cerro La Silla. For this study, bentonite horizons were sampled at Cerro La Chilca and Talacasto.

(Astini et al., 1995). The Famatina magmatic belt of the Sierra Pampeanas lies to the east, which consists primarily of igneous rocks with calc-alkaline continental margin affinities (Astini et al., 1995). The Famatinian volcanic arc, in particular, developed on and within basement metasedimentary and gneissic lithologies with protoliths derived, according to zircon ages, from Proterozoic to Cambrian sources (Pankhurst et al., 1998; Rapela et al., 2001).

2.2. Distribution of K-bentonites within the Precordilleran terrane

Numerous bentonite horizons have been reported in the upper San Juan and lower Gualcamayo Formations in the Argentine Precordillera (Huff et al., 1997; 1998; 2004; Fanning et al., 2004). These deposits are widespread in the Precordillera, where they occur interbedded with sub-tidal, storm-dominated carbonate deposits of the upper San Juan Formation and basinal shale of the Gualcamayo/Los Azules Formation. K-bentonites have been reported from sections at Talacasto La Chilca, Las Chacritas, Cerro Viejo and Rio Gualcamayo sections, and are here reported, as well, from the uppermost San Juan Formation strata at Pachaco. Bentonites are notably absent, however, from coeval, shallow-subtidal deposits of the San Juan Formation at its type section at La Silla, likely because bioturbation and wave action mixed ash deposits with underlying sediment, obscuring boundaries between carbonate deposition and ash deposits. By contrast, the absence of bentonites in strata of the lower San Juan Formation, from all sections, likely reflects the geographic distance of the Precordilleran terrane from the western Gondwanan margin at initiation of Famatina volcanism (Astini et al., 2007).

Major and trace element analyses show K-bentonites from the Talacasto section (Fanning et al., 2004) are high-silica rhyolites (>75% SiO_2), and are strikingly similar in composition to those collected by Huff et al., (1998) at the Cerro Viejo section, suggesting lateral continuity of volcanic ash falls across the Precordilleran terrane. Geochemical data further demonstrates the similarity of K-bentonites from both of these localities with magmas of the Chaschuil rhyolite in the Famatinian arc system (Fanning et al., 2004), suggesting that Famatinian magma is the likely parent body for widespread ash falls. A Famatinian origin for Precordilleran bentonites is further supported by chronological data (Fanning et al., 2004) that indicates, within uncertainty, that

ages of Precordilleran bentonites overlap with those from a porphyritic rhyolite from the Famatinian magmatic arc near Rio Chaschuil (468.3±3.4 Ma; Pankhurst et al., 2000).

2.3. Stratigraphic framework of San Juan Formation bentonites

In the Argentine Precordillera, bentonite deposits of the San Juan and Gualcamayo formations span the latest Floian to the mid-Darriwilian (Huff et al., 2003; Astini, *personal communication*). For this study, we report ages only from bentonite horizons within the San Juan Formation from the Talacasto and Cerro La Chilca exposures (Figure 4.2). These bentonites dissect a prominent, yet low magnitude, carbon isotope excursion wherein the isotopic composition of marine carbonates drop from 0‰ to approximately 2‰ before rising again to values near 0‰ (Figure 4.3). This negative isotopic excursion has been correlated to a near identical excursion in the lower Table Head Formation, Western Newfoundland (Thompson and Kah, *in review*; Thompson et al., *in review*). Overlying strata of the Table Head and Table Cove formations in Newfoundland (as well as strata of the Las Chacritas and Las Aguaditas formations in Argentina, show continued rise in marine carbon isotope composition in the aftermath of this excursion to values near +1.5‰ (Thompson et al., *in review*). These elevated values are considered equivalent to the MDICE event (Ainsaar et al., 2004). The MDICE is the oldest of seven positive marine carbon isotope excursions in the Middle to Late Ordovician that have been recognized and named (Bergström et al., 2009). The MDICE has been recorded broadly across Baltica (Ainsaar et al., 2004; 2010; Kaljo et al., 2007), China (Schmitz et al., 2010), and potentially North America (Saltzman and Young, 2005). North American marine carbon isotope records, however, are ambiguous as to the positive aspect of this excursion (cf. Saltzman and Young, 2005), so we consider the combined dataset from Argentina and Newfoundland to represent the first clear record of the MDICE in the western hemisphere.

The negative carbon isotope excursion considered here is potentially correlative to low magnitude (<2‰) negative excursions that are widely recognized to directly precede the MDICE event (Ainsaar et al., 2004; 2010; Saltzman and Young, 2005; Kaljo et al., 2007; Schmitz et al., 2010). The biostratigraphic correlation of this negative isotopic excursion, however, is at present

poorly constrained. In the Argentine Precordillera, bentonite deposits of the San Juan and Gualcamayo formations span the uppermost *O. evae* through *P. suecicus* conodont zones (Huff et al., 2008) and the *victoriae* to *elegans* graptolite zones (Huff et al., 1998; Astini et al., 2007), indicating an age of latest Floian (FL3) or earliest Dapingian (DP1) to late Darriwilian (DW3) (Bergström et al., 2008). Current U-Pb geochronology of the Precordilleran K-bentonites provide ages broadly consistent with biostratigraphic zonations: with bentonite horizons yielding ages of 469.5±3.2 Ma and 470.1±3.3 Ma (Fanning et al., 2004) to 464±2 Ma (Huff et al., 1997). Fanning et al., (2004) noted, however, that the latter age was calculated by merging three concordant data points with one discordant point. A recalculated age that excluded the discordant point, provided a mean $^{207}Pb/^{206}Pb$ age of 470.9±3.4 Ma, and suggests that the Famatinian bentonite suite occurs largely within the upper Dapingian to lower Darriwilian.

Across Baltica and China, the pre-MDICE negative isotope excursion occurs largely within the *L. variabilis* to the *E. suecicus* conodont zones (Ainsaar et al., 2004; 2010; Kaljo et al., 2007; Schmitz et al., 2010). Although regional biostratigraphic data from the Argentine Precordillera are consistent with an early to mid-Darriwilian (*M. parva* to *L. variabilis*) age for this event (Buggisch et al., 2003), recent correlation of carbon isotope records from Argentina and Western Newfoundland (Thompson and Kah, *in review*; Thompson et al., *in review*) show this excursion in the lower Table Head Formation (Figure 4.3), which requires that the excursion lies substantially below the top of the *L. variabilis* zone which defines the top of the overlying Table Cove Formation (Maletz, 2009). These correlations would place the observed negative excursion in the Dapingian to early Darriwilian, which is broadly consistent with current geochronological constraints but inconsistent with its identification as the pre-MDICE negative excursion. Much of the current uncertainty in the age of this chemostratigraphic event arises from the regional diachroneity of the top of the Middle Ordovician San Juan Formation, which undergoes both rapid deepening and differential erosion with tectonic loading and migration of the peripheral bulge as the Precordilleran terrane approaches and begins to dock with the western Gondwanan margin (Thomas and Astini, 1996; 2003).

3. Geochronology of Precordilleran bentonites

Figure 4.3. Biostratigraphic and chemostratigraphic correlation of the San Juan Formation, Argentina. A) Proposed biostratigraphic framework for carbon isotope stratigraphy from Buggisch et al. (2003) based on regional maximum duration of the San Juan Formation. This biostratigraphic calibration is complicated by differential subsidence and/or uplift across the Precordilleran terrane during the Middle Ordovician convergence of the Precordillera with western Gondwana. This ultimately resulted in substantial diachroneity for the top of the San Juan Formation. B) Proposed biostratigraphic framework for carbon isotope stratigraphy from Thompson and Kah (in review) based on chemostratigraphic correlation of strata from Argentina and Newfoundland combined with of biostratigraphic constraints from these two geographically disparate units. Stage slices are from Bergström et al. (2008) and time slices are from Webby et al. (2004).

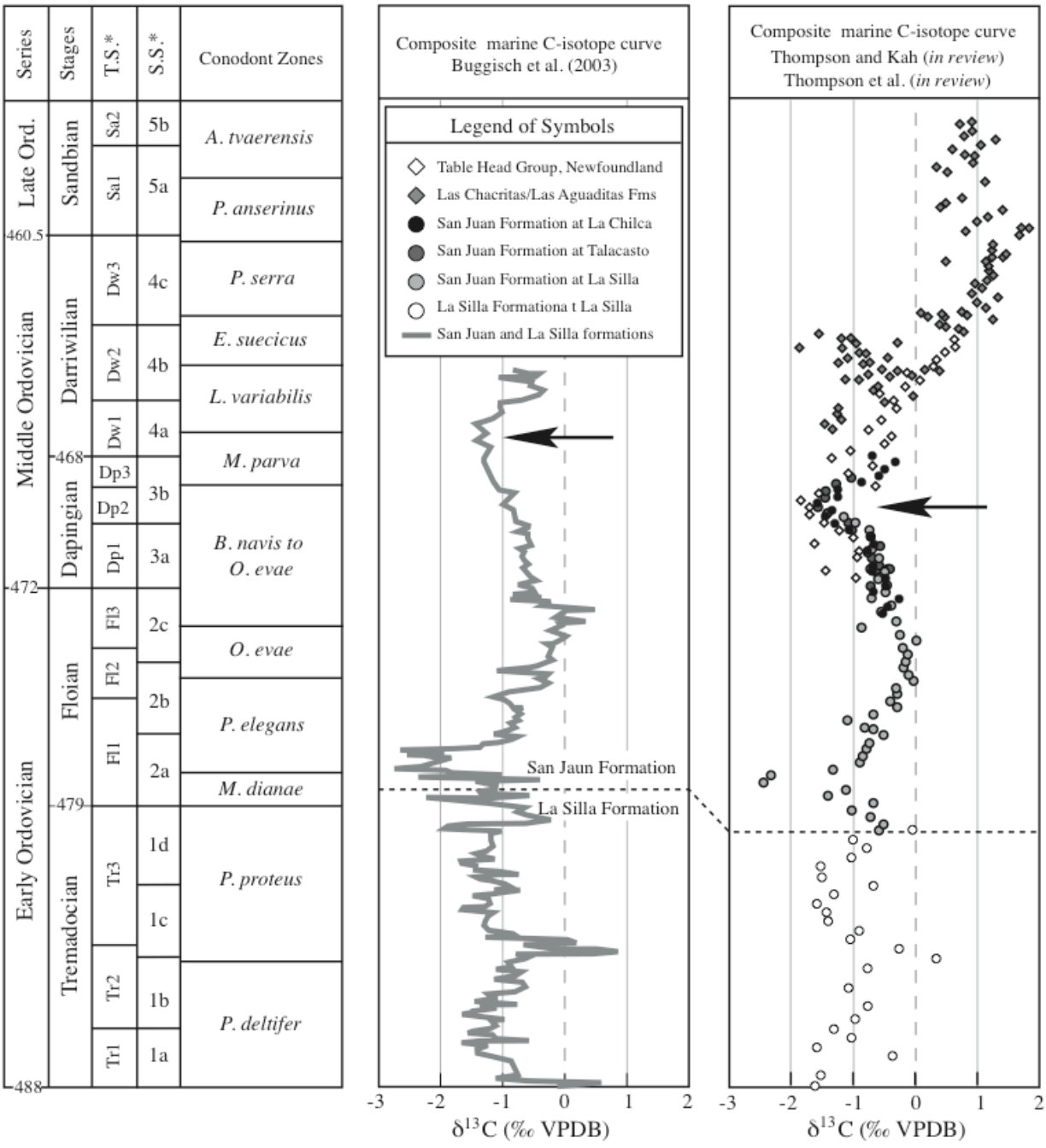
Series
Stages
T.S.*
S.S.*
Conodont Zones
Late Ord.
Middle Ordovician
Early Ordovician
Sandbian
Darriwilian
Dapingian
Floian
Tremadocian
460.5
468
472
479
488
Sa2
Sa1
Dw3
Dw2
Dw1
Dp3
Dp2
Dp1
Fl3
Fl2
Fl1
Tr3
Tr2
Tr1
5b
5a
4c
4b
4a
3b
3a
2c
2b
2a
1d
1c
1b
1a
A. tvaerensis
P. anserinus
P. serra
E. suecicus
L. variabilis
M. parva
B. navis to
O. evae
O. evae
P. elegans
M. dianae
P. proteus
P. deltifer
Composite marine C-isotope curve
Buggisch et al. (2003)
Legend of Symbols
Table Head Group, Newfoundland
Las Chacritas/Las Aguaditas Fms
San Juan Formation at La Chilca
San Juan Formation at Talacasto
San Juan Formation at La Silla
La Silla Formationa t La Silla
San Juan and La Silla formations
San Jaun Formation
La Silla Formation
-3
-2
-1
0
1
2
δ13C (‰ VPDB)
Composite marine C-isotope curve
Thompson and Kah (in review)
Thompson et al. (in review)
-3
-2
-1
0
1
2
δ13C (‰ VPDB)

3.1. Sample collection

K-bentonites were sampled from measured section of the San Juan Formation at Cerro La Chilca (30º 36´16.9″S, 69º47´41.0″W) and Talacasto (31º00´35.5″S, 68º46´12.0″W). Carbonate samples for stable isotopic (C, S, O) analysis were collected from the same measured sections (Thompson and Kah, *in review*). The San Juan Formation at Talacasto consists of an incomplete, composite section: lowermost strata of the San Juan Formation are deformed by chevron folds above a basal detachment and duplicated by numerous secondary faults; and the uppermost strata of the formation are erosionally removed and overlain by Silurian green shale. All samples for geochemical analysis were collected from the upper 125 meters of the section, which represent an incomplete, yet continuous and non-faulted section of the San Juan Formation. More than 70 bentonites appear in the measured Talacasto section, and 11 were sampled for this study. Similarly, the uppermost 180 meters of the San Juan Formation at the Cerro La Chilca section were measured and sampled for stable isotopic and geochronological analysis. At Cerro La Chilca, bentonites are concentrated in the upper 50 meters of the formation, and in the transitional beds that mark the boundary between the San Juan Formation and the overlying Gualcamayo Formation. More than 50 bentonites occur in the Cerro La Chilca section, and 10 were sampled for this study. In both localities, sampling was concentrated on well-preserved, relatively undisturbed bentonite horizons with distinct, normal grading. These horizons are interpreted to represent single, discrete ash fall events. Before sampling, surficial material was removed to expose the freshest material, and sampling focused on the lowest, most coarse-grained interval was collected since zircons are expected to be concentrated in these intervals. In the sections sampled for this study (Talacasto and Cerro La Chilca; Figure 4.4A, B), K-bentonites occur as discrete units that range in thickness from <1 cm to approximately 30 cm, with most ranging from 3-8 cm. K-bentonites are typically tan to buff colored, are clay-rich, and are typically recessed relative to the host carbonate rocks. Strata underlying bentonite horizons are iron-stained and commonly contain a cephalopod-rich death assemblage. Most bentonite horizons occur as single ash-fall deposits (Figure 4.4C), although several composite K-bentonite deposits were also observed (Figure 4.4D). Composite K-bentonites are identified by

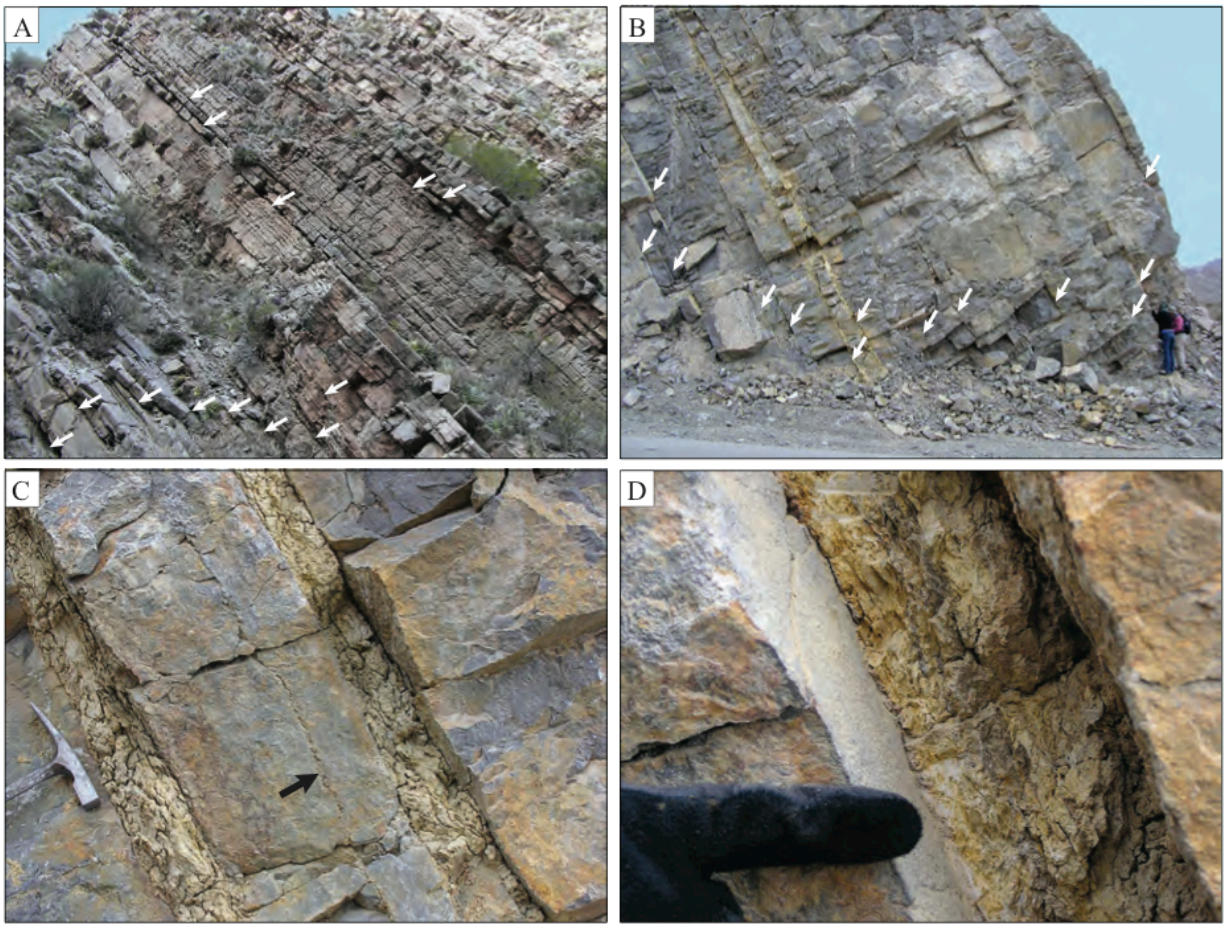

Figure 4.4. Stratigraphic occurrence of K-bentonites at Cerro La Chilca and Talacasto. A) Strata of the San Juan Formation at Cerro La Chilca with arrows locating a number of bentonite horizons. Bentonites occur predominantly in the upper 50 meters of the San Juan Formation and through the transitional beds that mark the onset of the Gualcamayo Formation. B) The uppermost strata of the San Juan Formation at Talacasto with arrows location a number of prominent bentonite horizons. More than 70 bentonite horizons occur in the upper 125 meters of section, which is truncated and unconformably overlain by Silurian aged strata. C) Two prominent K-bentonites in the upper San Juan Formation at Talacasto (see B). Bentonite horizons range from several millimeters in thickness (arrow) to approximately 20 cm. D) Composite bentonite horizon consisting of two distinct ash fall unites marked by distinct, normal grading.

superposition of two or more events that show distinct normal grading. Grading is not observed within all horizons, and may reflect a combination of depositional and modern (i.e. rooting, or rodent burrowing) homogenization processes.

3.2. Sample preparation and analysis

Zircon grains were dated using single grain ID-TIMS techniques (Schoene et al., 2006) at the Massachusetts Institute of Technology (MIT). Bentonites were processed using conventional magnetic and heavy liquid (methylene iodide) techniques to extract and separate zircon populations. Heavy mineral separates were hand picked in ethanol under an optical microscope to separate and classify zircons based on size, shape, clarity, and occurrence of inclusions. When possible, clear, elongate zircons with minimal inclusions were chosen for geochronological analysis in order to analyze the most rapidly formed, unaltered zircons. Internal zoning patterns were observed via SEM-cathodoluminescence (Figure 4.4). Grains were treated using chemical abrasion techniques, wherein zircons were annealed in quartz beakers at ~900°C for 60 hours (Mattinson, 2005) and leached in concentrated HF at 210°C for 12 hours to remove metamict grains or metamict grain portions.

Once samples were chemically abraded and annealed, all additional sample processing took place in a clean lab. Any common Pb in zircon analyses was considered to be procedural contamination during zircon dissolution. Zircons were transferred to Teflon beakers and cleaned by fluxing with 30% HNO_3 for 30-40 min, sonication, and rinsing in ultrapure water. Initial cleaning was repeated with another fluxing with 6.2N HCl for 30-40 min, followed by sonication and rinsing. Individual zircons were then dissolved in concentrated HF for 48 hours in teflon microvials at 210°C after being spiked with Earthtime ET535 ^{205}Pb-^{233}U-^{235}U tracer solution.

Uranium and lead were collected by HCl-based anion exchange procedures modified from Krogh (1973). Pre-cleaned columns were filled with 200-400 μm microbead resin and cleaned by flushing with 6N HCl (to flush any possible Pb contaminant), ultra-pure Milli-Q water, 6N HCl, 0.1N HCl (to flush any possible U contaminant), and 3N HCl. After cleaning, dissolved zircon

fractions were loaded in each column, which was then flushed with 3N HCl three times to remove zirconium. Pb was then released by flushing with 6N HCl, and U was released by flushing with 0.1N HCl. Pb and U were collected in clean Teflon beakers placed underneath the columns. Teflon beakers were cleaned by fluxing alternately with 6N HCl and 6N HF on a hot plate overnight (four times total). Pb and U were loaded together on a single Re filament using a silica-gel. U-Pb isotopic measurements were performed on a VG Sector-54 multi-collector thermal-ionization mass spectrometer at MIT. Error and weighted means were calculated using U-Pb Redux (McLean et al., 2008, 2009) and is reported as 2σ. Errors on the weighted mean are reported in a tripartite ±X/Y/Z scheme that denotes, respectively, the internal laboratory error, the tracer calibration error, and the tracer calibration and decay constant errors of Jaffey et al., (1971). Once ages have been reported with full error calculation, they will be referred to only in terms of the error that includes both the tracer calibration and decay constant errors.

4. Results and interpretation

Geochronological data from zircons of the San Juan Formation K-bentonites is summarized in Table 4.1. C-, S-, and O-isotope and major and trace element results are detailed in Thompson et al., (*in review*) and Thompson and Kah (*in review*).

Heavy mineral fractions were separated from a total of nine K-bentonites (KB-1, KB-3, KB-7, KB-10, KBT-1, KBT-3, KBT-4, KBT-7, and KBT-10). These samples represent a combination of the lowermost and uppermost San Juan Formation bentonites from the La Chilca (KB samples) and Talacasto (KBT) measured sections, and therefore maximized the potential to resolve discrete depositional ages even under conditions of high sedimentation rate. One sample yielded no recoverable zircons (KB-10), and geochronological analyses were ultimately carried out on the five samples (KB-1, KB-3, KBT-3, KBT-7 and KBT-10) that yielded the greatest abundance of zircons. These five K-bentonite horizons also are positioned to define the lower portion and apex of a prominent, yet low magnitude (~2‰) negative carbon isotope excursion that occurs prior to the MDICE carbon isotope event (Figure 4.3). KBT-3 was deposited in the

lower third of this $\delta^{13}C$ excursion, whereas KBT-7, KBT-10, KB-1 and KB-3 were deposited as $\delta^{13}C$ reached its negative apex and began to return to heavier isotopic values.

4.1. Zircon morphology and textures

Zircons extracted from San Juan Formation K-bentonites are typically small (<100 μm) and show a range of morphologies, although most are euhedral, lozenge to needle shaped, and have bipyramidal terminations with no evidence for significant transport. Broken grains retain sharp edges along broken surfaces suggesting recent breakage, perhaps during extraction or by handling after the annealing process. Zircons are generally clear, although some contain distinct inclusions. Overall, grains display fine-scale, oscillatory-zoning under cathodoluminescence, with only a few recording more complicated internal structures such as rounded, internal cores; truncated zoning; and inclusions. Zircons with simple, zoned patterns and those that lacked cores were chosen for analyses.

Zircons from KBT-3 and KBT-7 are small (<100 μm in length) and euhedral (Figure 4.5A, B), and zircons from KBT-3 display bimodal, stubby and acicular, morphologies. We chose to analyze acicular grains (length to width ratios >3:1) since this morphology is often associated with rapid crystallization and therefore are likely to reflect an age that is closer to the eruption age (Corfu et al., 2003). Zircons extracted from samples KBT-10 and KB-1 are generally larger (>100 μm in length), and display predominantly acicular morphologies with length to width ratios >3:1 (Figure 4.5C, D, E). Finally, zircons from KB-3 are typically small (<100 μm in length) and euhedral, although many grains display oscillatory-zoning with internal voids or rounded cores (Figure 4.5F).

4.2. Geochronology of San Juan Formation zircons

4.2.1. Sample KBT-3N

Figure 4.5. Cathodoluminescence images of San Juan Formation zircons. A) Zircon grain from sample KBT-3N (Talacasto section) showing fine-scale oscillatory zoning. B) Zircon grain from sample KBT-7 (Talacasto section) showing fine-scale oscillatory zoning and bipyramidal terminations. C) Fragment of acicular zircon grain from sample KBT-10 (Talacasto section) showing fine-scale oscillatory zoning. D) Acicular zircon grain from sample KBT-10 (Talacasto section) showing fine-scale oscillatory zoning and a small inclusion. E) Zircon grain from KB-1 (Cerro La Chilca section) showing oscillatory zoning that is similar to zircons from the Talacasto section. F) Zircon grain from KB-3 (Cerro La Chilca) showing sub-rounded, inherited core. Scale bars are 50 μm in all photomicrographs.

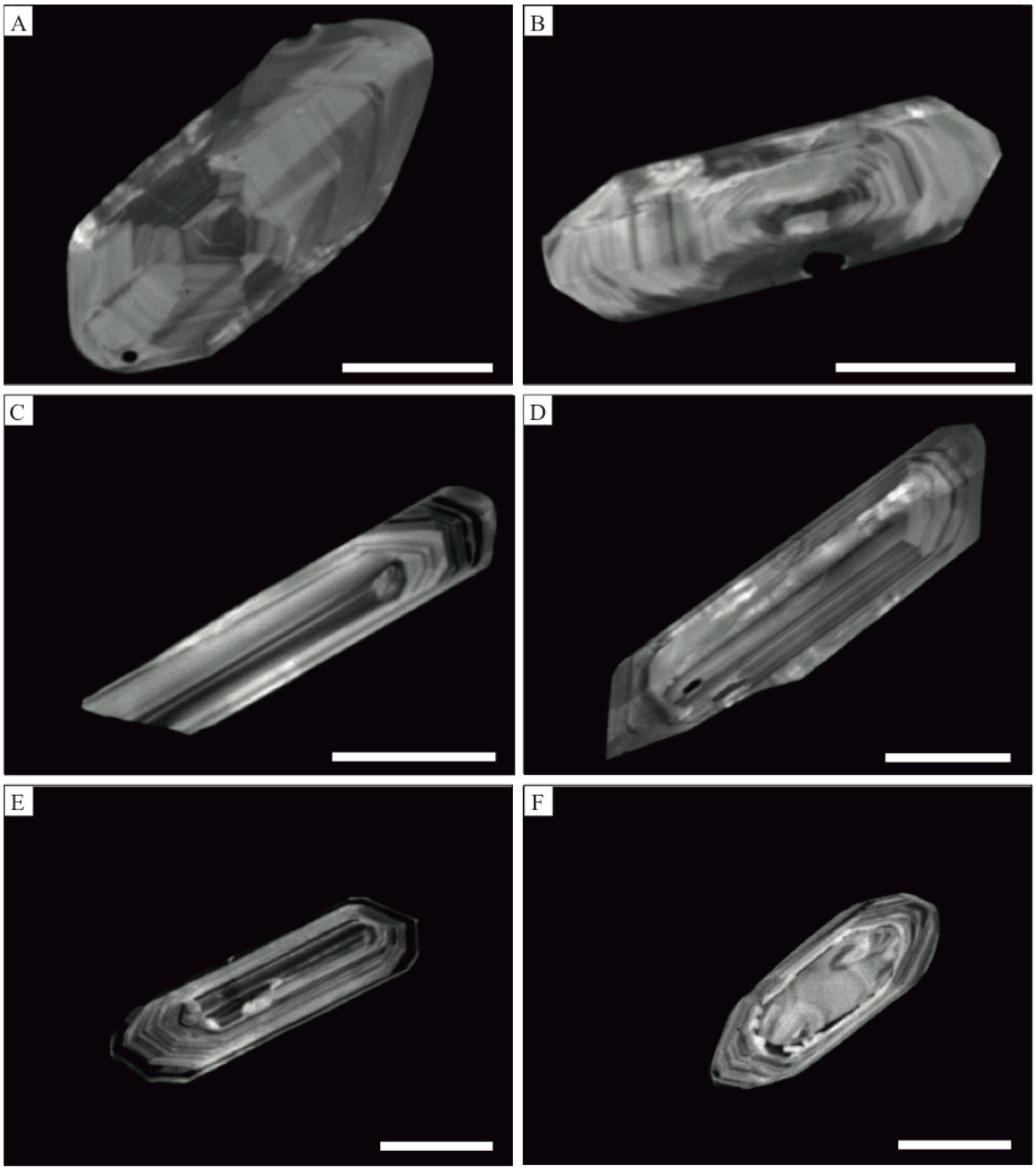
A
B
C
D
E
F

Five grains from sample KBT-3 were analyzed. Grain Z3 yielded an age that is older than the other grains and, because this sample had low common Pb (0.33 pg) and the KBT-3N (needle-shaped grain) population displayed potential for inherited cores, this age is considered to reflect inheritance. On a concordia plot (Figure 4.5), the remaining four analyses form a group near or within uncertainty of the concordia curve. A weighted mean of the remaining four analyses yields a mean age of 473.45 ±0.40/0.49/0.70 with MSWD = 0.65. The acicular shape and oscillatory-zoning, which is typical of magmatic grains (Corfu et al., 2003), suggests resolution at or near the eruption age [473.45 ±0.70] of the volcanic ash.

4.2.2. Sample KBT-7

Eight grains from sample KBT-7 were analyzed. Grains Z7 and Z8 were excluded from age calculation because of their high common lead content (1.37 and 1.49 pg, respectively), which likely represents procedural contamination. On a concordia plot (Figure 4.6), Z1 and Z3 fall largely outside uncertainty of the concordia curve and are, therefore, excluded from the age calculation. The remaining four analyses form a group near or within uncertainty of the concordia curve. A weighted mean of these four analyses gives an age of 469.86 ±0.33/0.42/0.65 with MSWD = 1.4. Fine-scale oscillatory-zoning that is typical of magmatic grains (Corfu et al., 2003) suggests resolution at or near the eruption age [469.86 ±0.65] of the volcanic ash.

4.2.3. Sample KBT-10

Eight grains from sample KBT-10 were analyzed. Grain Z10 was excluded from age calculations because of its high common lead content (1.93 pg), which likely reflect procedural contamination. On a concordia plot (Figure 4.5), Z6 and Z9 fall well outside uncertainty of the concordia curve and, therefore, are excluded from the age calculation. The remaining five analyses form a group near or within uncertainty of the concordia curve A weighted mean of these grains yields a mean age of 469.63 ±0.21/0.33/0.60 with MSWD = 0.97. The acicular shape and oscillatory-zoning, which is typical of magmatic grains (Corfu et al., 2003) suggests resolution at or near the eruption age [469.63 ±0.60] of the volcanic ash.

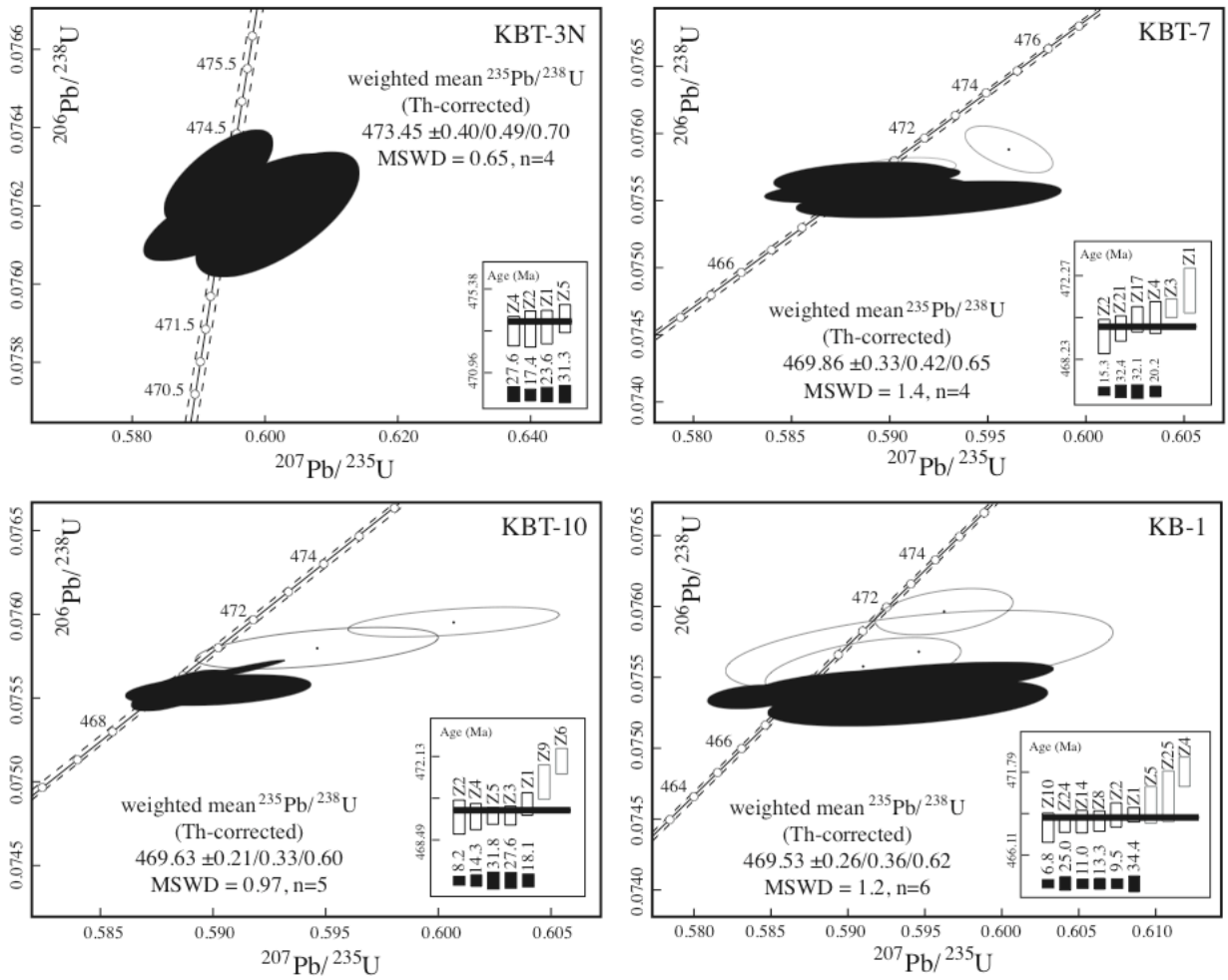

Figure 4.6. U-Pb concordia diagrams of whole grain zircon analyses from the upper San Juan Formation at Talacasto (KBT) and Cerro La Chilca (KB), with internal error without systematic error, tracer calibration error, and combined tracer calibration and decay constant errors. Shaded ellipses represent analyses that were included in mean age calculations. Black bars represent the weight fraction that each analysis represents in mean age calculations. Thin dotted lines represent the concordia error range that results from propagation of decay constant counting statistic error (2σ) from Jaffey et al. (1971).

4.2.4. Sample KB-1

Nine grains from sample KB-1 were analyzed. On a concordia plot (Figure 4.5), zircons Z4, Z5 and Z25 fall well outside uncertainty of the concordia curve and, therefore, are excluded from the age. These grains could represent contamination from inclusions. The remaining six analyses form a group near or within uncertainty of the concordia curve. A weighted mean of these six grains yields a mean age of 469.53 ±0.26/0.36/0.62 with MSWD = 1.2. This is interpreted as the eruption age of the volcanic ash. The acicular shape and oscillatory-zoning, which is typical of magmatic grains (Corfu et al., 2003) suggests resolution at or near the eruption age [469.53 ±0.62] of the volcanic ash.

4.2.5. Sample KB-3

The two grains from sample KB-3 that were analyzed each yielded Proterozoic ages (1060 and 1330 Ma). These ages suggest the zircons are potentially sourced from basement metasediments and gneisses of the Famatina and Pampeanas arc terranes (Figure 4.2A), which have yielded zircons with continental affinities that range in age from 500 to 2000 Ma (Casquet et al., 2001; Rapela et al., 2001). Zircons analyzed from KB-3, therefore, were interpreted as inherited and no further analyses were conducted.

5. Discussion

5.1. Defining Precordilleran chronology

The resolved age of sample KBT-3 falls within the Floian stage of the 2009 GSA Geologic Time Scale (Walker and Geissman, 2009); mean ages of the remaining samples fall entirely within the Dapingian stage. The ages of KBT-3, KBT-7, KBT-10, and KB-1 are within error of mean U-Pb zircon ages previously reported for the Talacasto section (469.5±3.2 Ma and 470.1±3.3 Ma; Fanning et al., 2004). All bentonites analyzed in this study are older than the U-Pb zircon mean

age reported for the Cerro Viejo section (464±2 Ma; Huff et al., 1997), but agree well with a recalculation of this age to 470.9±3.4 Ma (Fanning et al., 2004).

Difficulty arises, however, when considering these ages within a biostratigraphic framework for the San Juan Formation. The biostratigraphic age of the San Juan Formation is well constrained at its base to the *Macerodus dianae* zone, which is considered coeval with the uppermost Tremadocian *P. deltifer* conodont zone (Albanesi et al., 1998; Buggisch et al., 2003). The top of the formation, however, is regionally diachronous, with biostratigraphic determinations spanning an 8-10 Myr range from conodont zones *O. evae* to *L. variabilis* (Albanesi et al., 1998; Albanesi et al., 1999; Cañas and Aguirre, 2005) or *E. suecicus* (Sarmiento, 1991). Diachroneity of the uppermost San Juan Formation is recorded through the eastern Precordillera by a north-to south shift in depositional facies to deeper-water facies of the Gualcamayo, Las Chacritas, and Las Aguaditas formations (cf. Keller et al., 1993; Keller, 1999), or by truncation—either structurally, as at its type section of La Silla (Buggisch et al., 2003), or stratigraphically, as at Talacasto where it is unconformably overlain by deposits of Silurian-aged shale (Keller, 1999). Chemostratigraphic correlation of the San Juan Formation and conformably overlying Gualcamayo, Las Chacritas, and Las Aguaditas formations with carbonate strata of the Table Point and Table Cove formations, Western Newfoundland (Thompson and Kah, *in review;* Thompson et al., *in review*), suggest a similar mid-Dapingian to mid-Darriwilian (or approximately 470-464 Ma) diachroneity for the upper San Juan Formation. In sharp contrast to the correlation of biostratigraphic and chemostratigraphic profiles (Figure 4.3) proposed by Buggisch et al., (2003), the addition of biostratigraphic markers provided by chemostratigraphic correlation with Western Newfoundland (Thompson and Kah, *in review;* Thompson et al., *in review*) require that the uppermost strata of the San Juan Formation at both Talacasto and Cerro La Chilca reside close to the Dapingian-Darriwilian boundary. Combined chemo-biostratigraphic correlations are entirely consistent with geochronological data reported here. Close correspondence between the stratigraphic C-isotope profiles for Cerro La Chilca and Talacasto measured sections suggest similar deposition rates recorded by these strata. Geochronological constraints give a duration between KBT-3 and KBT-10 of the Talacasto section of 3.8±0.45 Myr, which, assuming a field measurement error of ±5%, gives a sedimentation rates of 21.8±2.8

(19 to 24.6) meters/Myr. These sedimentation rates place the top of the San Juan Formation (defined as the top of the 20.9 meter thick "transitional beds" which mark the boundary between the San Juan and overlying Gualcamayo Formation), which lies 45.2 meters above sample KB-1, at approximately 467 Ma, or within the earliest Darriwilian.

5.2. Calibration of marine carbon isotopes

San Juan Formation bentonites occur across a prominent, low-magnitude (<2‰) negative carbon isotope excursion. Radiometric calibration of the San Juan Formation marine carbon isotope curve (Figure 4.7) requires revision of the current biostratigraphic interpretation (Buggisch et al., 2003). Although marine carbonate rocks attributed to the San Juan Formation extend into the Middle Darriwilian *E. suecicus* conodont zone (Sarmiento, 1991), it has been well-documented that the top of the San Juan Formation is diachronous across the Precordillera (Albanesi et al., 1998; Albanesi et al., 1999; Cañas and Aguirre, 2005). Both the Talacasto and Cerro La Chilca sections of the San Juan Formation occur near its type locality at Cerro La Silla (Figure 4.2). Chronometric calibration of the marine carbon isotope curve indicates that the top of the San Juan Formation in this region occurs within the earliest Darriwilian. This revised calibration (Figure 4.7) demonstrates that the observed negative carbon isotope event was initiated in the latest Floian (*O. Evae* conodont zone), reached its minima in the middle Dapingian (*B. navis* conodont zone), and returned to near 0‰ values near the in the early to middle Darriwilian (uppermost *L. variabilis* to lowermost *E. suecicus* conodont zone)—well above the top of the San Juan Formation near its type locality.

This revised calibration suggests, as well, the need to evaluate the behavior of the marine carbon isotope record leading up to the mid-Darriwilian MDICE event. Everywhere where the MDICE event has been established, including within Latvia and Estonia (Ainsaar et al., 2004; 2010; Kaljo et al., 2007), Sweden (Sweden, Bergström, 2007; Schmitz et al., 2010), China (Schmitz et al., 2010), Newfoundland (this study) and Argentina (this study), positive carbon isotope excursions are initiated near the base of the *E. suecicus* conodont zone and continue above the *E. suecicus* zone into the Late Darriwilian *P. serra* conodont zone. Carbon isotope values then

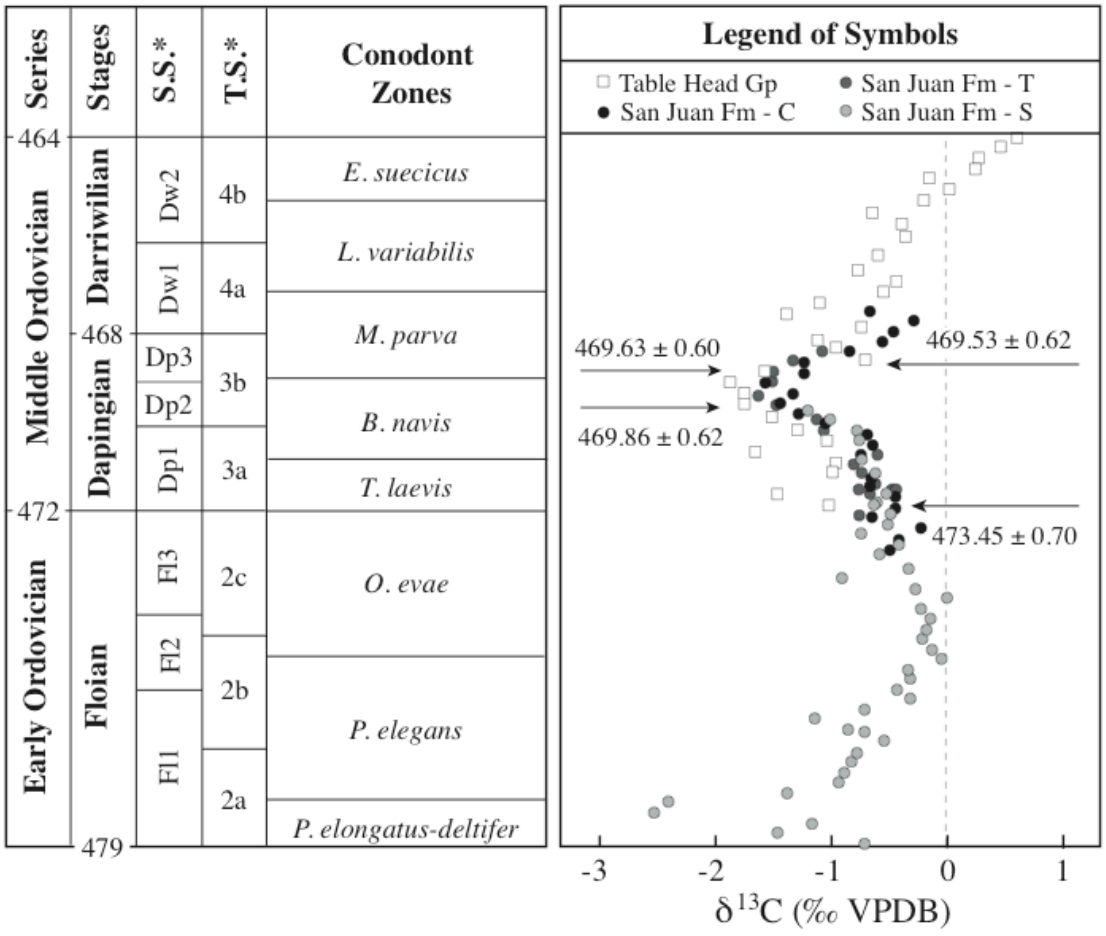

Figure 4.7. Geochronological constraints on carbon isotope chemostratigraphy. Carbon isotope chemostratigraphic correlation of Early and Middle Ordovician strata from Argentina (San Juan Formation) and Western Newfoundland (Table Head Group, including the Table Point and Table Cove formations) across a prominent, yet low magnitude negative carbon isotope excursion. New radiometric ages are consistent with biostratigraphic calibration suggested by Thompson and Kah (in review; see Fig. 3) and suggest that this low magnitude negative carbon isotope event spans from the late Floian (*O. evae* conodont zone) to the mid-Darriwilian (uppermost *L. variabilis* conodont zone). The trend to more positive carbon isotope values (to 1.5‰ in the late Darriwilian, (see Fig. 3) begins in the mid-Darriwilian (*E. suecicus* conodont zone) and is interpreted to reflect the first clear identification of the MDICE excursion (Ainsaar et al., 2010) in both Laurentia (Western Newfoundland) and South America (Argentine Precordillera). Stage slices are from Bergström et al. (2008) and time slices are from Webby et al. (2004).

remain elevated until the latest Darriwilian (*P. anserius* conodont zone) before they begin to decline. The structure of the pre-MDICE carbon isotope record, however, is variable. In sections representing deposition in deep-water (deep shelf-to-slope) environments, such as the Jurmala borehole in Latvia (Ainsaar et al., 2010) or the Western Newfoundland (this study; for lithologic descriptions and depositional environments, see Thompson et al., *in review*), marine carbon isotope records reveal a broad (6-8 Myr duration) negative excursion that reaches its nadir in the *B. navis* conodont zone. By contrast, stratigraphic sections that represent shallower-water (mid-shelf) environments, such as the Kerguta and Mehikoorma boreholes (Kaljo et al., 2007; Ainsaar et al., 2010) and Tallinn section (Ainsaar et al., 2004) in Estonia, the Kargärd section in Sweden (Bergström, 2007), and the Las Chacritas and Las Aguaditas sections of Argentina (this study; for lithologic descriptions and depositional environments, see Thompson et al., *in review*), show an initial decrease in marine carbon isotope composition followed by a distinct kick to more positive values in the *L. variabilis* conodont zone and an additional decline downward in the section to an isotopic nadir in the *B. navis* conodont zone.

Sections representing deposition in environments transitional between these two states, such as the Hallekis Quarry section in Sweden, or the Puxi River and Maocaopu sections of China (Schmitz et al., 2010), appear to record a combination of these two signals wherein strata record a broad negative isotope excursion with a small positive increase (<0.5‰) in the *L. variabilis* conodont zone.

That the pre-MDICE carbon isotope excursion appears to be quite low in its magnitude (< 2‰), long in its duration (6-8 Myr), and strongly correlated with depositional environment suggests that the excursion may simply reflect an isotopic depth gradient in the ocean and its interaction with different marine environments. In this scenario the isotopic "kick" in the *L. variabilis* conodont zone, and increased isotopic variability represented by sections representing the shallowest-water marine environments, such as the Tallinn section in Estonia (Ainsaar et al., 2004) or the Antelope Valley section in the United States (Saltzman and Young, 2005), may represent the inherent variability within these environments. Regardless, the marine carbon isotope records from Argentina and Newfoundland appear to accurately reflect marine carbon

record as preserved globally, suggesting that this pre-MDICE negative carbon isotope excursion—despite its environmentally-controlled variation— may be used as a discrete chronologic marker.

5.3. Climate consequences of explosive volcanism in the Middle Ordovician

One of the largest, most rapid drops in $^{87}Sr/^{86}Sr$ (~0.7088 to ~0.7078; Figure 4.8) in the Phanerozoic occurs in the mid-Ordovician beginning in the *P. serra* conodont zone (late Darriwilian; Veizer and Compston, 1974; Burke et al., 1982; Veizer et al., 1986; Qing et al., 1998; Shields et al., 2003) and broadly coincident with Late Ordovician explosive volcanism, as marked by widespread bentonites deposition across Laurentia and Baltica (Huff et al., 1992; 1996; Bergström et al., 1995). This rapid drop has been attributed to a combination of waning Pan-African orogenic activity, decreased continental weathering associated with a major transgression of sea level, and an increase in either sea floor spreading (Shields et al., 2003) or weathering of young basaltic provinces associated with arc magmatism (Young et al., 2009).

It has further been suggested that this rapid drop in $^{87}Sr/^{86}Sr$ reflected potentially significant CO_2 and global cooling prior to Hirnantian glaciation (Buggisch et al., 2010). If significant CO_2 drawdown occurred, however, it does not appear to be reflected in the marine sea surface temperature record. Oxygen-isotopic signatures from both conodonts (Trotter et al., 2008; Herrmann et al., 2011) and clumped isotope paleothermometry (Finnegan et al., 2011) suggest that after a protracted decline in sea surface temperature from the Early through the Middle Ordovician (Trotter et al., 2008), sea surface temperatures stabilized in the mid-to-late Darriwilian and remained stable until the mid-to-late Katian when temperatures dropped dramatically with the onset of Hirnantian glaciation. Young et al., (2009) suggest that sea surface temperatures during this period were stabilized by explosive volcanism via a balance between volcanic outgassing and basalt weathering. In this scenario, late-Katian to Hirnantian cooling resulted from a combination of the cessation of volcanic outgassing associated with explosive volcanism, and continued weathering of arc-related basalts and their associated CO_2 drawdown.

Figure 4.8. Timing of biospheric events in the Ordovician with respect to the distribution of explosive volcanic events. Two distinct suites of K-bentonite deposition occur in the Early-Middle Ordovician (Famatina suite, Argentina) and the Late Ordovician (Millbrig-Diecke-Kinnekulle suite). These bentonites span intervals of both subdued and more volatile marine carbon isotope signatures and have been implicated as a driver to biospheric change during these intervals. It is not clear, however, that causal relationships exist. The older, Famatinian bentonite suite occurs during rising to relatively stable sea level, stable marine strontium isotope composition, and near the end of a long-term cooling event. By contrast, the younger, Millbrig-Diecke-Kinnekulle bentonite suite occurs during rising to stable sea level, just after a major drop in marine strontium isotopic composition, and during a period of relatively stable sea surface temperatures. Stage slices are from Bergström et al. (2008) and time slices are from Webby et al. (2004). K-bentonite distribution is from Huff et al. (2008), composite carbon isotope curve is modified from Bergström et al. (2008), sea surface temperature curve (broad grey line) is from Trotter et al. (2008), and composite $^{87}Sr/^{86}Sr$ curve (dashed line) is modified from Shields et al. (2003), Young et al., (2009), and Thompson et al. (in review).

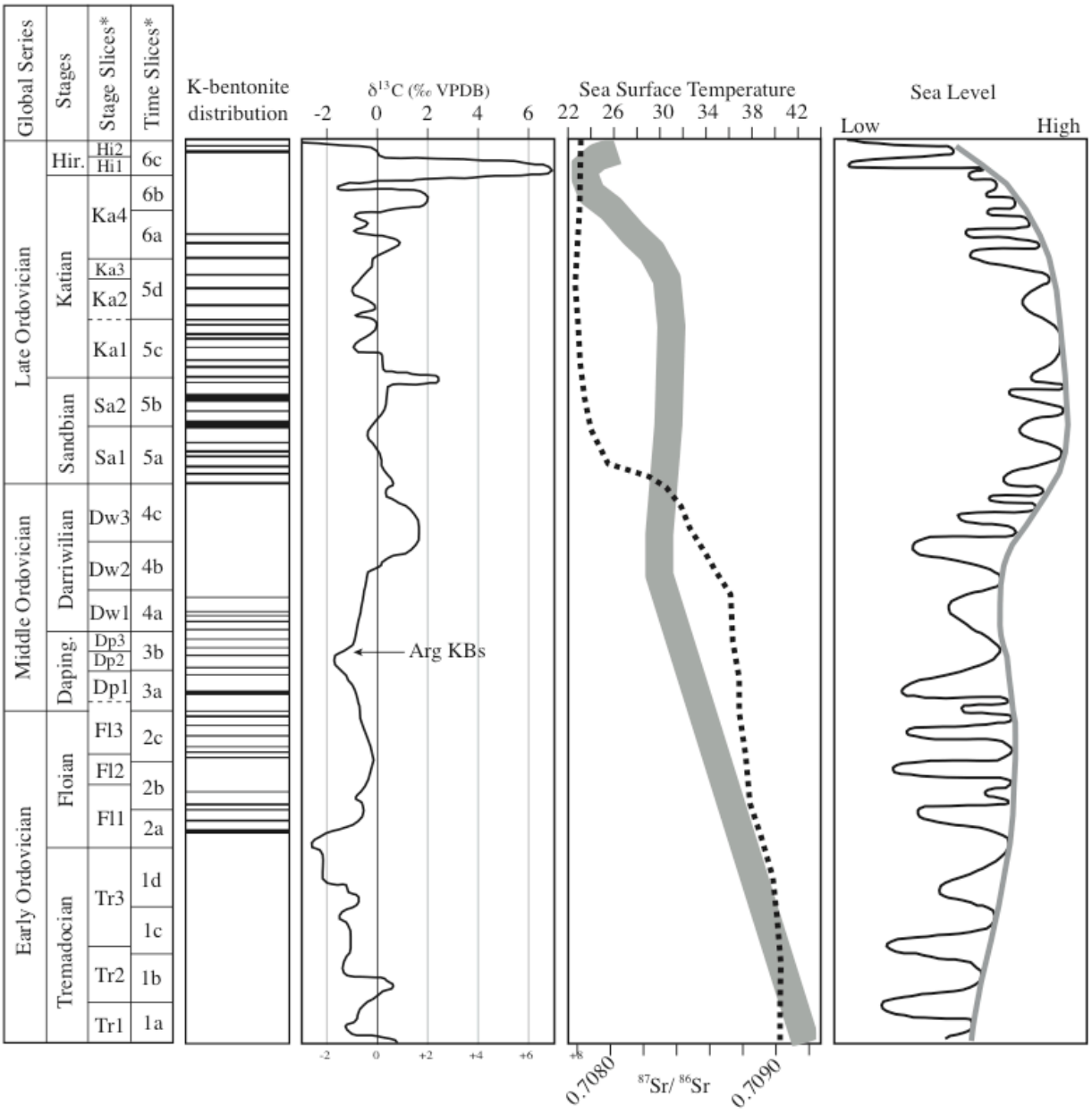
Global Series
Stages
Stage Slices*
Time Slices*
Late Ordovician
Middle Ordovician
Early Ordovician
Hir.
Katian
Sandbian
Darriwilian
Daping.
Floian
Tremadocian
Hi2
Hi1
Ka4
Ka3
Ka2
Ka1
Sa2
Sa1
Dw3
Dw2
Dw1
Dp3
Dp2
Dp1
Fl3
Fl2
Fl1
Tr3
Tr2
Tr1
6c
6b
6a
5d
5c
5b
5a
4c
4b
4a
3b
3a
2c
2b
2a
1d
1c
1b
1a
K-bentonite distribution
δ13C (‰ VPDB)
-2
0
2
4
6
Arg KBs
Sea Surface Temperature
22
26
30
34
38
42
87Sr/86Sr
0.7080
0.7090
Sea Level
Low
High

In sharp contrast to the Middle Ordovician strontium isotope record, stable, yet elevated $^{87}Sr/^{86}Sr$ values in the Early to Middle Ordovician have been attributed primarily to extensive weathering of Pan-African orogenic rocks (Qing et al., 1998; Shields et al., 2003). During the Early Ordovician, a small decline in marine $^{87}Sr/^{86}Sr$ (0.7090 to 0.7088; Shields et al., 2003) broadly coincides with the onset of Famatina volcanic activity (Figure 4.8). Comparison of the timing of Argentina K-bentonite deposition to sea surface temperature records shows that explosive volcanism occurred near the end of a long (>25 Myr) gradual decline in sea surface temperature, so there is no apparent link in the rate of oceanic cooling associated with the onset of Famatinian explosive volcanism (Huff et al., 2008). If a mechanism similar to that invoked by Young et al., (2009) were operating in the Early to Middle Ordovician, gradual cooling through the Early to Middle Ordovician would require basalt weathering to consume CO_2 faster than it was produced by volcanic outgassing. Furthermore, in order to retain the marked stability and radiogenic isotopic composition of the $^{87}Sr/^{86}Sr$ record, basaltic weathering would also have to be balanced, over the long term, by a continental weathering input. Combined, these arguments suggest that explosive volcanism recorded by widespread bentonites in the Argentine Precordillera played only a very limited role in changes to the global biosphere.

The gradual decline in sea surface temperature observed through the Early and Middle Ordovician has also been attributed to an increase in productivity and organic carbon burial as a result of increased biodiversification in the Ordovician (Trotter et al., 2008). Biodiversification during the GOBE also resulted in a transition from dominantly benthic grazers to suspension feeders (Bottjer et al., 2001). It has been hypothesized that this transition in feeding structure may have been driven by phytoplankton biodiversity expansion with new food source for animal consumption (Bambach, 1983; 1993; Signor and Vermeij, 1994). It is thus necessary to explore whether explosive volcanism in the Middle Ordovician, which can provide a variety of metals, such as iron and phosphorus, which are essential for organic matter production (Gaddy and Parker, 1986; Felitsyn and Kirianov, 2002), may have had played a direct role in the expansion of life in the Middle Ordovician. Explosive volcanism in the Famatinian arc system appears to have been active through much of the early stages of the GOBE (Webby et al., 2004). Volcanic ash deposits potentially may have acted as a fertilizer to enhance bioproductivity (Gaddy and

Parker, 1986) during this time. If this is the case, the effects of increased nutrient input should be reflected in marine biogeochemical cycles.

Marine C-isotope composition is considered to reflect a balance between organic carbon burial and delivery of inorganic carbon to the ocean. The deposition of Famatina K-bentonites coincides with an interval of unusually stable marine carbon isotope composition, wherein short-term excursions of <1‰ superimposed over a long-term variation between -2‰ and 0‰ from the mid-Floian to the mid-Darriwilian (Figure 4.8). Subdued carbon isotope signatures in the Early to Middle Ordovician are commonly attributed to generally low rates of organic carbon burial (fraction of total carbon buried as organic carbon = 0.1 to 0.2) associated with decreased nutrient availability during greenhouse times (Saltzman, 2005). Such an interpretation is supported by sulfur isotope data that indicates widespread euxinia and potential for a net flux of nutrients to the sedimentary substrate (Thompson and Kah, *in review*). Under these conditions, initiation of Famatina arc volcanism in the Floian would be expected to enhance nutrient fluxes to the surface oceans, resulting in a net increase in marine productivity and organic carbon. The broad negative carbon isotope excursion recorded through the late Floian and Dapingian is inconsistent with such an interpretation. However, because marine carbon and sulfur isotope cycles are linked via the availability of reactive marine organic matter for bacterial sulfate reduction, the sulfur isotope record may provide additional insight into changes in marine productivity.

The isotopic composition of marine sulfate in the Early to Middle Ordovician marine sulfate records short-term oscillation that has been attributed to small scale changes in the bacterial sulfate reduction and bacterial sulfate oxidation within an ocean that otherwise maintains a dynamic equilibrium between distinct sulfate (surface ocean) and hydrogen sulfide (deep ocean) reservoirs (Thompson and Kah, *in review*). An abrupt shift in the average isotopic composition of marine sulfate, however, occurs near the Middle-Late Ordovician boundary. This sulfur isotope event coincides with a long-term minimum in sea surface temperature (Trotter et al., 2008) and has been hypothesized to represent the onset of vigorous oceanic circulation and downwelling of cool, oxygen-rich waters that resulted in substantial oxidation of the deep-ocean

hydrogen sulfide reservoir (Thompson et al., *in review*). This event and the subsequent reorganization of marine biogeochemical cycles (*see* Thompson et al., *in review*), however, occur well after the end of explosive volcanism associated with Famatinian arc magmatism. Prior to this biogeochemical reorganization, the long-term stability of the marine sulfur isotope record—which was maintained both before and after the onset of Famatinian volcanism—suggests no clear influence of explosive volcanism on marine environmental conditions.

Together, these observations suggest that the relationship between explosive volcanism and environmental change in the Middle Ordovician is not straightforward, and that the extent of volcanism represented by the Famatina bentonite suite was insufficient to affect global surface environments. Instead we suggest that expansion of phytoplankton (Servais et al., 2008; 2010), zooplankton (Noble and Danelian, 2004; Paris et al., 2004), and ultimately marine metazoan diversity in the earliest stages of the GOBE appear to be more closely related to expansion of ecospace ultimately driven by plate tectonic reconfiguration and changes in sea level (Figure 4.8).

Distinguishing between sea level and nutrient input from explosive volcanism, however, and the apparent inability of Famatinian volcanism to affect the global biosphere may be related most clearly to the limited spatial extent of ash falls along the western Gondwanan margin (Huff et al., 1998; Astini et al., 2007).

6. Conclusions

Ordovician strata of the Early to Middle Ordovician of Argentina preserve an extensive record of explosive volcanism related to convergence of the Precordillera terrane with the western Gondwanan margin and the development and ultimate demise of the Famatina arc system. High-resolution ID-TIMS U-Pb ages on zircons within K-bentonites of the San Juan Formation, Argentine Precordillera provide stratigraphically consistent ages that range from 473.45±0.70 Ma to 469.53±0.62 Ma. The substantially higher precision of these new ages, and their correlation with high-resolution marine geochemical records, permits evaluation of explosive volcanism as an agent of global biospheric evolution.

Dated bentonites within the Famatina bentonite suite span a low-magnitude (2‰), globally-recorded negative excursion in marine carbon isotopic composition that provides an independent mechanism for global time-correlation. New geochronological ages are consistent with recent carbon isotope correlation suggesting that the San Juan Formation in the region of its type section is coeval with only the base of the often-correlated Table Head Group of Western Newfoundland and highlights the difficulties in using regional biostratigraphic data—particularly within erosionally truncated or otherwise diachronous units—to define the time-frame of carbon isotope chemostratigraphy. New geochronological data also suggest that the negative carbon isotope excursion of the San Juan and Table Head formations is correlative to a globally recognized pre-MDICE negative excursion, and indicates that this aspect of the marine carbon isotope record can be used as a discrete chronologic marker. San Juan Formation bentonites, however, cannot be discretely correlated with observed, environmentally significant changes in the Middle Ordovician marine geochemical records of carbon, sulfur, strontium, or sea surface temperature, and suggests that the extent of volcanism represented by the Famatina bentonite suite was insufficient to affect global surface environments. These results emphasize that the relationship between explosive volcanism and environmental change is not straightforward and needs to be carefully evaluated, even for more extensive bentonite suites, such as the Millbrig-Diecke-Kinnekulle suite of the Late Ordovician.

Acknowledgements

Funding for this project was provided by the National Geographic Society (NGS 7866-05 to Kah), National Science Foundation (NSF-EAR 0745768 to Kah), and the American Chemical Society (ACS-PRF 48166 to Kah), along with student grants from Sigma Xi, the Geological Society of America, and SEPM (to Thompson). We give special thanks to Ricardo Astini and Fernando Gomez (University of Cordoba) and Geoff Gilleaudeau (University of Tennessee) for help in conducting field work in Argentina; and Lisa Pratt and Seth Young (Indiana University) and Zhenghua Li (University of Tennessee) for help with isotopic and elemental analyses.

References cited

Achab, A., Paris, F., 2007. The Ordovician chitinozoan biodiversification and its leading factors. Palaeogeography, Palaeoclimatology, Palaeoecology 245, 5-19.

Ainsaar, L., Meidla, T., Tinn, O., 2004. Middle and Upper Ordovician stable isotope stratigraphy across the facies belts in the East Baltic. In: Hints, O., Ainsaar, L. (Eds.), WOGOGOB-2004 Conference Materials. Tartu University Press, Tartu, 11–12.

Ainsaar, L., Kaljo, D., Martma, T., Meidla, T., Männik, P., Nõlvak, J., Tinn, O., 2010. Middle and Upper Ordovician carbon isotope chemostratigraphy in Baltoscandia: a correlation standard and clues to environmental history. Palaeogeography, Palaeoclimatology, Palaeoecology 294, 189-201.

Albanesi G.L, Ortega, G., 2002. Advances on conodont-graptolite biostratigraphy of the Ordovician system of Argentina. Serie Correlacion Geologica 16, 143-165.

Albanesi G.L., Hünicken, M.A., Barnes, C.R., 1998. Bioestratigrafía de conodontes de las secuencias ordovícicas del cerro Potrerillo, Precordillera Central de San Juan, R. Argentina. Actas XII Academia Nacional de Ciencias, Córdoba, 7-72 (*in Spanish*).

Albanesi G.L., Ortega, G., Barnes, C.R. Hünicken. M.A. 1999. Conodont-graptolite biostratigraphy of the Gualcamayo Formation (Middle Ordovician) in the Gualcamayo-Guandacol rivers area, Argentina Precordillera. Acta Univesitatis Carolinae Geologica 43, 45-48.

Astini, R.A., 2003. Ordovician basins of Argentina. In: Benedetto, J.L. (Ed.), Ordovician Fossils of Argentina. Universidad Nacional de Córdoba, 1-74.

Astini, R.A., Benedetto, J.L., Vaccari, N.E., 1995. The early Paleozoic evolution of the Argentine Precordillera as a Laurentian rifted, drifted, and collided terrane: A geodynamic model. Geological Society of America Bulletin 107, 253-273.

Astini, R.A., Collo, G., Martina, F., 2007. Ordovician K-bentonites in the upper-plate active margin of Western Gondwana, (Famatina Ranges): Stratigraphic and palaeogeographic significance. Gondwana Research 11, 311-325.

Astini, R.A., Dávila, F.M., 2004. Ordovician back arc foreland and Ocloyic thrust belt development on the western Gondwana margin as a response to Precordillera terrane accretion. Tectonics 23, TC4008, doi:10.1029/2003TC001620.

Bambach, R.K.,1993. Seafood through time: changes in biomass, energetics, and productivity in the marine ecosystem. Paleobiology 19, 372-397.

Barnes, C.R., 2004. Was there an Ordovician superplume event. In: Webby, B.D., Droser, M.L., Paris, F., Percival, I.G. (Eds.), The Great Ordovician Biodiversification Event. Columbia University Press, New York, 77-80.

Benedetto, J.L., 1998. Early Paleozoic brachiopods and associated shelly faunas from western Gondwana: its bearing on the geodynamic history of the pre-Andean margin. In: Pankhurst, R.J., Rapela, C.W. (Eds.), The proto-Andean margin of Gondwana. Geological Society of London, Special Publication 142, 57-83.

Benedetto, J.L., 2004. The allochthony of the Argentine Precordillera ten years later (1993-2003): a new paleobiologic test of the microcontinent model. Gondwana Research 7, 1027-1039.

Benedetto, J.L., Sánchez, T.M., Carrera, M.G., Brussa, E.D., Salas, M.J., 1999. Paleontological constraints on successive paleogeographic positions of Precordillera terrane during the early Paleozoic. Geological Society of America, Special Paper 336, 21-42.

Bergström, S.M., 2007. The Ordovician conodont biostratigraphy in the Siljan region, south-central Sweden: a brief review of an international reference standard. In: Ebbestad, J.O.R.,

Wickström, L.M., Högström, A.E.S. (Eds.), WOGOGOB 2007. Field Guide and Abstracts: Sveriges Geologiska Undersökning, Rapporter och Meddelanden 128, 26–41.

Bergström, S.M., Huff, W., Kolata, D., Bauert, H., 1995. Nomenclature, stratigraphy chemical fingerprinting, and real distribution of some middle Ordovician bentonites in Baltoscandia. GFF 117, 1-13.

Bergström, S.M., Huff, W.D., Saltzman, M.R., Kolata, D.R., Leslie, S.A., 2004. The greatest volcanic ash falls in the Phanerozoic: Millbrig and Kinekulle K-bentonites. The Sedimentary Record 2, 4-7.

Bergström, S.M., Chen, X., Gutierrez-Marco, J.C., Dronov, A., 2008. The new chronostratigraphic classification of the Ordovician System and its relations to major regional series and stages and to $\delta^{13}C$ chemostratigraphy. Lethaia 42, 97-107.

Berner, R.A., Kothavala, Z., 2001. GEOCARB III: a revised model of atmospheric CO_2 over Phanerozoic time. American Journal of Science 301, 182-204.

Bottjer, D.J., Droser, M.L., Sheehan, P.M., McGhee Jr., G.R., 2001. The ecological architecture of major events in the Phanerozoic history of marine life. In: Allmon, W.D., Bottjer, D.J. (Eds.), Evolutionary Paleoecology. The Ecological Context of Macroevolutionary Change. Columbia University Press, New York, 35–61.

Brenchley, P.J., Marshall, J.D., Carden, G.A.F., Robertson, D.B.R., Long, D.G.F., Meidla, T., Hints, L., Anderson, T.F., 1994. Bathymetric and isotopic evidence for a short-lived Late Ordovician glaciation in a greenhouse period. Geology 22, 295-298.

Buggisch, W., Keller, M., Lehnert, O., 2003. Carbon isotope record of the Late Cambrian to Early Ordovician carbonates of the Argentine Precordillera. Palaeogeography, Palaeoclimatology, Palaeoecology 195, 357-373.

Buggisch, W., Joachimski, M.M., Lehnert, O., Bergström, S.M., Repetski, J.E., Webers, G.F., 2010. Did intense volcanism trigger the first Late Ordovician icehouse? Geology 38, 327-330.

Burke, W.H., Denison, R.E., Hetherington, E.A., Koepnick, R.B., Nelson, H.F., Otto, J.B., 1982. Variation of seawater $^{87}Sr/^{86}Sr$ throughout Phanerozoic time. Geology 10, 516-519.

Calner, M., Lehnert, O., Nolvak, J., 2010. Palaeokarst evidence for widespread regression and subaerial exposure in the middle Katian (Upper Ordovician) of Baltoscandia: significance for global climate. Palaeogeography, Palaeoclimatology, Palaeoecology 296, 235-247.

Cañas, F.L., 1999. Facies and sequences of the Late Cambrian–Early Ordovician carbonates of the Argentine Precordillera: a stratigraphic comparison with Laurentian platforms. In: Ramos, V.A., Keppie, J.D. (Eds.), Laurentia–Gondwana connections before Pangea: Geological Society of America, Special Paper 336, 43-62.

Cañas, F.L., Aguirre, H.D., 2005. High-resolution stratigraphy of the San Juan Formation (Lower Ordovician, Precordillera of Cuyo, San Juan, Argentina; preliminary results. Actas del Congresa Geologico Argentino 16, 365-370 (*in Spanish*).

Cardenas, A.L., Harries, P.J., 2010. Effect of nutrient availability on marine origination rates throughout the Phanerozoic eon. Nature Geoscience 3, 430-434.

Casquet, C., Baldo, E., Pankhurst, R., Rapela, C., Galindo, C., Fanning, C., Saawedra, J., 2001. Involvement of the Argentine Precordillera terrane in the Famatinian mobile belt: U-Pb SHRIMP and metamorphic evidence from the Sierra de Pie de Palo. Geology 29, 703-706.

Cherns, L., Wheeley, J.R., 2007. A pre-Hirnantian (Late Ordovician) interval of global cooling —the Boda event re-assessed. Palaeogeography, Palaeoclimatology, Palaeoecology 251, 449-460.

Crame, J.A., Owen, A.W. (Eds.), 2002. Palaeobiogeography and biodiversity change: the Ordovician and Mesozoic–Cenozoic Radiations: Geological Society, London, Special Publications 194, 206.

Corfu, F., Hanchar, J.M., Hoskin, P.W.O., Kinny, P. 2003. Atlas of zircon textures. In: Hanchar, J.M., Hoskin, P.W.O. (Eds.) Zircon. Mineralogical Society of America 53, 468-500.

Droser, M.L., Sheehan, P.M., 1997. Palaeoecology of the Ordovician Radiation: resolution of large-scale patterns with individual clade histories, palaeogeography and environments. Geobios 20, 221-229.

Droser, M.L., Finnegan, S., 2003. The Ordovician radiation: a follow-up to the Cambrian explosion. Integrative Comparative Biology 43, 178-184.

Fanning, C.M., Pankhurst, R.J., Rapela, C.W., Baldo, E.G., Casquet, C., Galindo, C., 2004. K-bentonites in the Argentine Precordillera contemporaneous with rhyolite volcanism in the Famatinian Arc. Journal of the Geological Society, London 161, 747-756.

Felitsyn, S.B., Kirianov, V.Y., 2002. Mobility of phosphorus during the weathering of volcanic ashes. Lithology and Mineral Resources 37, 275-278.

Finnegan, S., Bergmann, K., Eiler, J.M., Jones, D.S., Fike, D.A., Eisenman, I., Hughes, N.C., Tripati, A.K., Fischer, W.W., 2011. The magnitude and duration of Late Ordovician-Early Silurian Glaciation. Science 331, 903-906.

Gaddy, A.J., Parker, R.A., 1986. Zooplankton grazing activity and assimilation in the presence of Mount St. Helens ash. Northwest Science 60, 47-51.

Gomez, F.J., Ogle, N., Astini, R.A., Kalin, R.M., 2007. Paleoenvironmental and carbon-oxygen isotope record of Middle Cambrian carbonates (La Laja Formation) in the Argentine Precordillera. Journal of Sedimentary Research 77, 826-842.

Hamoumi, N., 1999. Upper Ordovician glaciation spreading and its sedimentary record in Moroccan North Gondwana margin. Acta Universitatis Carolinae Geologica 43, 11-14.

Haq, B.U., Schutter, S.R., 2008. A chronology of Paleozoic sea-level changes. Science 322, 64-68.

Harper, D.A.T., 2006. The Ordovician biodiversification: Setting and agenda for marine life. Palaeogeography, Palaeoclimatology, Palaeoecology 232, 148-166.

Herrmann, A., Patzkowsky, M., Pollard, D., 2004. The impact of paleogeography, pCO_2, poleward ocean heat transport and sea level change on global cooling during the Late Ordovician. Palaeogeography, Palaeoclimatology, Palaeoecology 206, 59-74.

Herrmann, A.D., MacLeod, K.G., Leslie, S.A., 2010. Did a volcanic mega-eruption cause global cooling during the Late Ordovician? Palaios 25, 831-836.

Hints, O., Delabroye, A., Nõlvak, J., Servais, T., Uutela, A., Wallin, A., 2010. Biodiversity patterns of Ordovician marine microphytoplankton from Baltica: Comparison with other fossil groups and sea-level changes. Palaeogeography, Palaeoclimatology, Palaeoecology 294, 161-173.

Huff, W., Bergström, S.M., Kolata, D., 1992. Gigantic Ordovician ash fall in North America and Europe: biological, tectonomagmatic, and event stratigraphic significance. Geology 20, 875-878.

Huff, W.D., Kolata, D.R., Bergström, S.M., Zhang, Y-S., 1996, Large-magnitude Middle Ordovician volcanic ash falls in North America and Europe: dimensions, emplacement and post-emplacement characteristics. Journal of Volcanology and Geothermal Research 73, 285-301.

Huff, W.D., Davis, D., Bergström, S.M., Krekeler, M.P.S., Kolata, D.R., Cingolani, C., 1997. A biostratigraphically well-constrained K-bentonite U-Pb zircon age of the lowermost Darriwilian State (Middle Ordovician) from the Argentine Precordillera. Episodes 20, 29-33.

Huff, W.D., Bergström, S.M., Kolata, D.R., Cingolani, C.A., Astini, R.A., 1998. Ordovician K-bentonites in the Argentine Precordillera: relations to Gondwana margin evolution. In: Pankhurst, R.J., Rapela, C.W. (Eds.), The Proto-Andean Margin of Gondwana. Geological Society, London, Special Publication 142, 107-126.

Huff, W.D., 2008. Ordovician K-bentonites: Issues in interpreting and correlating ancient tephras. Quaternary International 178, 276-287.

Huff, W.D., Bergström, S.M., Kolata, D.R., 2010. Ordovician explosive volcanism. Geological Society of America, Special Paper 466, 13-28.

Huff, W.D., 2008. Ordovician K-bentonites: Issues in interpreting and correlating ancient tephras. Quaternary International 178, 276-287.

Jablonski, D., 1991. Extinctions: a paleontological perspective. Science 253, 754-757.

Kaljo, D., Martma, T., Saadre, T., 2007. Post-Hunnebergian Ordovician carbon isotope trend in Baltoscanadia, its environmental implications and some similarities with that of Nevada. Palaeogeography, Palaeoclimatology, Palaeoecology 245, 138-155.

Keller, M., Eberlein, S., Lehnert, O., 1993. Sedimentology of Middle Ordovician carbonates in the Argentine Precordillera: evidence of regional relative sea-level changes. Geologische Rundschau 82, 362-377.

Keller, M. 1999. Argentine Precordillera: sedimentary and plate tectonic history of a Laurentian crustal fragment in South America. Geological Society of America, Special Paper 341, 131.

Keller, M., Lehnert, O., 2010. Ordovician paleokarst and quartz sand: Evidence of volcanically triggered extreme climates? Palaeogeography, Palaeoclimatology, Palaeoecology 296, 297-309.

Keller, M., Eberlein, S., Lehnert, O., 1993. Sedimentology of Middle Ordovician carbonates in the Argentine Precordillera: evidence of regional relative sea-level changes. Geologische Rundschau 82, 362-377.

Kidder, D.L., Worsley, D.L., 2010. Phanerozoic Large Igneous Provinces (LIPs), HEATT (Haline Euxinic Acidic Thermal Transgression) episodes, and mass extinctions. Palaeogeography, Palaeoclimatology, Palaeoecology, 295, 162-191.

Kolata, D.R., Huff, W.D., Bergström, S.M., 1996. Ordovician K-bentonites of eastern North America. GSA Special Paper 313, 1-84.

Kump, L.R., Gibbs, M.T., Arthur, M.A., Patzkowsky, M.E., Sheehan, P.M., 1995. Hirnantian glaciation and the carbon cycle. In: Cooper, J.D. et al., (Eds.), Ordovician Odyssey: Short Papers for the 7th International Symposium on the Ordovician System. Pacific Section, Society for Sedimentary Geology, Fullerton, CA, 299302.

Kump, L.R., Arthur, M.A., Patzkowsky, M., Gibbs, M., Pinkus, D., Sheehan, P., 1999. A weathering hypothesis for glaciation at high atmospheric pCO_2 during the Late Ordovician. Palaeogeography, Palaeoclimatology, Palaeoecology 152, 173-187.

Krogh, T.E., 1973. A low contamination method for hydrothermal decomposition of zircon and extraction of U and Pb for isotopic age determination. Geochimica et Cosmochimica Acta 37, 485-494.

Lefebvre, V., Servais, T., François, L., Averbuch, O., 2010. Did a Katian large igneous province trigger the Late Ordovician glaciation? A hypothesis tested with a carbon cycle model. Palaeogeography, Palaeoclimatology, Palaeoecology 296, 310-319.

Mattinson, J.M., 2005. Zircon U–Pb chemical-abrasion (CA-TIMS) method: combined annealing and multi-step dissolution analysis for improved precision and accuracy of zircon ages. Chemical Geology 220, 47-56.

McLean, N.M., Bowring, J.F., Bowring, S.A., Schoene, R.B., 2008. More than just an age: Quantitative analysis of geochronological data and uncertainty. Geological Society of America Abstracts with Programs 40, 134.

McLean, N., Bowring, J.F., Bowring, S.A., 2009. Using statistics and software to maximize precision and accuracy in U-Pb geochronological measurements. American Geophysical Union Abstract No. V33B-2033.

Noble, P.J., Danelian, T., 2004. Radiolarians. In: Webby, B.D., Droser, M.L., Paris, F., Percival, I.G. (Eds.) The Great Ordovician Biodiversification Event. Columbia University Press, New York, 97-101.

Owen, A.W., Crame, J.A., 2002. Palaeobiogeography and the Ordovician and Mesozoic-Cenozoic radiations. In: Crame, J.A., Owen, A.W. (Eds.), Palaeobiogeography and Biodiversity Change: The Ordovician and Mesozoic–Cenozoic Radiations: Geological Society, London, Special Publications 194, 1-11.

Pankhurst R.J., Rapela, C.W., Casquet, C., Baldo, E., Saavedra, J., Galindo, C., 1998. Early Paleozoic evolution of the Gondwana margin of South America. Journal of African Earth Sciences 27, 145-146.

Pankhurst, R.J., Rapela, C.W., Fanning, C.M., 2000. Age and origin of coeval TTG, I- and S-type granites in the Famatinian belt of NW Argentina. Transactions of the Royal Society of

Edinburgh, Earth Science 91, 151-168.

Paris, F., Achab, A., Chen, X., Grahn, Y., Nolvak, J., Obut, O., Samuelsson, J., Sennikov, N., Vecoli, M., Verniers, J., Wang, X., Winchester-Seeto, T., 2004. Chitinozoans. In: Webby, B.D., Droser, M.L., Paris, F., Percival, I.G., (Eds.), The Great Ordovician Biodiversification Event. Columbia University Press, New York, 294-311.

Pope, M.C., Read, J.F., 1998. Ordovician meter-scale cycles: Implications for Ordovician climate and eustatic fluctuations in the central Appalachian Basin, USA. Palaeoclimatology, Palaeogeography, Palaeoecology 138, 27-42.

Pope, M.C., Steffan, J.B., 2003. Widespread, prolonged late Middle to Late Ordovician upwelling in North America: a proxy record of glaciation. Geology 31, 63-66.

Qing, H., Barnes, C.R., Buhl, D., Veizer, J., 1998. The strontium isotopic composition of Ordovician and Silurian brachiopods and conodonts: Relationships to geological events and implications for coeval seawater. Geochimica et Cosmochimica Acta 62, 1721-1733.

Ramos, V.A. (1988) The Tectonics of the Central Andes : 30°-33° S latitude. In: Burchfiel, C., Suppe, J. (Eds.), Processes in continental lithospheric deformation, Geological Society of America, Special Paper 218, 31-54.

Ramos, V.A., 2004. Cuyania, an exotic block to Gondwana: review of a historical success and the present problems. Gondwana Research 7, 1009-1026.

Rapela, C.W., Pankhurst, R.J., Casquet, C., Baldo, E., Saavedra, J., Galindo, C., 1998. Early Evolution of the Proto-Andean margin of South America. Geology 26, 707-710.

Rapela, C.W., Pankhurst, R.J., Baldo, E., Casquet, C., Galindo, C., Fanning, C.M. Saavedra, J., 2001. Ordovician metamorphism in the Sierras Pampeanas: New U-Pb shrimp ages in central-east Valle Fértil and the Velasco batholith. 3° S. American Symposium on Isotope Geology, 616-

619.

Saltzman, M.R., 2005. Phosphorus, nitrogen, and the redox evolution of the Paleozoic oceans. Geology 33, 7, 573-576.

Saltzman, M.R., Young, S.A., 2005. Long-lived glaciation in the Late Ordovician? Isotopic and sequence-stratigraphic evidence from western Laurentia. Geology 33, 109-112.

Sarmiento, G.N., 1991. Conodonts of the Suecicus Zone (lower Llanvirnian) in the Sierra de Villicum, San Juan Precordillera, Argentina. Revista Espanola de Micropaleontologica 23, 113-132 (*in Spanish*).

Schmitz, B., Harper, D.A.T., Peucker-Ehrenbrink, B., Stouge, S., Alwmark, C., Cronholm, A., Bergström, S.M., Tassinari, M., Wang, X.F., 2008. Asteroid breakup linked to the Great Ordovician Biodiversification Event. Nature Geoscience 1, 49-53.

Schmitz, B., Bergström, S.M., Xiaofeng, W., 2010. The middle Darriwilian (Ordovician) $\delta^{13}C$ excursion (MDICE) discovered in the Yangtze Platform succession in China: implications of its first recorded occurrences outside Baltoscanadia. Journal of the Geological Society, London 167, 249-259.

Schoene, B., Crowley, J.L., Condon, D.J., Schmitz, M.D., Bowring, S.A., 2006. Reassessing the uranium decay constants for geochronology using ID-TIMS U-Pb data. Geochimica et Cosmochimica Acta 70, 426-445.

Scotese, C.R., McKerrow, W.S., 1990. Revised world maps and introduction. In: McKerrow, W.S., Scotese, C.R. (Eds.), Palaeozoic Palaeogeography and Biogeography: Memoir of the Geological Society of London 12, 1-21.

Servais, T., Lehnert, O., Li, J., Mullins, G.L., Munnecke, A., Nutzel, A., Vecoli, M., 2008. The

Ordovician Biodiversification: revolution in the oceanic trophic chain. Lethaia 41, 99-109.

Servais, T., Harper, D.A.T., Li, J., Munnecke, A., Owen, A.W., Sheehan, P.M., 2009. Understanding the Great Ordovician biodiversification Event (GOBE): Influences of paleogeography, paleoclimate, or paleoecology? GSA Today 19, 4-10.

Servais, T., Owen, A.W., Harper, D.A.T., Kröger, B., Munnecke, A., 2010. The Great Ordovician Biodiversification Event (GOBE): the palaoecological dimension. Palaeogeography, Palaeoclimatology, Palaeoecology 294, 99-119.

Sheehan, P.M., 2001. The Late Ordovician mass extinction. Annual Reviews of Earth and Planetary Sciences 29, 331-364.

Shields, G.A., Carden, G.A.F., Veizer, J., Meidla, T., Rong, J.Y., Rong, Y.L., 2003. Sr, C, and O isotope geochemistry of Ordovician brachiopods: a major isotopic event around the Middle–Late Ordovician transition. Geochimica Cosmochimica Acta 67, 2005-2025.

Signor, P.W., Vermeij, G., 1994. The plankton and the benthos: origins and early history of an evolving relationship. Paleobiology 20, 297-319.

Theron, J.N., 1994. The Ordovician System in South Africa; correlation chart and explanatory notes. In: Williams, S.H. (Ed.), The Ordovician System in Greenland and South Africa: International Union of Geological Sciences 29, 1-5.

Thomas,W.A., Astini, R.A., 1996. The Argentine Precordillera: a traveler from the Ouachita embayment of North American Laurentia. Science 273, 752-757.

Thomas, W.A., Astini, R.A., 1999. Simple-shear conjugate rift margins of the Argentine Precordillera and the Ouachita embayment of Laurentia. Geological Society of America, Bulletin 111, 1069-1079.

Thomas, W.A., Astini, R.A., 2003. Ordovician accretion of the Argentine Precordillera terrane to Gondwana: a review. Journal of South America Earth Science 16, 667-679.

Thompson, C.K., Kah, L.C., *in review.* Sulfur isotope evidence for widespread euxinia and a fluctuating oxycline in Early to Middle Ordovician greenhouse oceans. Palaeogeography, Palaeoclimatology, Palaeoecology.

Thompson, C.K., Kah, L.C., Kaufman, A.J., *in review*. Did ventilation of euxinic oceans herald the end of Ordovician greenhouse climate? Nature Geoscience.

Trotter, J.A., Williams, I.S., Barnes, C.R., Lécuyer, C., Nicoll, R.S., 2008. Did cooling oceans trigger Ordovician biodiversification? Evidence from conodont thermometry. Science 321, 550-554.

Veizer, J., Compston, W., 1974. $^{87}Sr/^{86}Sr$ in Precambrian carbonates as an index of crustal evolution. Geochimica et Cosmochimica Acta 40, 905-914.

Veizer, J., Fritz, P., Jones, B., 1986. Geochemistry of brachiopods, oxygen, and carbon isotopic records of Paleozoic oceans. Geochimica et Cosmochimica Acta 50, 1679-1696.

Walker, J.D., Geissman, J.W., 2009. GSA 2009 geologic time scale. GSA Today 19, 60-61.

Walker, L.J., Wilkinson, B.H., Ivany, L.C., 2002. Continental drift and Phanerozoic carbonate accumulation in shallow-shelf and deep-marine settings. The Journal of Geology 110, 75-87.

Webby, B.D., Paris, F., Droser, M.L., Percival, I.G., 2004. The Great Ordovician Biodiversification Event. Columbia University Press, New York, 1-484.

Young, S.A., Saltzman, M.R., Bergström, S.M., 2005. Upper Ordovician (Mohawkian) carbon isotope ($\delta^{13}C$) stratigraphy in eastern and central North America: Regional expression of a

perturbation of the global carbon cycle. Palaeogeography, Palaeoclimatology, Palaeoecology 222, 53-76.

Young, S.A., Saltzman, M.R., Bergström, S.M., Leslie, S.A., Chen, X., 2008. Paired δ^{13}Ccarb and $\delta^{13}C_{org}$ records of Upper Ordovician (Sandbian-Katian) carbonates in North America and China: implications for paleoceanographic change. Palaeogeography, Palaeoclimatology, Palaeoecology 270, 166-178.

Young, S.A., Saltzman, M.R., Foland, K.A., Linder, J.S., Kump, L.R., 2009. A major drop in seawater $^{87}Sr/^{86}Sr$ during the Middle Ordovician (Darriwilian): links to volcanism and climate. Geology 37, 951-954.

Young, S.A., Saltzman, M.R., Ausich, W.I., Desrochers, A., Kaljo, D., 2010. Did changes in atmospheric CO_2 coincide with latest Ordovician glacial-interglacial cycles? Palaeogeography, Palaeoclimatology, Palaeoecology 296, 376-388.

Zhang, T., Shen, Y., Algeo, T.J., 2010. High-resolution carbon isotopic records from the Ordovician of South China: Links to climatic cooling and the Great Ordovician Biodiversification Event (GOBE), Palaeogeography, Palaeoclimatology, Palaeoecology 289, 102-112.

Appendix

	Composition				Isotopic Ratios							Isotopic Ages (Ma)						
Sample[a]	$\frac{Th^{b}}{U}$	Pb^{*c} (pg)	Pb_c^{c} (pg)	$\frac{Pb^{*c}}{Pb_c}$	$\frac{^{206}Pb^{d}}{^{204}Pb}$	$\frac{^{206}Pb^{e,f}}{^{238}U}$	±2σ %	$\frac{^{207}Pb^{e}}{^{235}U}$	±2σ %	$\frac{^{207}Pb^{e,f}}{^{206}Pb}$	±2σ %	$\frac{^{206}Pb^{*f,g}}{^{238}U}$	±2σ abs.	$\frac{^{207}Pb^{g}}{^{235}U}$	±2σ abs.	$\frac{^{207}Pb^{f,g}}{^{206}Pb}$	±2σ abs.	corr. coef.
KB-1																		
z1	0.66	10.8	0.74	15	854	0.075446	0.098	0.5882	0.76	0.056545	0.7	468.88	0.44	469.7	2.9	474	15	0.69
z2	0.71	9.77	1.46	7	396	0.075438	0.19	0.5928	1.7	0.056988	1.5	468.83	0.84	472.6	6.3	491	34	0.66
z4	0.6	4.78	0.26	18	1090	0.075936	0.22	0.5955	0.75	0.056877	0.69	471.82	0.98	474.4	2.8	487	15	0.41
z5	0.76	6.27	0.31	20	1149	0.075548	0.27	0.5903	1.1	0.056668	0.96	469.5	1.2	471	4	479	21	0.54
z8	0.83	17	0.31	55	3031	0.075365	0.16	0.5862	0.33	0.05641	0.28	468.4	0.71	468.4	1.3	468.5	6.3	0.53
z10	1.09	5.52	0.69	8	433	0.075293	0.22	0.5932	1.5	0.057139	1.4	467.96	0.99	472.9	5.8	497	32	0.43
z14	1.03	8.55	0.58	15	790	0.075361	0.17	0.5908	0.97	0.056854	0.91	468.37	0.78	471.3	3.7	486	20	0.43
z24	0.8	11.2	0.41	27	1536	0.075333	0.11	0.5831	0.5	0.056141	0.48	468.21	0.52	466.5	1.9	458	11	0.32
z25	0.99	8.87	0.161	6	309	0.075654	0.38	0.594	2.1	0.056934	2	470.1	1.7	473.3	8	489	43	0.46
KB-3																		
z1	0.75	45.2	0.89	51	2843	0.17883	0.062	1.8464	0.19	0.07488	0.16	1060.58	0.61	1062.1	1.2	1065.4	3.2	0.592
z3	0.48	2.22	0.39	6	351	0.2294	1.8	2.674	2.4	0.0846	1.4	1331	22	1321	18	1305	26	0.821
KBT-1																		
z1	0.71	10.2	0.26	39	2245	0.075881	0.23	0.5961	0.38	0.056972	0.55	471.5	1	474.7	1.4	490	12	-0.6
z2	0.74	22.7	2.46	9	536	0.075509	0.18	0.592	1.1	0.056862	1.1	469.26	0.83	472.1	4.3	486	24	0.48
z3	0.58	10.9	0.28	39	2297	0.075747	0.097	0.5909	0.43	0.056575	0.41	470.68	0.44	471.4	1.6	475	9.2	0.23
z4	0.58	8.47	0.41	21	1240	0.075669	0.16	0.5886	0.78	0.05642	0.75	470.22	0.73	470	2.9	469	17	0.29
z7	0.49	1.74	1.37	1	94	0.074635	1	0.532	11	0.051715	10	464	4.5	433	38	273	240	0.4
z8	0.5	2.21	1.49	1	107	0.073824	0.91	0.618	6.4	0.060679	6	459.2	4	488	25	628	130	0.51
z17	0.59	9.44	0.56	17	993	0.075651	0.13	0.589	0.78	0.05647	0.71	470.11	0.58	470.2	2.9	471	16	0.6
z21	0.56	8.52	0.71	12	724	0.075578	0.13	0.5887	0.87	0.056495	0.82	469.68	0.57	470.1	3.3	472	18	0.48
KBT-3N																		
z1	0.77	3.62	0.81	4	267	0.076195	0.18	0.596	2.4	0.056714	2.2	473.37	0.82	474.6	9	480	50	0.8
z2	0.83	2.35	0.38	6	360	0.076176	0.21	0.602	2.1	0.057302	1.9	473.26	0.96	478.4	7.9	503	42	0.65
z3	0.82	6.36	0.33	19	1067	0.077161	1.6	0.607	1.7	0.057079	1.4	479.2	7.4	481.8	6.5	495	30	0.66
z4	0.9	15.5	0.59	26	1437	0.076162	0.17	0.5949	0.53	0.056655	0.48	473.17	0.76	474	2	478	11	0.47
z5	0.71	4.17	0.48	9	510	0.076274	0.16	0.593	1.4	0.056383	1.3	473.85	0.72	472.8	5.3	467	28	0.71
KBT-10																		
z1	0.6	13.1	0.56	23	1372	0.075643	0.11	0.5904	0.47	0.056606	0.36	470.06	0.5	471.1	1.8	476.2	8	0.97
z2	0.46	17	0.35	49	2980	0.075546	0.16	0.5885	0.37	0.056501	0.28	469.48	0.74	469.9	1.4	472.1	6.3	0.68

	Composition				Isotopic Ratios							Isotopic Ages (Ma)						
Sample[a]	$\frac{Th}{U}$[b]	Pb*[c] (pg)	Pb_c[c] (pg)	$\frac{Pb^*}{Pb_c}$[c]	$\frac{^{206}Pb}{^{204}Pb}$[d]	$\frac{^{206}Pb}{^{238}U}$[e,f]	±2σ %	$\frac{^{207}Pb}{^{235}U}$[e]	±2σ %	$\frac{^{207}Pb}{^{206}Pb}$[e,f]	±2σ %	$\frac{^{206}Pb^*}{^{238}U}$[f,g]	±2σ abs.	$\frac{^{207}Pb}{^{235}U}$[g]	±2σ abs.	$\frac{^{207}Pb}{^{206}Pb}$[f,g]	±2σ abs.	corr. coef.
z3	0.81	25.5	0.34	75	4130	0.075558	0.089	0.5894	0.31	0.05658	0.27	469.55	0.4	470.5	1.2	475.2	6	0.51
z4	0.7	9.23	0.49	19	1090	0.075547	0.12	0.5902	0.7	0.05666	0.67	469.49	0.56	471	2.7	478	15	0.34
z5	0.6	37.1	0.84	44	2589	0.075555	0.083	0.5887	0.26	0.056507	0.24	469.54	0.37	470.02	0.99	472.4	5.2	0.47
z6	0.76	8.75	0.62	14	810	0.075953	0.12	0.6007	0.78	0.057359	0.73	471.92	0.53	477.7	3	505	16	0.49
z9	0.86	8.17	0.6	14	762	0.075799	0.16	0.5946	0.91	0.056894	0.84	471	0.74	473.8	3.4	487	18	0.5
z10	0.83	8.5	1.93	4	260	0.075989	0.51	0.6	2.4	0.057308	2.2	471.2	2.3	477.5	9.3	503	49	0.48

Blank composition: $^{206}Pb/^{204}Pb = 18.24 \pm 0.21$; $^{207}Pb/^{204}Pb = 15.34 \pm 0.16$; $^{208}Pb/^{204}Pb = 37.35 \pm 0.20$

[a] Single-grain fraction descriptors: KBT = Talacasto, KB = Cerro La Chilca, N = needles

[b] [Th] calculated from radiogenic ^{208}Pb and the ^{207}Pb and the $^{207}Pb/^{235}U$ date of the sample, assuming concordance between U-Th-Pb systems: $\lambda(^{232}Th) = 4.9475X10^{-11}/yr$.

[c] Pb* and Pb_c represent radiogenic Pb and common Pb, respectively

[d] Measured ratio corrected for fractionation and spike contribution only.

[e] Measured ratios corrected for fractionation, spike, blank and initial common Pb.

[f] Corrected for Initial Th/U disequilibrium using radiogenic ^{208}Pb and Th/U [magma] = 2.8

[g] Isotopic dates calculated using the decay constants of Steiger and Jager (1976): $\lambda(^{235}U) = 9.8485X10^{-10}/yr$ and $\lambda(^{238}U) = 1.55125X10^{-10}/yr$.

Part 5
Conclusions

The results of this study represent the first long-term, high-resolution marine sulfate sulfur isotope records for the Ordovician. Both short and long-term variation in marine sulfate sulfur isotopic composition is consistent with the existence of a relatively large, deep-ocean hydrogen sulfide reservoir in the Early and Middle Ordovician. A major perturbation in the late Middle Ordovician sulfur cycle is best explained by the near complete oxidation of this deep-ocean hydrogen sulfide reservoir. Coeval records of declining sea surface temperature suggest this event was likely driven by downwelling of cool, oxygen-rich waters that perhaps signal the start of climate change that resulted in widespread glaciation and mass extinction in the terminal Ordovician. With the addition of new, high-resolution U-Pb zircon dates from K-bentonites from the Argentine Precordillera, evaluation of the timing of explosive volcanism suggests it was not the primary driver of climate change throughout the Ordovician.

Vita

Cara K. Thompson was born in Lancaster, CA on June 11, 1979. She was raised in Roanoke, VA where she graduated from Northside High School in May 1997. She attended Virginia Western Community College where she graduated with her Associate's in Science Degree in 1999. Her Bachelor's degree in Environmental Science was completed at the University of Virginia, Charlottesville in May 2001. She attended core courses in geosciences at Virginia Polytechnic Institute and State University in Blacksburg, VA before beginning her Master's in Geology at Earth and Planetary Sciences at the University of Tennessee, Knoxville. After completion of her M.S. in December 2005, she began a Doctor of Philosophy degree in Geology with a concentration in carbonate and stable isotope geochemistry in the Earth and Planetary Sciences Department at the University of Tennessee, Knoxville. Cara was awarded a National Science Foundation Postdoctoral Fellowship to work with Troy Rasbury at Stony Brook State University of New York beginning in May, 2011.